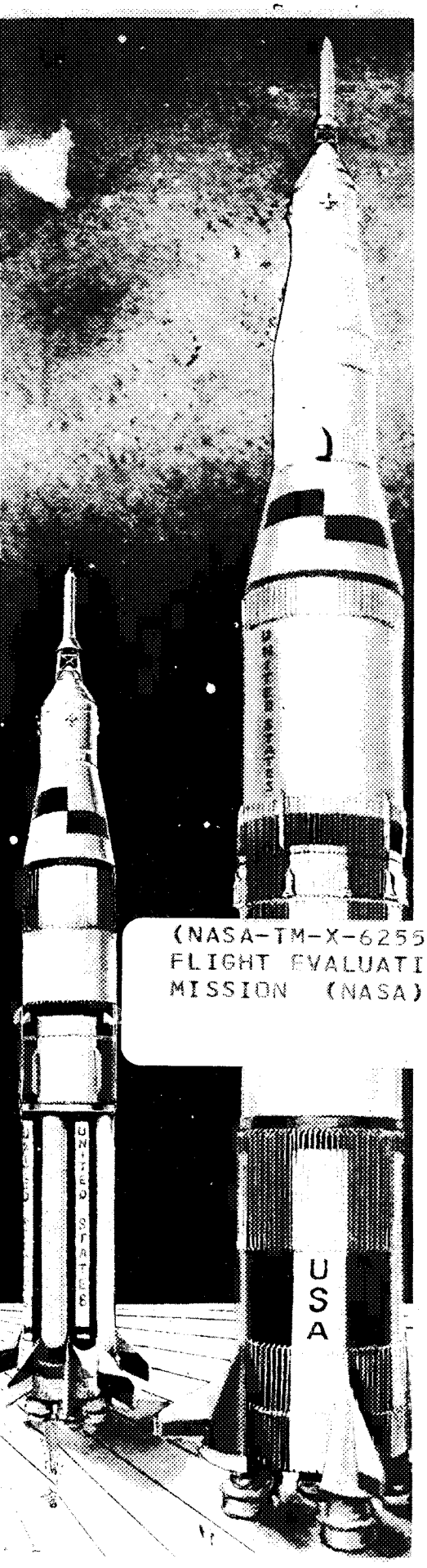

GEORGE C. MARSHALL SPACE FLIGHT CENTER

SATURN

MPR - SAT - FE - 69 - 9 SEPTEMBER 20, 1969

SATURN V LAUNCH VEHICLE FLIGHT EVALUATION REPORT-AS-506 APOLLO 11 MISSION

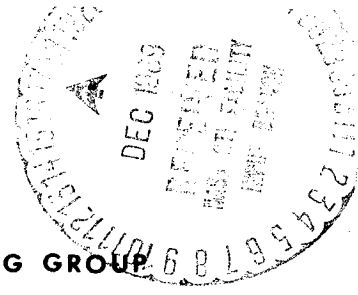

PREPARED BY

SATURN FLIGHT EVALUATION WORKING GROUP

NATIONAL AERONAUTICS AND SPACE ADMINISTRATION

GEORGE C. MARSHALL SPACE FLIGHT CENTER

MPR-SAT-FE-69-9

SATURN V LAUNCH VEHICLE
FLIGHT EVALUATION REPORT - AS-506
APOLLO 11 MISSION

PREPARED BY

SATURN FLIGHT EVALUATION WORKING GROUP

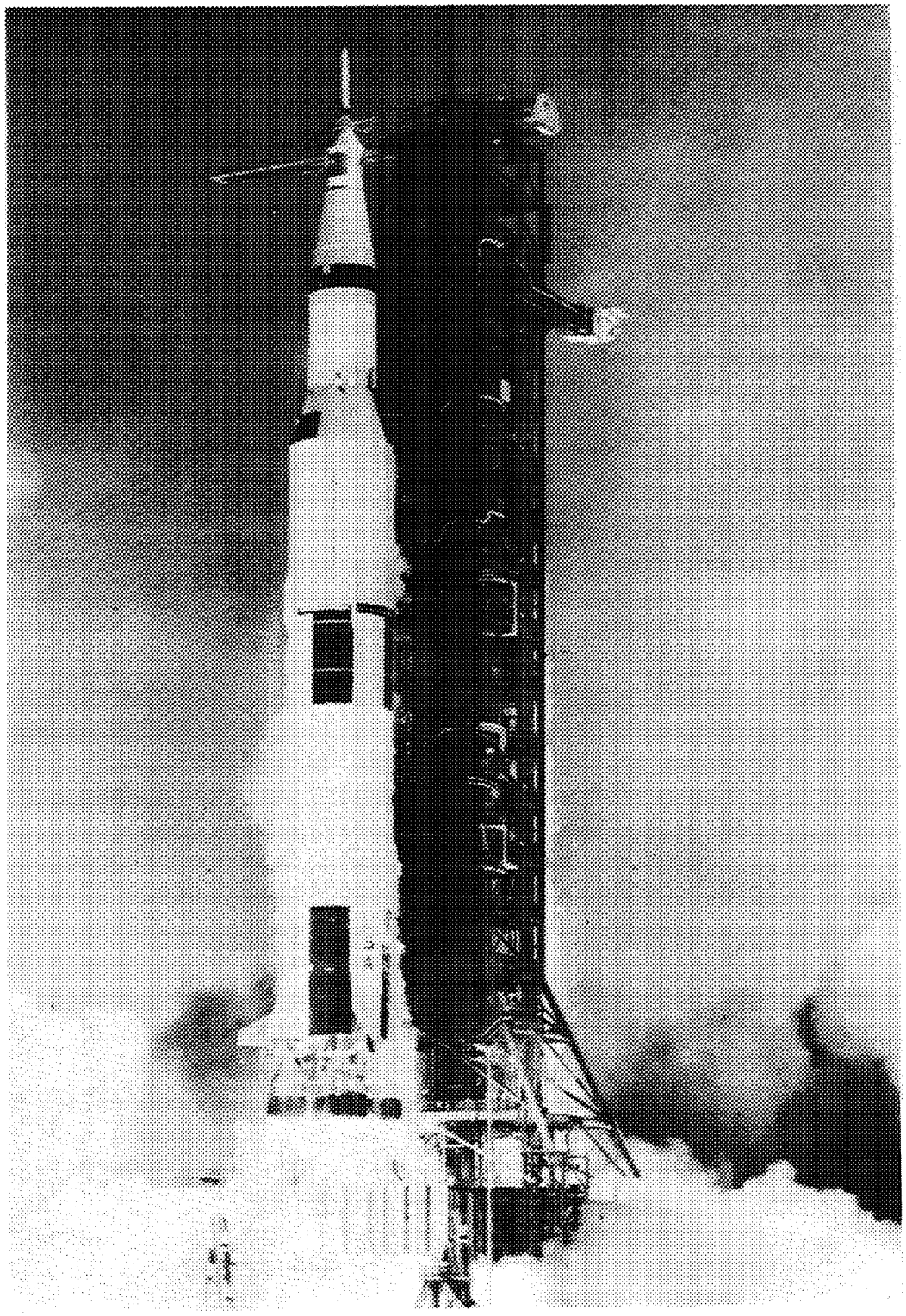

AS-506 LAUNCH VEHICLE

MPR-SAT-FE-69-9

SATURN V LAUNCH VEHICLE FLIGHT EVALUATION REPORT - AS-506

APOLLO 11 MISSION

BY

Saturn Flight Evaluation Working Group
George C. Marshall Space Flight Center

ABSTRACT

Saturn V AS-506 (Apollo 11 Mission) was launched at 09:32:00 Eastern Daylight Time on July 16, 1969, from Kennedy Space Center, Complex 39, Pad A. The vehicle lifted off on schedule on a launch azimuth of 90 degrees east of north and rolled to a flight azimuth of 72.058 degrees east of north.

The launch vehicle successfully placed the manned spacecraft in the planned translunar injection coast mode. The S-IVB/IU was placed in a solar orbit with a period of 342 days by a combination of continuous LH_2 vent, a LOX dump and APS ullage burn.

The Principal and Secondary Detailed Objectives of this mission were completely accomplished. No failures, anomalies, or deviations occurred that seriously affected the flight or mission.

Any questions or comments pertaining to the information contained in this report are invited and should be directed to:

Director, George C. Marshall Space Flight Center
Huntsville, Alabama 35812
Attention: Chairman, Saturn Flight Evaluation Working Group, S&E-CSE-LE (Phone 453-2575)

TABLE OF CONTENTS

Section			Page
	TABLE OF CONTENTS		iii
	LIST OF ILLUSTRATIONS		xi
	LIST OF TABLES		xvi
	ACKNOWLEDGEMENT		xix
	ABBREVIATIONS		xx
	MISSION PLAN		xxiii
	FLIGHT TEST SUMMARY		xxv
1	INTRODUCTION		
	1.1	Purpose	1-1
	1.2	Scope	1-1
2	EVENT TIMES		
	2.1	Summary of Events	2-1
	2.2	Variable Time and Commanded Switch Selector Events	2-2
3	LAUNCH OPERATIONS		
	3.1	Summary	3-1
	3.2	Prelaunch Milestones	3-1
	3.3	Countdown Events	3-1
	3.4	Propellant Loading	3-1
	3.4.1	RP-1 Loading	3-1
	3.4.2	LOX Loading	3-3
	3.4.3	LH_2 Loading	3-3
	3.4.4	Auxiliary Propulsion System Propellant Loading	3-4
	3.5	S-II Insulation, Purge and Leak Detection	3-4

TABLE OF CONTENTS (CONTINUED)

Section			Page
	3.6	Ground Support Equipment	3-4
	3.6.1	Ground/Vehicle Interface	3-4
	3.6.2	MSFC Furnished Ground Support Equipment	3-5
	3.6.3	Camera Coverage	3-6
4	TRAJECTORY		
	4.1	Summary	4-1
	4.2	Tracking Data Utilization	4-2
	4.2.1	Tracking During the Ascent Phase of Flight	4-2
	4.2.2	Tracking During Orbital Flight	4-2
	4.2.3	Tracking During the Injection Phase of Flight	4-2
	4.2.4	Tracking During the Post Injection Phase of Flight	4-3
	4.3	Trajectory Evaluation	4-3
	4.3.1	Ascent Trajectory	4-3
	4.3.2	Parking Orbit Trajectory	4-6
	4.3.3	Injection Trajectory	4-6
	4.3.4	Post TLI Trajectory	4-10
	4.3.5	S-IVB/IU Post Separation Trajectory	4-11
5	S-IC PROPULSION		
	5.1	Summary	5-1
	5.2	S-IC Ignition Transient Performance	5-1
	5.3	S-IC Mainstage Performance	5-3
	5.4	S-IC Engine Shutdown Transient Performance	5-5
	5.5	S-IC Stage Propellant Management	5-6
	5.6	S-IC Pressurization Systems	5-7
	5.6.1	S-IC Fuel Pressurization System	5-7
	5.6.2	S-IC LOX Pressurization System	5-7
	5.7	S-IC Pneumatic Control Pressure System	5-8
	5.8	S-IC Purge Systems	5-8
	5.9	S-IC POGO Suppression System	5-9

TABLE OF CONTENTS (CONTINUED)

Section			Page
6	S-II PROPULSION		
	6.1	Summary	6-1
	6.2	S-II Chilldown and Buildup Transient Performance	6-2
	6.3	S-II Mainstage Performance	6-4
	6.4	S-II Shutdown Transient Performance	6-8
	6.5	S-II Stage Propellant Management	6-8
	6.6	S-II Pressurization Systems	6-9
	6.6.1	S-II Fuel Pressurization System	6-9
	6.6.2	S-II LOX Pressurization System	6-11
	6.7	S-II Pneumatic Control Pressure System	6-13
	6.8	S-II Helium Injection System	6-13
7	S-IVB PROPULSION		
	7.1	Summary	7-1
	7.2	S-IVB Chilldown and Buildup Transient Performance for First Burn	7-1
	7.3	S-IVB Mainstage Performance for First Burn	7-3
	7.4	S-IVB Shutdown Transient Performance for First Burn	7-5
	7.5	S-IVB Parking Orbit Coast Phase Conditioning	7-5
	7.6	S-IVB Chilldown and Restart for Second Burn	7-8
	7.7	S-IVB Mainstage Performance for Second Burn	7-12
	7.8	S-IVB Shutdown Transient Performance for Second Burn	7-12
	7.9	S-IVB Stage Propellant Management	7-12
	7.10	S-IVB Pressurization System	7-14
	7.10.1	S-IVB Fuel Pressurization System	7-14
	7.10.2	S-IVB LOX Pressurization System	7-19

TABLE OF CONTENTS (CONTINUED)

Section			Page
	7.11	S-IVB Pneumatic Control System	7-25
	7.12	S-IVB Auxiliary Propulsion System	7-25
	7.13	S-IVB Orbital Safing Operations	7-27
	7.13.1	Fuel Tank Safing	7-27
	7.13.2	LOX Tank Dump and Safing	7-27
	7.13.3	Cold Helium Dump	7-29
	7.13.4	Ambient Helium Dump	7-29
	7.13.5	Stage Pneumatic Control Sphere Safing	7-29
	7.13.6	Engine Start Sphere Safing	7-31
	7.13.7	Engine Control Sphere Safing	7-31
8	HYDRAULIC SYSTEMS		
	8.1	Summary	8-1
	8.2	S-IC Hydraulic System	8-1
	8.3	S-II Hydraulic System	8-1
	8.4	S-IVB Hydraulic System	8-2
9	STRUCTURES		
	9.1	Summary	9-1
	9.2	Total Vehicle Structures Evaluation	9-1
	9.2.1	Longitudinal Loads	9-1
	9.2.2	Bending Moments	9-2
	9.2.3	Vehicle Dynamic Characteristics	9-3
	9.2.3.1	Longitudinal Dynamic Characteristics	9-3
	9.2.3.2	Lateral Dynamic Characteristics	9-12
10	GUIDANCE AND NAVIGATION		
	10.1	Summary	10-1
	10.1.1	Flight Program	10-1
	10.1.2	Instrument Unit Components	10-1
	10.2	Guidance Comparisons	10-1
	10.2.1	Late S-II Stage EMR Shift	10-4
	10.3	Navigation and Guidance Scheme Evaluation	10-9
	10.4	Guidance System Component Evaluation	10-10
	10.4.1	LVDC Performance	10-10
	10.4.2	LVDA Performance	10-10
	10.4.3	Ladder Outputs	10-10

TABLE OF CONTENTS (CONTINUED)

Section			Page
	10.4.4	Telemetry Outputs	10-10
	10.4.5	Discrete Outputs	10-13
	10.4.6	Switch Selector Functions	10-13
	10.4.7	ST-124M-3 Inertial Platform	10-14
11	CONTROL SYSTEM		
	11.1	Summary	11-1
	11.2	S-IC Control System Evaluation	11-1
	11.2.1	Liftoff Clearances	11-2
	11.2.2	S-IC Flight Dynamics	11-2
	11.3	S-II Control System Evaluation	11-6
	11.4	S-IVB Control System Evaluation	11-13
	11.4.1	Control System Evaluation During First Burn	11-13
	11.4.2	Control System Evaluation During Parking Orbit	11-13
	11.4.3	Control System Evaluation During Second Burn	11-14
	11.4.4	Control System Evaluation After S-IVB Second Burn	11-15
12	SEPARATION		
	12.1	Summary	12-1
	12.2	S-IC/S-II Separation Evaluation	12-1
	12.3	S-II/S-IVB Separation Evaluation	12-1
	12.4	S-IVB/IU/LM/CSM Separation Evaluation	12-1
	12.5	Lunar Module Docking and Ejection Evaluation	12-2
13	ELECTRICAL NETWORKS		
	13.1	Summary	13-1
	13.2	S-IC Stage Electrical System	13-1
	13.3	S-II Stage Electrical System	13-2
	13.4	S-IVB Stage Electrical System	13-3
	13.5	Instrument Unit Electrical System	13-6
14	RANGE SAFETY AND COMMAND SYSTEMS		
	14.1	Summary	14-1
	14.2	Secure Range Safety Command Systems	14-1

TABLE OF CONTENTS (CONTINUED)

Section			Page
	14.3	Command and Communications System	14-1
15	EMERGENCY DETECTION SYSTEM		
	15.1	Summary	15-1
	15.2	System Evaluation	15-1
	15.2.1	General Performance	15-1
	15.2.2	Propulsion System Sensors	15-1
	15.2.3	Flight Dynamics and Control Sensors	15-1
16	VEHICLE PRESSURE ENVIRONMENT		
	16.1	Summary	16-1
	16.2	Base Pressures	16-1
	16.2.1	S-IC Base Pressures	16-1
	16.2.2	S-II Base Pressures	16-1
	16.3	Surface Pressure and Compartment Venting	16-5
	16.3.1	S-IC Stage	16-5
	16.3.2	S-II Stage	16-5
17	VEHICLE THERMAL ENVIRONMENT		
	17.1	Summary	17-1
	17.2	S-IC Base Heating	17-1
	17.3	S-II Base Region Environment	17-4
	17.4	Vehicle Aeroheating Thermal Environment	17-7
	17.4.1	S-IC Stage Aeroheating Environment	17-7
	17.4.2	S-II Stage Aeroheating Environment	17-8
18	ENVIRONMENTAL CONTROL SYSTEM		
	18.1	Summary	18-1
	18.2	S-IC Environmental Control	18-1
	18.3	S-II Environmental Control	18-2
	18.4	IU Environmental Control	18-2
	18.4.1	Thermal Conditioning System	18-2
	18.4.2	Gas Bearing Supply System	18-7
19	DATA SYSTEMS		
	19.1	Summary	19-1
	19.2	Vehicle Measurement Evaluation	19-1
	19.3	Airborne Telemetry Systems	19-2

TABLE OF CONTENTS (CONTINUED)

Section			Page
	19.4	RF Systems Evaluation	19-6
	19.4.1	Telemetry System RF Propagation Evaluation	19-6
	19.4.2	Tracking Systems RF Propagation Evaluation	19-6
	19.4.3	Command Systems RF Evaluation	19-8
	19.5	Optical Instrumentation	19-12
20	MASS CHARACTERISTICS		
	20.1	Summary	20-1
	20.2	Mass Evaluation	20-1
21	MISSION OBJECTIVES ACCOMPLISHMENT		21-1
22	FAILURES, ANOMALIES AND DEVIATIONS		
	22.1	Summary	22-1
	22.2	System Failures and Anomalies	22-1
	22.3	System Deviations	22-1
23	SPACECRAFT SUMMARY		23-1
Appendix			
A	ATMOSPHERE		
	A.1	Summary	A-1
	A.2	General Atmospheric Conditions at Launch Time	A-1
	A.3	Surface Observations at Launch Time	A-1
	A.4	Upper Air Measurements	A-1
	A.4.1	Wind Speed	A-1
	A.4.2	Wind Direction	A-1
	A.4.3	Pitch Wind Component	A-2
	A.4.4	Yaw Wind Component	A-2
	A.4.5	Component Wind Shears	A-2
	A.4.6	Extreme Wind Data in the High Dynamic Region	A-3
	A.5	Thermodynamic Data	A-3
	A.5.1	Temperature	A-3
	A.5.2	Atmospheric Pressure	A-10

TABLE OF CONTENTS (CONTINUED)

Appendix			Page
	A.5.3	Atmospheric Density	A-10
	A.5.4	Optical Index of Refraction	A-13
	A.6	Comparison of Selected Atmospheric Data for Saturn V Launches	A-13
B.	AS-506 SIGNIFICANT CONFIGURATION CHANGES		
	B.1	Introduction	B-1

LIST OF ILLUSTRATIONS

Figure		Page
2-1	Telemetry Time Delay	2-2
4-1	Ascent Trajectory Position Comparison	4-3
4-2	Ascent Trajectory Space-Fixed Velocity and Flight Path Angle Comparisons	4-4
4-3	Ascent Trajectory Acceleration Comparison	4-5
4-4	Dynamic Pressure and Mach Number Comparisons	4-6
4-5	Ground Track	4-12
4-6	Injection Phase Space-Fixed Velocity and Flight Path Angle Comparisons	4-13
4-7	Injection Phase Acceleration Comparison	4-14
4-8	Slingshot Maneuver Longitudinal Velocity Increase	4-15
4-9	Trajectory Conditions Resulting from Slingshot Maneuver Velocity Increments	4-18
4-10	S-IVB/IU Velocity Relative to Earth Distance	4-18
5-1	S-IC LOX Start Box Requirements	5-2
5-2	S-IC Engines Buildup Transients	5-3
5-3	S-IC Stage Propulsion Performance Parameters	5-4
5-4	S-IC Fuel Ullage Pressure	5-8
5-5	S-IC LOX Tank Ullage Pressure	5-9
5-6	S-IC LOX Suction Duct Pressure, Engine No. 5	5-10
6-1	S-II Engine Start Tank Performance	6-3
6-2	S-II Engine Pump Inlet Start Requirements	6-5
6-3	S-II Steady-State Operation	6-6
6-4	S-II Fuel Tank Ullage Pressure	6-10
6-5	S-II Fuel Pump Inlet Conditions	6-12
6-6	S-II LOX Tank Ullage Pressure	6-13
6-7	S-II LOX Pump Inlet Conditions	6-14

LIST OF ILLUSTRATIONS (CONTINUED)

Figure		Page
7-1	S-IVB Start Box and Run Requirements - First Burn	7-2
7-2	S-IVB Steady-State Performance - First Burn	7-4
7-3	S-IVB CVS Performance - Coast Phase	7-6
7-4	S-IVB Ullage Conditions During Repressurization Using O_2/H_2 Burner	7-9
7-5	S-IVB O_2/H_2 Burner Thrust and Pressurant Flowrates	7-10
7-6	S-IVB Start Box and Run Requirements - Second Burn	7-11
7-7	S-IVB Steady-State Performance - Second Burn	7-13
7-8	S-IVB LH_2 Ullage Pressure - First Burn and Parking Orbit	7-15
7-9	S-IVB LH_2 Ullage Pressure - Second Burn and Translunar Coast	7-16
7-10	S-IVB Fuel Pump Inlet Conditions - First Burn	7-17
7-11	S-IVB Fuel Pump Inlet Conditions - Second Burn	7-18
7-12	S-IVB LOX Tank Ullage Pressure - First Burn and Parking Orbit	7-19
7-13	S-IVB LOX Tank Ullage Pressure - Second Burn and Translunar Coast	7-21
7-14	S-IVB LOX Pump Inlet Conditions - First Burn	7-22
7-15	S-IVB LOX Pump Inlet Conditions - Second Burn	7-23
7-16	S-IVB Cold Helium Supply History	7-24
7-17	S-IVB APS Propellants Remaining Versus Range Time, Module No. 1 and Module No. 2	7-26
7-18	S-IVB LOX Dump and Orbital Safing Sequence	7-28
7-19	S-IVB LOX Dump	7-30
8-1	S-IVB Hydraulic System - Second Burn	8-3
8-2	S-IVB Engine Driven Hydraulic Pump Schematic	8-4
9-1	Release Rod Force Time History Comparison	9-2
9-2	Longitudinal Load at Maximum Bending Moment, CECO and OECO	9-3
9-3	Maximum Bending Moment Near Max Q	9-4
9-4	First Longitudinal Modal Frequencies During S-IC Powered Flight	9-4

LIST OF ILLUSTRATIONS (CONTINUED)

Figure		Page
9-5	Longitudinal Acceleration at CM and IU	9-6
9-6	Peak Amplitudes of Vehicle First Longitudinal Mode for AS-504, AS-505, and AS-506	9-7
9-7	Frequency and Amplitude of Longitudinal Oscillations During S-IC Boost	9-8
9-8	Frequency and Amplitude of Longitudinal Oscillations During S-II Stage Boost	9-9
9-9	S-IVB AS-506 and AS-505 17- to 20-Hertz Oscillations Comparison	9-9
9-10	AS-506 S-IVB First Burn Maximum Response	9-10
9-11	AS-506 and AS-505 First Burn Response	9-10
9-12	Comparison of 45-Hertz Oscillations During AS-505 and AS-506 Second Burn	9-11
9-13	AS-506 Lateral Analysis/Measured Modal Frequency Correlation	9-12
10-1	Trajectory and ST-124M-3 Platform Velocity Comparison (Trajectory Minus Guidance)	10-2
10-2	Trajectory and ST-124M-3 Platform Velocity Comparison Second S-IVB Burn (Trajectory Minus Guidance)	10-3
10-3	AS-506 Characteristic Velocity Error	10-9
10-4	Attitude Commands During Active Guidance Period	10-11
10-5	Attitude Angles During S-IVB Second Burn	10-12
11-1	Pitch Plane Dynamics During S-IC Burn	11-3
11-2	Yaw Plane Dynamics During S-IC Burn	11-4
11-3	Roll Plane Dynamics During S-IC Burn	11-5
11-4	Normal Acceleration During S-IC Burn	11-8
11-5	Pitch and Yaw Plane Wind Velocity and Free-Stream Angles-of-Attack During S-IC Burn	11-9
11-6	Pitch Plane Dynamics During S-II Burn	11-10
11-7	Yaw Plane Dynamics During S-II Burn	11-11
11-8	Roll Plane Dynamics During S-II Burn	11-12
11-9	Pitch Plane Dynamics During S-IVB First Burn	11-14

LIST OF ILLUSTRATIONS (CONTINUED)

Figure		Page
11-10	Yaw Plane Dynamics During S-IVB First Burn	11-15
11-11	Roll Plane Dynamics During S-IVB First Burn	11-16
11-12	Pitch Plane Dynamics During Coast In Parking Orbit	11-17
11-13	Pitch Plane Dynamics During S-IVB Second Burn	11-17
11-14	Yaw Plane Dynamics During S-IVB Second Burn	11-18
11-15	Roll Plane Dynamics During S-IVB Second Burn	11-18
11-16	Pitch and Yaw Plane Dynamics Following Translunar Injection	11-19
11-17	Pitch, Yaw and Roll Plane Dynamics During the Maneuver to TD&E Attitude	11-20
11-18	Pitch, Yaw and Roll Plane Dynamics During the Maneuver to Slingshot Attitude	11-21
13-1	S-IVB Stage Forward Battery No. 1 Voltage and Current	13-4
13-2	S-IVB Stage Forward Battery No. 2 Voltage and Current	13-4
13-3	S-IVB Stage Aft Battery No. 1 Voltage and Current	13-5
13-4	S-IVB Stage Aft Battery No. 2 Voltage and Current	13-5
13-5	Battery 6D10 Voltage, Current, and Temperature	13-7
13-6	Battery 6D30 Voltage, Current, and Temperature	13-7
13-7	Battery 6D40 Voltage, Current, and Temperature	13-8
16-1	S-IC Base Heat Shield Pressure Loading	16-2
16-2	S-II Heat Shield Aft Face Pressure	16-3
16-3	S-II Heat Shield Forward Face Pressure	16-3
16-4	S-II Thrust Cone Pressure	16-4
16-5	S-II Forward Skirt Pressure Loading	16-6
17-1	S-IC Base Heat Shield Measurement Locations	17-2
17-2	S-IC Base Heat Shield Total Heating Rate	17-3
17-3	S-IC Base Heat Shield Gas Temperature	17-3
17-4	S-II Heat Shield Aft Face Heat Rate	17-4

LIST OF ILLUSTRATIONS (CONTINUED)

Figure		Page
17-5	Heat Shield Aft Radiation Heat Rate	17-5
17-6	S-II Base Gas Temperature	17-6
17-7	Forward Location of Separated Flow	17-7
18-1	S-IC Forward Compartment Ambient Temperature	18-3
18-2	S-IC Aft Compartment Temperature	18-4
18-3	Sublimator Performance During Ascent	18-5
18-4	TCS Coolant Control Parameters	18-6
18-5	TCS GN_2 Sphere Pressure (D25-601)	18-7
18-6	IU Selected Component Temperatures	18-8
18-7	Inertial Platform GN_2 Pressures	18-9
18-8	GBS GN_2 Sphere Pressure (D10-603)	18-10
19-1	VHF Telemetry Coverage Summary	19-7
19-2	C-Band Radar Coverage Summary	19-9
19-3	CCS Signal Strength Fluctuations at Hawaii	19-10
19-4	CCS Signal Strength Fluctuations at GDS Wing Station	19-11
19-5	CCS Coverage Summary	19-13
A-1	Scalar Wind Speed at Launch Time of AS-506	A-4
A-2	Wind Direction at Launch Time of AS-506	A-5
A-3	Pitch Wind Speed Component (W_X) at Launch Time of AS-506	A-6
A-4	Yaw Wind Speed Component (W_Z) at Launch Time of AS-506	A-7
A-5	Pitch (S_X) and Yaw (S_Z) Component Wind Shears at Launch Time of AS-506	A-8
A-6	Relative Deviation of Temperature and Density From the PRA-63 Reference Atmosphere, AS-506	A-11
A-7	Relative Deviation of Pressure and Absolute Deviation of the Index of Refraction From the PRA-63 Reference Atmosphere, AS-506	A-12

LIST OF TABLES

Table		Page
2-1	Time Base Summary	2-3
2-2	Significant Event Times Summary	2-4
2-3	Variable Time and Commanded Switch Selector Events	2-10
3-1	AS-506 Prelaunch Milestones	3-2
4-1	Comparison of Significant Trajectory Events	4-7
4-2	Comparison of Cutoff Events	4-8
4-3	Comparison of Separation Events	4-9
4-4	Stage Impact Location	4-10
4-5	Parking Orbit Insertion Conditions	4-11
4-6	Translunar Injection Conditions	4-16
4-7	Comparison of Slingshot Maneuver Velocity Increment	4-16
4-8	Comparison of Lunar Closest Approach Parameters	4-19
4-9	Heliocentric Orbit Parameters	4-19
5-1	S-IC Engine Performance Deviations	5-5
5-2	S-IC Stage Propellant Mass History	5-6
6-1	S-II Engine Performance Deviations (ESC +61 Seconds)	6-7
6-2	S-II Propellant Mass History	6-10
7-1	S-IVB Steady-State Performance - First Burn (STDV +137-Second Time Slice at Standard Altitude Conditions)	7-5
7-2	S-IVB Steady-State Performance - Second Burn (STDV +172-Second Time Slice at Standard Altitude Conditions)	7-14
7-3	S-IVB Stage Propellant Mass History	7-14
7-4	S-IVB APS Propellant Conditions	7-25
7-5	S-IVB APS Propellant Consumption	7-27

LIST OF TABLES (CONTINUED)

Table		Page
10-1	Inertial Platform Velocity Comparisons	10-5
10-2	Guidance Comparisons	10-6
10-3	Guidance Components Differences	10-8
10-4	Start and Stop Times for IGM Guidance Commands	10-10
10-5	Parking Orbit Insertion Parameters	10-13
10-6	Translunar Injection Parameters	10-13
11-1	AS-506 Misalignment and Liftoff Conditions Summary	11-6
11-2	Maximum Control Parameters During S-IC Burn	11-7
11-3	Maximum Control Parameters During S-II Burn	11-13
11-4	Maximum Control Parameters During S-IVB First Burn	11-16
11-5	Maximum Control Parameters During S-IVB Second Burn	11-19
13-1	S-IC Stage Battery Power Consumption	13-1
13-2	S-II Stage Battery Power Consumption	13-2
13-3	S-IVB Stage Battery Power Consumption	13-3
13-4	IU Battery Power Consumption	13-6
14-1	Command and Communication System GDS Commands History	14-2
18-1	TCS Coolant Flowrates and Pressures	18-6
19-1	AS-506 Measurement Summary	19-2
19-2	AS-506 Flight Measurements Waived Prior to Launch	19-3
19-3	AS-506 Measurement Malfunctions	19-4
19-4	AS-506 Launch Vehicle Telemetry Links	19-5
20-1	Total Vehicle Mass - S-IC Burn Phase - Kilograms	20-3
20-2	Total Vehicle Mass - S-IC Burn Phase - Pounds Mass	20-4
20-3	Total Vehicle Mass - S-II Burn Phase - Kilograms	20-5
20-4	Total Vehicle Mass - S-II Burn Phase - Pounds Mass	20-6
20-5	Total Vehicle Mass - S-IVB First Burn Phase - Kilograms	20-7

LIST OF TABLES (CONTINUED)

Table		Page
20-6	Total Vehicle Mass - S-IVB First Burn Phase - Pounds Mass	20-8
20-7	Total Vehicle Mass - S-IVB Second Burn Phase - Kilograms	20-9
20-8	Total Vehicle Mass - S-IVB Second Burn Phase - Pounds Mass	20-10
20-9	Flight Sequence Mass Summary	20-11
20-10	Mass Characteristics Comparison	20-13
21-1	Mission Objectives Accomplishment Summary	21-1
22-1	Summary of Deviations	22-2
A-1	Surface Observations at AS-506 Launch Time	A-2
A-2	Solar Radiation at AS-506 Launch Time, Launch Pad 39A	A-3
A-3	Systems Used to Measure Upper Air Wind Data for AS-506	A-9
A-4	Maximum Wind Speed in High Dynamic Pressure Region for Apollo/Saturn 501 through Apollo/ Saturn 506 Vehicles	A-9
A-5	Extreme Wind Shear Values in the High Dynamic Pressure Region for Apollo/Saturn 501 through Apollo/Saturn 506 Vehicles	A-10
A-6	Selected Atmospheric Observations for Apollo/ Saturn 501 through Apollo/Saturn 506 Vehicle Launches at Kennedy Space Center, Florida	A-13
B-1	S-IC Significant Configuration Changes	B-2
B-2	S-II Significant Configuration Changes	B-2
B-3	S-IVB Significant Configuration Changes	B-3
B-4	IU Significant Configuration Changes	B-4

ACKNOWLEDGEMENT

This report is published by the Saturn Flight Evaluation Working Group--composed of representatives of Marshall Space Flight Center, John F. Kennedy Space Center, and MSFC's prime contractors--and in cooperation with the Manned Spacecraft Center. Significant contributions to the evaluation have been made by:

George C. Marshall Space Flight Center

Science and Engineering

Central Systems Engineering
Aero-Astrodynamics
Astrionics Laboratory
Computation Laboratory
Astronautics Laboratory

Program Management

John F. Kennedy Space Center

Manned Spacecraft Center

The Boeing Company

McDonnell Douglas Astronautics Company

International Business Machines Corporation

North American Rockwell/Space Division

North American Rockwell/Rocketdyne Division

ABBREVIATIONS

ACN	Ascension
AGC	Automatic Gain Control
ANT	Antigua
AOS	Acquisition of Signal
APS	Auxiliary Propulsion System
ARIA	Apollo Range Instrument Aircraft
ASI	Augmented Spark Igniter
AUX	Auxiliary
AVP	Address Verification Pulse
BDA	Bermuda
CCS	Command and Communications System
CDDT	Countdown Demonstration Test
CECO	Center Engine Cutoff
CG	Center of Gravity
CIF	Central Information Facility
CM	Command Module
CNV	Cape Kennedy
CRO	Carnarvon
CRP	Computer Reset Pulse
CSM	Command and Service Module
CVS	Continuous Vent System
CYI	Grand Canary Island
DDAS	Digital Data Acquisition System
DEE	Digital Events Evaluator
DTS	Data Transmission System
EBW	Exploding Bridge Wire
ECO	Engine Cutoff
ECS	Environmental Control System
EDS	Emergency Detection System
EDT	Eastern Daylight Time
EMR	Engine Mixture Ratio
EPO	Earth Parking Orbit
ESC	Engine Start Command
EVA	Extra-Vehicular Activity
FCC	Flight Control Computer
FM/FM	Frequency Modulation/ Frequency Modulation
FRT	Flight Readiness Test
GBI	Grand Bahama Island
GBM	Grand Bahama
GBS	Gas Bearing System
GET	Ground Elapse Time
GFCV	GOX Flow Control Valve
GDS	Goldstone
GG	Gas Generator
GOX	Gaseous Oxygen
GRR	Guidance Reference Release
GSE	Ground Support Equipment
GSFC	Goddard Space Flight Center
GTK	Grand Turk Island
GWM	Guam
GYM	Guaymas

HAW	Hawaii
HDA	Holddown Arm
HFCV	Helium Flow Control Valve
HSK	Honeysuckle (Canberra)
IGM	Iterative Guidance Mode
IMU	Inertial Measurement Unit
IP&C	Instrumentation Program and Components
IU	Instrument Unit
KSC	Kennedy Space Center
LCC	Launch Control Center
LES	Launch Escape System
LET	Launch Escape Tower
LH_2	Liquid Hydrogen
LIEF	Launch Information Exchange Facility
LM	Lunar Module
LOI	Lunar Orbit Insertion
LOS	Loss of Signal
LOX	Liquid Oxygen
LUT	Launch Umbilical Tower
LV	Launch Vehicle
LVDA	Launch Vehicle Data Adapter
LVDC	Launch Vehicle Digital Computer
MAD	Madrid
MAP	Message Acceptance Pulse
MCC-H	Mission Control Center - Houston
MER	Mercury (ship)
MFCV	Modulating Flow Control Valve
MILA	Merritt Island Launch Area
MOV	Main Oxidizer Valve
MR	Mixture Ratio
MSC	Manned Spacecraft Center
MSFC	Marshall Space Flight Center
MSFN	Manned Space Flight Network
MSS	Mobile Service Structure
MTF	Mississippi Test Facility
M/W	Methanol Water
NPSP	Net Positive Suction Pressure
NPV	Non Propulsive Vent
NASA	National Aeronautics and Space Administration
OAFPL	Overall Fluctuating Pressure Level
OASPL	Overall Sound Pressure Level
OAT	Overall Test
OCP	Orbital Correction Program
OECO	Outboard Engine Cutoff
OIS	Operational Intercom System
OMNI	Omni Directional
OT	Operational Trajectory
PAM/ FM/FM	Pulse Amplitude Modulation/ Frequency Modulation/ Frequency Modulation
PAFB	Patrick Air Force Base
PCM	Pulse Code Modulation
PCM/ FM	Pulse Code Modulation/ Frequency Modulation
PDO	Principal Detailed Objective
PMR	Programed Mixture Ratio
PRA	Patrick Reference Atmosphere
PSD	Power Spectral Density
PTCR	Pad Terminal Connection Room
PTCS	Propellant Tanking Control System
PU	Propellant Utilization

RED	Redstone (ship)
RF	Radio Frequency
RMS	Root Mean Square
RP-1	Designation for S-IC Stage Fuel (kerosene)
SA	Service Arm
SC	Spacecraft
SDO	Secondary Detailed Objective
SLA	Spacecraft LM Adapter
SM	Service Module
SMC	Steering Misalignment Correction
SPL	Sound Pressure Level
SPS	Service Propulsion System
SRSCS	Secure Range Safety Command System
SS/FM	Single Sideband/Frequency Modulation
STDV	Start Tank Discharge Valve
SV	Space Vehicle
T_1	Time Base 1
T_{1i}	Time to go in 1st Stage IGM
T_{2i}	Time to go in 2nd Stage IGM
TAN	Tananarive
TCS	Thermal Conditioning System
TD&E	Transposition, Docking and Ejection
TEI	Transearth Injection
TEX	Corpus Christi (Texas)
TLC	Translunar Coast
TLI	Translunar Injection
TM	Telemeter, Telemetry
TMR	Triple Modular Redundant
TSM	Tail Service Mast
TVC	Thrust Vector Control
USB	Unified S-Band
UT	Universal Time
VAN	Vanguard (ship)
VHF	Very High Frequency
WHS	White Sands

MISSION PLAN

The AS-506 flight (Apollo 11 Mission) is the sixth flight of the Apollo/Saturn V flight test program. The primary objective of the mission is to land astronauts on the lunar surface and return them safely to earth. The crew consists of Neil Armstrong (Mission Commander), Lt. Col. Michael Collins (Command Module Pilot), and Lt. Col. Edwin Aldrin, Jr. (Lunar Module Pilot).

The AS-506 flight vehicle is composed of the S-IC-6, S-II-6, and S-IVB-6N stages; Instrument Unit (IU)-6; Spacecraft/Lunar Module Adapter (SLA)-14; and Spacecraft (SC). The SC consists of Command and Service Module (CSM) -107 and Lunar Module (LM)-5.

Vehicle launch from Complex 39A at Kennedy Space Center (KSC) is along a 90 degree azimuth with a roll to a variable flight azimuth of 72 to 108 degrees measured east of true north. Vehicle mass at S-IC ignition is 2,941,221 kilograms (6,484,282 lbm). The S-IC stage powered flight is approximately 161 seconds; the S-II stage provides powered flight for approximately 389 seconds. Following S-IVB first burn (approximately 144 seconds duration), the S-IVB/IU/SLA/LM/CSM is inserted into a 183.8 by 186.5 kilometer (99.2 by 100.7 n mi) altitude (referenced to a spherical earth) Earth Parking Orbit (EPO). Vehicle mass at orbit insertion is 135,669 kilograms (229,099 lbm).

At approximately 10 seconds after EPO insertion, the vehicle is aligned with the local horizontal. Continuous hydrogen venting is initiated shortly after EPO insertion and the Launch Vehicle (LV) and CSM systems are checked in preparation for the Translunar Injection (TLI) burn. During the second or third revolution in EPO, the S-IVB stage is reignited and burns for approximately 349 seconds. This burn injects the S-IVB/IU/SLA/LM/CSM into a free-return, translunar trajectory.

Approximately 15 minutes after TLI, the vehicle initiates an inertial attitude hold for CSM separation, docking and LM ejection. Following the attitude freeze, the CSM separates from the LV and the SLA panels are jettisoned. The CSM then transposes and docks to the LM. After docking, the CSM/LM is spring ejected from the S-IVB/IU. Following CSM/LM ejection, the S-IVB/IU configuration achieves a co-rotational slingshot trajectory by using propulsive venting of hydrogen (LH_2), dumping of oxygen (LOX) and by firing the Auxiliary Propulsion System (APS) ullage engines. The slingshot trajectory results in a solar orbit for the S-IVB/IU.

During the 3 day translunar coast, the astronauts perform star-earth landmark sightings, Inertial Measurement Unit (IMU) alignments, general lunar navigation procedures and possibly four midcourse corrections. At approximately 76 hours, a Service Propulsion System (SPS), Lunar Orbit Insertion (LOI) burn of approximately 359 seconds inserts the CSM/LM into a 111 by 315 kilometer (60 by 170 n mi) altitude parking orbit.

After two revolutions in lunar orbit, a 16-second SPS burn circularizes the orbit to 111 kilometers (60 n mi) altitude at 80 hours. The LM is entered by astronauts Armstrong and Aldrin and checkout is accomplished. During the eleventh revolution in orbit at 100 hours, the LM separates from the CSM and prepares for the lunar descent. The LM descent propulsion system is used to brake the LM into the landing trajectory, approach the landing site and perform the landing at 103 hours.

Following lunar landing, the two astronauts execute a 2.66 hour simultaneous lunar Extra-Vehicular Activity (EVA). After the EVA, the astronauts prepare the ascent propulsion system for lunar ascent. The total lunar stay time for Apollo 11 is approximately 22 hours.

The CSM performs a plane change approximately 17 hours prior to lunar ascent. At approximately 124.5 hours, the ascent stage inserts the LM into a 16.7 by 83.3 kilometer (9 by 45 n mi) altitude lunar orbit, and rendezvous and docks with the CSM. The astronauts reenter the CSM, jettison the LM and prepare for Transearth Injection (TEI). TEI is accomplished at approximately 135 hours with a 149-second SPS burn. The time and duration of the SPS TEI burn is dependent on an optional astronaut rest period.

During the 60-hour transearth coast, the astronauts perform navigation procedures, star-earth-moon sightings and possibly three midcourse corrections. The Service Module (SM) separates from the Command Module (CM) 15 minutes prior to reentry. Splashdown occurs in the Pacific Ocean approximately 195 hours after liftoff.

After the recovery operations, a biological quarantine is imposed on the crew and CM. An incubation period of 18 days from splashdown (21 days from lunar ascent) is required for the astronauts. The hardware incubation period is the time required to analyze certain lunar samples.

FLIGHT TEST SUMMARY

The fourth manned Saturn V Apollo space vehicle, AS-506 (Apollo 11 (Mission) was launched at 09:32:00 Eastern Daylight Time (EDT) on July 16, 1969 from Kennedy Space Center (KSC), Complex 39, Pad A. This sixth launch of the Saturn V/Apollo successfully performed the three principal detailed objectives mandatory for successful accomplishment of the primary mission objective which was to perform a lunar landing and return. The secondary detailed objective was also successfully accomplished.

The launch countdown was completed without any unscheduled countdown holds. Ground system performance was satisfactory. Damage to the pad, Launch Umbilical Tower (LUT) and support equipment was minor.

The trajectory parameters of AS-506 from launch to Translunar Injection (TLI) were close to nominal. The vehicle was launched on an azimuth 90 degrees east of north. A roll maneuver was initiated at 13.2 seconds that placed the vehicle on a flight azimuth of 72.058 degrees east of north. The space-fixed velocity at S-IC Outboard Engine Cutoff (OECO) was 8.5 m/s (27.9 ft/s) greater than nominal. The space-fixed velocity at S-II OECO was 22.8 m/s (74.8 ft/s) less than nominal. The space-fixed velocity at S-IVB first guidance cutoff was 0.2 m/s (0.6 ft/s) less than nominal. The altitude at S-IVB first guidance cutoff was 0.2 kilometer (0.1 n mi) lower than nominal and the surface range was 1.7 kilometer (1.0 n mi) less than nominal. The space-fixed velocity at parking orbit insertion was equal to nominal. The apogee and perigee were 0.5 kilometer (0.3 n mi) and 0.6 kilometer (0.3 n mi) less than nominal, respectively. The parameters at TLI were also close to nominal. The space-fixed velocity was 3.2 m/s (10.5 ft/s) greater than nominal, the altitude was 3.1 kilometers (1.6 n mi) less than nominal and C_3 was 16,877 m^2/s^2 (181,663 ft^2/s^2) greater than nominal. Following Lunar Module (LM) extraction, the vehicle maneuvered to a slingshot attitude frozen relative to local horizontal. The retrograde velocity change necessary to achieve S-IVB/IU lunar slingshot maneuver was accomplished by a LOX dump, Auxiliary Propulsion System (APS) burn, and LH_2 vent. The S-IVB/IU closest approach of 3379 kilometers (1825 n mi) above the lunar surface occurred at 78.7 hours into the mission.

All S-IC propulsion systems performed satisfactorily and the propulsion performance level was very close to nominal. Stage site thrust (averaged from liftoff to OECO) was 0.62 percent lower than predicted. Total propellant consumption rate was 0.40 percent lower than predicted with the total consumed Mixture Ratio (MR) 0.10 percent lower than predicted.

Specific impulse was 0.16 percent lower than predicted. Total propellant consumption from Holddown Arm (HDA) release to OECO was low by 1.12 percent. Center Engine Cutoff (CECO) was commanded by the IU as planned. OECO, initiated by the LOX low level sensors, occurred 0.55 second later than predicted.

The S-II propulsion system performed satisfactorily throughout the flight. The S-II stage operation time of 385.18 seconds was 4.0 seconds shorter than predicted. Early CECO successfully avoided high amplitude low frequency oscillations experienced on the AS-503 and AS-504 flights. Total stage thrust at 61 seconds after S-II Engine Start Command (ESC) was 0.20 percent below predicted. Total propellant flowrate (including pressurization flow) was 0.13 percent below predicted and vehicle specific impulse was 0.07 percent below predicted at this time slice. Stage propellant MR was 0.36 percent above predicted. The engine servicing system Ground Support Equipment (GSE) performed satisfactorily except that the engine No. 1 start tank pressure was 2.8 N/cm^2 (4 psi) below redline at prelaunch commit (-33 seconds). All start tank pressures and temperatures were well within requirements at S-II ESC.

The J-2 engine operated satisfactorily throughout the operational phase of S-IVB first and second burn. Shutdowns for both burns were normal. S-IVB first burn duration was 147.1 seconds which was 3.4 seconds more than predicted. The engine performance during first burn, as determined from standard altitude reconstruction analysis, deviated from the predicted by +0.20 percent for thrust and +0.05 percent for specific impulse. The S-IVB stage first burn Engine Cutoff (ECO) was initiated by the Launch Vehicle Digital Computer (LVDC) at 699.34 seconds. The Continuous Vent System (CVS) adequately regulated LH_2 tank ullage pressure during orbit, and the Oxygen/Hydrogen (O_2/H_2) burner satisfactorily achieved LH_2 and LOX tank repressurization for restart. Engine restart conditions were within specified limits. The restart at full open Propellant Utilization (PU) valve position was successful. S-IVB second burn duration was 346.9 seconds which was 1.7 seconds less than predicted. The engine performance during second burn, as determined from the standard altitude reconstruction analysis, deviated from the predicted by -0.56 percent for thrust and +0.05 percent for specific impulse. Subsequent to second burn, the stage propellant tanks were safed satisfactorily.

The stage hydraulic systems performed satisfactorily on the S-IC, S-II, and first burn and coast phase of the S-IVB stage. During this period all parameters were within specification limits. Just after stage reignition the S-IVB hydraulic system pressure exceeded the upper limit by 0.6 percent. At 202 seconds into the burn, a step decrease in system pressure to a nominal operating level occurred and the pressure remained at this level for the remainder of the burn. The pump manufacturer does not consider this condition to indicate impending malfunction of the engine driven pump.

The structural loads and dynamic environments experienced by the AS-506 launch vehicle were well within the vehicle structural capability. The longitudinal loads experienced during flight were nominal. The maximum bending moment condition, 3.75 x 10^6 N-m (33.2 x 10^6 lbf-in.), was experienced at 91.5 seconds and was lower than that experienced on any previous flight. Low level first mode longitudinal oscillations similar to those of previous flights were evident during each stage burn but caused no problems.

The navigation and guidance system performed satisfactorily. The parking orbit and TLI parameters were well within tolerance. The S-IVB LOX dump, LH_2 vent and APS ullage burn resulted in a heliocentric orbit of the S-IVB/IU as planned. The actual S-II Engine Mixture Ratio (EMR) shift occurred approximately 9.5 seconds later than indicated by the final stage propulsion prediction. About 4 seconds of this deviation was attributed to the change in LVDC nominal characteristic velocity presetting predictions and variation in actual from predicted flight performance. Approximately 5.5 seconds of the deviation is attributed to improper scaling in the flight program calculation of characteristic velocity. The LVDC, the Launch Vehicle Data Adapter (LVDA), and the ST-124M-3 inertial platform functioned satisfactorily. The platform-measured crossrange velocity ($\dot{Y}$) exhibited a negative shift of approximately 1.8 m/s (5.9 ft/s) at 3.3 seconds after liftoff. The probable cause was the Y accelerometer head momentarily contacting an internal mechanical stop. This had negligible effect on launch vehicle performance.

The AS-506 Flight Control Computer (FCC), Thrust Vector Control (TVC) and APS satisfied all requirements for vehicle attitude control during the flight. All maneuvers were properly accomplished. All separations occurred as expected without producing significant attitude deviations.

The AS-506 launch vehicle electrical systems performed satisfactorily throughout all phases of flight. Performance of the Secure Range Safety Command Systems (SRSCS) was nominal on all powered stages. The SRSCS was properly safed by ground command from Bermuda (BDA). Performance of the Command and Communications System (CCS) was satisfactory except for the Radio Frequency (RF) problem noted. The Emergency Detection System (EDS) performance was nominal with no abort limits exceeded.

Vehicle base pressure environments were generally in good agreement with postflight predictions and compared well with previous flight data. There was no instrumentation provided on the AS-506 vehicle which would permit a direct evaluation of the surface and compartment pressure environments. The one ambient pressure measurement located in the S-II forward skirt was used to calculate the pressure loading acting on that area, and indicated good agreement with postflight predictions and previous flight data.

Base thermal environments were similar to those experienced on earlier flights with the exception that S-II heat shield aft radiation heating rates were approximately 20 percent higher than the maximum values measured during previous flights. Aerodynamic heating environments were not measured on AS-506.

The Environmental Control System (ECS) performed satisfactorily. The IU ECS coolant temperatures, pressure, and flowrates were continuously maintained within required ranges and design limits. One deviation from specification was observed. The inertial platform gas bearing differential pressure drifted above the 10.7 N/cm^2 (15.5 psid) maximum to 11.2 N/cm^2 (16.3 psid). This condition has occurred on previous flights and caused no detrimental effect on the missions.

All elements of the data system performed satisfactorily except for a problem with the CCS downlink during translunar coast. Measurement performance was excellent as evidenced by 99.9 percent reliability. This is the highest reliability attained on any Saturn V flight. Telemetry performance was nominal, with the exception of a minor calibration deviation. Very High Frequency (VHF) telemetry Radio Frequency (RF) propagation was generally good, though the usual problems due to flame effects and staging were experienced. VHF data were received to 17,800 seconds (04:56:40). Command systems RF performance for both the SRSCS and CCS was nominal except for the CCS downlink problem noted. Goldstone (GDS) reported receiving CCS signals to 35,779 seconds (9:56:19). Good tracking data were received from the C-Band radar, with Patrick Air Force Base (PAFB) indicating final LOS at 42,912 seconds (11:55:12). The 75 ground engineering cameras provided good data during the launch.

SECTION 1

INTRODUCTION

1.1 PURPOSE

This report provides the National Aeronautics and Space Administration (NASA) Headquarters, and other interested agencies, with the launch vehicle evaluation results of the AS-506 flight test. The basic objective of flight evaluation is to acquire, reduce, analyze, evaluate and report on flight test data to the extent required to assure future mission success and vehicle reliability. To accomplish this objective, actual flight failures, anomalies and deviations must be identified, their causes accurately determined, and complete information made available so that corrective action can be accomplished within the established flight schedule.

1.2 SCOPE

This report presents the results of the early engineering flight evaluation of the AS-506 launch vehicle. The contents are centered on the performance evaluation of the major launch vehicle systems, with special emphasis on the deviations. Summaries of launch operations and spacecraft performance are included for completeness.

The official George C. Marshall Space Flight Center (MSFC) position at this time is represented by this report. It will not be followed by a similar report unless continued analysis or new information should prove the conclusions presented herein to be significantly incorrect. Final stage evaluation reports will, however, be published by the stage contractors. Reports covering major subjects and special subjects will be published as required.

SECTION 2

EVENT TIMES

2.1 SUMMARY OF EVENTS

Range zero time, the basic time reference for this report, is 9:32:00 Eastern Daylight Time (EDT) (13:32:00 Universal Time [UT]). This time is based on the nearest second prior to S-IC tail plug disconnect which occurred at 9:32:00.6 EDT. Range time is calculated as the elasped time from range zero time and, unless otherwise noted, is the time used throughout this report. The actual and predicted range times are adjusted to ground telemetry received times. The Time-From-Base times are presented as vehicle times. Figure 2-1 shows the time delay of ground telemetry received time versus Launch Vehicle Digital Computer (LVDC) time and indicates the magnitude and sign of corrections applied to correlate range time and vehicle time in Tables 2-1, 2-2 and 2-3.

Guidance Reference Release (GRR) occurred at -16.97 seconds and start of Time Base 1 (T_1) occurred at 0.63 seconds. GRR was established by the Digital Events Evaluator (DEE-6) and T_1 was initiated at detection of liftoff signal provided by de-energizing the liftoff relay in the Instrument Unit (IU) at IU umbilical disconnect.

Range time for each time base used in the flight sequence program and the signal for initiating each time base are presented in Table 2-1.

Start of T_2 was within nominal expectations for this event. Start of T_3, T_4 and T_5 were initiated approximately 0.6 second late and 3.5 and 0.1 seconds early, respectively, due to variations in the stage burn times. These variations are discussed in Sections 5, 6 and 7 of this document. Start of T_6, which was initiated by the LVDC upon solving the restart equation, was 0.9 second later than predicted. Start of T_7 was 1.0 second earlier than predicted. T_8, which was initiated by the receipt of a ground command, was started 63.2 seconds later than the predicted time.

A summary of significant events for AS-506 is given in Table 2-2. Since not all events listed in Table 2-2 are IU commanded switch selector functions, deviations are not to be construed as failures to meet specified switch selector tolerances. The events in Table 2-2 associated with guidance, navigation, and control have been identified as being accurate to within a major computation cycle.

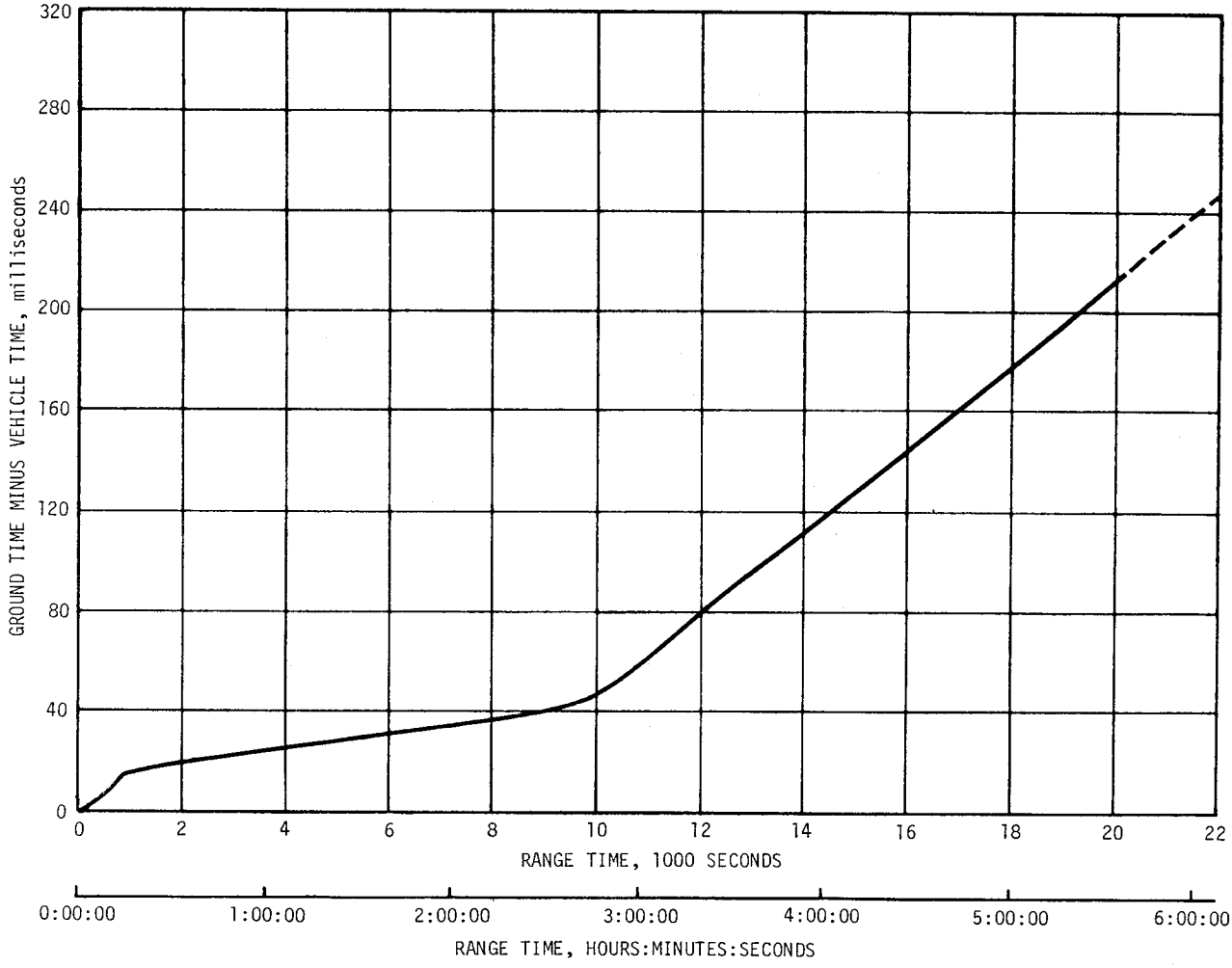

Figure 2-1. Telemetry Time Delay

The predicted times for establishing actual minus predicted times in Table 2-2 have been taken from 40M33626B, "Interface Control Document Definition of Saturn SA-506 Flight Sequence Program", and from the "AS-506 G Mission Launch Vehicle Operational Trajectory", dated July 14, 1969.

2.2 VARIABLE TIME AND COMMANDED SWITCH SELECTOR EVENTS

Table 2-3 lists the switch selector events which were issued during the flight but were not programed for specific times. The range times are adjusted to ground telemetry received times. The water coolant valve open and close switch selector commands were issued based on the condition of two thermal switches in the Environmental Control System (ECS). The outputs of these switches were sampled once every 300 seconds, beginning at 180 seconds, and a switch selector command was issued to open or close the water valve. The valve was opened if the sensed temperature was too high and the valve was closed if the temperature was too low.

Table 2-1. Time Base Summary

TIME BASE	RANGE TIME SEC (HR:MIN:SEC)	SIGNAL START
T_0	-16.97	Guidance Reference Release
T_1	0.63	IU Umbilical Disconnect Sensed by LVDC
T_2	135.27	S-IC CECO Sensed by LVDC
T_3	161.66	S-IC OECO Sensed by LVDC
T_4	548.24	S-II OECO Sensed by LVDC
T_5	699.57	S-IVB ECO (Velocity) Sensed by LVDC
T_6	9278.24 (2:34:38.24)	Restart Equation Solution
T_7	10,203.33 (2:50:03.33)	S-IVB ECO (Velocity) Sensed by LVDC
T_8	17,467.64 (4:51:07.64)	Enabled by Ground Command

Table 2-3 also contains the special sequence of switch selector events which were programed to be initiated by telemetry station acquisition and included the following calibration sequence:

Function	Stage	Time (Sec)
Telemetry Calibrator In-Flight Calibrate ON	IU	Acquisition +60.0
TM Calibrate ON	S-IVB	Acquisition +60.4
TM Calibrate OFF	S-IVB	Acquisition +61.4
Telemetry Calibrator In-Flight Calibrator OFF	IU	Acquisition +65.0

Table 2-2. Significant Event Times Summary

EVENT DESCRIPTION	RANGE TIME		TIME FROM BASE	
	ACTUAL SEC	ACT-PRED SEC	ACTUAL SEC	ACT-PRED SEC
1 GUIDANCE REFERENCE RELEASE (GRR)	-17.0	0.0	-17.6	0.0
2 S-IC ENGINE START SEQUENCE COMMAND (GROUND)	-8.9	0.0	-9.5	0.0
3 S-IC ENGINE NO.1 START	-6.1	0.0	-6.8	0.0
4 S-IC ENGINE NO.2 START	-5.9	0.0	-6.5	0.0
5 S-IC ENGINE NO.3 START	-6.1	0.0	-6.7	0.0
6 S-IC ENGINE NO.4 START	-6.0	0.0	-6.6	0.0
7 S-IC ENGINE NO.5 START	-6.4	0.0	-7.1	0.0
8 ALL S-IC ENGINES THRUST OK	-1.6	-0.1	-2.2	-0.1
9 RANGE ZERO	0.0		-0.6	
10 ALL HOLDDOWN ARMS RELEASED (FIRST MOTION)	0.3	0.0	-0.3	0.1
11 IU UMBILICAL DISCONNECT, START OF TIME BASE 1 (T1)	0.6	-0.1	0.0	0.0
12 BEGIN TOWER CLEARANCE YAW MANEUVER*	1.7	0.0	1.0	0.0
13 END YAW MANEUVER*	9.7	-1.0	9.0	-1.0
14 BEGIN PITCH AND ROLL MANEUVER*	13.2	-0.6	12.6	-0.5
15 S-IC OUTBOARD ENGINE CANT	20.6	-0.1	20.0	0.0
16 END ROLL MANEUVER *	31.1	-0.7	30.5	-0.6
17 MACH 1	66.3	0.7	65.7	0.7
18 MAXIMUM DYNAMIC PRESSURE (MAX Q)	83.0	1.7	82.4	1.8
19 S-IC CENTER ENGINE CUTOFF (CECO)	135.20	-0.08	134.56	-0.06
20 START OF TIME BASE 2 (T2)	135.3	0.0	0.0	0.0
21 END PITCH MANEUVER (TILT ARREST)*	160.0	-0.8	24.7	-0.8
22 S-IC OUTBOARD ENGINE CUTOFF (OECO)	161.63	0.55	26.36	0.59
23 START OF TIME BASE 3 (T3)	161.7	0.6	0.0	0.0
24 START S-II LH2 TANK HIGH PRESSURE VENT MODE	161.7	0.5	0.1	0.0

*Time is accurate to major computation cycle dependent upon length of computation cycles.

Table 2-2. Significant Event Times Summary (Continued)

EVENT DESCRIPTION	RANGE TIME		TIME FROM BASE	
	ACTUAL SEC	ACT-PRED SEC	ACTUAL SEC	ACT-PRED SEC
25 S-II LH2 RECIRCULATION PUMPS OFF	161.8	0.5	0.2	0.0
26 S-II ULLAGE MOTOR IGNITION	162.1	0.5	0.5	0.0
27 S-IC/S-II SEPARATION COMMAND TO FIRE SEPARATION DEVICES AND RETRO MOTORS	162.3	0.5	0.7	0.0
28 S-II ENGINE START COMMAND (ESC)	163.0	0.5	1.4	0.0
29 S-II ENGINE SOLENOID ACTIVATION (AVERAGE OF FIVE)	164.0	0.5	2.4	0.0
30 S-II ULLAGE MOTOR BURN TIME TERMINATION (THRUST REACHES 75%)	166.1	0.4	4.4	-0.2
31 S-II MAINSTAGE	166.2	0.7	4.6	0.2
32 S-II CHILLDOWN VALVES CLOSE	168.0	0.5	6.4	0.0
33 ACTIVATE S-II PU SYSTEM	168.5	0.5	6.9	0.0
34 S-II SECOND PLANE SEPARATION COMMAND (JETTISON S-II AFT INTERSTAGE)	192.3	0.5	30.7	0.0
35 LAUNCH ESCAPE TOWER (LET) JETTISON	197.9	0.4	36.2	-0.2
36 ITERATIVE GUIDANCE MODE (IGM) PHASE 1 INITIATED*	204.1	1.5	42.4	0.9
37 S-II LOX STEP PRESSURIZATION	261.6	0.2	100.0	0.0
38 S-II CENTER ENGINE CUTOFF (CECO)	460.6	0.5	299.0	0.0
39 S-II LH2 STEP PRESSURIZATION	461.6	0.5	300.0	0.0
40 GUIDANCE SENSED TIME TO BEGIN EMR SHIFT (IGM PHASE 2 INITIATED & START OF ARTIFICIAL TAU MODE)*	494.8	6.0	333.2	5.5
41 S-II LOW ENGINE MIXTURE RATIO (EMR) SHIFT (ACTUAL)	498.0		336.3	
42 END OF ARTIFICIAL TAU MODE *	504.2	4.9	342.5	4.3
43 S-II OUTBOARD ENGINE CUTOFF (OECO)	548.22	-3.50	386.56	-4.07
44 S-II ENGINE CUTOFF INTERRUPT, START OF TIME BASE 4 (T4) (START OF IGM PHASE 3)	548.2	-3.5	0.0	0.0

*Time is accurate to major computation cycle dependent upon length of computation cycles.

Table 2-2. Significant Event Times Summary (Continued)

EVENT DESCRIPTION	RANGE TIME		TIME FROM BASE	
	ACTUAL SEC	ACT-PRED SEC	ACTUAL SEC	ACT-PRED SEC
45 S-IVB ULLAGE MOTOR IGNITION	548.9	-3.4	0.7	0.0
46 S-II/S-IVB SEPARATION COMMAND TO FIRE SEPARATION DEVICES AND RETRO MOTORS	549.0	-3.4	0.8	0.0
47 S-IVB ENGINE START COMMAND (FIRST ESC)	549.2	-3.4	1.0	0.0
48 FUEL CHILLDOWN PUMP OFF	550.4	-3.5	2.2	0.0
49 S-IVB IGNITION (STDV OPEN)	552.2	-3.5	4.0	0.0
50 S-IVB MAINSTAGE	554.7	-3.5	6.5	0.0
51 START OF ARTIFICIAL TAU MODE*	555.6	-5.7	7.3	-2.3
52 S-IVB ULLAGE CASE JETTISON	561.0	-3.4	12.8	0.0
53 END OF ARTIFICIAL TAU MODE *	562.4	-8.9	14.2	-5.4
54 BEGIN TERMINAL GUIDANCE*	665.2	-0.3	116.9	3.0
55 END IGM PHASE 3 *	691.6	-0.2	143.4	3.3
56 BEGIN CHI FREEZE *	691.6	-0.2	143.4	3.3
57 S-IVB VELOCITY CUTOFF COMMAND (FIRST GUIDANCE CUTOFF) (FIRST ECO)	699.34	-0.15	-0.23	-0.03
58 S-IVB ENGINE CUTOFF INTERRUPT, START OF TIME BASE 5 (T5)	699.6	-0.1	0.0	0.0
59 S-IVB APS ULLAGE ENGINE NO. 1 IGNITION COMMAND	699.8	-0.2	0.3	0.0
60 S-IVB APS ULLAGE ENGINE NO. 2 IGNITION COMMAND	699.9	-0.2	0.4	0.0
61 LOX TANK PRESSURIZATION OFF	700.7	-0.2	1.2	0.0
62 PARKING ORBIT INSERTION	709.34	-0.15	9.77	-0.04
63 BEGIN MANEUVER TO LOCAL HORIZONTAL ATTITUDE *	719.3	-0.5	19.8	-0.3
64 S-IVB LH2 CONTINUOUS VENT SYSTEM (CVS) ON	758.5	-0.2	59.0	0.0
65 S-IVB APS ULLAGE ENGINE NO. 1 CUTOFF COMMAND	786.5	-0.2	87.0	0.0
66 S-IVB APS ULLAGE ENGINE NO. 2 CUTOFF COMMAND	786.6	-0.2	87.1	0.0
67 FIRST ORBITAL NAVIGATION CALCULATIONS*	801.1	0.8	101.5	0.9

*Time is accurate to major computation cycle dependent upon length of computation cycles.

Table 2-2. Significant Event Times Summary (Continued)

EVENT DESCRIPTION	RANGE TIME		TIME FROM BASE	
	ACTUAL SEC	ACT-PRED SEC	ACTUAL SEC	ACT-PRED SEC
68 BEGIN S-IVB RESTART PREPARATIONS, START OF TIME BASE 6 (T6)	9278.2	0.9	0.0	0.0
69 S-IVB O2/H2 BURNER LH2 ON	9319.5	0.9	41.3	0.0
70 S-IVB O2/H2 BURNER EXCITERS ON	9319.8	0.9	41.6	0.0
71 S-IVB O2/H2 BURNER LOX ON (HELIUM HEATER ON)	9320.2	0.9	42.0	0.0
72 S-IVB LH2 VENT OFF (CVS OFF)	9320.4	0.9	42.2	0.0
73 S-IVB LH2 REPRESSURIZATION CONTROL VALVE ON	9326.3	0.9	48.1	0.0
74 S-IVB LOX REPRESSURIZATION CONTROL VALVE ON	9326.5	0.9	48.3	0.0
75 S-IVB AUX HYDRAULIC PUMP FLIGHT MODE ON	9497.2	0.9	219.0	0.0
76 S-IVB LOX CHILLDOWN PUMP ON	9527.2	0.9	249.0	0.0
77 S-IVB LH2 CHILLDOWN PUMP ON	9532.2	0.9	254.0	0.0
78 S-IVB PREVALVES CLOSED	9537.2	0.9	259.0	0.0
79 S-IVB PU MIXTURE RATIO 4.5 ON	9728.3	0.9	450.1	0.0
80 S-IVB APS ULLAGE ENGINE NO. 1 IGNITION COMMAND	9774.5	0.9	496.3	0.0
81 S-IVB APS ULLAGE ENGINE NO. 2 IGNITION COMMAND	9774.6	0.9	496.4	0.0
82 S-IVB O2/H2 BURNER LH2 OFF (HELIUM HEATER OFF)	9775.0	0.9	496.8	0.0
83 S-IVB O2/H2 BURNER LOX OFF	9779.5	0.9	501.3	0.0
84 S-IVB LH2 CHILLDOWN PUMP OFF	9847.6	0.9	569.4	0.0
85 S-IVB LOX CHILLDOWN PUMP OFF	9847.8	0.9	569.6	0.0
86 S-IVB ENGINE RESTART COMMAND (FUEL LEAD INITIATION) (SECOND ESC)	9848.2	0.9	570.0	0.0
87 S-IVB APS ULLAGE ENGINE NO. 1 CUTOFF COMMAND	9851.2	0.9	573.0	0.0
88 S-IVB APS ULLAGE ENGINE NO. 2 CUTOFF COMMAND	9851.3	0.9	573.1	0.0
89 S-IVB SECOND IGNITION (STDV OPEN)	9856.2	0.7	578.0	-0.2

Table 2-2. Significant Event Times Summary (Continued)

EVENT DESCRIPTION	RANGE TIME		TIME FROM BASE	
	ACTUAL SEC	ACT-PRED SEC	ACTUAL SEC	ACT-PRED SEC
90 S-IVB MAINSTAGE	9858.7	0.7	580.5	-0.2
91 ENGINE MIXTURE RATIO (EMR) SHIFT	9974.4	-0.6	696.2	-1.5
92 S-IVB LH2 STEP PRESSURIZATION (SECOND BURN RELAY OFF)	10128.2	0.9	850.0	0.0
93 BEGIN TERMINAL GUIDANCE*	10174.5	-0.5	896.3	-1.4
94 BEGIN CHI FREEZE *	10201.9	0.6	923.7	-0.3
95 S-IVB SECOND GUIDANCE CUTOFF COMMAND (SECOND ECO)	10203.07	-1.0	-0.26	-0.06
96 S-IVB ENGINE CUTOFF INTERRUPT, START OF TIME BASE 7	10203.3	-1.0	0.0	0.0
97 LH2 VENT ON COMMAND	10203.8	-1.0	0.5	0.0
98 TRANSLUNAR INJECTION	10213.07	-1.0	9.74	-0.05
99 BEGIN MANEUVER TO LOCAL HORIZONTAL ATTITUDE *	10223.0	-2.8	19.7	-1.8
100 FIRST ORBITAL NAVIGATION CALCULATIONS*	10223.9	-1.9	20.6	-0.9
101 LH2 VENT OFF COMMAND	11103.1	-1.0	899.8	0.0
102 BEGIN MANEUVER TO TRANSPOSITION AND DOCKING ATTITUDE (TD&E) *	11103.9	-0.4	900.6	0.6
103 CSM SEPARATION	11723.0	18.7	1519.7	19.7
104 CSM DOCK	12243.7	109.3	2040.4	110.4
105 SC/LV FINAL SEPARATION	15423.0	418.6	5219.7	419.7
106 START OF TIME BASE 8 (T8)	17467.6	63.2	0.0	0.0
107 INITIATE MANEUVER TO SLINGSHOT ATTITUDE *	17467.6	63.3	0.0	0.0
108 S-IVB LH2 VENT ON (CVS ON)	17468.0	63.3	0.4	0.0
109 BEGIN LOX DUMP	18187.6	63.3	720.0	0.0
110 END LOX DUMP	18295.8	63.3	828.2	0.0
111 H2 NONPROPULSIVE VENT (NPV) ON	19500.6	63.1	2032.9	-0.1
112 S-IVB APS ULLAGE ENGINE NO. 1 IGNITION COMMAND	20267.6	63.3	2800.0	0.0
113 S-IVB APS ULLAGE ENGINE NO. 2 IGNITION COMMAND	20267.8	63.5	2800.2	0.0

*Time is accurate to major computation cycle dependent upon length of computation cycles.

Table 2-2. Significant Event Times Summary (Continued)

EVENT DESCRIPTION	RANGE TIME		TIME FROM BASE	
	ACTUAL SEC	ACT-PRED SEC	ACTUAL SEC	ACT-PRED SEC
114 S-IVB APS ULLAGE ENGINE NO. 1 CUTOFF COMMAND	20547.6	63.3	3080.0	0.0
115 S-IVB APS ULLAGE ENGINE NO. 2 CUTOFF COMMAND	20547.8	63.5	3080.2	0.0
116 INITIATE MANEUVER TO COMMUNICATIONS ATTITUDE	20568.8	64.5	3101.1	1.1

Table 2-3. Variable Time and Commanded Switch Selector Events

FUNCTION	STAGE	RANGE TIME (SEC)	TIME FROM BASE (SEC)	REMARKS
Water Coolant Valve Open	IU	181.0	T3 +19.4	LVDC Function
High (5.5) Engine Mixture Ratio Off	S-II	495.8	T3 +334.1	LVDC Function
Low (4.5) Engine Mixture Ratio On	S-II	496.0	T3 +334.3	LVDC Function
Water Coolant Valve Closed	IU	783.2	T5 +83.7	LVDC Function
TM Calibrate On	S-IVB	1057.7	T5 +358.1	CYI Rev 1
TM Calibrate Off	S-IVB	1058.7	T5 +359.1	CYI Rev 1
Water Coolant Valve Close	IU	3186.9	T5 +2487.4	LVDC Function
Telemetry Calibrator Inflight Calibrate On	IU	3201.3	T5 +2501.8	CRO Rev 1
TM Calibrate On	S-IVB	3201.7	T5 +2502.2	CRO Rev 1
TM Calibrate Off	S-IVB	3202.7	T5 +2503.2	CRO Rev 1
Telemetry Calibrator Inflight Calibrate Off	IU	3206.3	T5 +2506.8	CRO Rev 1
TM Calibrate Off	S-IVB	3642.6	T5 +2943.1	HSK Rev 1
Telemetry Calibrator Inflight Calibrate Off	IU	3646.2	T5 +2946.7	HSK Rev 1
Telemetry Calibrator Inflight Calibrate On	IU	5369.2	T5 +4669.7	GYM Rev 1
TM Calibrate On	S-IVB	5369.6	T5 +4670.1	GYM Rev 1
TM Calibrate Off	S-IVB	5370.6	T5 +4671.1	GYM Rev 1
Telemetry Calibrator Inflight Calibrate Off	IU	5374.2	T5 +4674.7	GYM Rev 1
Telemetry Calibrator Inflight Calibrate On	IU	7825.2	T5 +7125.7	TAN Rev 1
TM Calibrate On	S-IVB	7825.6	T5 +7126.1	TAN Rev 1
TM Calibrate Off	S-IVB	7826.6	T5 +7127.1	TAN Rev 1
Telemetry Calibrator Inflight Calibrate Off	IU	7830.2	T5 +7130.7	TAN Rev 1

Table 2-3. Variable Time and Commanded Switch Selector Events (Continued)

FUNCTION	STAGE	RANGE TIME (SEC)	TIME FROM BASE (SEC)	REMARKS
Telemetry Calibrator Inflight Calibrate On	IU	8793.3	T5 +8093.8	CRO Rev 2
TM Calibrate On	S-IVB	8793.7	T5 +8094.2	CRO Rev 2
TM Calibrate Off	S-IVB	8794.7	T5 +8095.2	CRO Rev 2
Telemetry Calibrator Inflight Calibrate Off	IU	8798.3	T5 +8098.8	CRO Rev 2
Telemetry Calibrator Inflight Calibrate On	IU	9678.4	T6 +400.2	ARIA No. 3 Rev 2
TM Calibrate On	S-IVB	9678.6	T6 +400.4	ARIA No. 3 Rev 2
TM Calibrate Off	S-IVB	9679.6	T6 +401.4	ARIA No. 3 Rev 2
Telemetry Calibrator Inflight Calibrate Off	IU	9683.4	T6 +405.2	ARIA No. 3 Rev 2
Water Coolant Valve Open	IU	13,409.5	T7 +3206.1	LVDC Function
Water Coolant Valve Close	IU	13,803.7	T7 +3507.1	LVDC Function
Water Coolant Valve Open	IU	17,319.4	T7 +7116.0	LVDC Function
Passivation Enable	S-IVB	18,503.5	T8 +1035.8	CCS Command
Engine He Control Valve Open On	S-IVB	18,505.0	T8 +1037.3	CCS Command
TM Calibrate On	IU	27,371.9	T8 +9904.0	} Acquisition by GYM during TLC
TM Calibrate Off	IU	27,372.0	T8 +9904.1	
Antenna switching times are not available due to noisy telemetry.				

SECTION 3

LAUNCH OPERATIONS

3.1 SUMMARY

The ground systems supporting the AS-506/Apollo 11 countdown and launch performed exceptionally well. Several systems experienced component failures and malfunctions which required corrective actions, but all repairs were accomplished in parallel with the scheduled countdown operations. No unscheduled holds were incurred. Propellant tanking was accomplished satisfactorily. The start of S-II LH_2 loading was delayed 25 minutes due to a communications problem in the Pad Terminal Connection Room (PTCR). However, this delay time was recovered during the scheduled hold at -3 hours 30 minutes. Launch occurred at 09:32:00 Eastern Daylight Time (EDT), July 16, 1969, from Pad 39A of the Saturn Complex. Damage to the pad, Launch Umbilical Tower (LUT) and support equipment was minor.

3.2 PRELAUNCH MILESTONES

A chronological summary of events and preparations leading to the launch of AS-506 is contained in Table 3-1.

3.3 COUNTDOWN EVENTS

The AS-506/Apollo 11 terminal countdown was picked up at -28 hours on July 14, 1969 at 17:00:00 EDT. Scheduled holds of 11 hours duration at -9 hours in the count, and 1 hour 32 minutes duration at -3 hours 30 minutes, were the only holds initiated. The start of S-II LH_2 loading was delayed 25 minutes due to a communications problem in the PTCR. However, this time was recovered during the hold at -3 hours 30 minutes and Space Vehicle (SV) activities were on schedule when the countdown resumed. Launch occurred at 09:32:00 EDT, July 16, 1969, from Pad 39A of the Saturn Complex.

3.4 PROPELLANT LOADING

3.4.1 RP-1 Loading

The RP-1 system supported the launch countdown satisfactorily. At approximately -21 hours the Propellant Tanking Control System (PTCS) RP-1 level indication from the propellant monitor program display became erratic. The problem was traced to a noisy RP-1 loading electronics unit. Since

Table 3-1. AS-506 Prelaunch Milestones

DATE	ACTIVITY OR EVENT
January 8, 1969	LM-5 Ascent Stage Arrival
January 10, 1969	SLA-14 Arrival
January 12, 1969	LM-5 Descent Stage Arrival
January 15, 1969	CSM Quads Arrival
January 19, 1969	S-IVB-6N Stage Arrival
January 22, 1969	CSM 107 Arrival
February 6, 1969	S-II-6 Stage Arrival
February 20, 1969	S-IC-6 Stage Arrival
February 21, 1969	S-IC Erection
February 27, 1969	IU-6 Arrival
March 4, 1969	S-II Erection
March 5, 1969	S-IVB and IU Erections
March 18, 1969	CSM Altitude Test with Prime Crew
March 21, 1969	LM Altitude Test with Prime Crew
March 27, 1969	Launch Vehicle (LV) Propellant Dispersion/ Malfunction Overall Test (OAT)
April 14, 1969	Spacecraft (SC) Erection
May 5, 1969	Space Vehicle (SV) Electrical Mate
May 14, 1969	SV OAT No. 1 (Plugs In)
May 20, 1969	SV Transfer to Complex 39, Pad A
May 22, 1969	MSS Transfer to Pad A
June 6, 1969	SV Flight Readiness Test (FRT) Completed
June 25, 1969	RP-1 Loading Completed
July 2, 1969	CDDT (Wet) Completed
July 3, 1969	CDDT (Dry) Completed
July 10, 1969	SV Launch Countdown Started
July 16, 1969	SV Launch on Schedule

the RP-1 level display was not a critical measurement, the disposition of the electronics unit was "use as is". However, the level indication was stable during the final 8 hours of countdown.

The RP-1 system vent trap closed prematurely during replenish operations at -13 hours, causing entrapped air to be pumped through the S-IC fuel tank. There were no serious consequences. The air, which is filtered to about 50 microns, was immediately vented from the stage. All subsequent system functions were normal, and replenishment was completed satisfactorily.

3.4.2 LOX Loading

The LOX system successfully supported the launch countdown. A premature closure of the S-II stage LOX tank vents during slow fill to 99 percent flight mass caused the LOX loading system to revert at about -6 hours 43 minutes. Recovery procedures were initiated, and flow was reestablished at about -6 hours 35 minutes. Launch vehicle loading and replenish operations were completed without further incident. A procedure change will be made to prevent cycling of the tank vents prior to reaching the 99 percent value during future cryogenic loadings.

3.4.3 LH_2 Loading

The LH_2 system supported the launch countdown satisfactorily. A communications problem in the Radio Frequency-Operational Intercom System (RF-OIS) caused a delay in the start of S-II LH_2 loading of 25 minutes. The RF-OIS/Pad A fault summary light illuminated at the Launch Control Center (LCC) during LOX loading. This condition could indicate, as a worse case, that pad OIS had switched to batteries or less critical, that an OIS amplifier had switched to secondary. Upon pad entry, an amplifier was found to have automatically switched to secondary; it was reset manually in the PTCR and the fault summary light in the LCC went off.

During LH_2 replenish operations at about -3 hours 20 minutes, a leak developed in the S-IVB stage replenish valve located on LUT level 200. The LH_2 system was drained and purged, and the valve bonnet and packing gland bolts were retorqued. No further leakage was detected when LH_2 loading operations were resumed at about -2 hours. However, to prevent problem recurrence that could cause countdown delay, the replenish valve was closed and subsequent S-IVB replenishment accomplished manually using the main fill valve in the reduced position.

About 7 minutes after liftoff, during automatic line drain and purge operations, the S-IC liftoff indication was lost causing an LH_2 system revert. Drain and purge operations were completed manually using the S-II/S-IVB fill line purge valve. Although this is not the normal manual configuration, a satisfactory purge was obtained. A change in the propellant system logic is presently being considered which will isolate the system from external influence once the liftoff signal is received.

3.4.4 Auxiliary Propulsion System Propellant Loading

Propellant loading of the S-IVB Auxiliary Propulsion System (APS) was accomplished satisfactorily. Total propellant mass in both modules at liftoff was 184.3 kilograms (406 lbm) of Nitrogen Tetroxide (N_2O_4) and 114.4 kilograms (252 lbm) of Monomethyl Hydrazine (MMH).

3.5 S-II INSULATION, PURGE AND LEAK DETECTION

The performance of the S-II stage insulation was highly satisfactory. Detailed inspection of all external insulation was conducted by operational television during the countdown and no significant leakage was detected. The total heat leakage through the insulation to the LH_2 was within specification limits. Satisfactory pressures and flows were maintained in all purge circuits during countdown. The leak detection system performed satisfactorily throughout the final countdown and contaminant gas concentrations remained within acceptable limits at all times. There were no problems during countdown with the leak detecting selector solenoid valve which presented a minor problem during Countdown Demonstration Test (CDDT).

3.6 GROUND SUPPORT EQUIPMENT (GSE)

3.6.1 Ground/Vehicle Interface

Detailed discussion of the GSE will be contained in the Kennedy Space Center Apollo/Saturn V (AS-506) Ground Systems Evaluation Reports. The performance of all ground systems was highly satisfactory. Overall damage to the pad, LUT and support equipment from the blast and flame impingement was minor. The Holddown Arms (HDA), Tail Service Masts (TSM) and Service Arms (SA) performed within design limits during the launch sequence.

The HDA's were released pneumatically at 0.3 second. HDA No. 1 protective hood did not close and the adjustable head and upper link received some blast damage. However, damage to the interior of HDA No. 1 was not greater than to any other arm. Warpage of the HDA protective hoods was negligible. As on AS-504 launch, the secondary Service Arm Control Switch (SACS) actuator arm on HDA No. 2 was broken off.

TSM retractions were normal and all protective hoods closed properly. The RP-1 mast cutoff valve in TSM 1-2 opened at liftoff, indicating a loss of valve GN_2 control pressure. The cause of pressure loss is being investigated.

SA systems total retract times to safe angle were within specifications. Damage to SA systems was slight. Control console door latches were bent or broken on all SA levels of the LUT; however, provisions incorporated for AS-506 restrained the doors and prevented their blowing open as had

occurred on previous launches. Hydraulic oil leakage from SA No. 2 upper and lower hinge areas was detected during postlaunch inspection and was observed to have leaked into SA No. 1. Investigation will be conducted to determine the source.

None of the ground/vehicle related problems experienced during launch preparations had sufficient impact such as to constrain the countdown operations. All system repairs and remedial actions were accomplished in parallel with countdown operations. At -13 hours 30 minutes, about 07:31:00 EDT on July 15, 1969, it was discovered that the LCC Data Transmission System (DTS) would not synchronize with the DTS transmitter at Pad A. Further investigation revealed severe attenuation of transmitted data. The basic problem was traced to a discrepant patch in the wideband video distributor. Satisfactory operation was restored at about 19:00:00 EDT of the same day.

3.6.2 MSFC Furnished Ground Support Equipment

Performance of the mechanical and electrical equipment supporting the launch operations was satisfactory. Blast damage to the equipment was considered normal. Minor GSE deviations encountered were as follows:

a. SA No. 1 (S-IC Intertank) umbilical carrier withdrawal time was approximately 0.06 second greater than the specification maximum of 5 seconds. Withdrawal time for this carrier under non-cryogenic conditions, based on the average of results obtained during system revalidation testing, is approximately 3 seconds. Total SA No. 1 retract time to safe angle was 9.9 seconds, which is within the specification limit of 10.5 seconds and was about 3.9 seconds before SA No. 2 retract command. (Failure to achieve SA No. 1 safe angle prior to time for SA No. 2 retract at -16.2 seconds would cause cutoff.) Cause of the slow withdrawal has not yet been determined. Slower than specification withdrawal times were also experienced during the AS-503 and AS-505 launch countdowns. The withdrawal time for the AS-504 launch, although within specification limits, was slower than the average obtained during validation testing under non-cryogenic conditions. Investigation is continuing.

b. The GH_2 dome regulator in the S-II stage pneumatic servicing console indicated erratic leakage during the -9 hour countdown hold and was replaced with a spare regulator. The new regulator was not adjusted to the high side tolerance of the 810 $\pm$10.3 N/cm^2 (1175 $\pm$15 psia) setting, as planned. During S-II start tank pressurization, the low regulator setting resulted in the start tank pressures being lower than the desired prelaunch values. At the prelaunch commit point (-33 seconds), S-II Engine No. 1 start tank pressure was 2.8 N/cm^2 (4 psi) below the redline requirement. The countdown was continued since the Central Instrumentation Facility (CIF) observer verified that the measurement was not below redline at -45 seconds.

The regulator pressures will be set to 827 ±10.3 N/cm^2 (1200 ±15 psia) for subsequent vehicles and this will alleviate the prelaunch low pressure conditions.

c. The S-II LH_2 heat exchanger delta pressure controller mode of control did not operate properly and the point sensor mode of control was initiated after the beginning of start tank chilldown. This mode of operation was utilized throughout the remaining portion of the countdown. Also, the heat exchanger would not refill properly during the start tank and thrust chamber chilldown sequences. However, the liquid level was sufficient to perform the required stage systems chilldown. The deviation will be investigated.

3.6.3 Camera Coverage

A total of 201 cameras were installed for the AS-506 launch of which 119 were committed to engineering data, and 82 to documentary coverage. Three cameras failed to acquire data. Upon review of film coverage of the GSE at launch, the following conditions were observed:

a. S-II stage forward SA umbilical covers did not secure upon SA withdrawal from the vehicle.

b. HDA No. 1 protective hood failed to close and the other three HDA hoods appeared to close late.

SECTION 4

TRAJECTORY

4.1 SUMMARY

The trajectory parameters from launch to Translunar Injection (TLI) were close to nominal. The vehicle was launched on an azimuth 90 degrees east of north. A roll maneuver was initiated at 13.2 seconds that placed the vehicle on a flight azimuth of 72.058 degrees east of north.

The space-fixed velocity at S-IC Outboard Engine Cutoff (OECO) was 8.5 m/s (27.9 ft/s) greater than nominal. The space-fixed velocity at S-II Outboard Engine Cutoff was 22.8 m/s (74.8 ft/s) less than nominal. The space-fixed velocity at S-IVB first guidance cutoff was 0.2 m/s (0.6 ft/s) less than nominal. The altitude at S-IVB first guidance cutoff was 0.2 kilometer (0.1 n mi) lower than nominal and the surface range was 1.7 kilometers (1.0 n mi) less than nominal.

The space-fixed velocity at parking orbit insertion was equal to nominal and the flight path angle was 0.013 degree greater than nominal. The eccentricity was 0.00001 less than nominal. The apogee and perigee were 0.5 kilometer (0.3 n mi) and 0.6 kilometer (0.3 n mi) less than nominal, respectively.

The parameters at translunar injection were also close to nominal. The eccentricity was 0.00029 greater than nominal, the inclination was 0.004 degree greater than nominal, the node was 0.019 degree lower than nominal, and C_3 was 16,877 m^2/s^2 (181,663 $ft^2/s2$) greater than nominal. The space-fixed velocity was 3.2 m/s (10.5 ft/s) greater than nominal and the altitude was 3.1 kilometers (1.6 n mi) less than nominal.

Following Lunar Module (LM) extraction, the vehicle maneuvered to a slingshot attitude frozen relative to local horizontal. The retrograde velocity to achieve S-IVB/IU lunar slingshot was accomplished by a LOX dump, Auxiliary Propulsion System (APS) burn, and LH_2 vent. The S-IVB/IU closest approach of 3379 kilometers (1825 n mi) above the lunar surface occurred at 78.7 hours into the mission.

The actual impact locations for the spent S-IC and S-II stages were determined by a theoretical free-flight simulation. The surface range for the S-IC impact point was 0.2 kilometer (0.1 n mi) greater than nominal. The surface range for the S-II impact point was 91.7 kilometers (49.5 n mi) less than nominal.

The event times reported in this section reflect the event as seen at the vehicle in order to enable direct comparison with times in the Guidance and Navigation section.

4.2 TRACKING DATA UTILIZATION

4.2.1 Tracking During the Ascent Phase of Flight

Tracking data were obtained during the period from the time of first motion through parking orbit insertion.

The best estimate trajectory was established by using telemetered guidance velocities as generating parameters to fit data from five different C-Band tracking stations. Approximately 30 percent of the various tracking data was eliminated due to inconsistencies. A comparison of the reconstructed ascent trajectory with the remaining tracking data yielded good agreement. The launch phase portion of the trajectory (liftoff to approximately 20 seconds) was established by constraining integrated telemetered guidance accelerometer data to the early phase of the best estimate trajectory.

4.2.2 Tracking During the Parking Orbit Phase of Flight

Orbital tracking was conducted by the NASA Manned Space Flight Network (MSFN). Eight C-Band radar stations furnished data for use in determining the parking orbit trajectory. There were also considerable S-Band tracking data available which were not used due to the abundance of C-Band radar data.

The parking orbit trajectory was obtained by integrating corrected insertion conditions forward to the S-IVB second burn restart preparation event. The insertion conditions, as determined by the Orbital Correction Program (OCP), were obtained by a differential correction procedure which adjusted the estimated insertion conditions to fit the C-Band radar tracking data in accordance with the weights assigned to the data. After all available C-Band radar tracking data were analyzed, the stations and passes providing the better quality data were used in the determination of the insertion conditions.

4.2.3 Tracking During the Injection Phase of Flight

C-Band radar data were obtained from the ship Redstone during the early portion of the injection phase of flight. These tracking data were found to be invalid and were not used in the trajectory determination.

The injection trajectory was established by integrating the telemetered guidance velocity data forward from the restart vector at 9715 seconds (obtained from the parking orbit trajectory) and constraining the end point to the TLI vector at 10,213.03 seconds (obtained from the post TLI trajectory).

4.2.4 Tracking During the Post Injection Phase of Flight

Tracking data from seven C-Band radar stations furnished data for use in determining the post TLI trajectory. The available S-Band tracking data were not used due to the availability of the C-Band radar data.

The post TLI trajectory was obtained by integrating corrected injection conditions forward to S-IVB/Command and Service Module (CSM) separation. The corrected injection conditions were determined by the same method outlined in paragraph 4.2.2.

4.3 TRAJECTORY EVALUATION

4.3.1 Ascent Trajectory

The vehicle was launched on an azimuth 90 degrees east of north. A roll maneuver was initiated at 13.2 seconds that placed the vehicle on a flight azimuth of 72.058 degrees east of north.

Actual and nominal altitude, surface range, and cross range for the ascent phase are presented in Figure 4-1. Actual and nominal space-fixed velocity and flight path angle during ascent are shown in Figure 4-2.

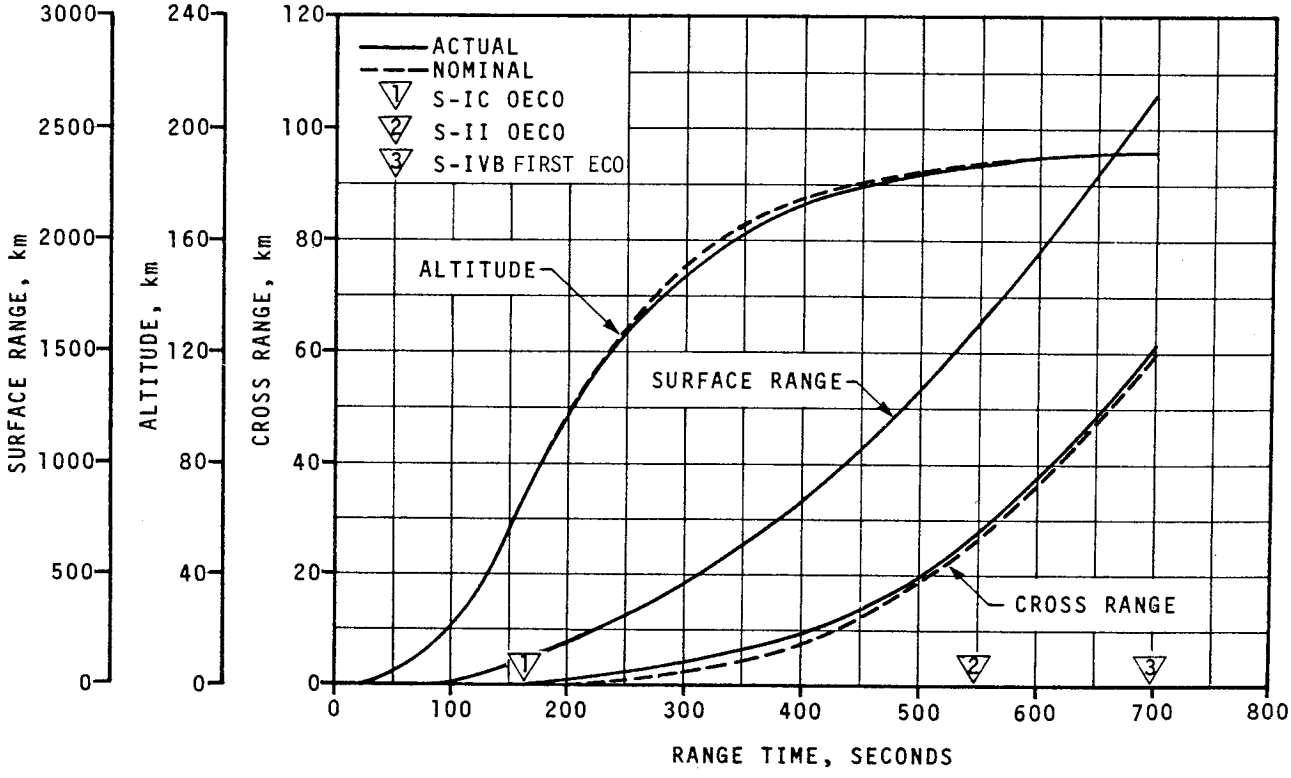

Figure 4-1. Ascent Trajectory Position Comparison

Comparisons of total inertial accelerations are shown in Figure 4-3. The maximum acceleration during S-IC burn was 3.94 g.

Mach number and dynamic pressure are shown in Figure 4-4. These parameters were calculated using meteorological data measured to an altitude of 56.0 kilometers (30.2 n mi). Above this altitude the measured data were merged into the U.S. Standard Reference Atmosphere.

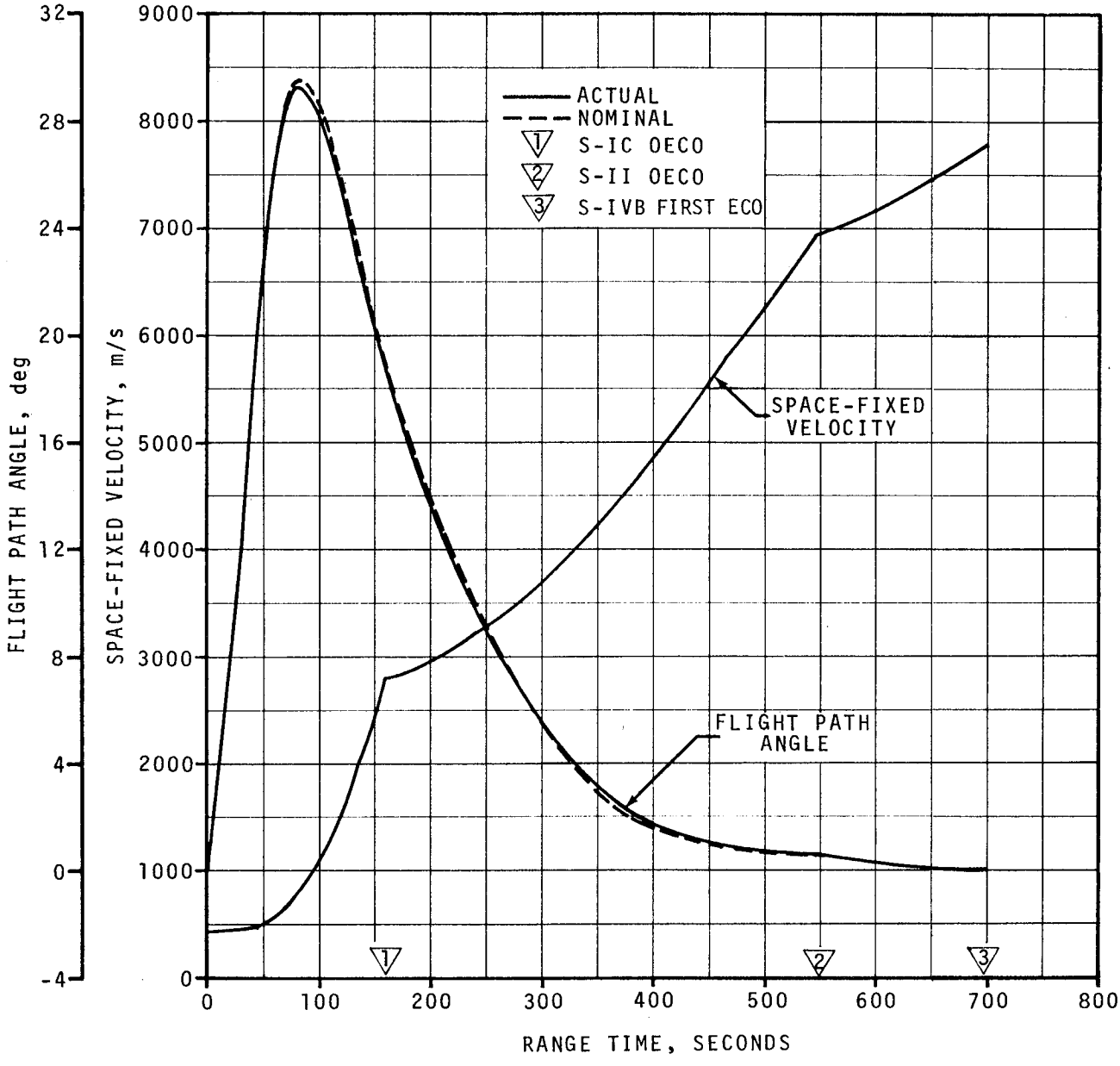

Figure 4-2. Ascent Trajectory Space-Fixed Velocity and Flight Path Angle Comparisons

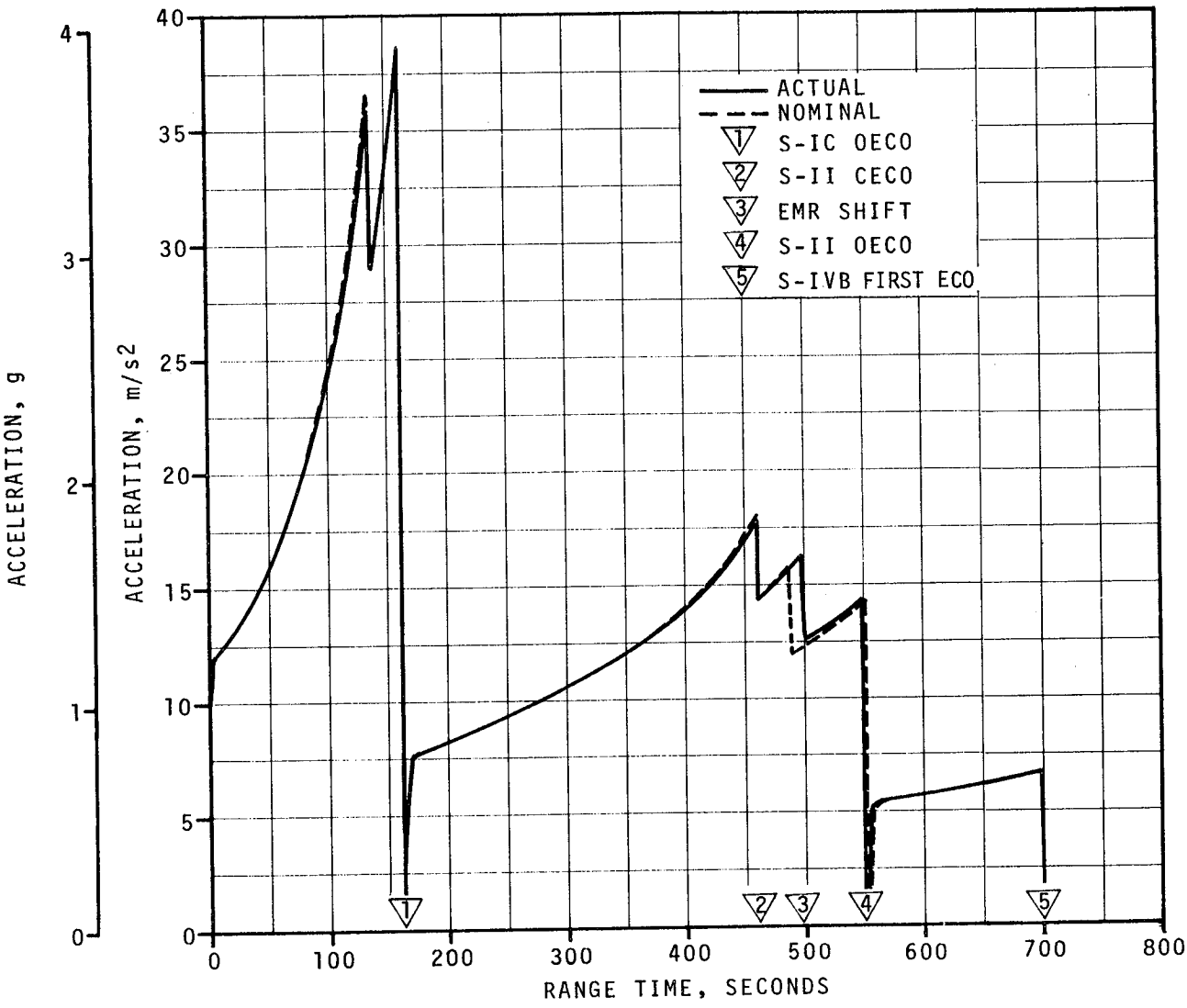

Figure 4-3. Ascent Trajectory Acceleration Comparison

Actual and nominal values of parameters at significant trajectory event times, cutoff events, and separation events are shown in Tables 4-1, 4-2, and 4-3, respectively.

The free-flight trajectories of the spent S-IC and S-II stages were simulated using initial conditions from the final postflight trajectory. The simulation was based upon the separation impulses for both stages and nominal tumbling drag coefficients. No tracking data were available for verification. Table 4-1 presents a comparison of free-flight parameters to nominal at apex for the S-IC and S-II stages. Table 4-4 presents a comparison of free-flight parameters to nominal at impact for the S-IC and S-II stages.

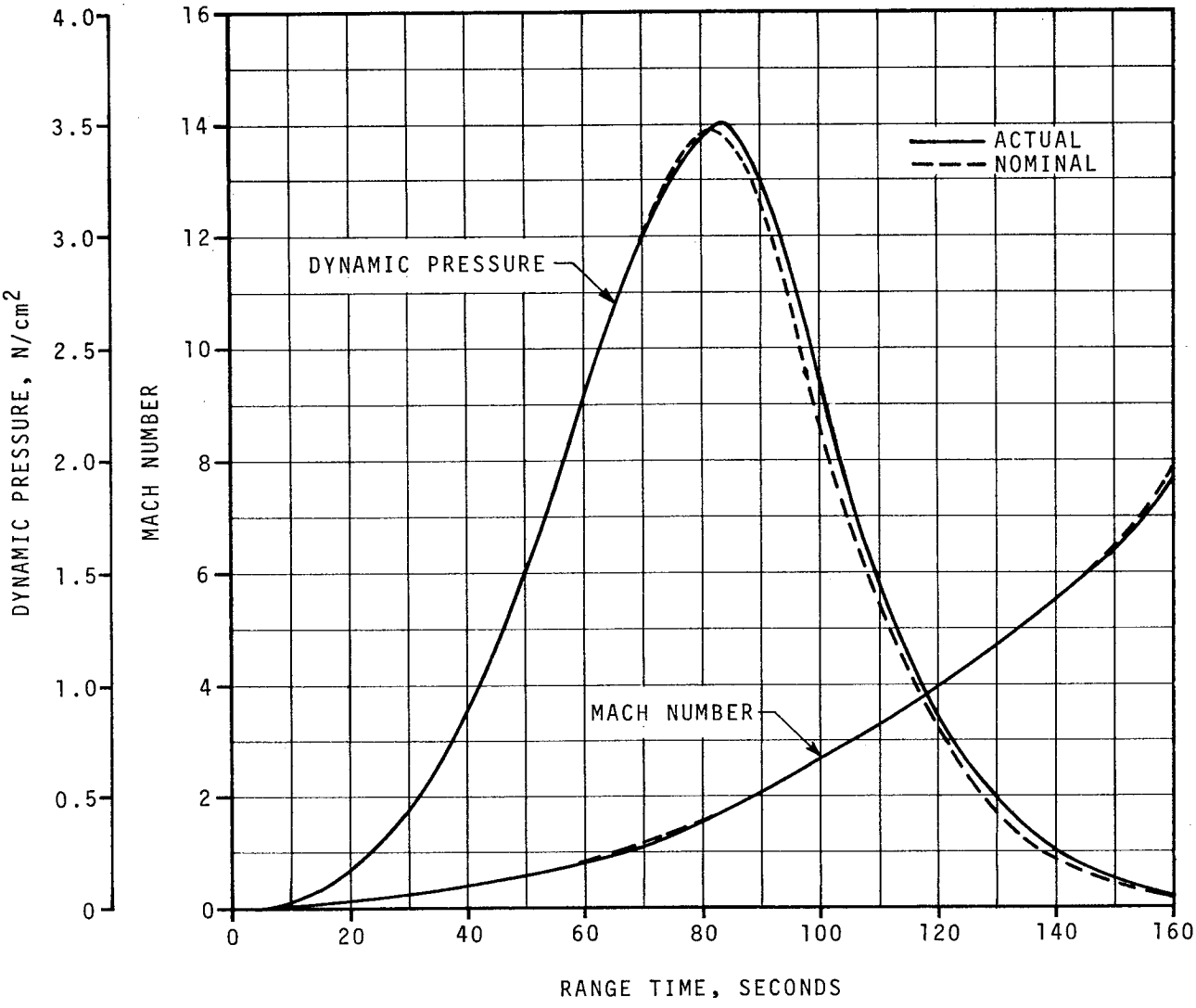

Figure 4-4. Dynamic Pressure and Mach Number Comparisons

4.3.2 Parking Orbit Trajectory

A family of values for the insertion parameters was obtained depending upon the combination of data used and the weights applied to the data. The solutions that were considered reasonable had a spread of about ±250 meters (±820 ft) in position components and ±0.7 m/s (±2.3 ft/s) in velocity components. The actual and nominal parking orbit insertion parameters are presented in Table 4-5. The ground track from insertion to S-IVB/CSM separation is given in Figure 4-5.

4.3.3 Injection Trajectory

Comparisons between the actual and nominal space-fixed velocity and flight path angle are shown in Figure 4-6. The actual and nominal total inertial acceleration comparisons are presented in Figure 4-7. Throughout the S-IVB second burn phase of flight, the space-fixed velocity and the flight

Table 4-1. Comparison of Significant Trajectory Events

EVENT	PARAMETER	ACTUAL	NOMINAL	ACT-NOM
First Motion	Range Time, sec	0.3	0.3	0.0
	Total Inertial Acceleration, m/s^2	10.47	10.61	-0.14
	(ft/s^2)	(34.35)	(34.81)	(-0.46)
	(g)	(1.07)	(1.08)	(-0.01)
Mach 1	Range Time, sec	66.3	65.6	0.7
	Altitude, km	7.8	7.6	0.2
	(n mi)	(4.2)	(4.1)	(0.1)
Maximum Dynamic Pressure	Range Time, sec	83.0	81.3	1.7
	Dynamic Pressure, N/cm^2	3.52	3.47	0.05
	(lbf/ft^2)	(735.2)	(724.7)	(10.5)
	Altitude, km	13.6	12.9	0.7
	(n mi)	(7.3)	(7.0)	(0.3)
Maximum Total Inertial Acceleration: S-IC	Range Time, sec	161.7	160.3	1.4
	Acceleration, m/s^2	38.61	38.13	0.48
	(ft/s^2)	(126.67)	(125.10)	(1.57)
	(g)	(3.94)	(3.89)	(0.05)
S-II	Range Time, sec	460.70	460.26	0.44
	Acceleration, m/s^2	17.84	17.99	-0.15
	(ft/s^2)	(58.53)	(59.02)	(-0.49)
	(g)	(1.82)	(1.83)	(-0.01)
S-IVB 1st Burn	Range Time, sec	699.41	699.57	-0.16
	Acceleration, m/s^2	6.73	6.66	0.07
	(ft/s^2)	(22.08)	(21.85)	(0.23)
	(g)	(0.69)	(0.68)	(0.01)
S-IVB 2nd Burn	Range Time, sec	10,203.11	10,204.14	-1.03
	Acceleration, m/s^2	14.23	14.17	0.06
	(ft/s^2)	(46.69)	(46.49)	(0.20)
	(g)	(1.45)	(1.44)	(0.01)
Maximum Earth-Fixed Velocity: S-IC	Range Time, sec	162.3	161.6	0.7
	Velocity, m/s	2,402.7	2,397.0	5.7
	(ft/s)	(7,882.9)	(7,864.2)	(18.7)
S-II	Range Time, sec	549.00	552.52	-3.52
	Velocity, m/s	6,515.7	6,538.8	-23.1
	(ft/s)	(21,377.0)	(21,452.8)	(-75.8)
S-IVB 1st Burn	Range Time, sec	709.33	709.49	-0.16
	Velocity, m/s	7,389.5	7,389.6	-0.1
	(ft/s)	(24,243.8)	(24,244.1)	(-0.3)
S-IVB 2nd Burn	Range Time, sec	10,203.50	10,204.46	-0.96
	Velocity, m/s	10,433.2	10,430.2	3.0
	(ft/s)	(34,229.7)	(34,219.8)	(9.9)
Apex: S-IC Stage	Range Time, sec	269.1	270.4	-1.3
	Altitude, km	115.0	117.3	-2.3
	(n mi)	(62.1)	(63.3)	(-1.2)
	Surface Range, km	327.4	326.9	0.5
	(n mi)	(176.8)	(176.5)	(0.3)
S-II Stage	Range Time, sec	587.0	593.7	-6.7
	Altitude, km	188.8	189.7	-0.9
	(n mi)	(101.9)	(102.4)	(-0.5)
	Surface Range, km	1,862.9	1,906.6	-43.7
	(n mi)	(1,005.9)	(1,029.5)	(-23.6)

Table 4-2. Comparison of Cutoff Events

PARAMETER	ACTUAL	NOMINAL	ACT-NOM	ACTUAL	NOMINAL	ACT-NOM
	S-IC CECO (ENGINE SOLENOID)			S-IC OECO (ENGINE SOLENOID)		
Range Time, sec	135.2	135.3	-0.1	161.6	161.1	0.5
Altitude, km (n mi)	44.0 (23.8)	44.6 (24.1)	-0.6 (-0.3)	66.1 (35.7)	66.7 (36.0)	-0.6 (-0.3)
Surface Range, km (n mi)	46.4 (25.1)	46.3 (25.0)	0.1 (0.1)	93.6 (50.5)	92.2 (49.8)	1.4 (0.7)
Space-Fixed Velocity, m/s (ft/s)	1,979.0 (6,492.8)	1,989.8 (6,528.2)	-10.8 (-35.4)	2,764.1 (9,068.6)	2,755.6 (9,040.7)	8.5 (27.9)
Flight Path Angle, deg	22.957	23.406	-0.449	19.114	19.635	-0.521
Heading Angle, deg	76.315	76.132	0.183	75.439	75.269	0.170
Cross Range, km (n mi)	0.2 (0.1)	0.0 (0.0)	0.2 (0.1)	0.5 (0.3)	0.0 (0.0)	0.5 (0.3)
Cross Range Velocity, m/s (ft/s)	5.4 (17.7)	-0.2 (-0.7)	5.6 (18.4)	12.6 (41.3)	4.3 (14.1)	8.3 (27.2)
	S-II CECO (ENGINE SOLENOID)			S-II OECO (ENGINE SOLENOID)		
Range Time, sec	460.6	460.1	0.5	548.2	551.7	-3.5
Altitude, km (n mi)	180.2 (97.3)	181.1 (97.8)	-0.9 (-0.5)	187.3 (101.1)	188.0 (101.5)	-0.7 (-0.4)
Surface Range, km (n mi)	1,114.3 (601.7)	1,112.5 (600.7)	1.8 (1.0)	1,617.0 (873.1)	1,640.8 (886.0)	-23.8 (-12.9)
Space-Fixed Velocity, m/s (ft/s)	5,707.5 (18,725.4)	5,724.0 (18,779.5)	-16.5 (-54.1)	6,916.1 (22,690.6)	6,938.9 (22,765.4)	-22.8 (-74.8)
Flight Path Angle, deg	0.897	0.772	0.125	0.608	0.661	-0.053
Heading Angle, deg	79.646	79.658	-0.012	82.389	82.529	-0.140
Cross Range, km (n mi)	15.0 (8.1)	13.6 (7.3)	1.4 (0.8)	27.4 (14.8)	26.8 (14.5)	0.6 (0.3)
Cross Range Velocity, m/s (ft/s)	111.9 (367.1)	114.5 (375.7)	-2.6 (-8.6)	174.1 (571.2)	176.9 (580.4)	-2.8 (-9.2)
	S-IVB 1ST GUIDANCE CUTOFF SIGNAL			S-IVB 2ND GUIDANCE CUTOFF SIGNAL		
Range Time, sec	699.3	699.5	-0.2	10,203.0	10,204.1	-1.1
Altitude, km (n mi)	191.1 (103.2)	191.3 (103.3)	-0.2 (-0.1)	320.9 (173.3)	323.8 (174.8)	-2.9 (-1.5)
Surface Range, km (n mi)	2,634.0 (1,422.2)	2,635.7 (1,423.2)	-1.7 (-1.0)			
Space-Fixed Velocity, m/s (ft/s)	7,791.2 (25,561.7)	7,791.4 (25,562.3)	-0.2 (-0.6)	10,841.0 (35,567.6)	10,838.7 (35,560.0)	2.3 (7.6)
Flight Path Angle, deg	0.015	-0.002	0.017	6.913	6.959	-0.046
Heading Angle, deg	88.416	88.419	-0.003	59.934	59.945	-0.011
Cross Range, km (n mi)	60.9 (32.9)	59.8 (32.3)	1.1 (0.6)			
Cross Range Velocity, m/s (ft/s)	274.3 (899.9)	273.3 (896.7)	1.0 (3.2)			
Eccentricity				0.97537	0.97542	-0.00005
C_3*, m^2/s^2 (ft^2/s^2)				-1,487,528 (-16,011,618)	-1,484,138 (-15,975,128)	-3,390 (-36,490)
Inclination, deg				31.386	31.381	0.005
Descending Node, deg				121.850	121.867	-0.017

* C_3 is twice the specific energy of orbit

$$C_3 = V^2 - \frac{2\mu}{R}$$

where V = Inertial Velocity
μ = Gravitational Constant
R = Radius vector from center of earth

Table 4-3. Comparison of Separation Events

PARAMETER	ACTUAL	NOMINAL	ACT-NOM
	S-IC/S-II SEPARATION		
Range Time, sec	162.3	161.8	0.5
Altitude, km (n mi)	66.7 (36.0)	67.4 (36.4)	-0.7 (-0.4)
Surface Range, km (n mi)	95.1 (51.3)	93.7 (50.6)	1.4 (0.7)
Space-Fixed Velocity, m/s (ft/s)	2,773.9 (9,100.7)	2,765.4 (9,072.8)	8.5 (27.9)
Flight Path Angle, deg	19.020	19.533	-0.513
Heading Angle, deg	75.436	75.266	0.170
Cross Range, km (n mi)	0.5 (0.3)	0.0 (0.0)	0.5 (0.3)
Cross Range Velocity, m/s (ft/s)	12.8 (42.0)	4.4 (14.4)	8.4 (27.6)
Geodetic Latitude, deg N	28.865	28.865	0.000
Longitude, deg E	-79.676	-79.691	0.015
	S-II/S-IVB SEPARATION		
Range Time, sec	549.0	552.4	-3.4
Altitude, km (n mi)	187.4 (101.2)	188.1 (101.6)	-0.7 (-0.4)
Surface Range, km (n mi)	1,623.4 (876.6)	1,645.9 (888.7)	-22.5 (-12.1)
Space-Fixed Velocity, m/s (ft/s)	6,918.8 (22,699.5)	6,941.9 (22,775.3)	-23.1 (-75.8)
Flight Path Angle, deg	0.611	0.653	-0.042
Heading Angle, deg	82.426	82.610	-0.184
Cross Range, km (n mi)	27.5 (14.8)	27.0 (14.6)	0.5 (0.2)
Cross Range Velocity, m/s (ft/s)	174.7 (573.2)	177.3 (581.7)	-2.6 (-8.5)
Geodetic Latitude, deg N	31.883	31.921	-0.038
Longitude, deg E	-64.147	-63.913	-0.234
	S-IVB/CSM SEPARATION		
Range Time, sec	11,723	11,704	19
Altitude, km (n mi)	7,065.7 (3,815.2)	6,963.2 (3,759.8)	102.5 (55.4)
Space-Fixed Velocity, m/s (ft/s)	7,608.6 (24,962.6)	7,637.6 (25,057.7)	-29.0 (-95.1)
Flight Path Angle, deg	45.148	44.922	0.226
Heading Angle, deg	93.758	93.449	0.309
Geodetic Latitude, deg N	31.246	31.275	-0.029
Longitude, deg E	-90.622	-91.105	0.483

Table 4-4. Stage Impact Location

PARAMETER	ACTUAL	NOMINAL	ACT-NOM
S-IC STAGE IMPACT			
Range Time, sec	543.7	546.1	-2.4
Surface Range, km (n mi)	661.4 (357.1)	661.2 (357.0)	0.2 (0.1)
Cross Range, km (n mi)	8.8 (4.8)	6.3 (3.4)	2.5 (1.4)
Geodetic Latitude, deg N	30.212	30.232	-0.020
Longitude, deg E	-74.038	-74.047	0.009
S-II STAGE IMPACT			
Range Time, sec	1,213.7	1,226.8	-13.1
Surface Range, km (n mi)	4392.5 (2371.8)	4484.2 (2421.3)	-91.7 (-49.5)
Cross Range, km (n mi)	143.0 (77.2)	147.0 (79.4)	-4.0 (-2.2)
Geodetic Latitude, deg N	31.535	31.403	0.132
Longitude, deg E	-34.844	-33.892	-0.952

path angle were close to nominal with deviations more noticeable towards the end of the time period.

The trajectory and targeting parameters at S-IVB second guidance cutoff and TLI are presented in Tables 4-2 and 4-6, respectively.

4.3.4 Post TLI Trajectory

A family of values for the injection parameters was obtained depending on the combination of data used and the weights applied to the data. The solutions that were considered reasonable had a spread of about ±500 meters (±1640 ft) in position components and ±1.0 m/s (±3.3 ft/s) in velocity components. A comparison of the actual and nominal S-IVB/CSM separation conditions is presented in Table 4-3.

Table 4-5. Parking Orbit Insertion Conditions

PARAMETER	ACTUAL	NOMINAL	ACT-NOM
Range Time, sec	709.3	709.5	-0.2
Altitude, km (n mi)	191.1 (103.2)	191.3 (103.3)	-0.2 (-0.1)
Space-Fixed Velocity, m/s (ft/s)	7793.1 (25,567.9)	7793.1 (25,567.9)	0.0 (0.0)
Flight Path Angle, deg	0.012	-0.001	0.013
Heading Angle, deg	88.848	88.854	-0.006
Inclination, deg	32.521	32.531	-0.010
Descending Node, deg	123.088	123.100	-0.012
Eccentricity	0.00021	0.00022	-0.00001
Apogee*, km (n mi)	186.0 (100.4)	186.5 (100.7)	-0.5 (-0.3)
Perigee*, km (n mi)	183.2 (98.9)	183.8 (99.2)	-0.6 (-0.3)
Period, min	88.18	88.20	-0.02
Geodetic Latitude, deg N	32.672	32.683	-0.011
Longitude, deg E	-52.694	-52.671	-0.023

* Based on a spherical earth of radius 6378.165 km (3443.934 n mi).

4.3.5 S-IVB/IU Post Separation Trajectory

After final LM separation, the S-IVB/IU was placed on a lunar slingshot trajectory. This trajectory was accomplished by slowing down the S-IVB/IU to make it pass by the trailing edge of the moon and obtain sufficient energy to continue to a solar orbit. This was accomplished by a combination of 108-second LOX dump, 280-second APS burn, and LH_2 vent. A time history of the velocity increase along the vehicle longitudinal axis for the slingshot maneuver is presented in Figure 4-8. Table 4-7 presents a comparison of the actual and nominal velocity increase due to the various

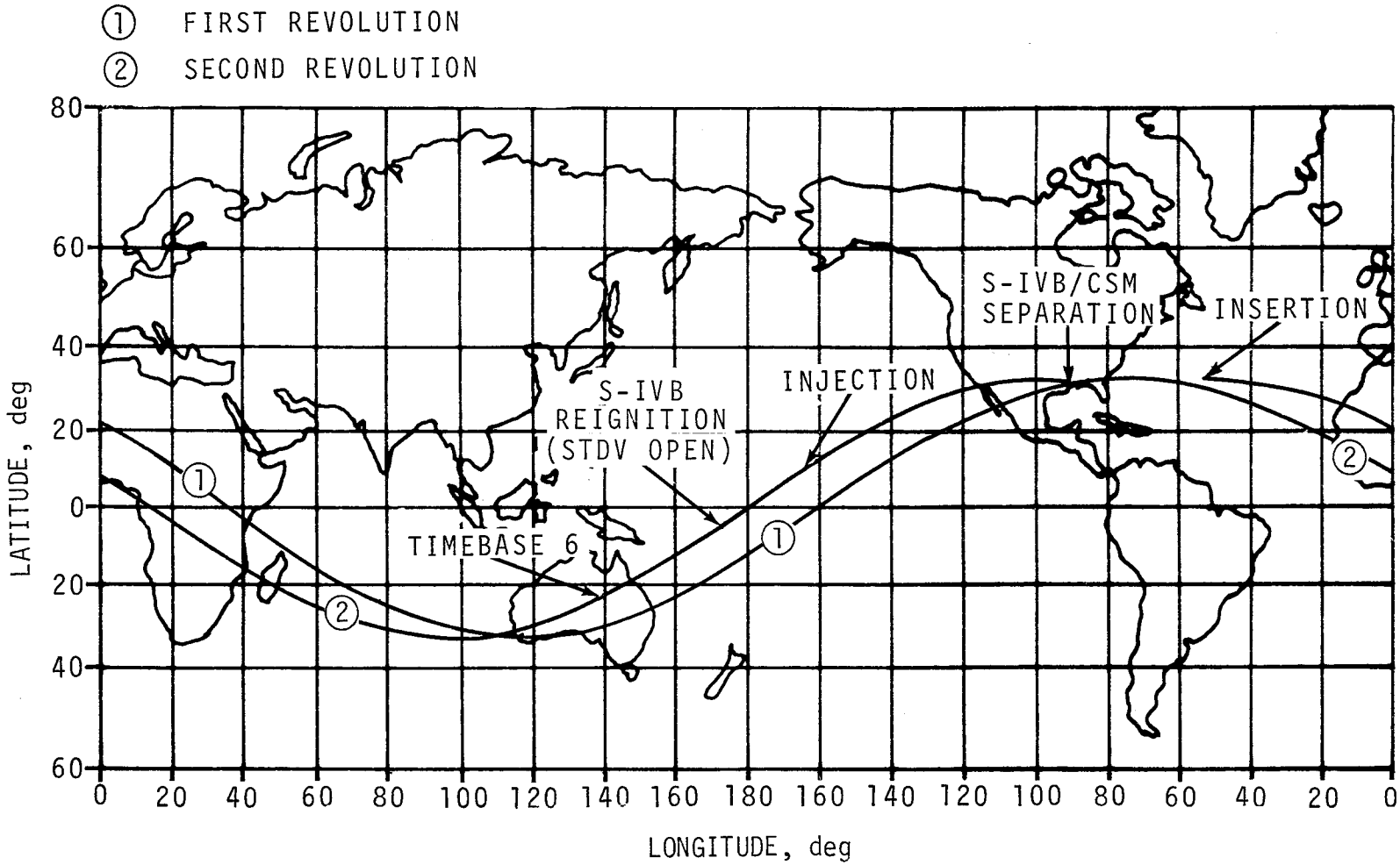

Figure 4-5. Ground Track

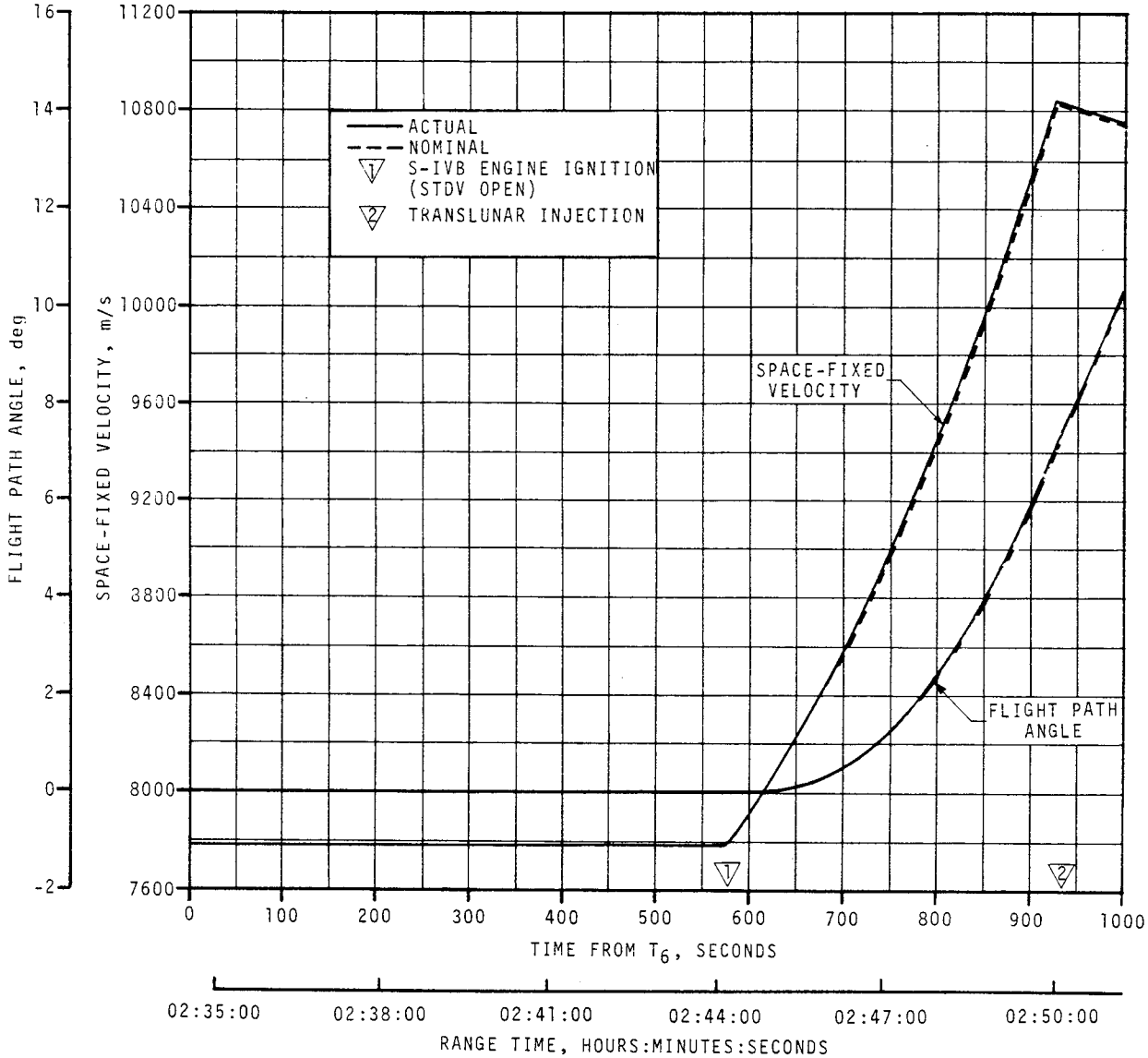

Figure 4-6. Injection Phase Space-Fixed Velocity and Flight Path Angle Comparisons

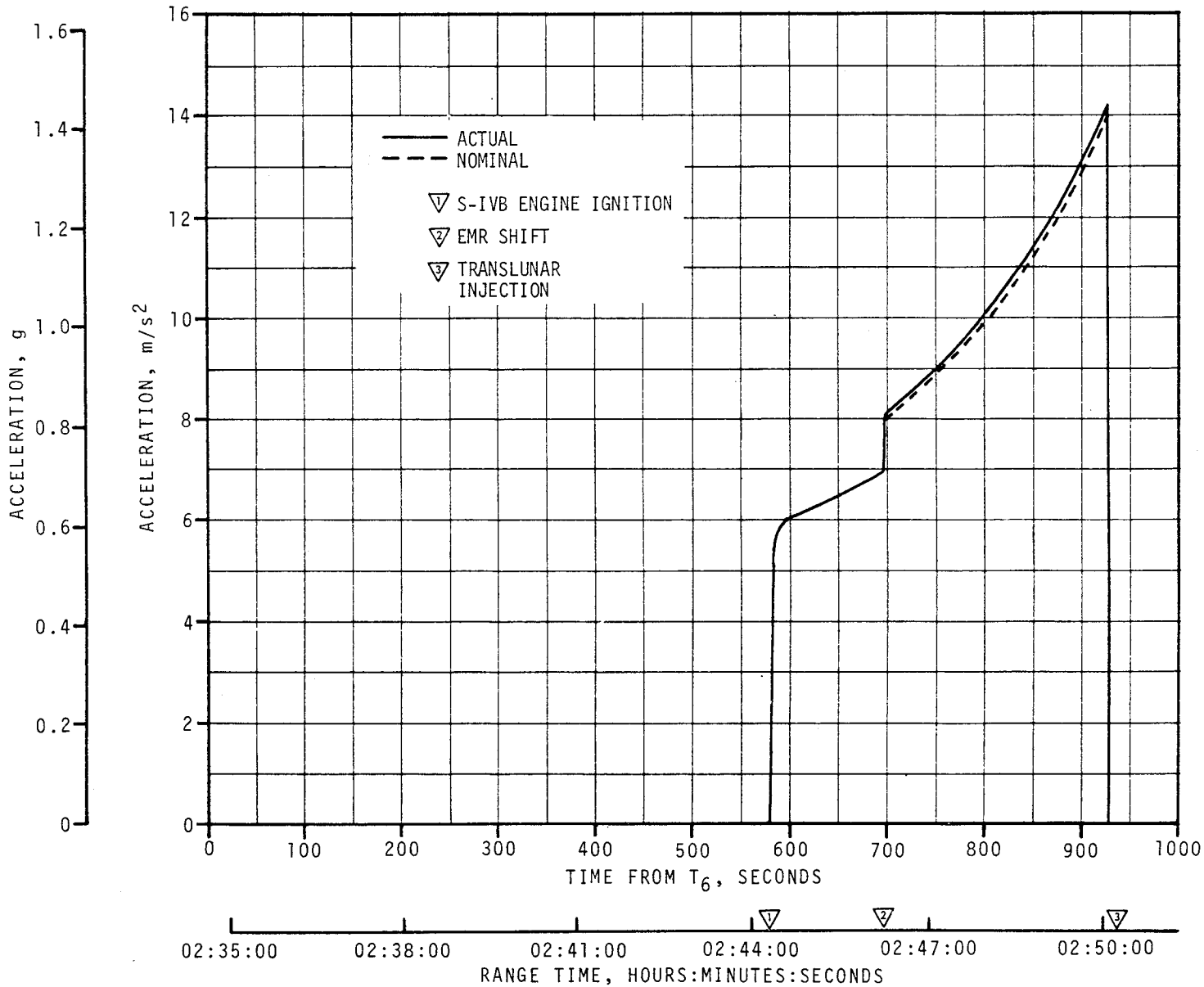

Figure 4-7. Injection Phase Acceleration Comparison

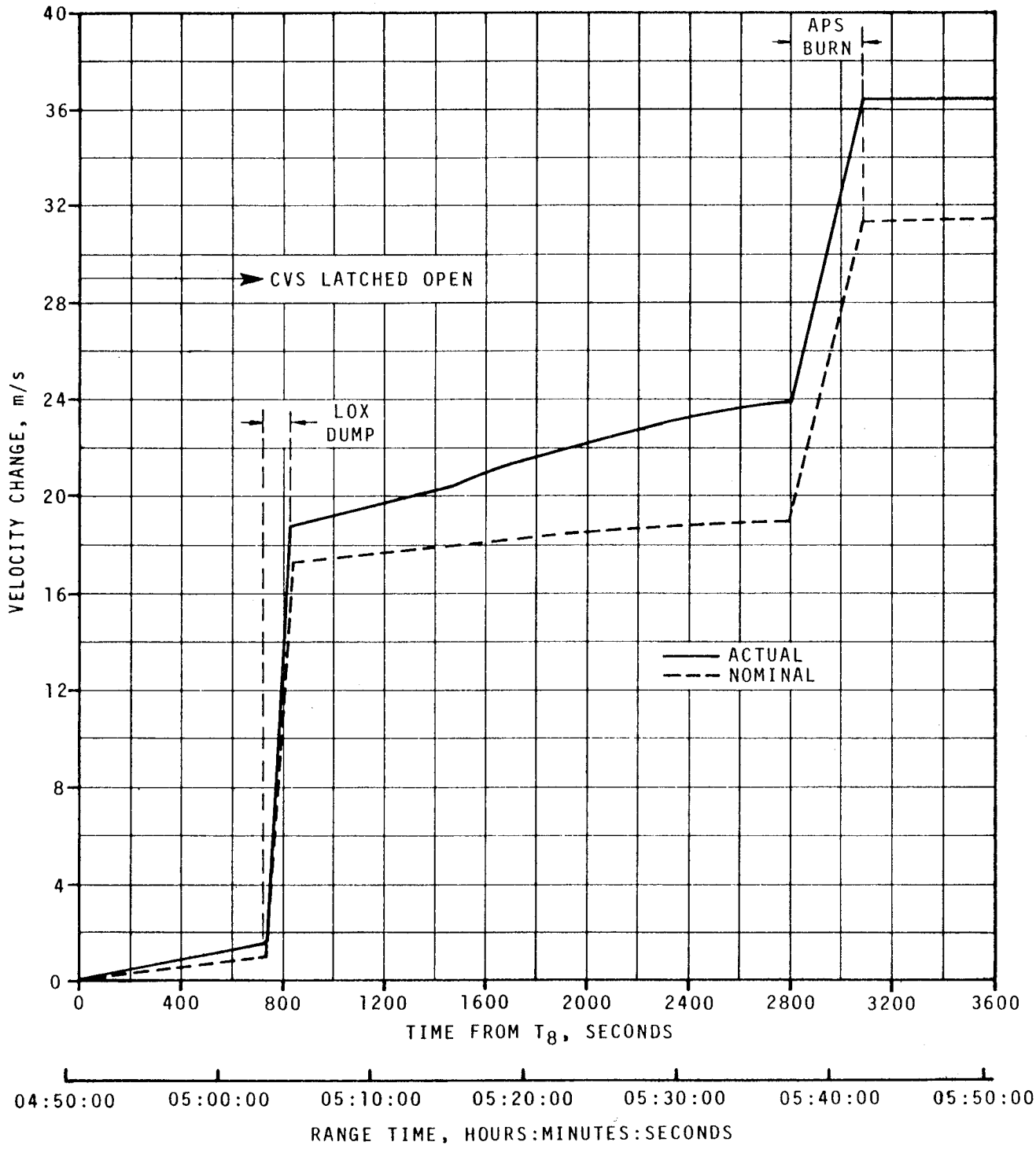

Figure 4-8. Slingshot Maneuver Longitudinal Velocity Increase

Table 4-6. Translunar Injection Conditions

PARAMETER	ACTUAL	NOMINAL	ACT-NOM
Range Time, sec	10,213.0	10,214.1	-1.1
Altitude, km (n mi)	334.4 (180.6)	337.5 (182.2)	-3.1 (-1.6)
Space-Fixed Velocity, m/s (ft/s)	10,834.3 (35,545.6)	10,831.1 (35,535.1)	3.2 (10.5)
Flight Path Angle, deg	7.367	7.412	-0.045
Heading Angle, deg	60.073	60.083	-0.010
Inclination, deg	31.383	31.379	0.004
Descending Node, deg	121.847	121.866	-0.019
Eccentricity	0.97696	0.97667	0.00029
C_3, m^2/s^2 (ft^2/s^2)	-1,391,607 (-14,979,133)	-1,408,484 (-15,160,796)	16,877 (181,663)

Table 4-7. Comparison of Slingshot Maneuver Velocity Increment

PARAMETER	ACTUAL	NOMINAL	ACT-NOM
Longitudinal Velocity Increase, m/s (ft/s)	36.3 (119.1)	31.5 (103.3)	4.8 (15.8)
LOX Dump, m/s (ft/s)	17.0 (55.8)	16.0 (52.5)	1.0 (3.3)
APS Burn, m/s (ft/s)	12.0 (39.4)	12.0 (39.4)	0.0 (0.0)
Continuous Vent System*, m/s (ft/s)	7.3 (24.0)	3.5 (11.5)	3.8 (12.5)

* Latched open at T_8.

phases of the maneuver. The major error contribution in total velocity increase is due to the resulting 7.3 m/s (24.0 ft/s) from the Continuous Vent System (CVS) as compared to 3.5 m/s (11.5 ft/s) for the predicted value. Figure 4-9 presents the resultant conditions for various velocity increases at the given attitude of the vehicle for the maneuver.

The S-IVB/IU closest approach of 3379 kilometers (1825 n mi) above the lunar surface occurred at 78.7 hours into the mission. The trajectory parameters were obtained by integrating forward a vector (furnished by Goddard Space Flight Center (GSFC) which was obtained from Unified S-Band (USB) tracking data during the active lifetime of the S-IVB/IU. The actual and nominal conditions at closest approach are presented in Table 4-8. Figure 4-10 illustrates the influence of the moon on the S-IVB/IU energy (velocity) relative to the earth, particularly as the spent stage passes through the lunar sphere of influence. Some of the heliocentric orbit parameters of the S-IVB/IU are presented in Table 4-9. The same parameters for the earths orbit are also presented for comparison.

ATTITUDE (LOCAL HORIZONTAL REFERENCE SYSTEM)

218° PITCH
0° YAW
170° ROLL

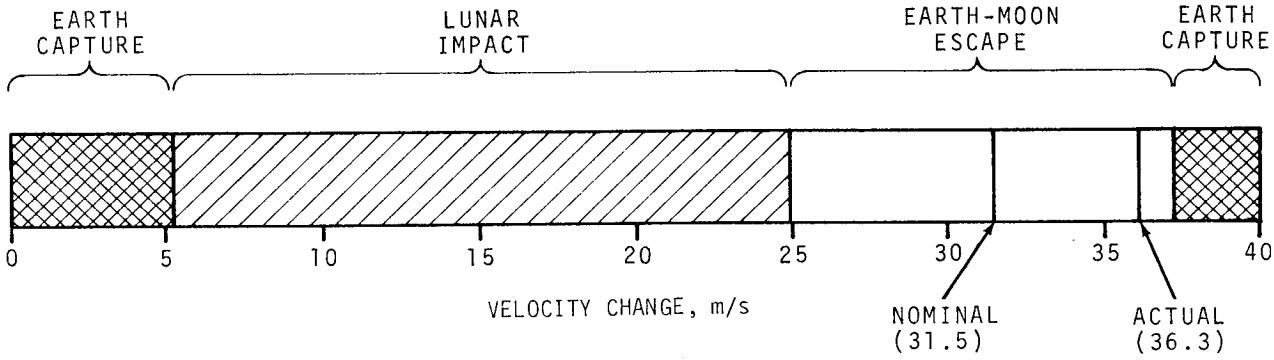

Figure 4-9. Trajectory Conditions Resulting from Slingshot Maneuver Velocity Increments

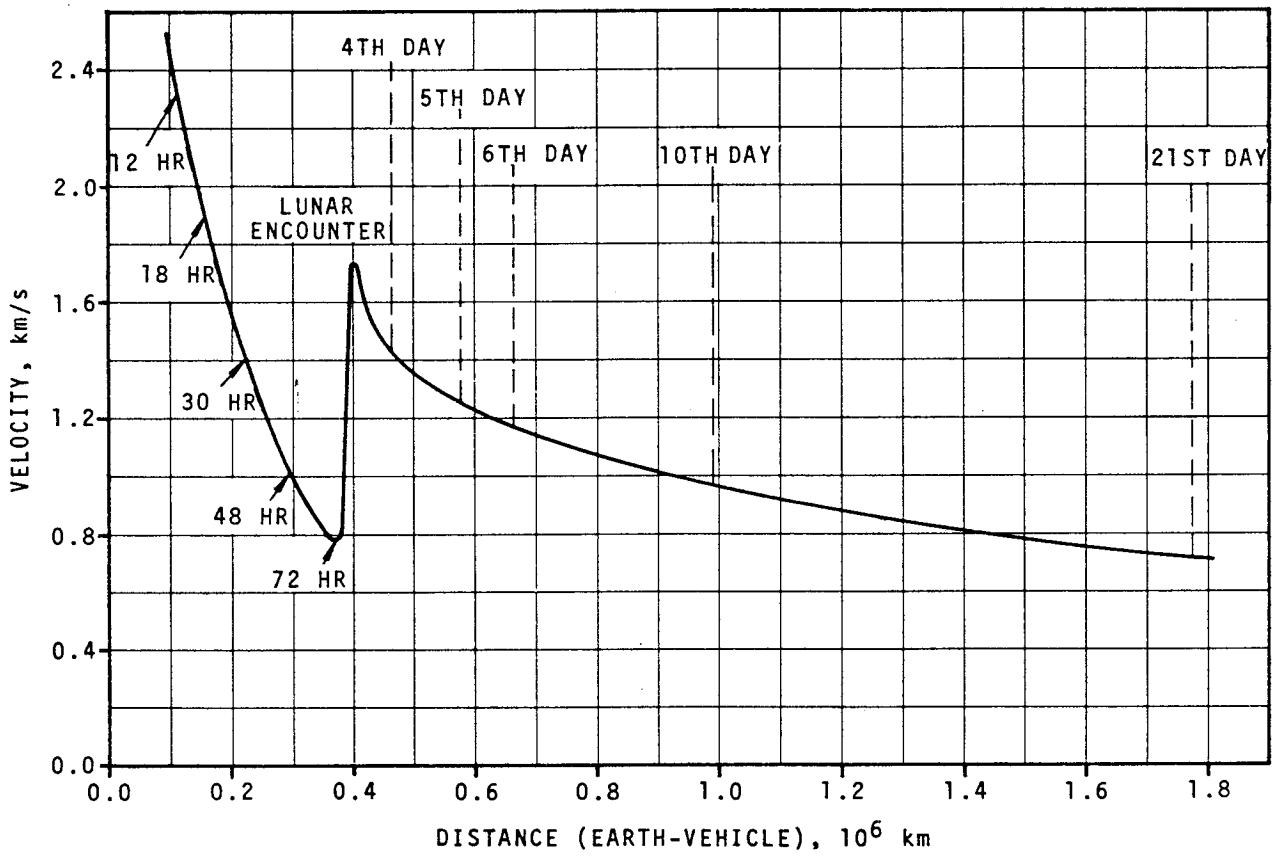

Figure 4-10. S-IVB/IU Velocity Relative to Earth Distance

Table 4-8. Comparison of Lunar Closest Approach Parameters

PARAMETER	ACTUAL	NOMINAL	ACT-NOM
Lunar Radius, km (n mi)	5117 (2763)	3700 (1998)	1417 (765)
Altitude Above Lunar Surface, km (n mi)	3379 (1825)	1962 (1059)	1417 (765)
Range Time, hr	78.7	78.4	0.3
Velocity Increase Relative to Earth from Lunar Encounter, km/s (n mi/s)	0.680 (0.367)	0.860 (0.464)	-0.180 (-0.097)

Table 4-9. Heliocentric Orbit Parameters

PARAMETER	S-IVB/IU	EARTH
Semimajor Axis, 10^6 km (10^6 n mi)	143.08 (77.26)	149.00 (80.45)
Aphelion, 10^6 km (10^6 n mi)	151.86 (82.00)	151.15 (81.61)
Perihelion, 10^6 km (10^6 n mi)	134.30 (72.52)	146.84 (79.29)
Inclination,* deg	0.3836	0.0000
Period, days	342	365

* Measured with respect to the ecliptic.

SECTION 5

S-IC PROPULSION

5.1 SUMMARY

All S-IC propulsion systems performed satisfactorily and the propulsion performance level was very close to nominal. Stage site thrust (averaged from liftoff to Outboard Engine Cutoff [OECO]) was 0.62 percent lower than predicted. Total propellant consumption rate was 0.40 percent lower than predicted with the total consumed Mixture Ratio (MR) 0.10 percent lower than predicted. Specific impulse was 0.16 percent lower than predicted. Total propellant consumption from Holddown Arm (HDA) release to OECO was low by 1.12 percent.

Center Engine Cutoff (CECO) was initiated by the Instrument Unit (IU) at 135.20 seconds as planned. OECO, initiated by LOX low level sensors, occurred at 161.63 seconds which was 0.55 second later than predicted. This is a small difference compared to the predicted 3-sigma limits of ±3.74 seconds. The LOX residual at OECO was 18,041 kilograms (39,772 lbm) compared to the predicted 18,177 kilograms (40,074 lbm). The fuel residual at OECO was 13,954 kilograms (30,763 lbm) compared to the predicted 14,354 kilograms (31,645 lbm).

5.2 S-IC IGNITION TRANSIENT PERFORMANCE

The fuel pump inlet preignition pressure was 31.6 N/cm^2 (45.9 psia) and within F-1 Engine Model Specification limits of 30.0 to 75.8 N/cm^2 (43.5 to 110 psia). The fuel pump inlet preignition temperatures were not available since these measurements were deleted from the S-IC-6 and subsequent stages.

The LOX pump inlet preignition pressure and temperature were 58.5 N/cm^2 (84.8 psia) and 96.1°K (-286.7°F) and were within the F-1 Engine Model Specification limits as shown in Figure 5-1.

Engine startup sequence was nominal. A 1-2-2 start was planned and attained. Engine position starting order was 5, 1-3, 4-2. Two engines are considered to start together if their combustion chamber pressures reach 68.9 N/cm^2 (100 psig) in a 100-millisecond time period.

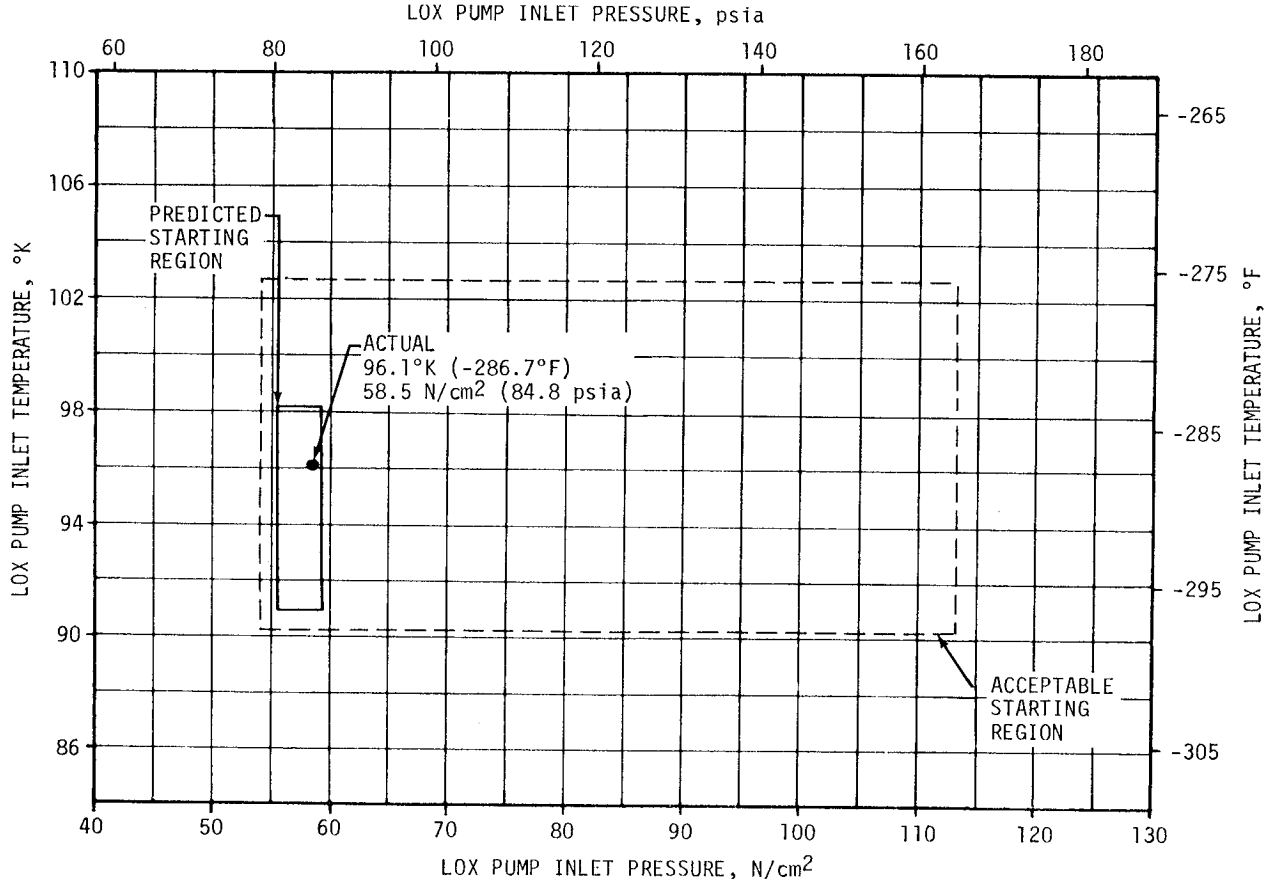

Figure 5-1. S-IC LOX Start Box Requirements

Figure 5-2 shows the thrust buildup of each engine indicative of the successful 1-2-2 start. The shift in thrust buildup near the 5,250,000 Newtons (1,180,000 lbf) level on the outboard engines is caused by ingestion of helium from the LOX prevalves during startup. The thrust shift is absent on the center engine since the POGO suppression helium accumulator system is not used on this engine. Engine combustion chamber pressure oscillograms show 79- to 80-hertz oscillations of approximately 445,000 Newtons (100,000 lbf) peak-to-peak amplitude during buildup. These oscillations are characteristic of normal F-1 engine thrust buildup. Engines No. 1 and 5 show normal inertial surge chamber pressure spikes of approximately 48.3 N/cm^2 (70 psi) and 50.3 N/cm^2 (73 psi), respectively, at 3.45 seconds after their individual start solenoids were energized. Engine No. 4 data indicate a large chamber pressure spike (approximately 80 percent of the mainstage level) at 3.42 seconds after engine No. 4 start solenoid energization. The unusual magnitude of this spike is believed to have been the result of a data problem and is a characteristic of the flight pressure transducer. Static firings of the F-1 engines have exhibited similar pressure spikes (measured with the flight pressure transducer) during the buildup transient, but failed to indicate the same

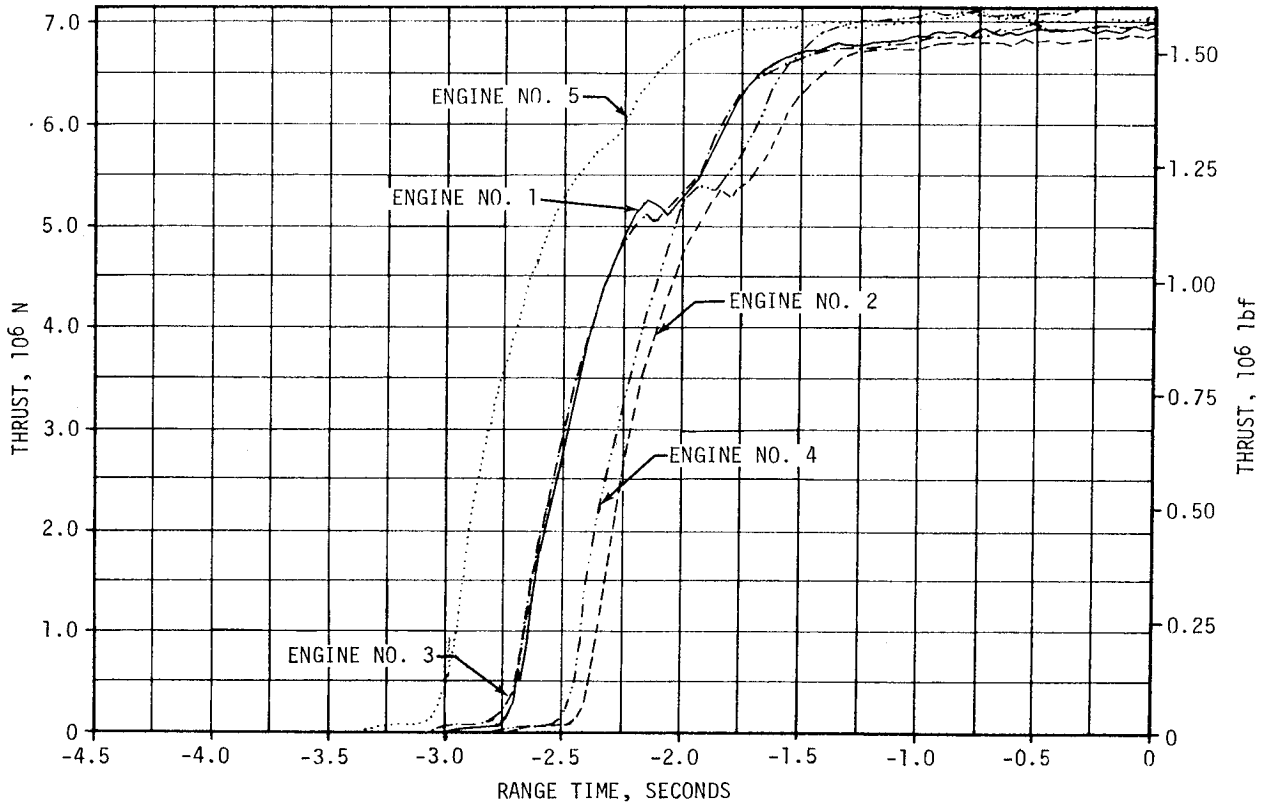

Figure 5-2. S-IC Engines Buildup Transients

spike on high frequency type ground firing instrumentation. The pressure spike has, therefore, been omitted from the thrust buildup curve shown in Figure 5-2.

The best estimate of propellants consumed between ignition and HDA release was 39,374 kilograms (86,803 lbm). The predicted consumption was 38,913 kilograms (85,790 lbm). Propellant loads at HDA release were 1,468,594 kilograms (3,237,697 lbm) for LOX and 637,830 kilograms (1,406,175 lbm) for fuel.

5.3 S-IC MAINSTAGE PERFORMANCE

S-IC stage propulsion performance was satisfactory. Site performance was very close to the predicted level as can be seen in Figure 5-3. The stage site thrust (averaged from liftoff to OECO) was 0.62 percent lower than predicted with the total propellant consumption rate 0.40 percent lower than predicted and the total consumed propellant MR 0.10 percent lower than predicted and the specific impulse 0.16 percent lower than predicted. Total propellant consumption from HDA release to OECO was low by 1.12 percent.

The F-1 engines performance levels during the AS-506 flight showed the smallest deviations from predicted levels of any S-IC flight.

Figure 5-3. S-IC Stage Propulsion Performance Parameters

For comparing F-1 engine flight performance with predicted performance, the flight performance has been analytically reduced to standard conditions and compared to the predicted performance which is based on ground firings and also reduced to standard conditions. These values are shown in Table 5-1 at the 35- to 38-second time slice. Individual engine deviations from predicted thrust ranged from 0.662 percent lower (engine No. 5) to 0.527 percent higher (engine No. 4). Individual engine deviations from predicted specific impulse ranged from 0.114 percent lower (engine No. 5) to 0.038 percent higher (engines No. 1 and 4).

5.4 S-IC ENGINE SHUTDOWN TRANSIENT PERFORMANCE

CECO was initiated by a signal from the IU at 135.20 seconds as planned. OECO, initiated by LOX low level sensors, occurred at 161.63 seconds which was 0.55 second later than predicted. This is a small difference compared to the predicted 3-sigma limits of $\pm$3.74 seconds. Most of the OECO deviation can be attributed to lower than predicted thrust, specific impulse, and propellant loads.

Thrust decay of the F-1 engines was nominal.

Table 5-1. S-IC Engine Performance Deviations

PARAMETER	ENGINE	PREDICTED	RECONSTRUCTION ANALYSIS	DEVIATION PERCENT	AVERAGE DEVIATION PERCENT
Thrust 10^3 N (10^3 lbf)	1	6727 (1512)	6740 (1515)	0.198	
	2	6695 (1505)	6674 (1500)	-0.332	
	3	6717 (1510)	6725 (1512)	0.132	-0.027
	4	6748 (1517)	6783 (1525)	0.527	
	5	6717 (1510)	6674 (1500)	-0.662	
Specific Impulse N-s/kg (lbf-s/lbm)	1	2598 (264.9)	2599 (265.0)	0.038	
	2	2599 (265.0)	2598 (264.9)	-0.038	
	3	2596 (264.7)	2596 (264.7)	0	-0.015
	4	2594 (264.5)	2595 (264.6)	0.038	
	5	2587 (263.8)	2584 (263.5)	-0.114	
Total Flowrate kg/s (lbm/s)	1	2589 (5708)	2594 (5718)	0.175	
	2	2576 (5679)	2569 (5664)	-0.264	
	3	2587 (5703)	2590 (5711)	0.140	-0.025
	4	2602 (5737)	2613 (5761)	0.418	
	5	2597 (5725)	2582 (5691)	-0.594	
Mixture Ratio LOX/Fuel	1	2.258	2.255	-0.133	
	2	2.244	2.241	-0.134	
	3	2.262	2.259	-0.133	-0.133
	4	2.254	2.251	-0.133	
	5	2.282	2.279	-0.131	

NOTE: Performance levels were reduced to standard sea level and pump inlet conditions at 35 to 38 seconds.

Engine cutoff impulse was approximately 10,612,096 N-s (2,385,694 lbf-s) or 11 percent higher than predicted for the outboard engines and approximately 2,659,605 N-s (597,903 lbf-s) or 7 percent lower than predicted for the center engine. The impulse values stated for the outboard engines are for the period from cutoff signal to stage separation, and the impulse value for the center engine is for the period from cutoff signal to zero thrust of the center engine. The flight cutoff impulse is based on chamber pressures. At cutoff, chamber pressure was high for engines No. 1, 3 and especially 4, and low for engine No. 5. These chamber pressure deviations yielded sufficient thrust to account for the cutoff impulse deviations.

5.5 S-IC STAGE PROPELLANT MANAGEMENT

The S-IC does not have an active Propellant Utilization (PU) system. Minimum residuals are obtained by attempting to load the mixture ratio expected to be consumed by the engines plus the predicted unusable residuals. An analysis of the usable residuals experienced during a flight is a good measure of the performance of the passive PU system.

OECO was initiated by the LOX low level sensors as planned, and resulted in residual propellants being very close to the predicted values. The residual LOX at OECO was 18,041 kilograms (39,772 lbm) compared to the predicted value of 18,177 kilograms (40,074 lbm). The fuel residual at OECO was 13,954 kilograms (30,763 lbm) compared to the predicted value of 14,354 kilograms (31,645 lbm). A summary of the propellants remaining at major event times is presented in Table 5-2.

Table 5-2. S-IC Stage Propellant Mass History

EVENT		PREDICTED		LEVEL SENSOR DATA		RECONSTRUCTED	
		LOX	FUEL	LOX	FUEL	LOX	FUEL
Ignition Command	kg (lbm)	1,500,418 (3,307,854)	646,854 (1,426,070)		646,323 (1,424,899)	1,499,479 (3,305,786)	646,319 (1,424,889)
Holddown Arm Release	kg (lbm)	1,469,966 (3,240,719)	638,393 (1,407,415)	1,468,792 (3,238,132)	637,386 (1,405,195)	1,468,594 (3,237,697)	637,830 (1,406,175)
CECO	kg (lbm)	211,956 (467,282)	97,465 (214,874)	217,230 (478,911)	99,475 (219,304)	216,633 (477,594)	99,059 (218,389)
OECO	kg (lbm)	18,177 (40,074)	14,354 (31,645)	19,009 (41,908)	14,202 (31,309)	18,041 (39,772)	13,954 (30,763)
Separation	kg (lbm)	15,594 (34,377)	13,263 (29,241)			15,651 (34,504)	12,705 (28,008)
Zero Thrust	kg (lbm)	15,406 (33,965)	13,063 (28,800)			15,408 (33,970)	12,517 (27,595)

NOTE: Predicted and reconstructed values do not include pressurization gas so they will compare with level sensor data.

5.6 S-IC PRESSURIZATION SYSTEMS

5.6.1 S-IC Fuel Pressurization System

The fuel tank pressurization system performed satisfactorily keeping ullage pressure within the acceptable limits during flight. Helium Flow Control Valves (HFCV's) No. 1 through 4 opened as planned and HFCV No. 5 was not required.

The low flow prepressurization system was commanded on at -97 seconds. High flow pressurization, accomplished by the onboard pressurization system, performed as expected. HFCV No. 1 was commanded on at -2.7 seconds and was supplemented by the high flow prepressurization system until umbilical disconnect.

Fuel tank ullage pressure was within the predicted limits throughout flight as shown in Figure 5-4. HFCV's No. 2, 3, and 4 were commanded open during flight by the switch selector within acceptable limits. Helium bottle pressure was 2137 N/cm^2 (3100 psia) at -2.8 seconds and decayed to 331 N/cm^2 (480 psia) at OECO. Total helium flowrate and heat exchanger performance were as expected.

Fuel pump inlet pressure was maintained above the required minimum Net Positive Suction Pressure (NPSP) during flight.

5.6.2 S-IC LOX Pressurization System

The LOX pressurization system performed satisfactorily and all performance requirements were met. The ground prepressurization system maintained ullage pressure within acceptable limits until launch commit. The onboard pressurization system subsequently maintained ullage pressure within the GOX Flow Control Valve (GFCV) band during flight.

The prepressurization system was initiated at -72 seconds. Ullage pressure increased to the prepressurization switch band and flow was terminated at -57 seconds. The low-flow system was cycled on two additional times at -40 and -17 seconds. At -4.7 seconds the high-flow system was commanded on and maintained ullage pressure within acceptable limits until launch commit.

The LOX tank ullage pressure during flight, shown in Figure 5-5, was maintained within the required limits throughout flight by the GFCV. The maximum GOX flowrate to the tank (at CECO) was 24.9 kg/s (55.0 lbm/s). The heat exchangers performed as expected.

The LOX pump inlet pressure met the minimum NPSP requirement throughout flight. The engine No. 5 LOX suction duct pressure decayed after CECO similar to previous flights as shown in Figure 5-6. The cause of these decays is still unknown.

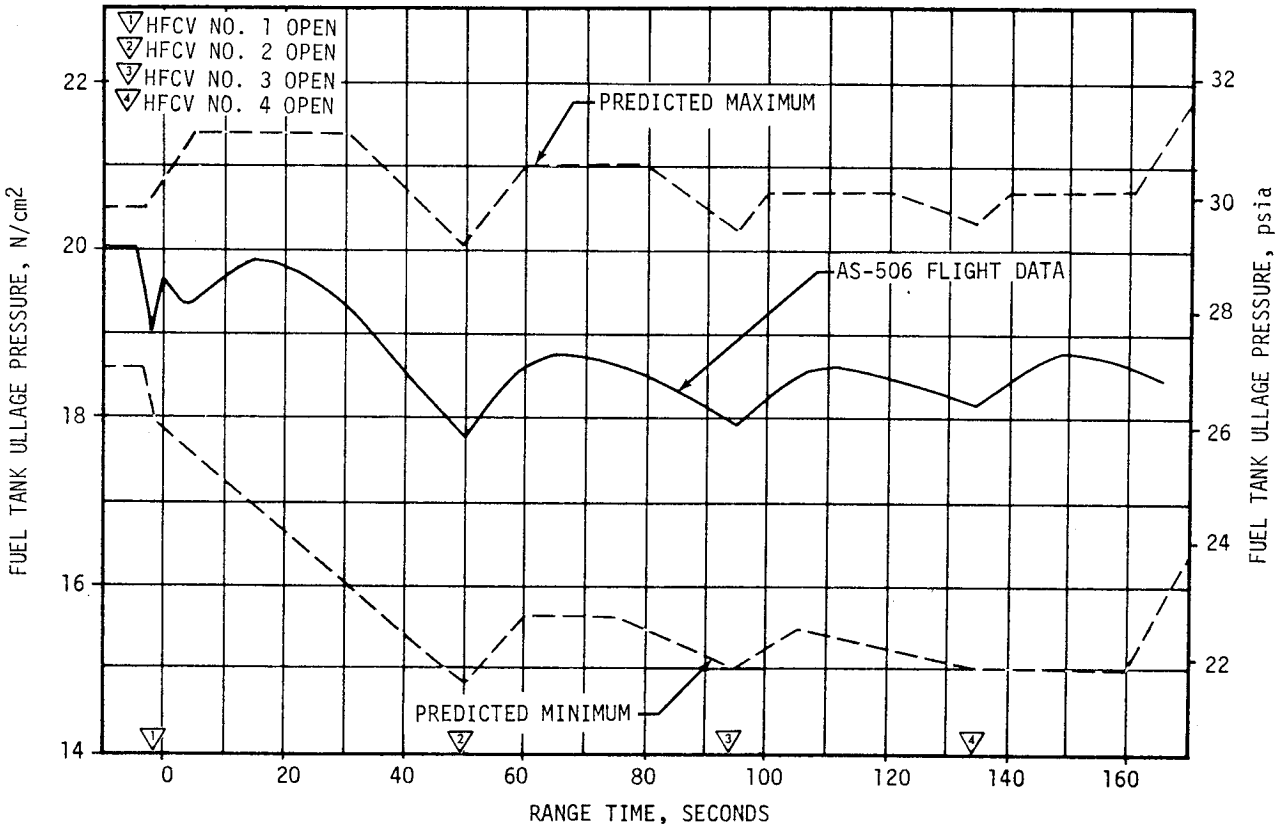

Figure 5-4. S-IC Fuel Ullage Pressure

5.7 S-IC PNEUMATIC CONTROL PRESSURE SYSTEM

The control pressure system functioned satisfactorily throughout the S-IC flight.

Sphere pressure was 2151 N/cm^2 (3120 psia) at liftoff and remained steady until CECO when it decreased to 2068 N/cm^2 (3000 psia). The decrease was due to center engine prevalve actuation. There was a further decrease to 1810 N/cm^2 (2625 psia) after OECO.

The engine prevalves were closed after engine cutoff as required. The engine No. 5 prevalves closed at approximately 137 seconds. The prevalves for the other four engines closed at approximately 163 seconds.

5.8 S-IC PURGE SYSTEMS

Performance of the S-IC purge systems was satisfactory during the flight.

The turbopump LOX seal purge storage sphere pressure was within the limits of 1862 to 2275 N/cm^2 (2700 to 3300 psia) until ignition and 2275 to 689 N/cm^2 (3300 to 1000 psia) from liftoff to cutoff. The radiation calorimeter purge system was not installed on S-IC-6 nor subsequent vehicles.

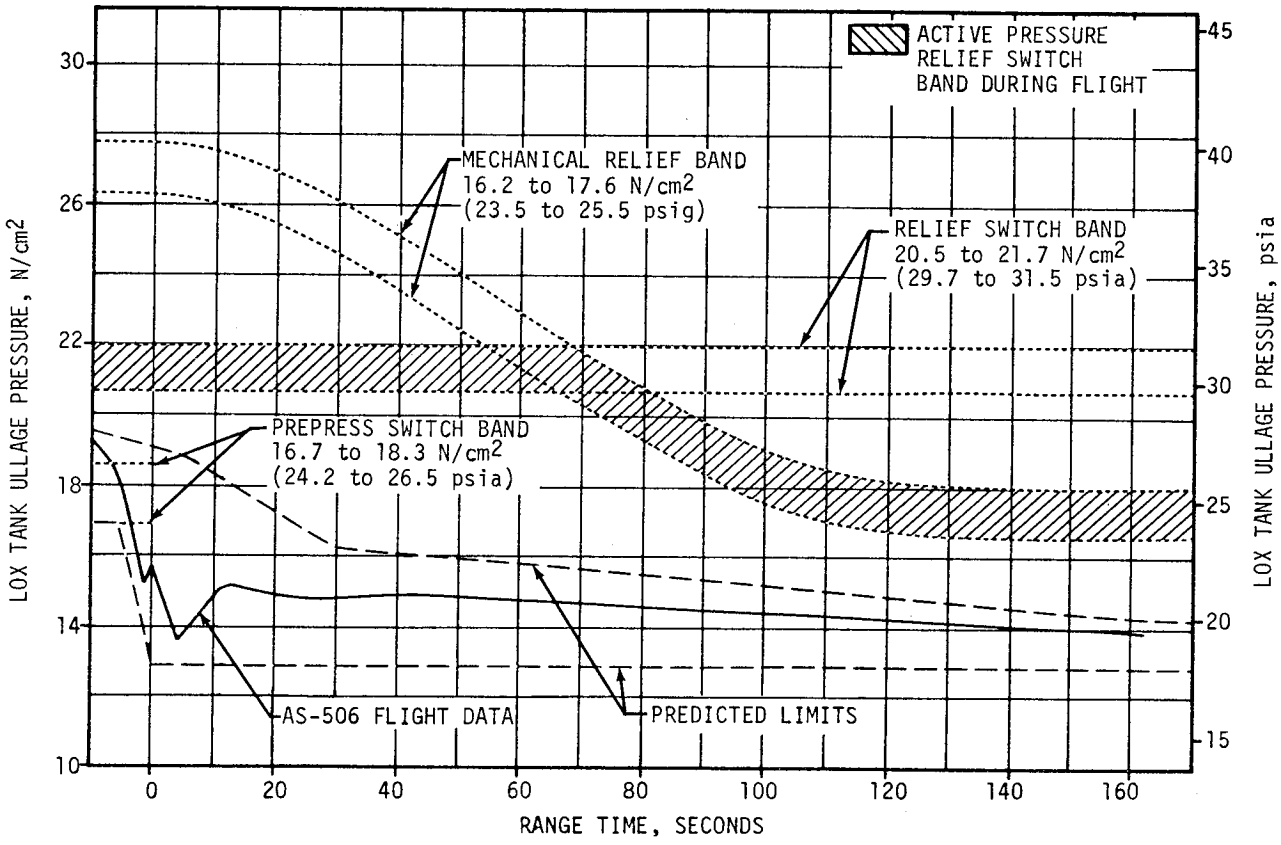

Figure 5-5. S-IC LOX Tank Ullage Pressure

5.9 S-IC POGO SUPPRESSION SYSTEM

The POGO suppression system performed satisfactorily during S-IC flight.

Outboard LOX prevalve temperature measurements indicated that the prevalve cavities were filled with helium prior to liftoff as planned. The measurements in the outboard prevalves went cold momentarily at liftoff indicating LOX sloshed on the probes. They remained warm throughout flight, indicating helium in the prevalves. At cutoff, the increased pressure forced LOX into the prevalves once more. The two measurements in the center engine prevalve indicated cold, which meant LOX was in this valve, as planned.

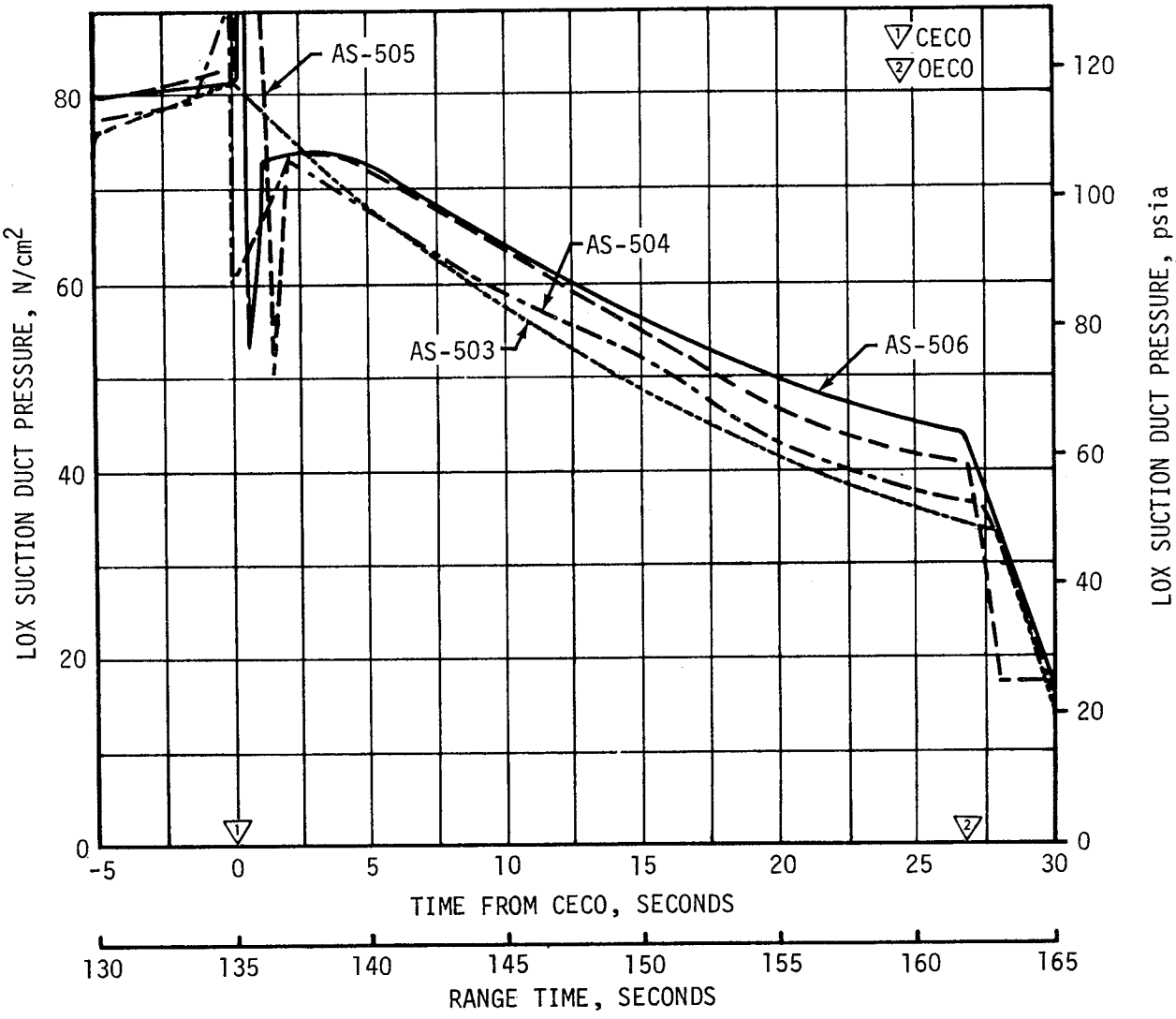

Figure 5-6. S-IC LOX Suction Duct Pressure, Engine No. 5

SECTION 6

S-II PROPULSION

6.1 SUMMARY

The S-II propulsion system performed satisfactorily throughout the flight. As sensed at the engines, Engine Start Command (ESC) occurred at 163.04 seconds and Outboard Engine Cutoff (OECO) at 548.22 seconds with an operation time of 385.18 seconds or 4.0 seconds shorter than predicted. Due to high amplitude low frequency oscillations on the AS-503 and AS-504 flights, the center engine was shut down early as on AS-505 and successfully avoided these oscillations. Center Engine Cutoff (CECO) occurred at 460.62 seconds. Total stage thrust, as determined by computer analysis of telemetered propulsion measurements, at 61 seconds after S-II ESC was 0.20 percent below predicted. Total propellant flowrate (including pressurization flow) was 0.13 percent below predicted and stage specific impulse was 0.07 percent below predicted at this time slice. Stage propellant Mixture Ratio (MR) was 0.36 percent above predicted.

The propellant management system performance was satisfactory. The system was similar to AS-505 in that it also used open-loop control of the engine Propellant Utilization (PU) valves. On AS-506, however, the Instrument Unit (IU) command to shift Engine Mixture Ratio (EMR) from high to low was initiated upon attainment of a preprogramed stage characteristic velocity as sensed by the Launch Vehicle Digital Computer (LVDC). An IU timed command served this function on AS-505. The IU EMR shift command occurred 6 seconds later than predicted and this deviation was due mainly to improper scaling in the LVDC velocity computations. The actual shift from high to low EMR occurred 9.5 seconds late when compared with the final propulsion prediction. The additional 3.5 seconds result from a propulsion and characteristic velocity presetting mismatch that was known prior to flight. Future preflight operational trajectory events, IU programed commands, and S-II propulsion prediction events will be reviewed for compatibility.

OECO, initiated by the LOX low level cutoff sensors, was achieved following a planned 1.5-second time delay. A small engine performance decay was noted just prior to cutoff similar to AS-505, but was less severe than that observed on AS-504 due to only four engines operating at cutoff. Residual propellant remaining in the tanks at OECO signal was 3388 kilograms (7471 lbm) compared to a prediction of 2623 kilograms (5783 lbm).

The performance of the LOX and LH_2 tank pressurization systems was satisfactory. Ullage pressure in both tanks was more than adequate to meet engine inlet Net Positive Suction Pressure (NPSP) requirements throughout mainstage. As commanded by the IU, step pressurization occurred at 261.6 seconds for the LOX tank and 461.6 seconds for the LH_2 tank.

The engine servicing system performed satisfactorily except that the engine No. 1 start tank pressure was 2.8 N/cm^2 (4 psi) below redline at prelaunch commit (-33 seconds). This low pressure was caused by a lower than planned setting of the Ground Support Equipment (GSE) regulator supplying hydrogen to the start tank. Corrective action being proposed includes increasing the nominal setting of the GSE regulator and relaxing the prelaunch commit redline to more closely approximate actual requirements. All start tank pressures and temperatures were well within requirements at S-II ESC.

The recirculation, pneumatic control and helium injection systems all performed satisfactorily.

6.2 S-II CHILLDOWN AND BUILDUP TRANSIENT PERFORMANCE

The prelaunch servicing operations satisfactorily accomplished the engine conditioning requirements. Thrust chamber temperatures were within predicted limits both at launch and engine start. The thrust chamber temperatures ranged between 101 and 119°K (-278 and -245°F) at prelaunch commit and 131 and 150°K (-223 and -190°F) at engine start. Thrust chamber temperature warmup rate during S-IC boost agreed closely with those experienced on previous flights.

Engine start tank temperatures at the conclusion of chilldown ranged between 95 and 100°K (-289 and -280°F) and were similar to AS-505. All start tank temperatures and pressures were within the prelaunch and engine start boxes, as shown in Figure 6-1, with the exception that engine No. 1 start tank pressure was 2.8 N/cm^2 (4 psi) low at prelaunch commit (-33 seconds).

The low start tank pressures at -33 seconds resulted from the start tanks being pressurized at 783 to 792 N/cm^2 (1135 to 1148 psia) instead of the required 810 $\pm$10.3 N/cm^2 (1175 $\pm$15 psia). It had been planned to set both the GSE S-II pneumatic console dome regulator and the start tank supply regulator at the high side of the tolerance. The dome regulator was replaced during the -9 hour launch countdown hold without adjustment to the high limit (refer to paragraph 3.6.2). Another factor contributing to the low start tank pressures was that the pressure gauge used to set the regulators was reading approximately 7.6 N/cm^2 (11 psi) high. It is planned to revise the pressurization regulator settings to provide a higher pressure level for subsequent stages. It has also been recommended that the minimum pressure line of the prelaunch redline box be lowered approximately 6.9 N/cm^2 (10 psi). Review of all previous launch data indicates a lower prelaunch pressure is compatible with the engine start box.

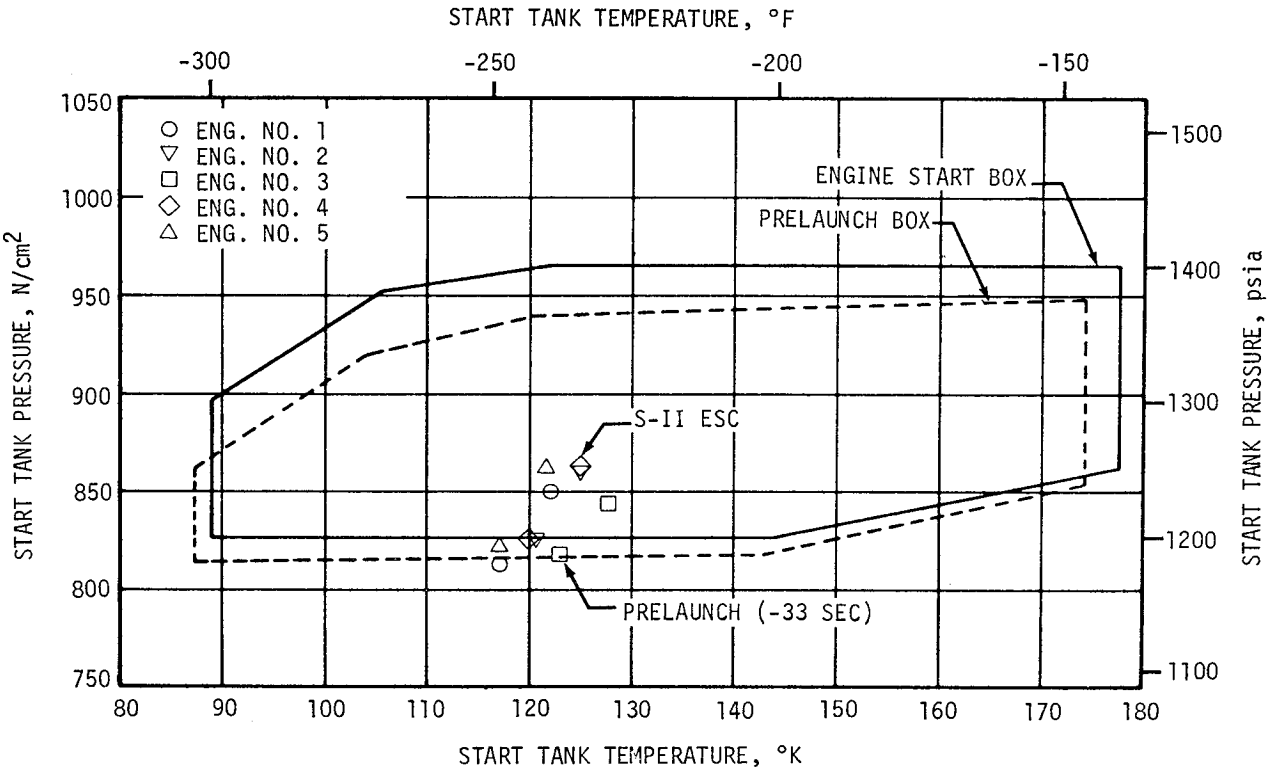

Figure 6-1. S-II Engine Start Tank Performance

All engine helium tank pressures were within the prelaunch and engine start limits of 1931 to 2379 N/cm^2 (2800 to 3450 psia). The helium supply line was manually vented at -277 seconds versus being vented at -30 seconds on previous launches. This allowed adequate time to monitor for leakage prior to the -19 second launch commit. No pressure decay of any significance occurred during this time period.

Engine No. 2 helium tank pressure decayed at a sharper rate than expected after S-II ESC. The decay assumed a more normal rate after approximately 30 seconds of operation. This condition has occurred on previous flights and has been coincident with shifts in the engine helium regulator outlet pressure. Engine regulator outlet pressure measurement was not provided on AS-506 so it can only be assumed that a regulator outlet pressure shift also occurred. On AS-505 flight, engine No. 5 regulator outlet pressure shifted from 281 to 276 N/cm^2 (408 to 400 psia) at approximately 63 seconds after ESC. On AS-504 flight, engine No. 3 regulator outlet pressure shifted from 279 to 276 N/cm^2 (405 to 400 psia) at approximately 43 seconds after ESC. Between ESC and regulator shift the decay rates were higher than expected, but following the shift the decay rates of all engines were comparable.

The higher than expected helium tank decay rates experienced to date are not critical for the S-II mission. Even if the initial decay rate continued throughout S-II burn, the supply pressure would be adequate to meet system demands with sufficient margin. The cause of this deviation has been assessed as internal leakage through the engine helium regulator.

The LOX and LH_2 recirculation systems used to chill the feed ducts, turbopumps, and other engine components performed satisfactorily during prelaunch and S-IC boost. Engine pump inlet temperatures and pressures at engine start were well within the requirements as shown in Figure 6-2. The LOX pump discharge temperatures at ESC were 7.5 to 8.9°K (13.5 to 16.1°F) subcooled, which is well below the 1.7°K (3°F) subcooling requirement.

Prepressurization of the propellant tanks was satisfactorily accomplished. Ullage pressures at S-II ESC were 26.9 N/cm^2 (39 psia) for LOX and 19.6 N/cm^2 (28.5 psia) for LH_2.

S-II ESC was received at 163.04 seconds and the Start Tank Discharge Valve (STDV) solenoid activation signal occurred 1.0 second later. The engine thrust buildup was satisfactory and was within the required thrust buildup envelope. The stage thrust reached mainstage level at 166.2 seconds. Engine thrust levels were between 861,496 and 895,080 Newtons (193,672 and 201,222 lbf) prior to "High EMR Select" command at 168.5 seconds.

6.3 S-II MAINSTAGE PERFORMANCE

Stage performance during the high EMR portion of the flight was very close to predicted as shown in Figure 6-3. At a time slice of ESC +61 seconds, total vehicle thrust was 5,141,516 Newtons (1,155,859 lbf) which is only 10,094 Newtons (2269 lbf) or 0.20 percent below the preflight prediction. Total propellant flowrate (including pressurization flow) was 1239 kg/s (2731 lbm/s) which was 0.13 percent below prediction. Stage specific impulse, including the effect of pressurization gas flowrate, was 4150.2 N-s/kg (423.2 lbf-s/lbm) which is 0.07 percent below the predicted level. Stage propellant MR was 0.36 percent above prediction.

At ESC +297.58 seconds (460.62 seconds) the center engine was shut down in order to prevent buildup of the low frequency oscillations that were observed on AS-503 and AS-504. This action reduced total vehicle thrust by 1,031,685 Newtons (231,932 lbf) to a level of 4,093,107 Newtons (920,167 lbf). Of this total, a thrust reduction of 1,017,255 Newtons (228,688 lbf) was directly due to CECO and the remaining 14,430 Newtons (3244 lbf) decrease resulted from the sum effect of fuel step pressurization (ESC +298.6 seconds) and loss of acceleration head.

The shift from high to low EMR operation occurred at approximately 335 seconds after ESC. The change of EMR resulted in further thrust reduction, and at ESC +351 seconds the total vehicle thrust was 3,082,769 Newtons (693,034 lbf); thus a decrease in thrust of 1,010,338 Newtons (227,133 lbf) is indicated between high and the average low EMR operation.

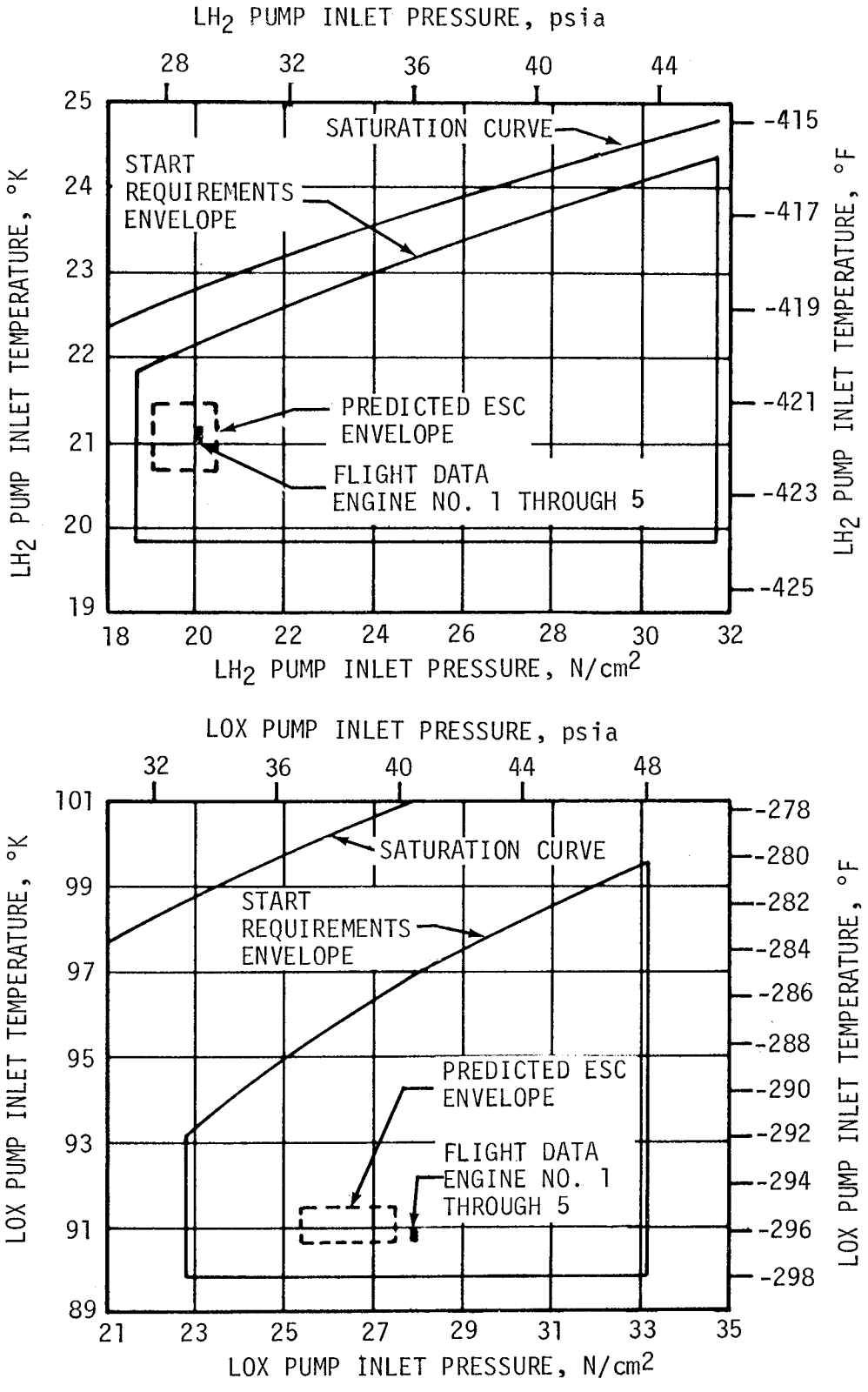

Figure 6-2. S-II Engine Pump Inlet Start Requirements

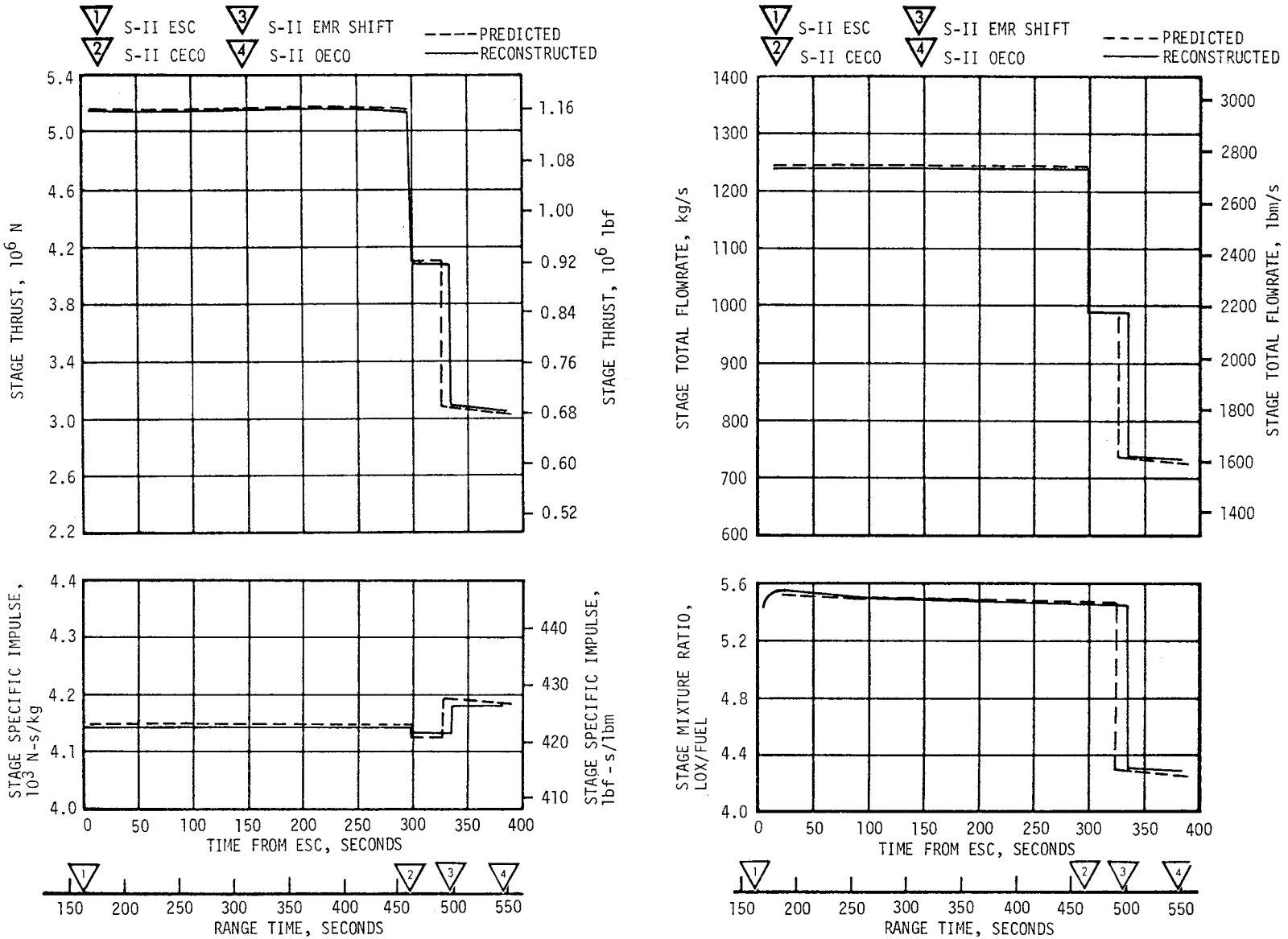

Figure 6-3. S-II Steady State Operation

Similar to AS-505 flight, the deviation of actual from predicted performance remained small at the lower mixture ratio levels. At ESC +381 seconds, total thrust was 3,059,402 Newtons (687,781 lbf) at an EMR of 4.29. Vehicle thrust and propellant flowrate deviations at this time were 18,683 Newtons (4200 lbf) and 5.1 kg/s (11.2 lbm/s), respectively.

Individual J-2 engine data, excluding the effects of pressurization flowrate, are presented in Table 6-1 for the ESC +61-second time point. Very good correlation between prediction and flight is indicated by the small magnitude of the deviations. Flight data reconstruction procedures were directed toward matching the engine and stage acceptance specific impulse values while maintaining the engine flow and pump speed data as a baseline.

Data presented in Table 6-1 are actual flight data and have not been adjusted to standard J-2 engine conditions. Considering data that have been adjusted to standard conditions through use of a computer program, very little difference from the results shown in Table 6-1 is observed. The adjusted data show all engine thrust levels to be within 0.40 percent of those achieved during vehicle acceptance test.

Three minor engine performance shifts were observed during S-II burn. Engine No. 1 experienced two performance increases, each approximately 6672 Newtons (1500 lbf), during the first 35 seconds of mainstage operation.

Table 6-1. S-II Engine Performance Deviations (ESC +61 Seconds)

PARAMETER	ENGINE	PREDICTED		RECONSTRUCTED		PERCENT INDIVIDUAL DEVIATION	PERCENT AVERAGE DEVIATION
Thrust, Newtons (lbf)	1	1,034,683	(232,606)	1,035,083	(232,696)	0.04	-0.20
	2	1,016,663	(228,555)	1,017,517	(228,747)	0.08	
	3	1,023,514	(230,095)	1,017,228	(228,682)	-0.61	
	4	1,042,085	(234,270)	1,039,576	(233,706)	-0.24	
	5	1,034,665	(232,602)	1,032,112	(232,028)	-0.25	
Specific Impulse N-s/kg (lbf-s/lbm)	1	4173.7	(425.6)	4169.8	(425.2)	-0.09	-0.06
	2	4159.0	(424.1)	4170.8	(425.3)	0.28	
	3	4175.7	(425.8)	4165.9	(424.8)	-0.23	
	4	4155.1	(423.7)	4157.0	(423.9)	0.05	
	5	4175.7	(425.8)	4162.9	(424.5)	-0.30	
Engine Flowrate kg/s (lbm/s)	1	247.9	(546.6)	248.2	(547.2)	0.11	-0.14
	2	244.5	(539.0)	244.0	(537.9)	-0.20	
	3	245.1	(540.4)	244.2	(538.3)	-0.39	
	4	250.8	(552.9)	250.1	(551.3)	-0.29	
	5	247.8	(546.3)	248.0	(546.7)	0.07	
Engine Mixture Ratio LOX/Fuel	1	5.57		5.57		0	0.29
	2	5.56		5.55		-0.18	
	3	5.59		5.57		-0.36	
	4	5.53		5.54		0.18	
	5	5.49		5.59		1.82	

NOTE: Values exclude pressurization flow.

A thrust decrease of about the same magnitude occurred in engine No. 2 after 64 seconds of mainstage operation. These shifts are indicative of changes in the Gas Generator (GG) oxidizer system flow resistance and are not considered detrimental to engine operation.

Amplified main chamber pressure processed with a 25 hertz low pass filter revealed no high amplitude, low frequency oscillations as experienced on AS-503 and AS-504. As in the flight of AS-505, CECO precluded any oscillation buildup.

6.4 S-II SHUTDOWN TRANSIENT PERFORMANCE

Engine shutdown sequence was initiated by the stage LOX low level sensors. The LOX depletion cutoff system again included a 1.5-second delay timer. As in the AS-504 and AS-505 flights, this resulted in engine performance decay prior to receipt of the cutoff signal. Due to early CECO however, the precutoff decay was greatly reduced compared to AS-504 without CECO. Only engine No. 1 exhibited a significant thrust chamber pressure decay, decreasing 77.9 N/cm^2 (113 psi) in the final 0.25 second before cutoff. All other outboard engines thrust chamber pressure decays were of the order of 20.7 N/cm^2 (30 psi).

At OECO signal (548.22 seconds), total vehicle thrust was down to 2,783,479 Newtons (625,751 lbf). Vehicle thrust dropped to 5 percent of this level within 0.75 second. The stage cutoff impulse through the 5 percent thrust level was estimated to be 581,916 N-s (130,820 lbf-s). No unusual features were apparent in the center engine thrust decay data following CECO, with the decay to 5 percent thrust occurring in approximately 0.3 second.

6.5 S-II STAGE PROPELLANT MANAGEMENT

The propellant management system performed satisfactorily during the propellant loading operation and during flight. The S-II stage employed an open-loop system utilizing fixed, open-loop commands from the IU rather than feedback signals from the tank mass sensing probes. (Open-loop operation was also used on AS-503 and AS-505. It is also planned for use on all subsequent vehicles.)

The facility Propellant Tanking Control System (PTCS) and the propellant management system successfully accomplished S-II loading and replenishment. During the prelaunch countdown, all propellant management subsystems operated properly with no problems noted.

Open-loop PU system operation commenced when "High EMR select" was commanded at ESC +5.5 seconds, as planned. The PU valves then moved to the high EMR position, providing a nominal high EMR of 5.50 for the first phase of Programed Mixture Ratio (PMR). The IU command to shift EMR from high to low was initiated at ESC +331.8 seconds (6 seconds later than predicted) upon attainment of a preprogramed characteristic velocity as sensed by the LVDC. Approximately 5.5 seconds of this deviation is attributed to improper scaling in the inflight calculations of velocity within the LVDC (refer to

paragraph 10.2.1), and the remainder is due to variations between the actual and predicted flight performance. The IU command caused the PU valves to be driven to the low EMR position, providing an average EMR of 4.34 (versus a predicted average EMR of 4.33) for the low mixture ratio portion of the flight.

The actual shift from high to low EMR occurred 9.5 seconds late when compared with the final propulsion prediction. The additional 3.5 seconds result from a propulsion and characteristic velocity presetting mismatch that was known prior to flight.

Engine No. 3 PU valve position monitor exhibited erratic characteristics during the S-IC and S-II boost operational periods. Analysis of the limited measurements available did not reveal any PU computer, telemetry or engine malfunction. The PU valve telemetry potentiometer is the most likely cause of this problem.

The open-loop PU control system responded as expected during flight and no instabilities were noted. The open-loop PU error at OECO was approximately +567 kilograms (+1250 lbm) LH_2 versus a 3-sigma tolerance of ±1134 kilograms (±2500 lbm).

Based on PU system data, propellant residuals (mass in tanks and sumps) at OECO were 816 kilograms (1800 lbm) LOX, and 2572 kilograms (5671 lbm) LH_2, versus the predicted 657 kilograms (1448 lbm) LOX and 1966 kilograms (4335 lbm) LH_2. An updated analysis using AS-505 LOX depletion data indicated a higher than predicted LOX residual would occur on AS-506. S-II burn time was reduced approximately 4 seconds and the LH_2 residual at OECO was increased 432 kilograms (952 lbm) due to the late PU valve step time.

Table 6-2 presents a comparison of propellant masses as measured by the PU probes and engine flowmeters. The best estimate propellant mass is based on integration of flowmeter data utilizing the propellant residuals determined from PU system data corrected for nominal tank mismatch at OECO. Best estimates of propellant mass loaded are 370,778 kilograms (817,425 lbm) LOX, and 71,615 kilograms (157,885 lbm) LH_2 which correlates closely with the postlaunch trajectory simulation. These mass values were 0.24 percent less than predicted for LOX and 0.07 percent less than predicted for LH_2.

6.6 S-II PRESSURIZATION SYSTEMS

6.6.1 S-II Fuel Pressurization System

LH_2 tank ullage pressure, actual and predicted, is presented in Figure 6-4 for autosequence, S-IC boost and S-II boost. The LH_2 tank vent valves were closed at -96 seconds and the ullage was pressurized to 24.8 N/cm^2 (36 psia) in approximately 27 seconds. One makeup cycle was required at -40 seconds as a result of thermal pressure decay. Venting occurred during S-IC boost as anticipated. One venting cycle was indicated on vent valve No. 1 between 93 and 100 seconds. There was no indication that vent valve No. 2 opened.

Table 6-2. S-II Propellant Mass History

EVENT RANGE TIME	UNITS	PREDICTED		PU SYSTEM ANALYSIS		ENGINE FLOWMETER INTEGRATION (BEST ESTIMATE)	
		LOX	LH_2	LOX	LH_2	LOX	LH_2
Ground Ignition	kg (lbm)	371,672 (819,397)	71,668 (158,000)	371,899 (819,896)	71,718 (158,111)	370,778 (817,425)	71,615 (157,885)
S-II ESC	kg (lbm)	371,672 (819,397)	71,668 (158,000)	371,697 (819,452)	71,627 (157,910)	370,778 (817,425)	71,615 (157,885)
S-II PU Valve Step (497.60 sec)	kg (lbm)	38,217 (84,254)	10,751 (23,703)	53,432 (117,797)	13,503 (29,768)	35,884 (79,111)	10,469 (23,080)
S-II OECO	kg (lbm)	657 (1448)	1966 (4335)	816 (1800)	2572 (5671)	816 (1800)	2572 (5671)
S-II Residual At Stage Separation	kg (lbm)	544 (1199)	1916 (4224)	730 (1609)	2531 (5579)	730 (1609)	2531 (5579)

NOTE: Table is based on mass in tanks and sump only. Propellant trapped external to tanks and LOX sump is not included.

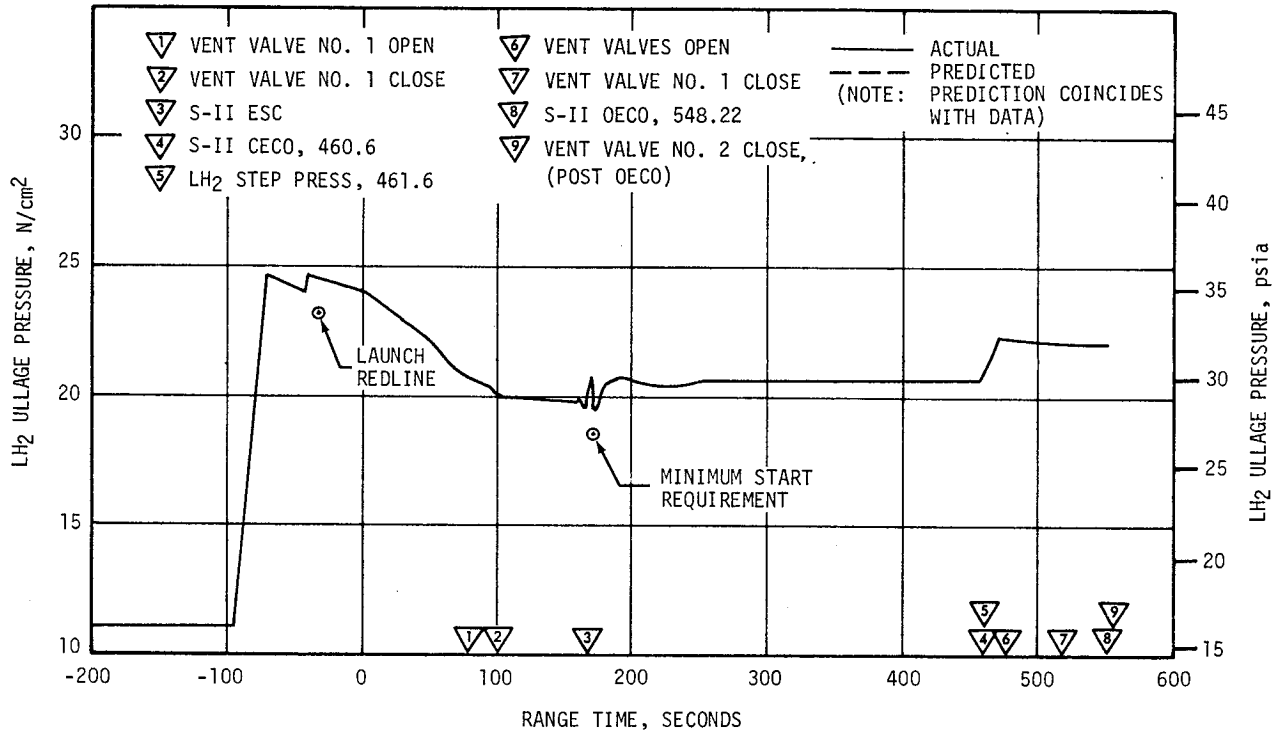

Figure 6-4. S-II Fuel Tank Ullage Pressure

Differential pressure across the vent valve was kept below the low-mode upper limit of 20.3 N/cm^2 (29.5 psid). Ullage pressure at S-II engine start was 19.6 N/cm^2 (28.5 psia) meeting the minimum engine start requirement of 18.6 N/cm^2 (27 psia). The LH_2 tank valves were switched to the high vent mode immediately prior to S-II engine start.

LH_2 tank ullage pressure was maintained within the regulator range of 19.7 to 20.7 N/cm^2 (28.5 to 30 psia) during burn until the LH_2 tank pressure regulator was stepped open at 461.6 seconds. Ullage pressure increased to 22.1 N/cm^2 (32 psia). The LH_2 vent valves started venting at 477 seconds and continued venting throughout the remainder of the S-II flight. Ullage pressure remained within the high-mode vent range of 21 to 22.7 N/cm^2 (30.5 to 33 psia).

Figure 6-5 shows LH_2 total inlet pressure, temperature and NPSP. The parameters were close to predicted values. The NPSP supplied exceeded that required throughout the S-II burn phase of the flight.

6.6.2 S-II LOX Pressurization System

LOX tank ullage pressure, actual and predicted, is presented in Figure 6-6 for autosequence, S-IC boost and S-II burn. After a two-minute cold helium chilldown flow through the LOX tank, the vent valves were closed at -185.3 seconds and the LOX tank was prepressurized to the pressure switch setting of 27.1 N/cm^2 (39.3 psia) in approximately 42 seconds. One pressure makeup cycle was required at -125 seconds as a result of pressure decay, which was followed by the slight pressure increase caused by LH_2 tank prepressurization. Ullage pressure was 26.9 N/cm^2 (39 psia) at engine start.

The LOX regulator remained at its minimum position until 240 seconds because the ullage pressure was above the regulator range of 24.8 to 26.5 N/cm^2 (36 to 38.5 psia). A slight decrease in ullage pressure prior to LOX regulator step pressurization indicated normal performance of the LOX regulator. LOX step pressurization (261.6 seconds) caused the usual characteristic surge in ullage pressure followed by a slower increase until LOX tank ullage pressure reached a maximum of 28.3 N/cm^2 (41 psia) at 383.4 seconds when the No. 1 vent valve cracked. Ullage pressure was 27.9 N/cm^2 (40.5 psia) at CECO. Vent valve No. 1 reseat occurred at 27.9 N/cm^2 (40.5 psia) after EMR shift. The LOX tank vent valve No. 2 did not open.

LOX pump total inlet pressure, temperature and NPSP are presented in Figure 6-7. The NPSP supplied exceeded the requirement throughout the S-II boost phase. The total magnitude of LOX liquid stratification was greater than predicted, but was similar to AS-505. The 1.5-second time delay in the LOX low level cutoff circuit makes it very difficult to predict an accurate cutoff temperature.

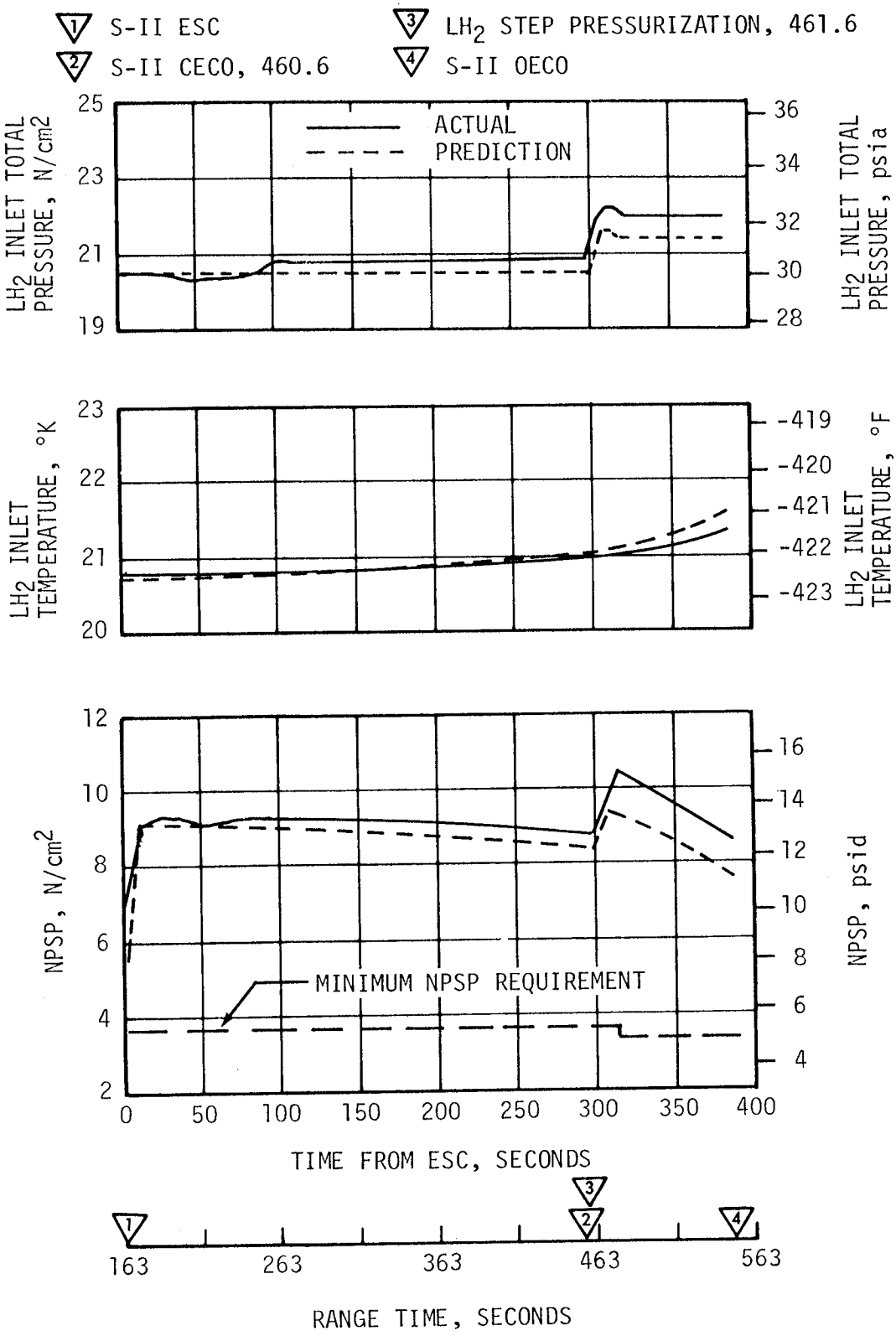

Figure 6-5. S-II Fuel Pump Inlet Conditions

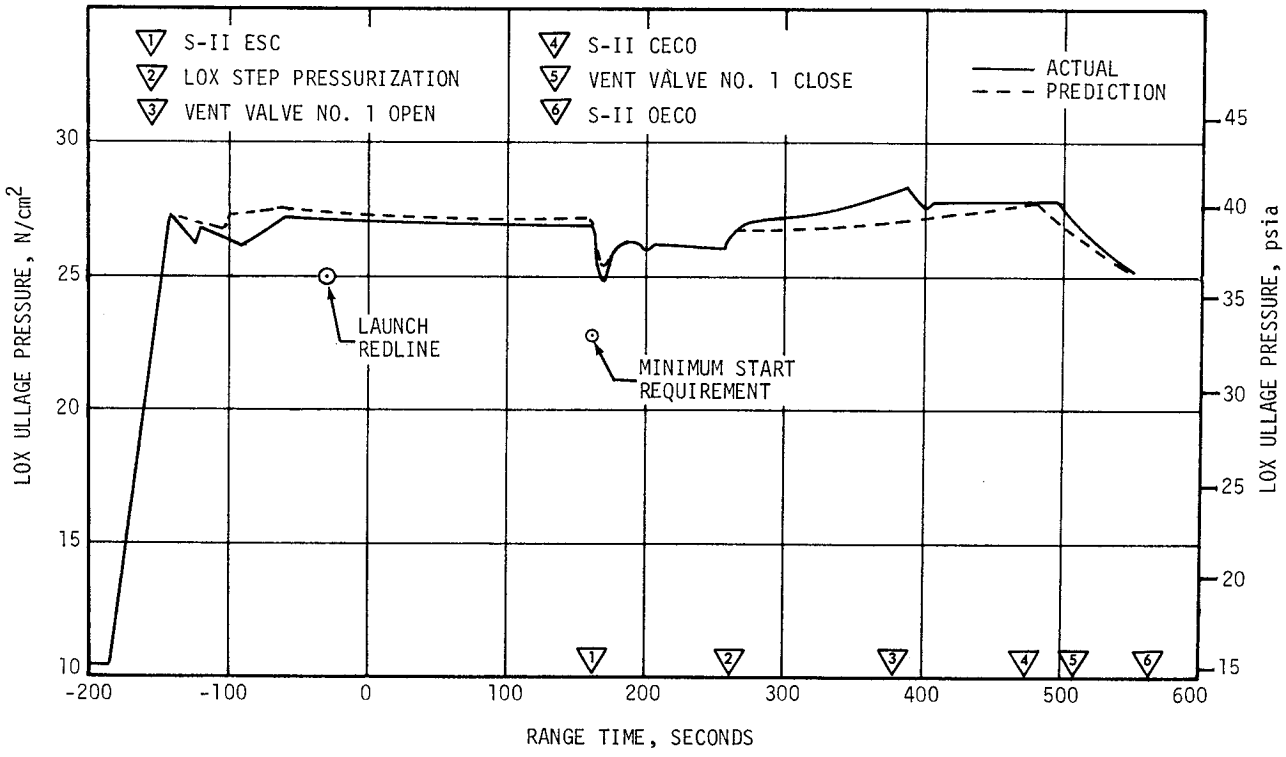

Figure 6-6. S-II LOX Tank Ullage Pressure

6.7 S-II PNEUMATIC CONTROL PRESSURE SYSTEM

Performance of the stage pneumatic control system was satisfactory. Main receiver pressure and regulator outlet pressure were within predicted limits throughout system operation. Regulator outlet pressure was within the operating band of 476 to 527 N/cm^2 (690 to 765 psia) except during valve actuations which follow S-II ESC, CECO and OECO events. The makeup period for the regulator outlet pressure to return to its operating band after valve closures did not exceed 17 seconds. This is within the normal recovery time.

Pressure decay in the main receiver from facility supply vent at -30 seconds to the initial valve actuation at 168 seconds was negligible. Main receiver pressure was 2086 N/cm^2 (3025 psia) at S-II engine start.

6.8 S-II HELIUM INJECTION SYSTEM

The performance of the helium injection system was satisfactory. Requirements were met and parameters were in good agreement with predictions. The supply bottle was pressurized to 2137 N/cm^2 (3100 psia) prior to liftoff and by ESC was 552 N/cm^2 (800 psia). Helium injection system average total flowrate during supply bottle blowdown (-30 to 163 seconds) was 2.0 SCMM (70.4 SCFM).

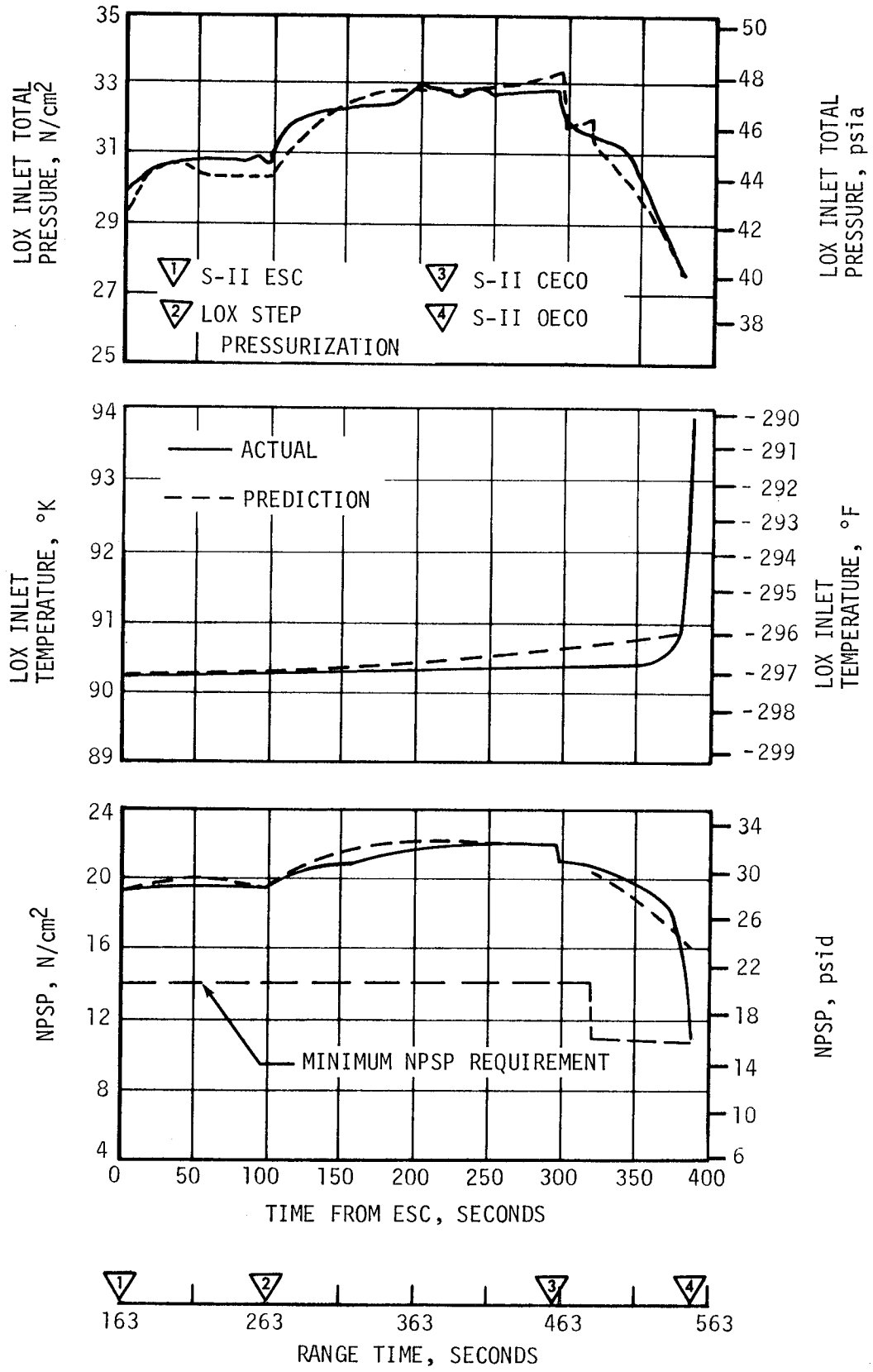

Figure 6-7. S-II LOX Pump Inlet Conditions

SECTION 7

S-IVB PROPULSION

7.1 SUMMARY

The J-2 engine operated satisfactorily throughout the operational phase of first and second burn. Shutdowns for both burns were normal. S-IVB first burn duration was 147.1 seconds which was 3.4 seconds more than predicted. The engine performance during first burn, as determined from standard altitude reconstruction analysis, deviated from the predicted by +0.20 percent for thrust and +0.05 percent for specific impulse. The S-IVB stage first burn Engine Cutoff (ECO) was initiated by the Launch Vehicle Digital Computer (LVDC) at 699.34 seconds.

The Continuous Vent System (CVS) adequately regulated LH_2 tank ullage pressure at 13.4 N/cm^2 (19.5 psia) during orbit, and the Oxygen/Hydrogen (O_2/H_2) burner satisfactorily achieved LH_2 and LOX tank repressurization for restart.

Engine restart conditions were within specified limits. The restart at full open Propellant Utilization (PU) valve position was successful.

S-IVB second burn duration was 346.9 seconds which was 1.7 seconds less than predicted. The engine performance during second burn, as determined from the standard altitude reconstruction analysis, deviated from the predicted by -0.56 percent for thrust and +0.05 percent for specific impulse. The S-IVB stage second burn ECO was initiated by the LVDC at 10,203.07 seconds.

Subsequent to second burn, the stage propellant tanks were safed satisfactorily, with LOX dump imparting a 17 m/s (55.8 ft/s) velocity change to the stage.

7.2 S-IVB CHILLDOWN AND BUILDUP TRANSIENT PERFORMANCE FOR FIRST BURN

The propellant recirculation system performed satisfactorily, meeting start and run box requirements for fuel and LOX as shown in Figure 7-1.

The thrust chamber temperature at launch was well below the maximum allowable redline limit of 172°K (-150°F). At S-IVB first burn Engine Start Command (ESC), the temperature was 164°K (-164°F), which is within the requirement of 150 ±61.1°K (-189.6 ±110°F).

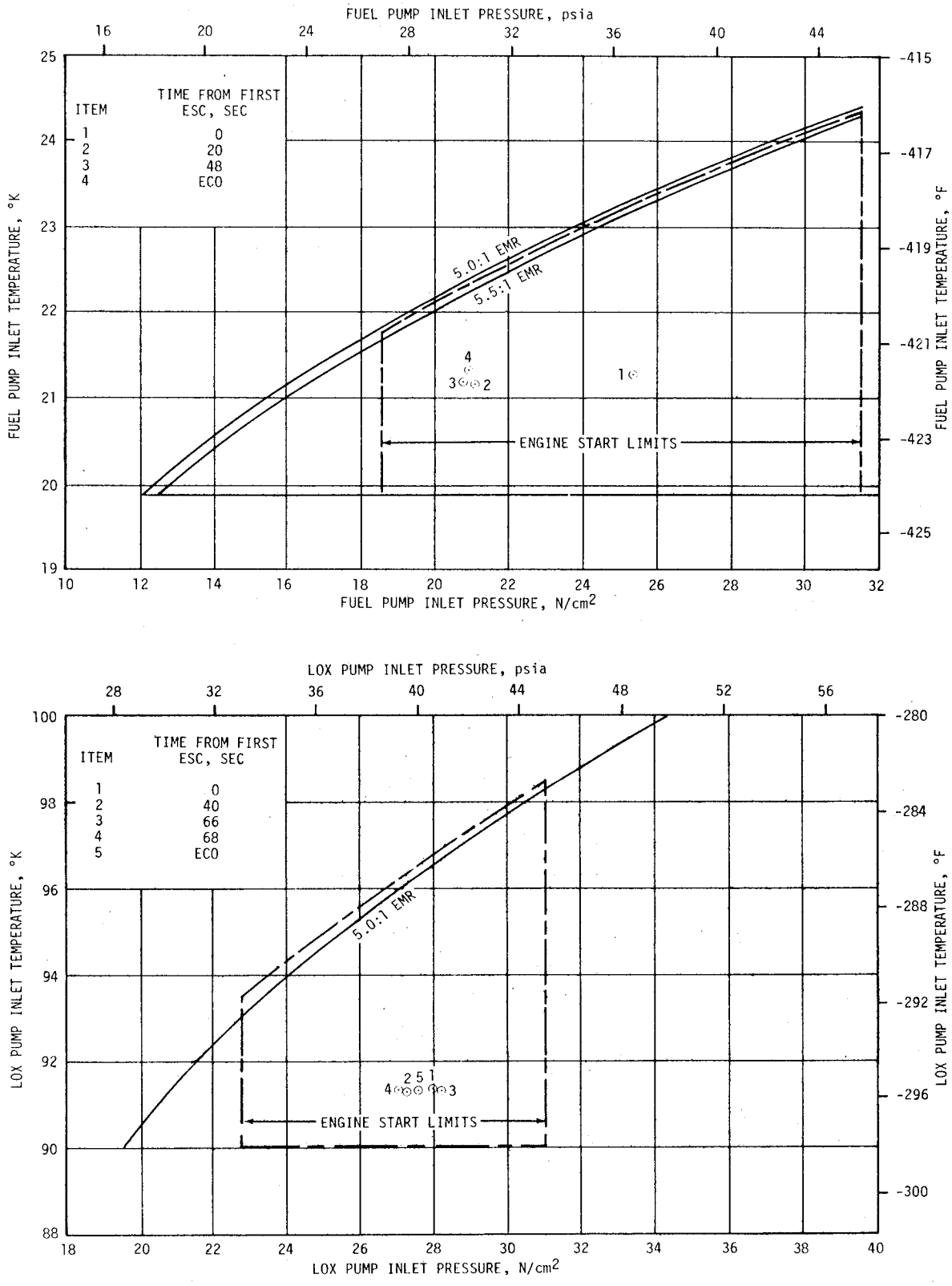

Figure 7-1. S-IVB Start Box and Run Requirements - First Burn

The chilldown and loading of the engine Gaseous Hydrogen (GH_2) start sphere and pneumatic control sphere prior to liftoff were satisfactory. The engine control bottle pressure and temperature at liftoff were 2124 N/cm^2 (3080 psia) and 163°K (-169°F), respectively. At first ESC the start tank conditions were within the required S-IVB region of 896.3 ±68.9 N/cm^2 and 133.1 ±44.4°K (1300 ±100 psia and -220 ±80°F). The discharge was completed and the refill initiated at first burn ESC +3.7 seconds. The refill was satisfactory. The first burn start transient was satisfactory with thrust buildup within the limits set by the engine manufacturer. This buildup was similar to the thrust buildups observed on the AS-501 through AS-505 flights. The PU valve was in proper null position prior to first start. The total impulse from first Start Tank Discharge Valve (STDV) open to STDV +2.5 seconds was 857,243 N-s (192,716 lbf-s). This was more than the value of 833,615 N-s (187,404 lbf-s) obtained during the same interval for the acceptance test.

First burn fuel lead generally followed the predicted pattern and resulted in satisfactory conditions as indicated by the thrust chamber and fuel injector temperatures.

7.3 S-IVB MAINSTAGE PERFORMANCE FOR FIRST BURN

The propulsion reconstruction analysis showed that the stage performance during mainstage operation was satisfactory. A comparison of predicted and actual performance of thrust, total flowrate, specific impulse, and mixture ratio versus time is shown in Figure 7-2. Table 7-1 shows the specific impulse, flowrates and mixture ratio deviations from the predicted at the STDV +137-second time slice when engine performance stabilized. This time slice performance is the standardized altitude performance which is comparable to engine tests. The 137-second time slice performance for first burn thrust was 0.20 percent higher than predicted. Specific impulse performance for first burn was 0.05 percent higher than predicted.

S-IVB burn duration was 147.1 seconds which was 3.4 seconds more than predicted.

The helium control system for the J-2 engine performed satisfactorily during first mainstage operation. Since the engine bottle was connected with the stage ambient repressurization bottles there was little pressure decay. Approximately 0.19 kilogram (0.42 lbm) of helium was consumed during first burn.

The PU valve position shifted slightly away from the null position during engine operation. This shift was in the closed (high Engine Mixture Ratio [EMR]) direction and amounted to 0.7 degree during first burn and 0.6 degree during second burn. These shifts are approximately the same as those observed on the AS-505 flight and the S-IVB-508 and S-IVB-509 acceptance tests. Valve position shifts during engine operation have occurred only in engines with PU valves containing rotated baffles. The magnitude

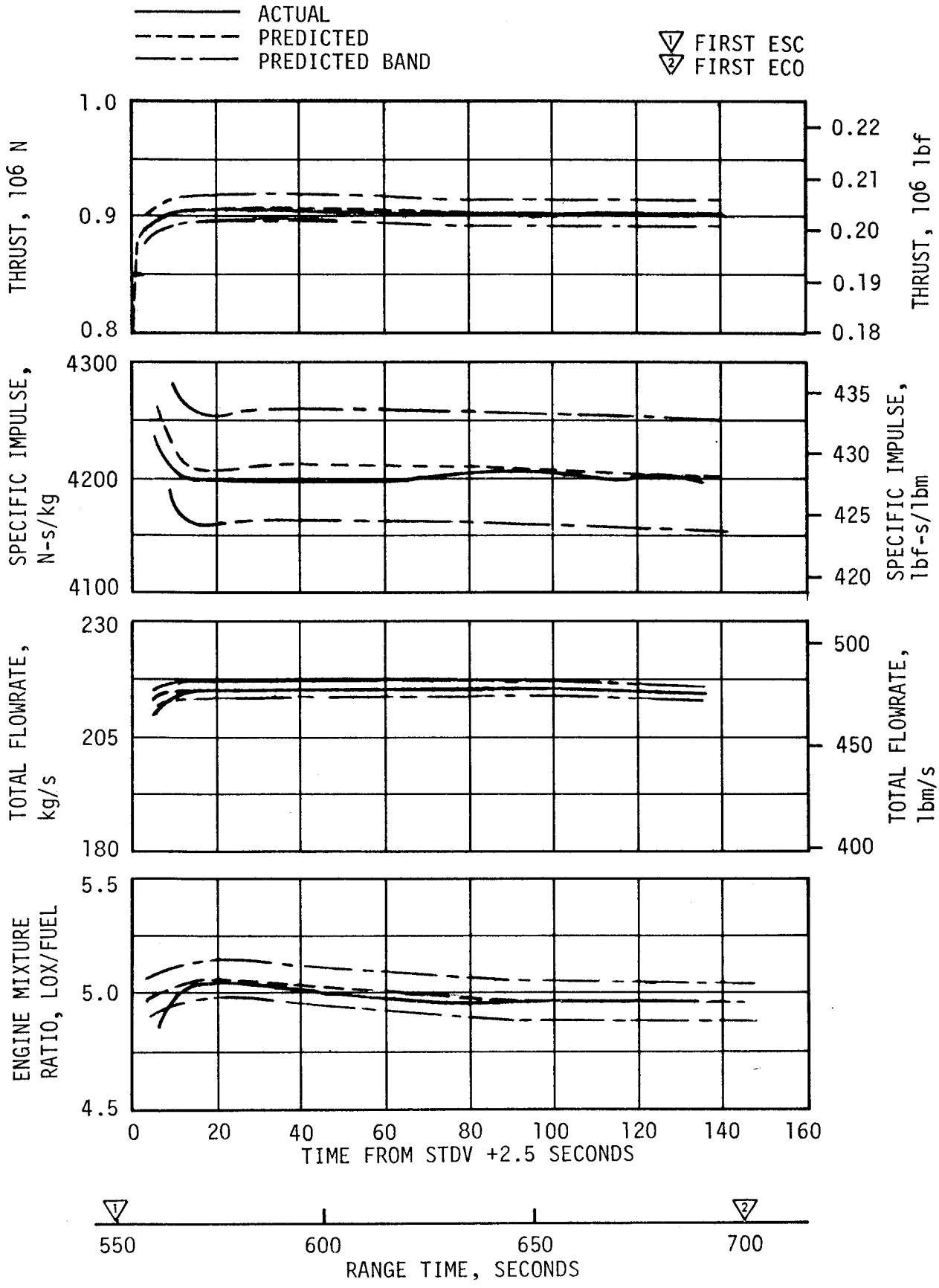

Figure 7-2. S-IVB Steady State Performance - First Burn

Table 7-1. S-IVB Steady State Performance - First Burn (STDV +137-Second Time Slice at Standard Altitude Conditions)

PARAMETER	PREDICTED	RECONSTRUCTION	FLIGHT DEVIATION	PERCENT DEVIATION FROM PREDICTED
Thrust N (lbf)	899,399 (202,193)	901,223 (202,603)	1824 (410)	0.20
Specific Impulse N-s/kg (lbf-s/lbm)	4202 (428.5)	4204 (428.7)	2 (0.2)	0.05
LOX Flowrate kg/s (lbm/s)	177.94 (392.30)	178.24 (392.95)	0.30 (0.65)	0.17
Fuel Flowrate kg/s (lbm/s)	36.09 (79.57)	36.14 (79.67)	0.05 (0.10)	0.14
Engine Mixture Ratio LOX/Fuel	4.930	4.932	0.002	0.04

of the flow forces for a PU valve with a rotated baffle (determined from recent engine manufacturer testing) combined with the PU electronics gain factor (feedback to control) results in an expected valve displacement of approximately 0.75 degree.

It was concluded that the shift in valve position during the AS-506 flight was due largely to the increased flow forces resulting from the rotated baffle and possibly partly due to an electrical phase change. This observed 0.6 to 0.8 degree shift in valve position during null PU operation is expected to occur on AS-507 and subsequent flights.

7.4 S-IVB SHUTDOWN TRANSIENT PERFORMANCE FOR FIRST BURN

S-IVB ECO was initiated at 699.34 seconds by a guidance velocity cutoff command. The ECO transient was satisfactory and agreed closely with the acceptance test and predictions. The total cutoff impulse to zero percent of rated thrust was 188,302 N-s (42,332 lbf-s). Cutoff occurred with the PU valve in the null position.

7.5 S-IVB PARKING ORBIT COAST PHASE CONDITIONING

The LH_2 CVS performed satisfactorily, maintaining the fuel tank ullage pressure at an average level of 13.4 N/cm^2 (19.5 psia).

The continuous vent regulator was activated at 758.5 seconds. Continuous venting was terminated at 9320.4 seconds. The CVS performance is shown in Figure 7-3.

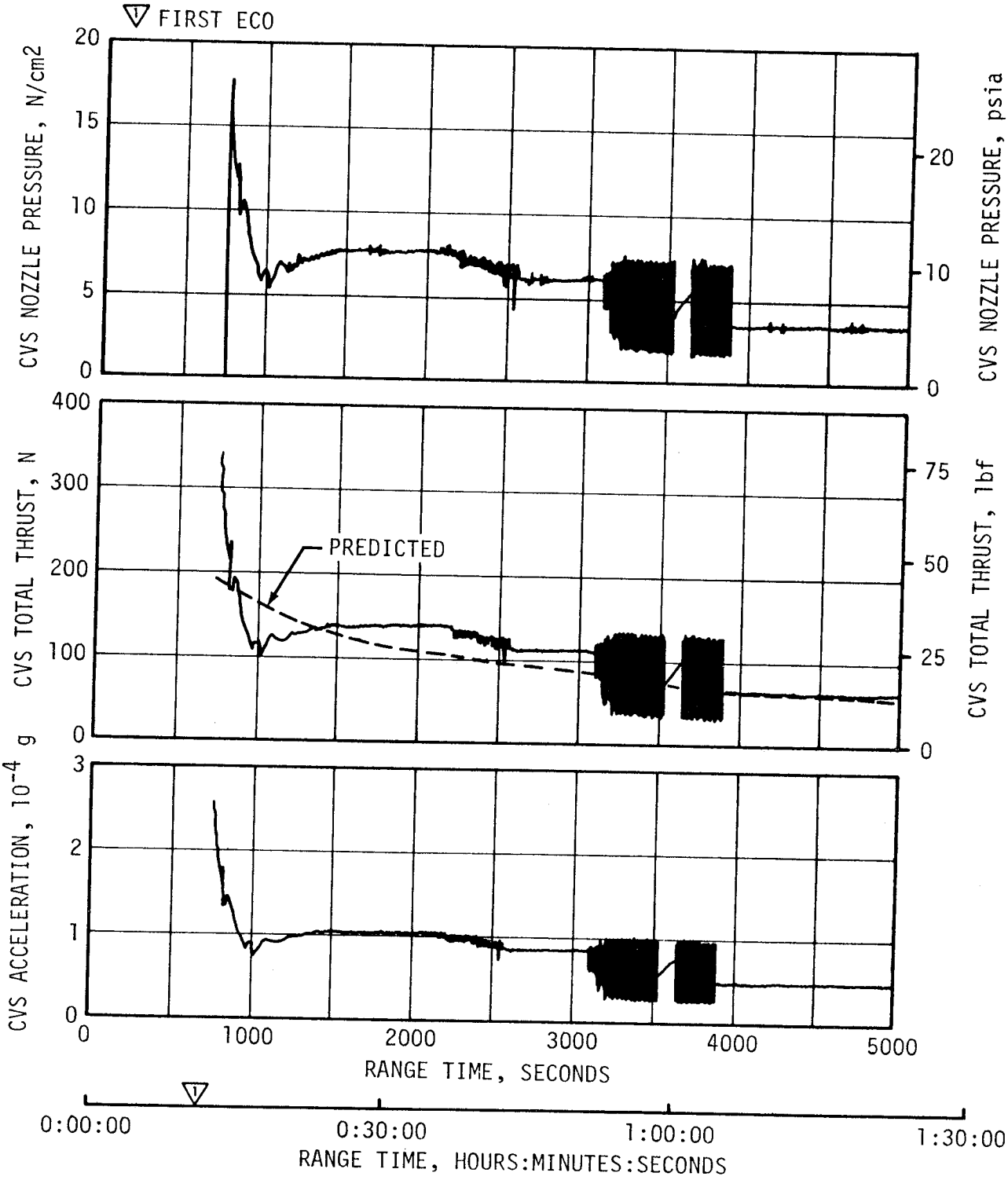

Figure 7-3. S-IVB CVS Performance - Coast Phase (Sheet 1 of 2)

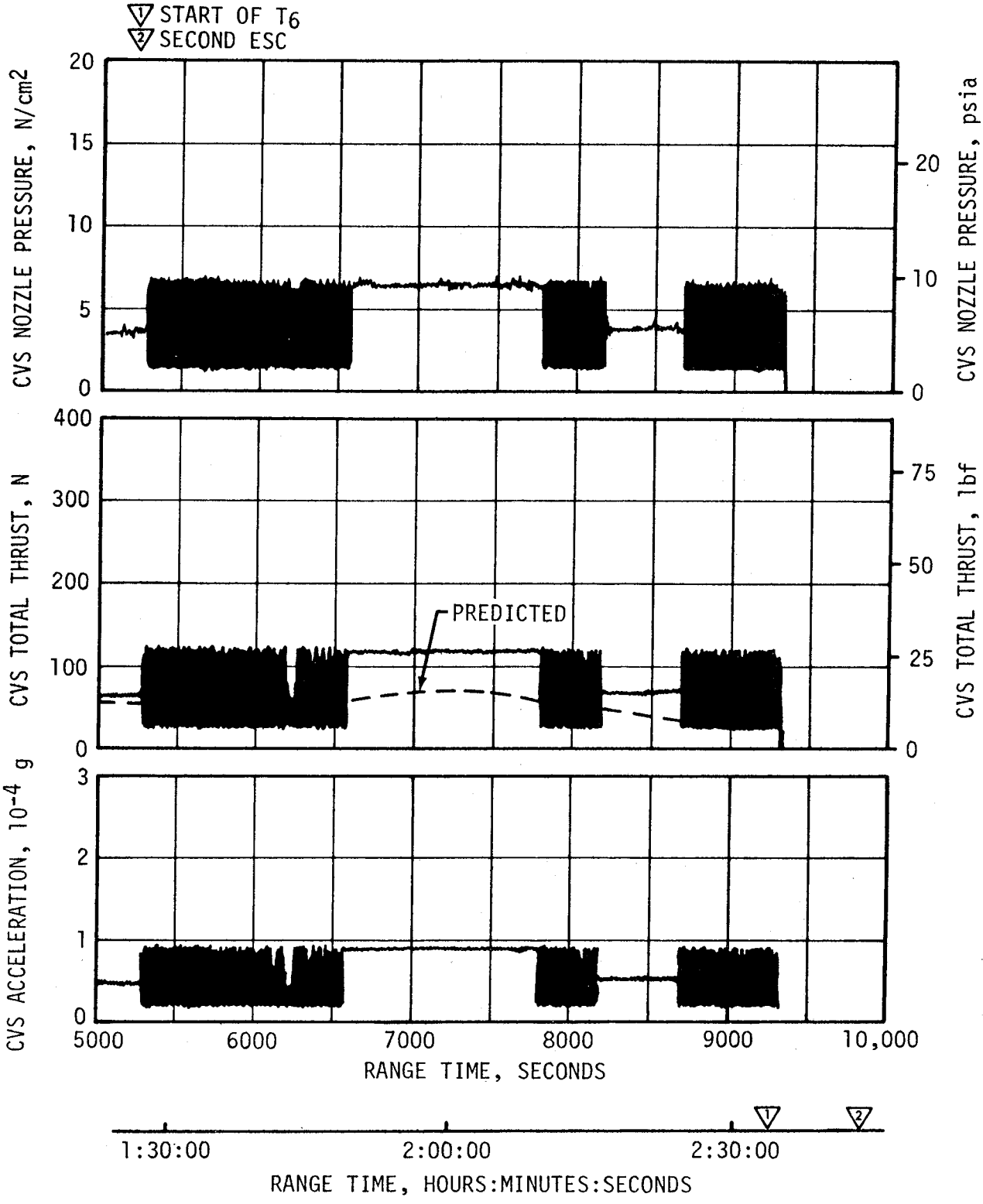

Figure 7-3. S-IVB CVS Performance - Coast Phase (Sheet 2 of 2)

Calculations based on estimated temperatures indicate that the mass vented during parking orbit was 966 kilograms (2130 lbm) and that the boiloff mass was 1081 kilograms (2383 lbm).

7.6 S-IVB CHILLDOWN AND RESTART FOR SECOND BURN

Repressurization of the LOX and LH_2 tanks was satisfactorily accomplished by the O_2/H_2 burner. Helium heater "ON" command was initiated at 9320.2 seconds. The LH_2 repressurization control valves were opened at helium heater "ON" +6.1 seconds and the fuel tank was repressurized from 13.4 to 20.8 N/cm^2 (19.5 to 30.2 psia) in 193.7 seconds. There were 12.1 kilograms (26.7 lbm) of cold helium used to repressurize the LH_2 tank. The LOX repressurization control valves were opened at helium heater "ON" +6.3 seconds and the LOX tank was pressurized from 25.0 to 27.8 N/cm^2 (36.2 to 40.3 psi) in 145.3 seconds. There were 1.95 kilograms (4.3 lbm) of helium used to repressurize the LOX tank. LH_2 and LOX ullage pressures are shown in Figure 7-4. The burner continued to operate for a total of 454.8 seconds providing nominal propellant settling forces. The performance of the AS-506 O_2/H_2 burner was satisfactory as shown in Figure 7-5.

The engine start sphere was recharged properly and maintained sufficient pressure during coast. Between first and second burns, the rate of pressure increase was less than predicted. Also the start bottle relief valve regulated higher than the nominal setting.

The engine control sphere gas usage was as predicted during the first burn; the ambient helium spheres recharged the control sphere to a nominal level adequate for a proper restart.

The S-IVB propellant recirculation systems performed satisfactorily and provided adequate conditioning of propellants to the J-2 engine for the restart as shown in Figure 7-6. Second burn fuel lead resulted in satisfactory conditions as indicated by the thrust chamber and fuel injector temperatures. The start tank performed satisfactorily during the second burn blowdown and recharge sequence.

The second burn start transient was satisfactory with thrust buildup similar to the thrust buildup on flights AS-501 through AS-505. The PU valve was in the proper full open (4.5 EMR) position prior to the second start.

The total impulse from STDV to STDV +2.5 seconds was 794,114 N-s (178,524 lbf-s). This was less than the value of 833,615 N-s (187,404 lbf-s) obtained during the same interval for the acceptance test.

The helium control system performed satisfactorily during second burn mainstage. There was little pressure decay during the burn due to the connection to the stage repressurization system. Approximately 0.553 kilogram (1.22 lbm) of helium was consumed during second burn.

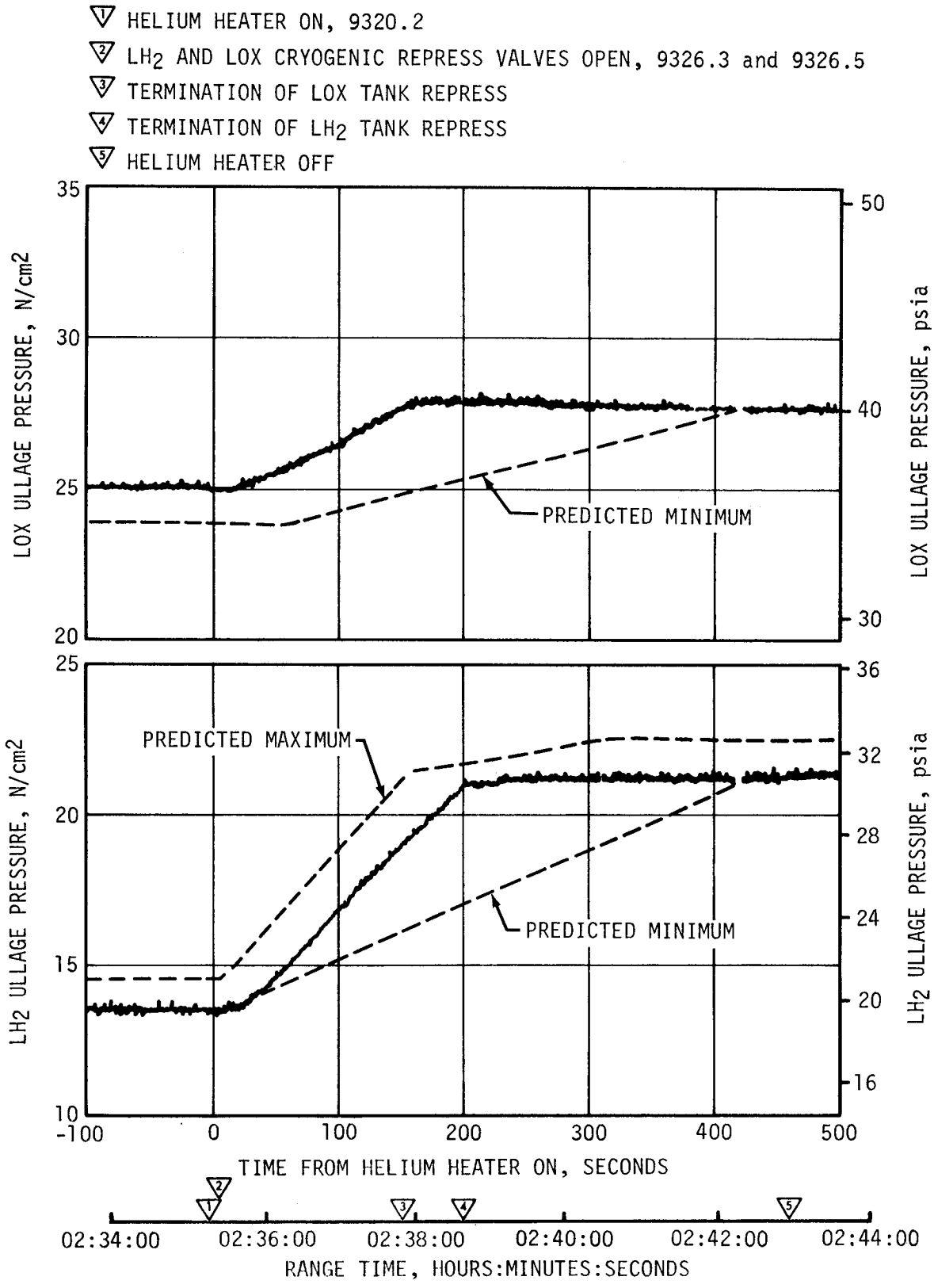

Figure 7-4. S-IVB Ullage Conditions During Repressurization Using O_2/H_2 Burner

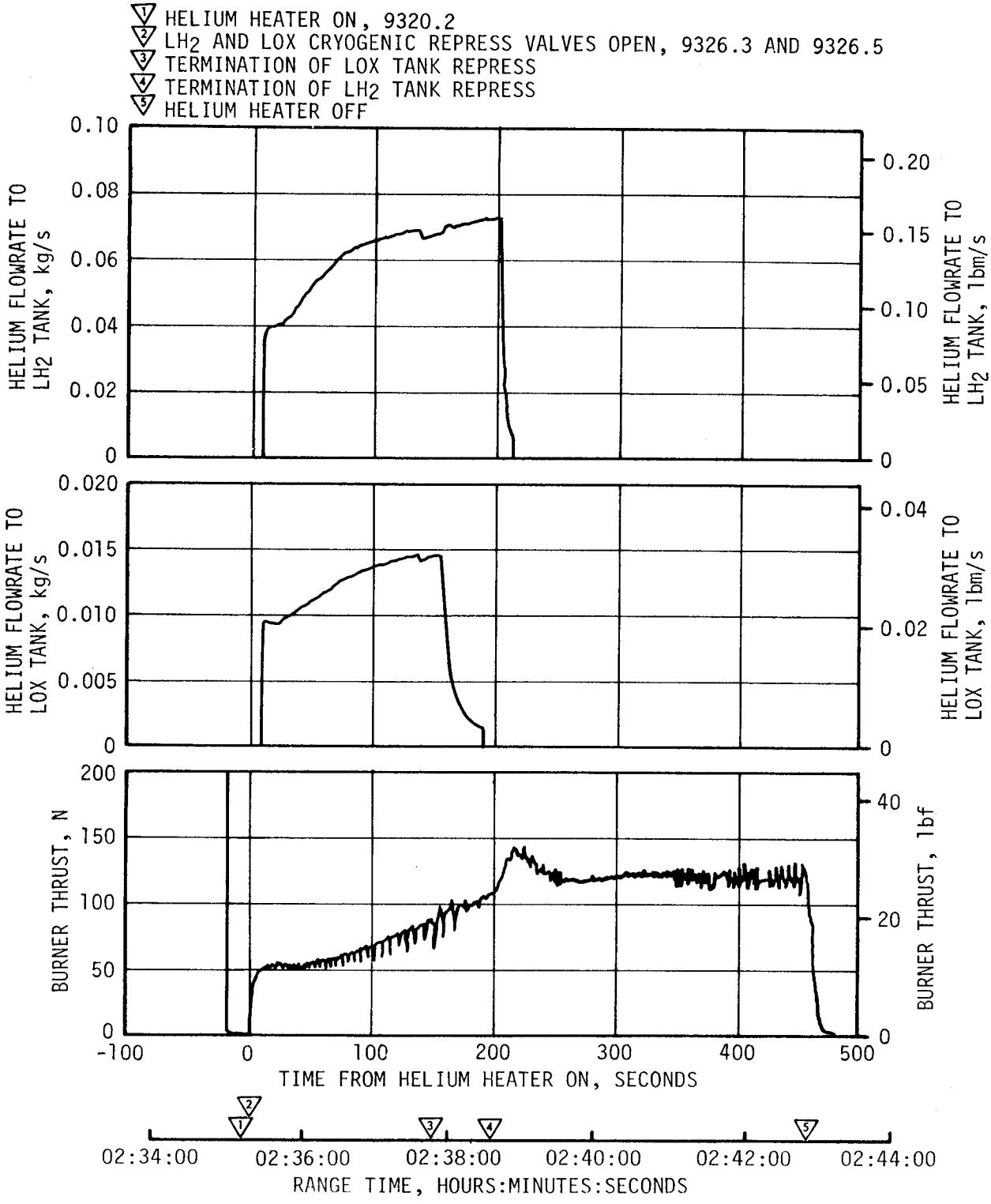

Figure 7-5. S-IVB O_2/H_2 Burner Thrust and Pressurant Flowrates

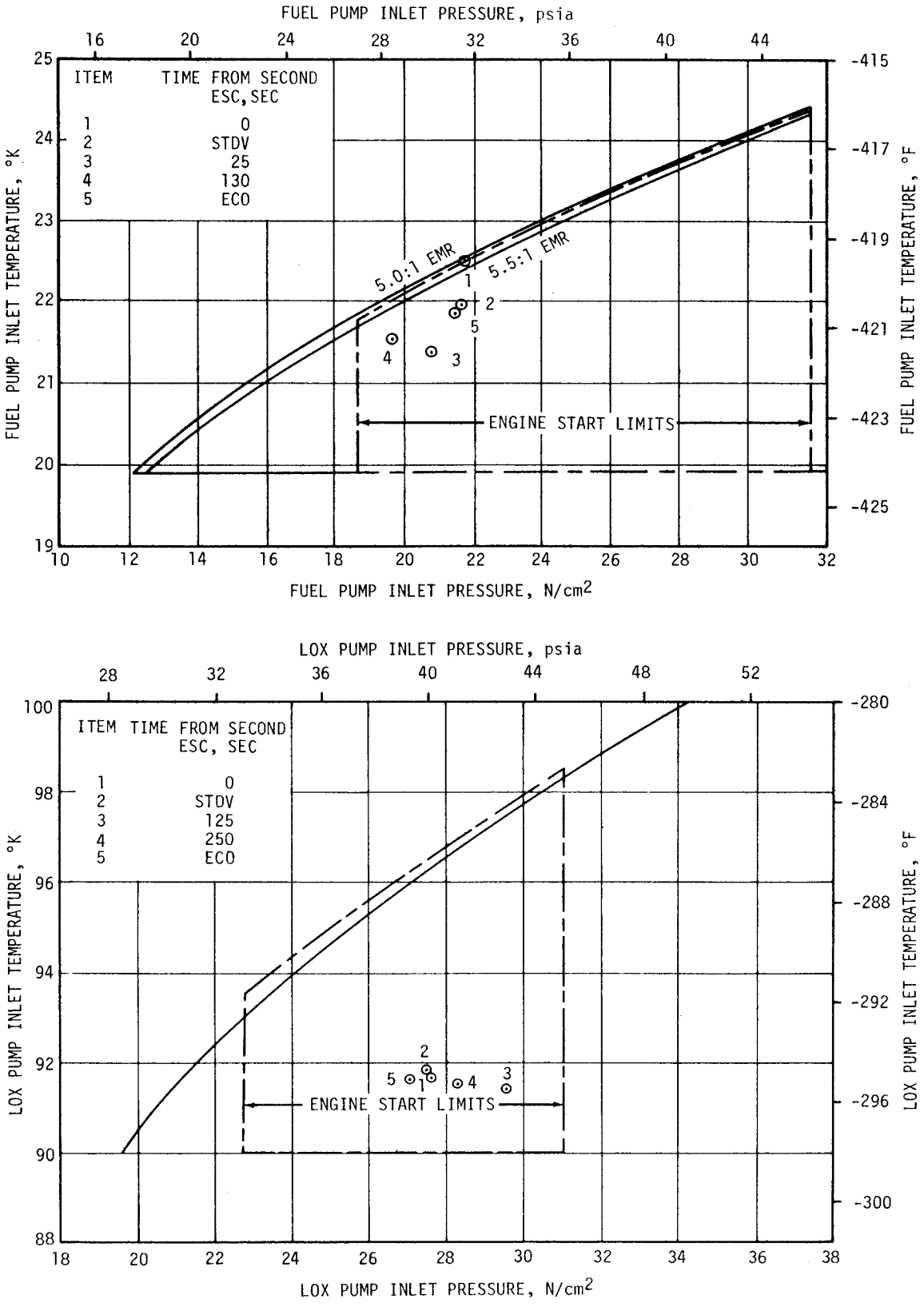

Figure 7-6. S-IVB Start Box and Run Requirements - Second Burn

7.7 S-IVB MAINSTAGE PERFORMANCE FOR SECOND BURN

The propulsion reconstruction analysis showed that the stage performance during mainstage operation was satisfactory. A comparison of predicted and actual performance of thrust, total flowrate, specific impulse, and mixture ratio versus time is shown in Figure 7-7. Table 7-2 shows the specific impulse, flowrates and mixture ratio deviations from the predicted at the STDV +172-second time slice. This time slice performance is the standardized altitude performance which is comparable to the first burn slice at 137 seconds.

The 172-second time slice performance for second burn thrust was 0.56 percent lower than predicted. Specific impulse performance for second burn was 0.05 percent higher than predicted. A shift in performance at the null PU valve position (-1.5 degrees) occurred during second burn. A shift in the Gas Generator (GG) system resistance is suspected as being the cause of the down shift of 6859 Newtons (1542 lbf). Also, during second burn several PU valve system resistance shifts are believed to have occurred.

S-IVB second burn duration was 346.9 seconds which was 1.7 seconds less than predicted.

7.8 S-IVB SHUTDOWN TRANSIENT PERFORMANCE FOR SECOND BURN

S-IVB ECO was initiated at 10,203.07 seconds by a guidance velocity cutoff command which resulted in 1.70 seconds shorter than predicted second burn time. The transient was satisfactory and agreed closely with the acceptance test and predictions. The total cutoff impulse to zero percent of rated thrust was 239,061 N-s (53,743 lbf-s). Cutoff occurred with the PU valve in the null position.

7.9 S-IVB STAGE PROPELLANT MANAGEMENT

The PU system was operated in the open-loop mode. The PU system successfully accomplished the requirements associated with propellant loading.

A comparison of propellant mass values at critical flight events, as determined by various analyses, is presented in Table 7-3. The best estimate full load propellant masses were 0.25 percent greater for LOX and 0.25 percent greater for LH_2 than the predicted values. These deviations were well within the required loading accuracies.

Extrapolation of propellant level sensor data to depletion, using propellant flowrates, indicated that a LOX depletion cutoff would have occurred approximately 12.4 seconds after second burn velocity cutoff.

During first burn, the PU valve was positioned at null for start and remained there, as programed, for the duration of the burn. The PU valve was commanded to the 4.5 EMR position 119.9 seconds prior to second burn start command, and remained there for 246.1 seconds. At second ESC +126.2

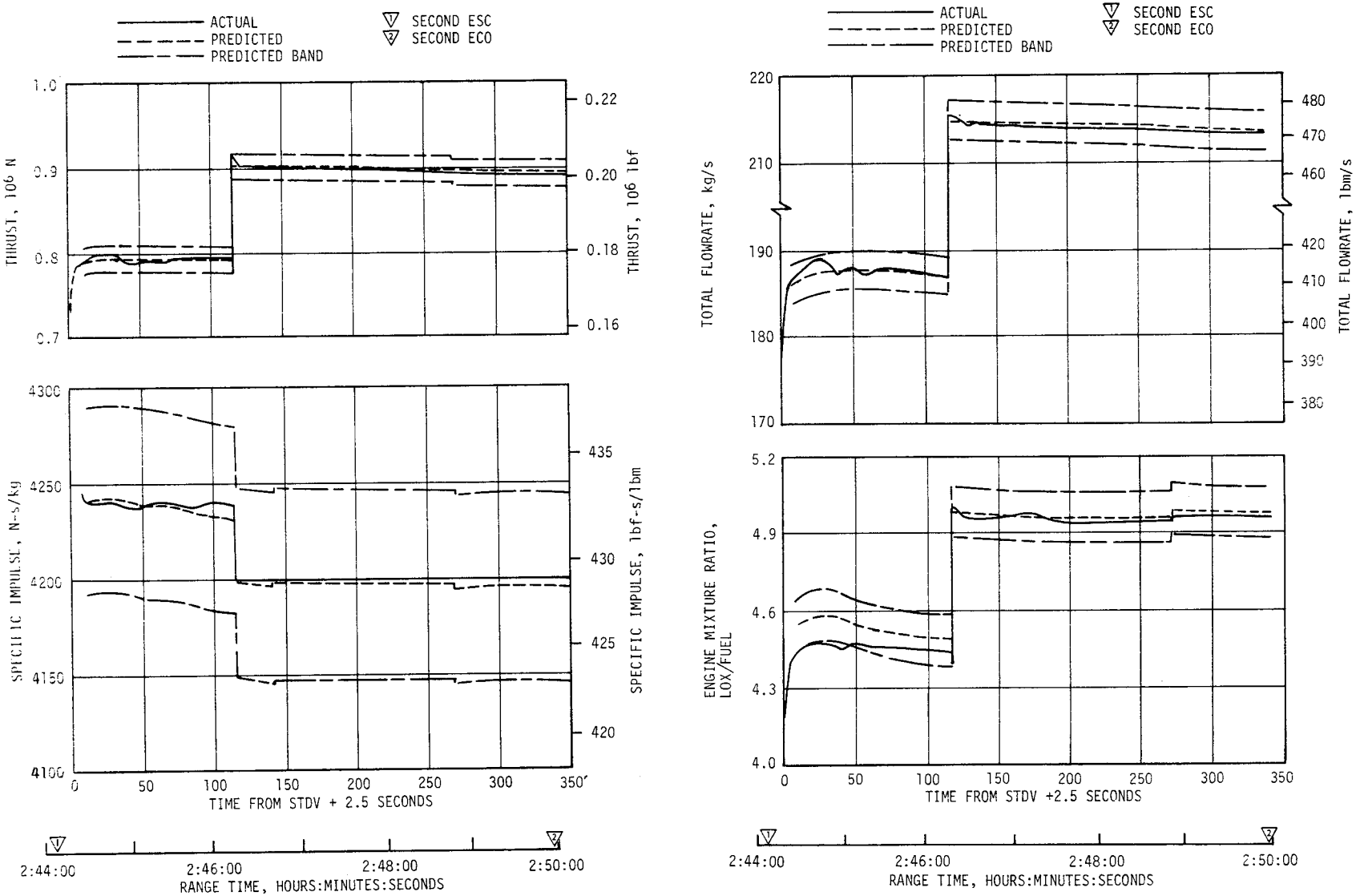

Figure 7-7. S-IVB Steady-State Performance - Second Burn

Table 7-2. S-IVB Steady State Performance - Second Burn (STDV +172-Second Time Slice at Standard Altitude Conditions)

PARAMETER	PREDICTED	SECOND BURN RECONSTRUCTION	FLIGHT DEVIATION	PERCENT DEVIATION FROM PREDICTED
Thrust N (lbf)	899,399 (202,193)	894,364 (201,061)	-5035 (-1132)	-0.56
Specific Impulse N-s/kg (lbf-s/lbm)	4202 (428.5)	4204 (428.7)	2 (0.2)	0.05
LOX Flowrate kg/s (lbm/s)	177.94 (392.30)	176.86 (389.90)	-1.1 (-2.4)	-0.61
Fuel Flowrate kg/s (lbm/s)	36.09 (79.57)	35.88 (79.10)	-0.21 (-0.47)	-0.59
Engine Mixture Ratio LOX/Fuel	4.930	4.929	-0.001	-0.02

Table 7-3. S-IVB Stage Propellant Mass History

EVENT	UNITS	PREDICTED		PU INDICATED (CORRECTED)		PU VOLUMETRIC		FLOW INTEGRAL		BEST ESTIMATE	
		LOX	LH_2	LOX	LH_2	LOX	LH_2	LOX	LH_2	LOX	LH_2
S-IC Ignition	kg (lbm)	87,100 (192,023)	19,731 (43,500)	87,187 (192,215)	19,761 (43,565)	87,360 (192,596)	19,791 (43,631)	87,119 (192,065)	19,753 (43,548)	87,315 (192,497)	19,780 (43,608)
First S-IVB Ignition	kg (lbm)	87,100 (192,023)	19,731 (43,500)	87,187 (192,215)	19,756 (43,555)	87,360 (192,596)	19,786 (43,621)	87,119 (192,065)	19,753 (43,548)	87,315 (192,497)	19,757 (43,557)
First S-IVB Cutoff	kg (lbm)	61,539 (135,670)	14,556 (32,091)	61,242 (135,016)	14,284 (31,491)	61,354 (135,262)	14,380 (31,702)	61,007 (134,497)	14,437 (31,829)	61,300 (135,144)	14,395 (31,736)
Second S-IVB Ignition	kg (lbm)	61,406 (135,377)	13,283 (29,284)	61,124 (134,756)	13,207 (29,116)	61,236 (135,002)	13,303 (29,327)	60,884 (134,227)	13,326 (29,378)	61,151 (134,817)	13,301 (29,324)
Second S-IVB Cutoff	kg (lbm)	2371 (5228)	926 (2043)	2489 (5487)	974 (2147)	2484 (5477)	968 (2133)	2441 (5381)	948 (2089)	2488 (5486)	970 (2139)

seconds the valve was commanded to the null position (approximately 5.0 EMR) and remained there throughout the remainder of the flight.

7.10 S-IVB PRESSURIZATION SYSTEM

7.10.1 S-IVB Fuel Pressurization System

The LH_2 pressurization system operationally met all engine performance requirements during prepressurization, boost, first burn, coast phase, and second burn.

Following the termination of prepressurization, the ullage pressure reached relief conditions, approximately 22.0 N/cm^2 (32.0 psia) and remained at that level until just after liftoff as shown in Figure 7-8. A small ullage collapse occurred during the first 5 seconds of boost, and then returned to the relief level at 70 seconds due to self pressurization. All during the burn the ullage pressure was at the relief level, as predicted.

The LH_2 ullage pressure was 21.4 N/cm^2 (31.0 psia) at second burn ESC as shown in Figure 7-9. Significant venting during second burn occurred at second ESC +280 seconds when step pressurization was initiated. This behavior was as predicted.

The LH_2 pump inlet Net Positive Suction Pressure (NPSP) was calculated from the pump interface temperature and total pressure. Throughout the burn, the NPSP had satisfactory agreement with the predicted. Figures 7-10 and 7-11 summarize the fuel pump inlet conditions for first and second burns, respectively.

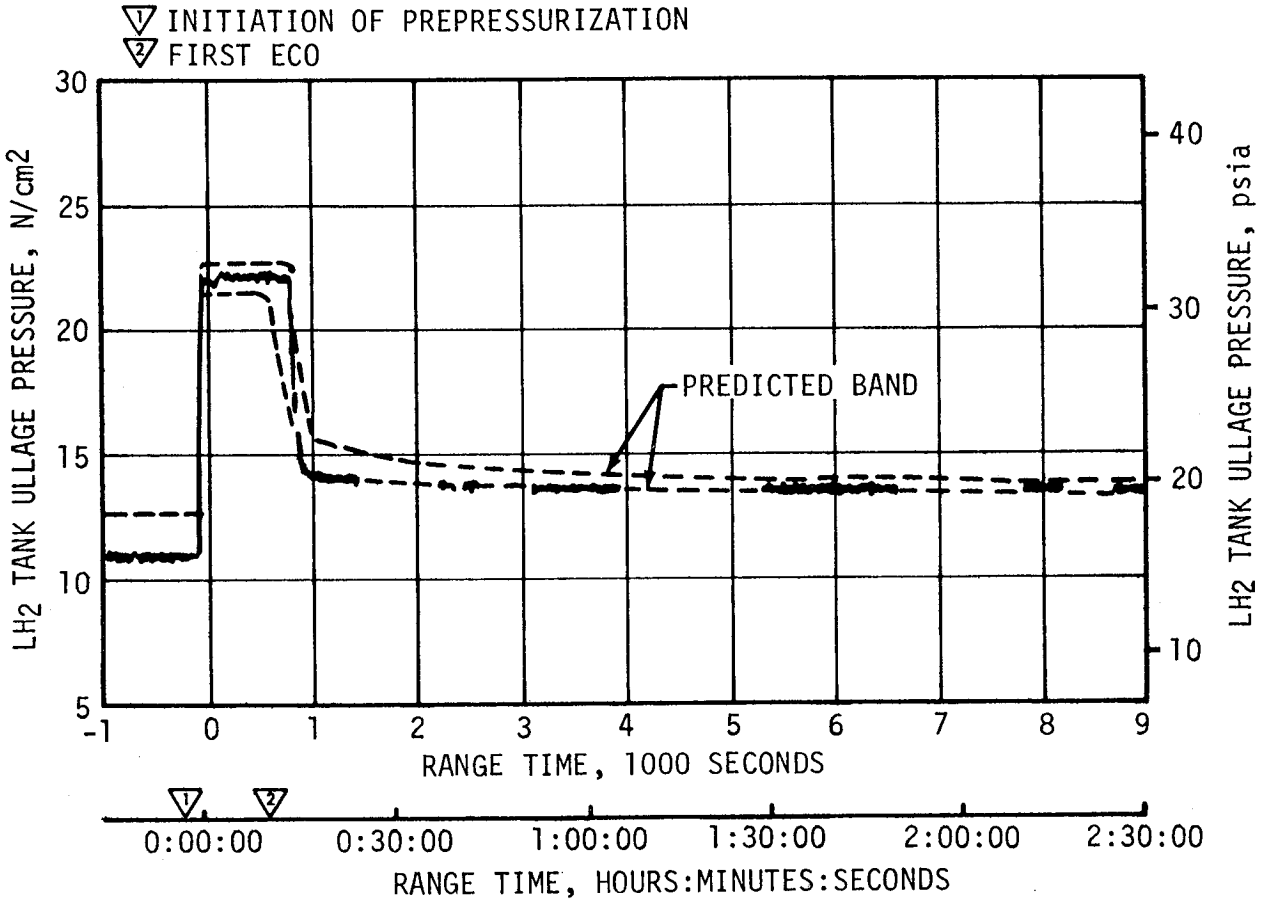

Figure 7-8. S-IVB LH_2 Ullage Pressure - First Burn and Parking Orbit

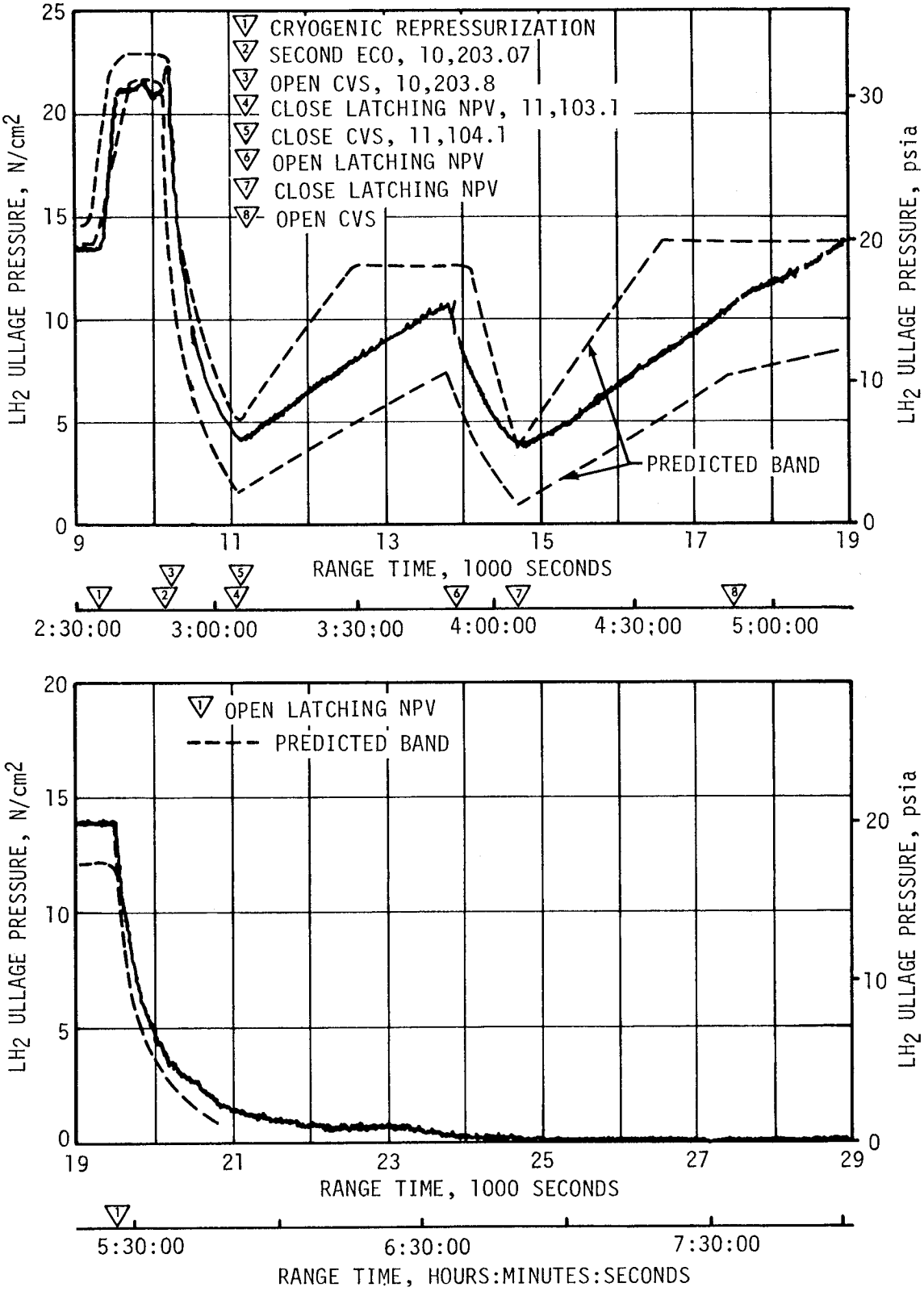

Figure 7-9. S-IVB LH_2 Ullage Pressure - Second Burn and Translunar Coast

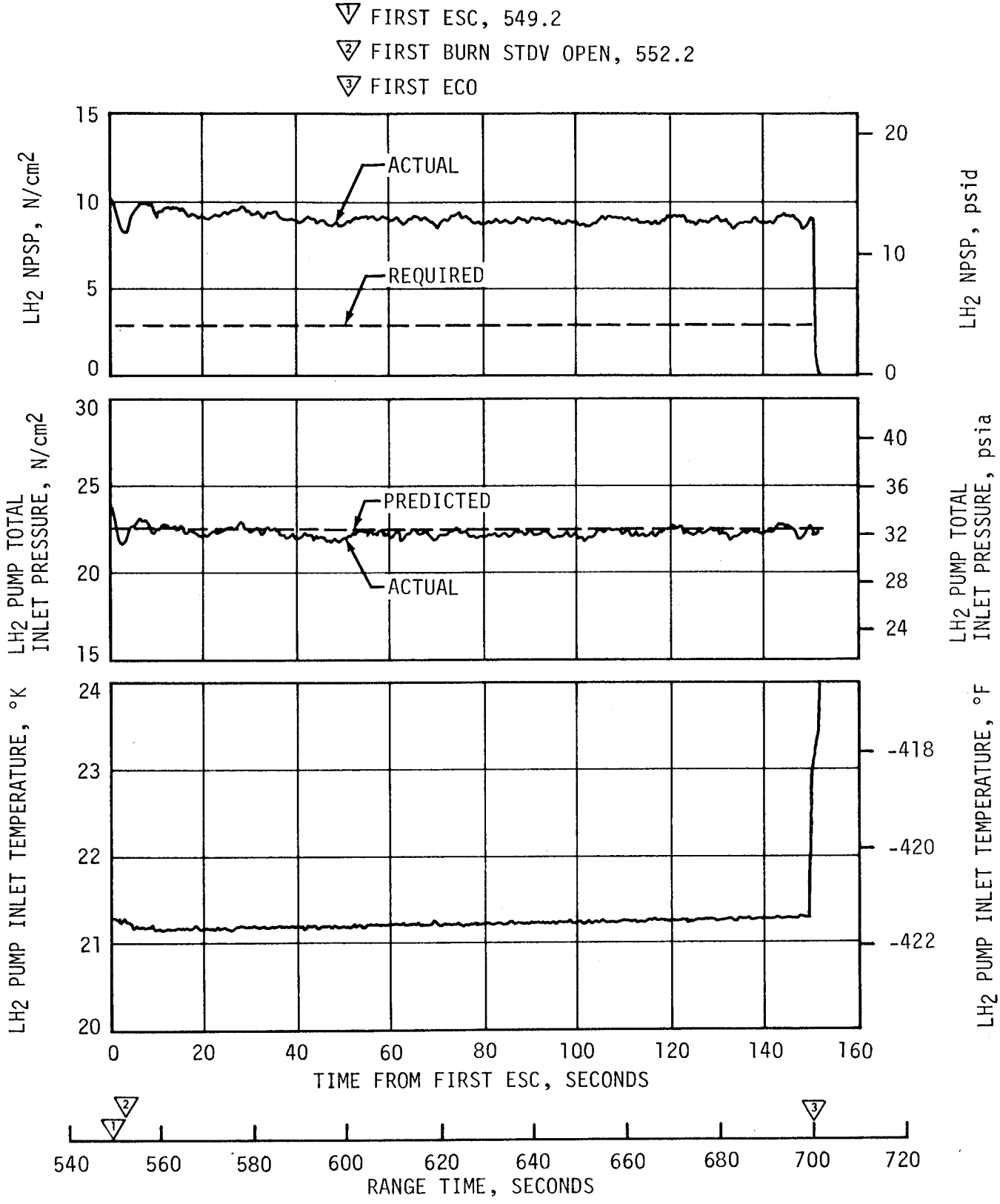

Figure 7-10. S-IVB Fuel Pump Inlet Conditions - First Burn

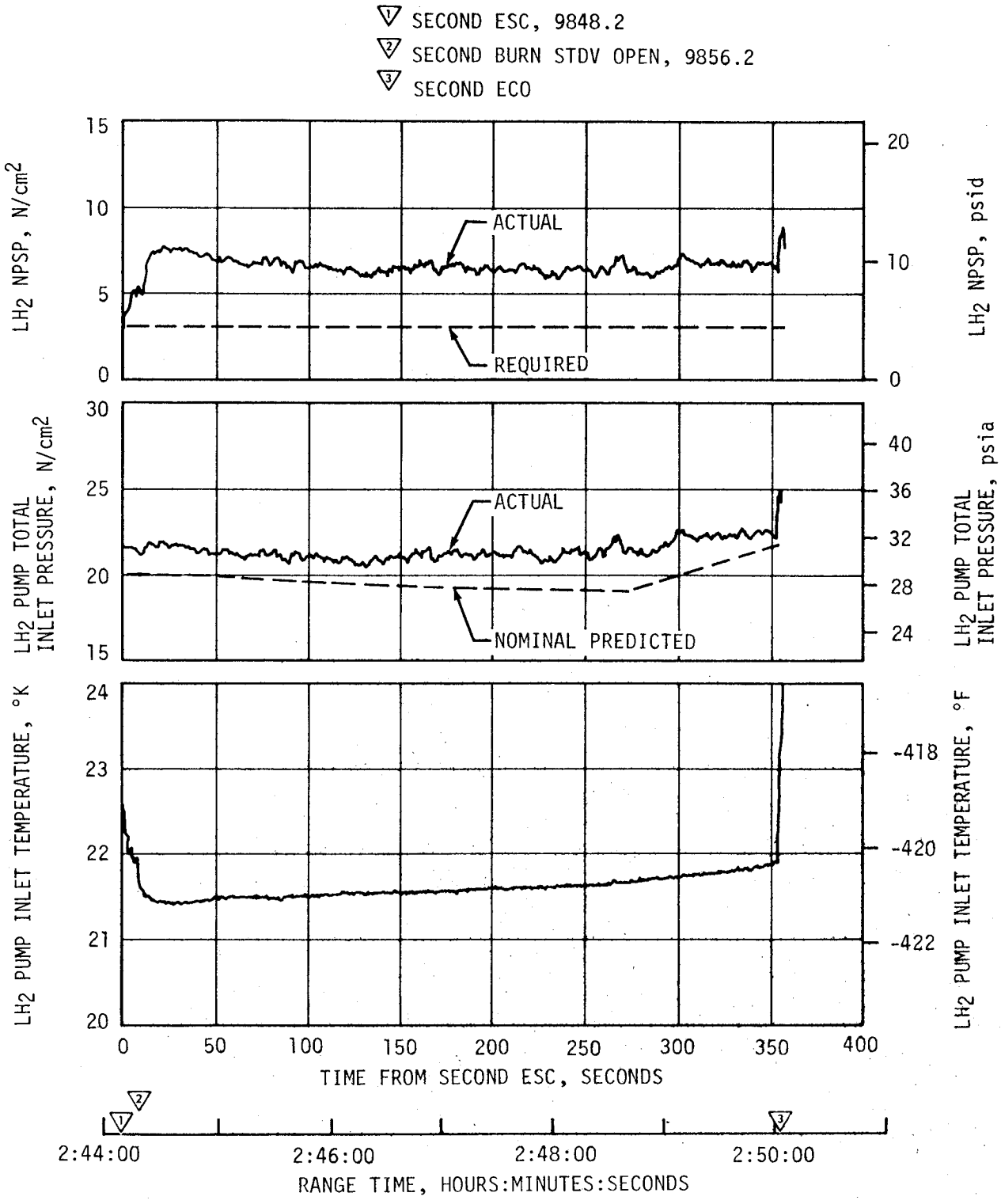

Figure 7-11. S-IVB Fuel Pump Inlet Conditions - Second Burn

7.10.2 S-IVB LOX Pressurization System

LOX tank prepressurization was initiated at -167.5 seconds and increased the LOX tank ullage pressure from ambient to 28.3 N/cm^2 (41.1 psia) within 18.5 seconds as shown in Figure 7-12. Three makeup cycles were required to maintain the LOX tank ullage pressure before the ullage temperature stabilized. At -96 seconds the LOX tank ullage pressure increased from 27.4 to 28.5 N/cm^2 (39.8 to 41.4 psia) due to fuel tank prepressurization, LOX tank vent purge, and LOX pressure sense line purge. These conditions plus boiloff caused the vent/relief valve to open, holding the pressure at 28.8 N/cm^2 (41.8 psia). The pressure remained at this level until lift-off.

During S-IC boost there was a relatively high rate of ullage pressure decay caused by an acceleration effect and subsequent thermal collapse, the decay necessitated one makeup cycle from the cold helium spheres as shown in Figure 7-12.

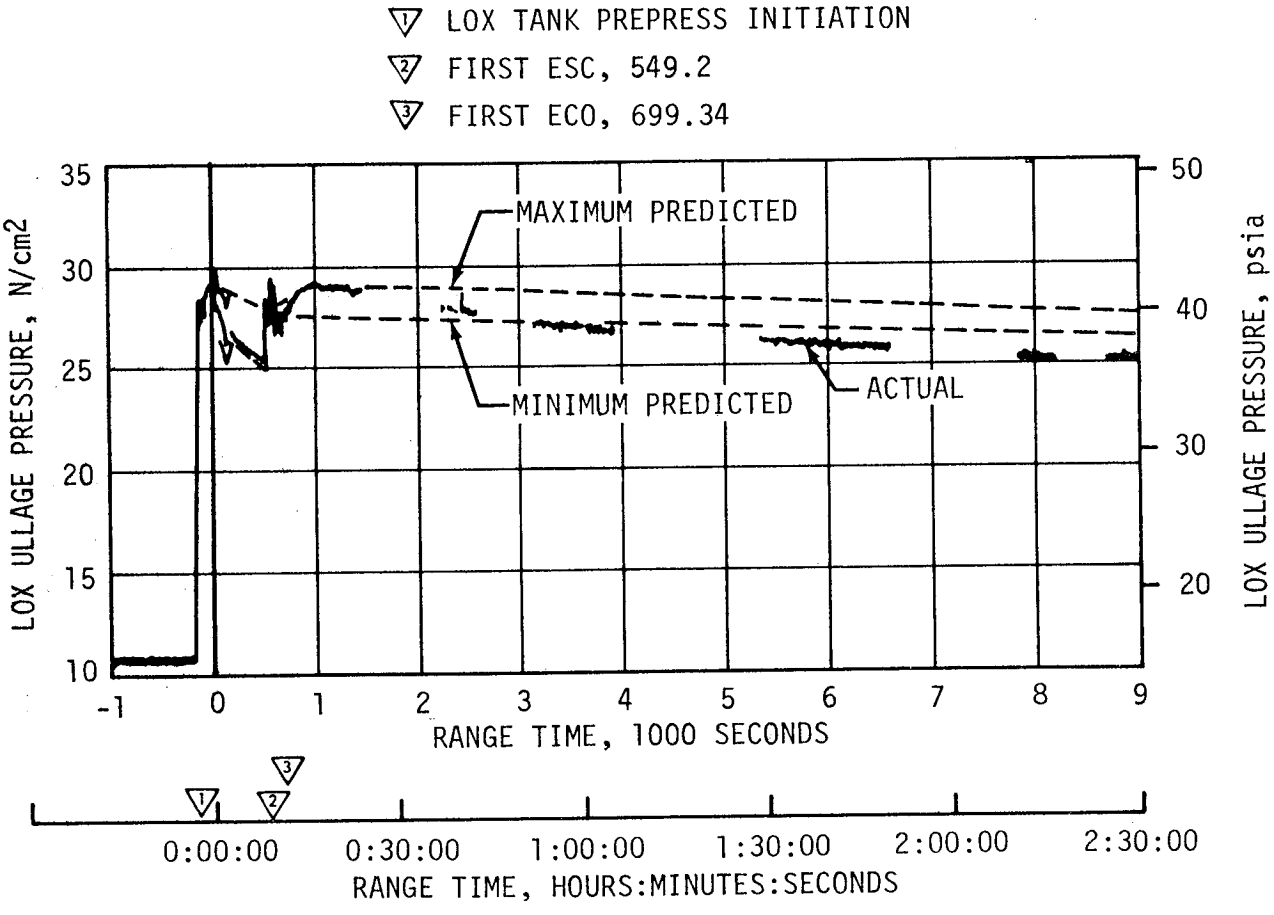

Figure 7-12. S-IVB LOX Tank Ullage Pressure - First Burn and Parking Orbit

One makeup cycle was also required during S-II boost. Although ullage cooling continued during this period, the major cause of the decay again appears to be response to the vehicle acceleration. The LOX tank ullage pressure was 27.7 N/cm^2 (40.2 psia) at ESC.

During S-IVB first burn, three over-control cycles were initiated, as predicted. Heat exchanger performance during first burn was satisfactory.

During the coast period between first and second burns the LOX ullage pressure decreased from 29.0 to 25.0 N/cm^2 (42.1 to 36.2 psia) which was approximately 5 percent below the predicted minimum. Although this decay was not a problem, it was greater than usual. The ullage pressure decay could have been the result of a combination of factors, including bulkhead heat transfer rate, initial coast ullage temperature, localized boiling rates, and perturbations of the stage. The above possibilities are still under investigation. The decay could also have been the result of leakage through the LOX vent system although a leak of this magnitude could not be detected by stage instrumentation, this possibility cannot be completely eliminated.

Repressurization of the LOX tank prior to second burn was required. The tank ullage pressure was increased from 25.0 to 27.9 N/cm^2 (36.2 to 40.4 psia) prior to second ESC. At ESC the pressure was 27.7 N/cm^2 (40.2 psia) satisfying engine start requirements as shown in Figure 7-13.

Pressurization system performance during second burn was satisfactory, having the same characteristics noted during first burn. As predicted, there were no over-control cycles. Heat exchanger performance was satisfactory.

The LOX NPSP calculated at the interface was 16.81 N/cm^2 (24.38 psid) at first burn STDV open. The minimum NPSP during burn was 17.1 N/cm^2 (24.8 psid) at 100 seconds after ESC. This was 11.4 N/cm^2 (16.6 psid) above the required NPSP at that time.

The LOX pump static interface pressure during first burn followed the cyclic trends of the LOX tank ullage pressure. The NPSP calculated at the engine interface was 16.02 N/cm^2 (23.24 psid) at second burn ESC. At all times during second burn, NPSP was above the required level. Figure 7-14 and 7-15 summarize the LOX pump conditions for the first burn and second burn, respectively.

The cold helium supply was adequate to meet all flight requirements. At first burn ESC the cold helium spheres contained 171 kilograms (378 lbm) of helium. At the end of the first burn, the helium mass had decreased to 147 kilograms (325 lbm). At second burn ESC the spheres contained 132 kilograms (292 lbm) of helium. At the end of second burn the helium mass had decreased to 75 kilograms (166 lbm). Figure 7-16 shows helium supply pressure history.

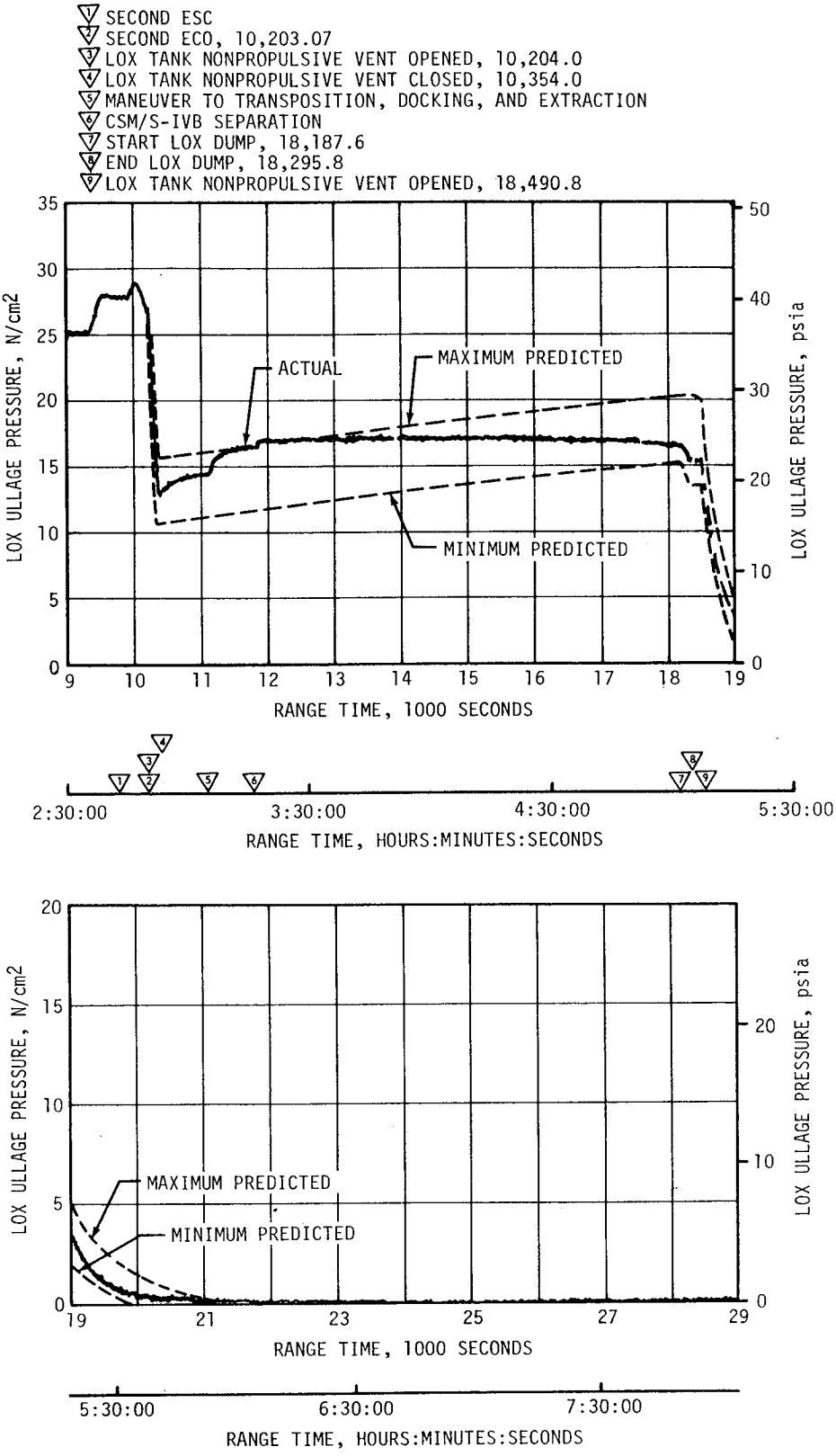

Figure 7-13. S-IVB LOX Tank Ullage Pressure - Second Burn and Translunar Coast

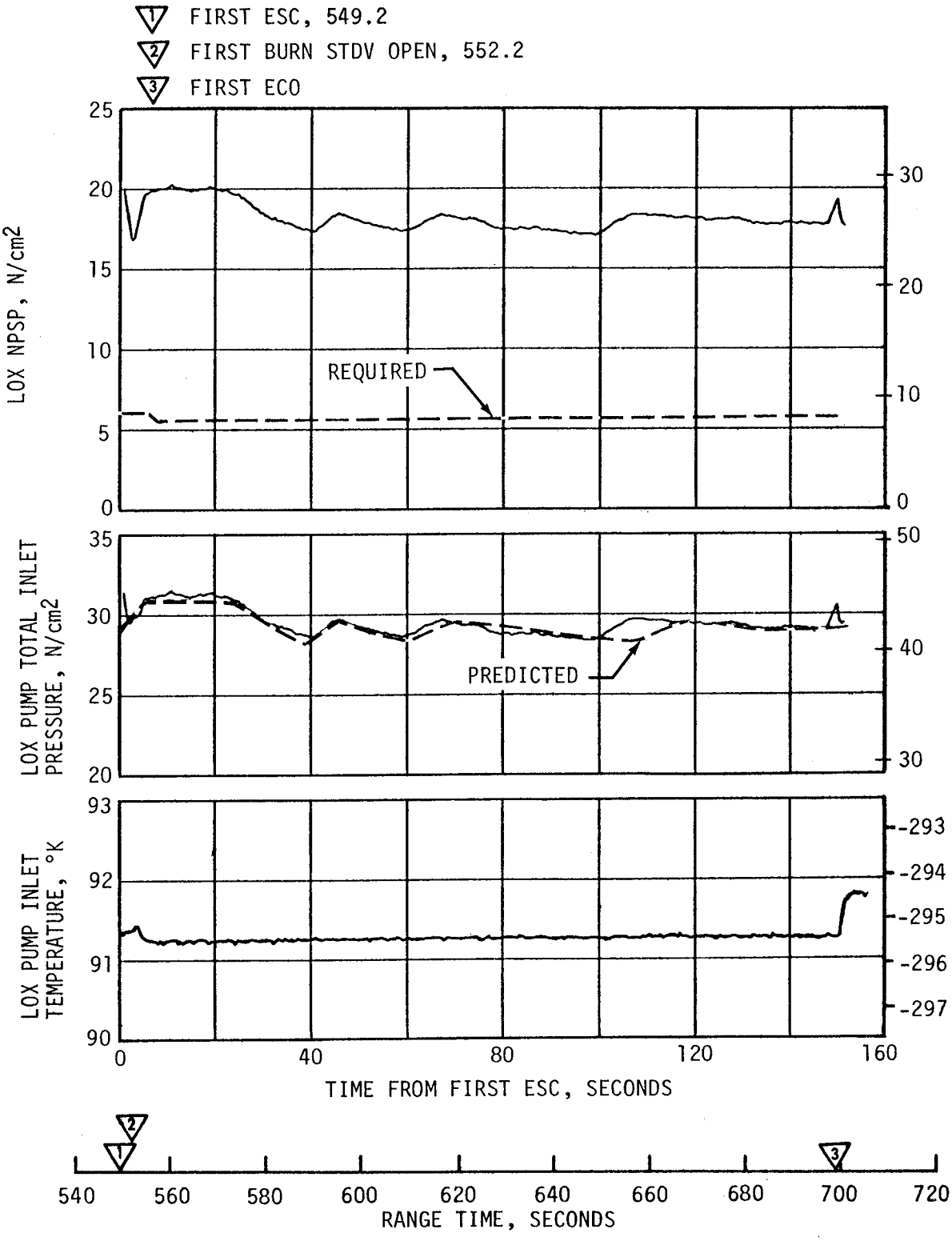

Figure 7-14. S-IVB LOX Pump Inlet Conditions - First Burn

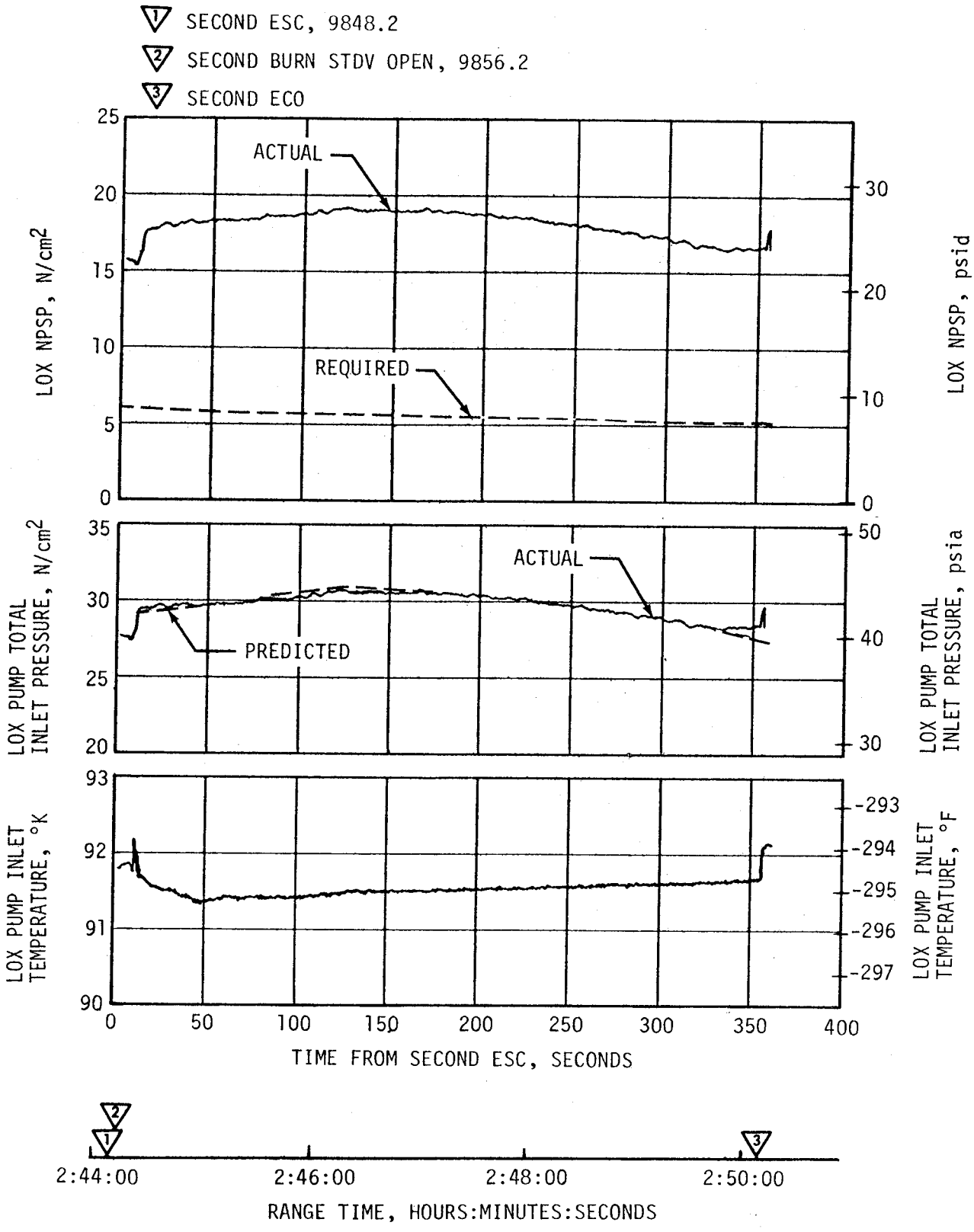

Figure 7-15. S-IVB LOX Pump Inlet Conditions - Second Burn

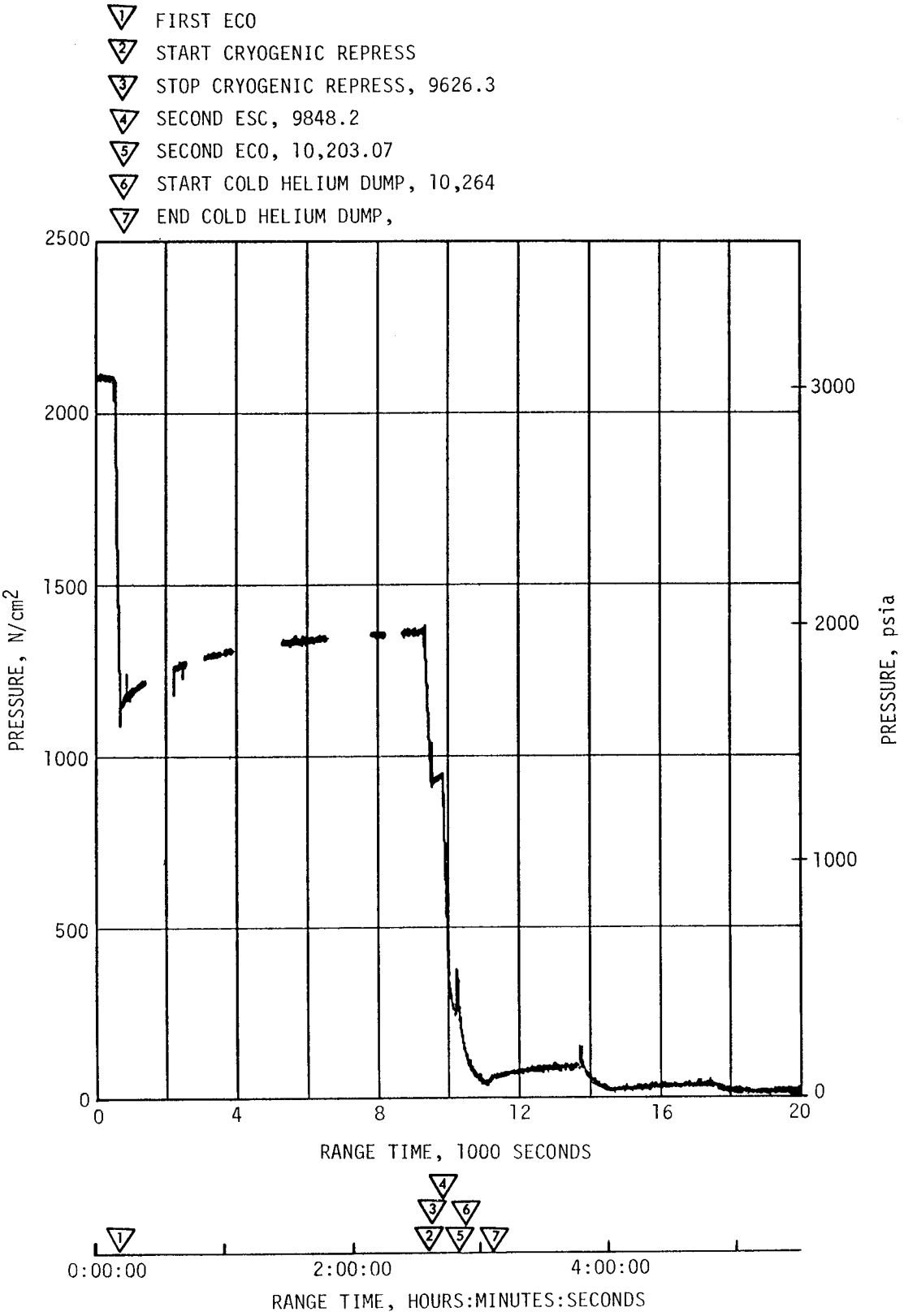

Figure 7-16. S-IVB Cold Helium Supply History

7.11 S-IVB PNEUMATIC CONTROL SYSTEM

The pneumatic control and purge system performed satisfactorily during all phases of the mission. System performance was nominal during boost and first burn operations.

7.12 S-IVB AUXILIARY PROPULSION SYSTEM

The Auxiliary Propulsion System (APS) pressurization system demonstrated nominal performance throughout the flight and met control system demands as required.

System pressures and propellant temperatures are presented in Table 7-4.

All APS engines performed satisfactorily with chamber pressures ranging from 62 to 69 N/cm^2 (90 to 100 psia).

The APS ullage engines were turned on at approximately 700 seconds and 9775 seconds for propellant settling and were turned on a third time at approximately 20,268 seconds to provide additional impulse for the slingshot maneuver.

The propellant consumption curves and predictions are presented in Figure 7-17. Table 7-5 presents the APS oxidizer and fuel consumption at significant events during the flight.

Table 7-4. S-IVB APS Propellant Conditions

PARAMETER	MODULE NO. 1		MODULE NO. 2	
	FUEL	OXIDIZER	FUEL	OXIDIZER
Ullage Pressure N/cm^2 (psia)	131 to 133 (190 to 193)	131 to 133 (190 to 193)	128 to 130 (186 to 188)	131 to 133 (190 to 193)
Propellant Manifold Pressure N/cm^2 (psia)	133 to 135 (193 to 196)	133 to 135 (193 to 196)	130 to 131 (188 to 190)	131 to 132 (190 to 192)
Propellant Temperature (Control Module) °K (°F)	297 to 304 (75 to 87)	300 to 309 (80 to 96)	303 to 315 (86 to 107)	302 to 315 (84 to 107)
Regulator Outlet Pressure N/cm^2 (psia)	128.2 to 134.4 (186 to 195)	128.2 to 134.4 (186 to 195)	134 to 135 (194 to 196)	134 to 135 (194 to 196)

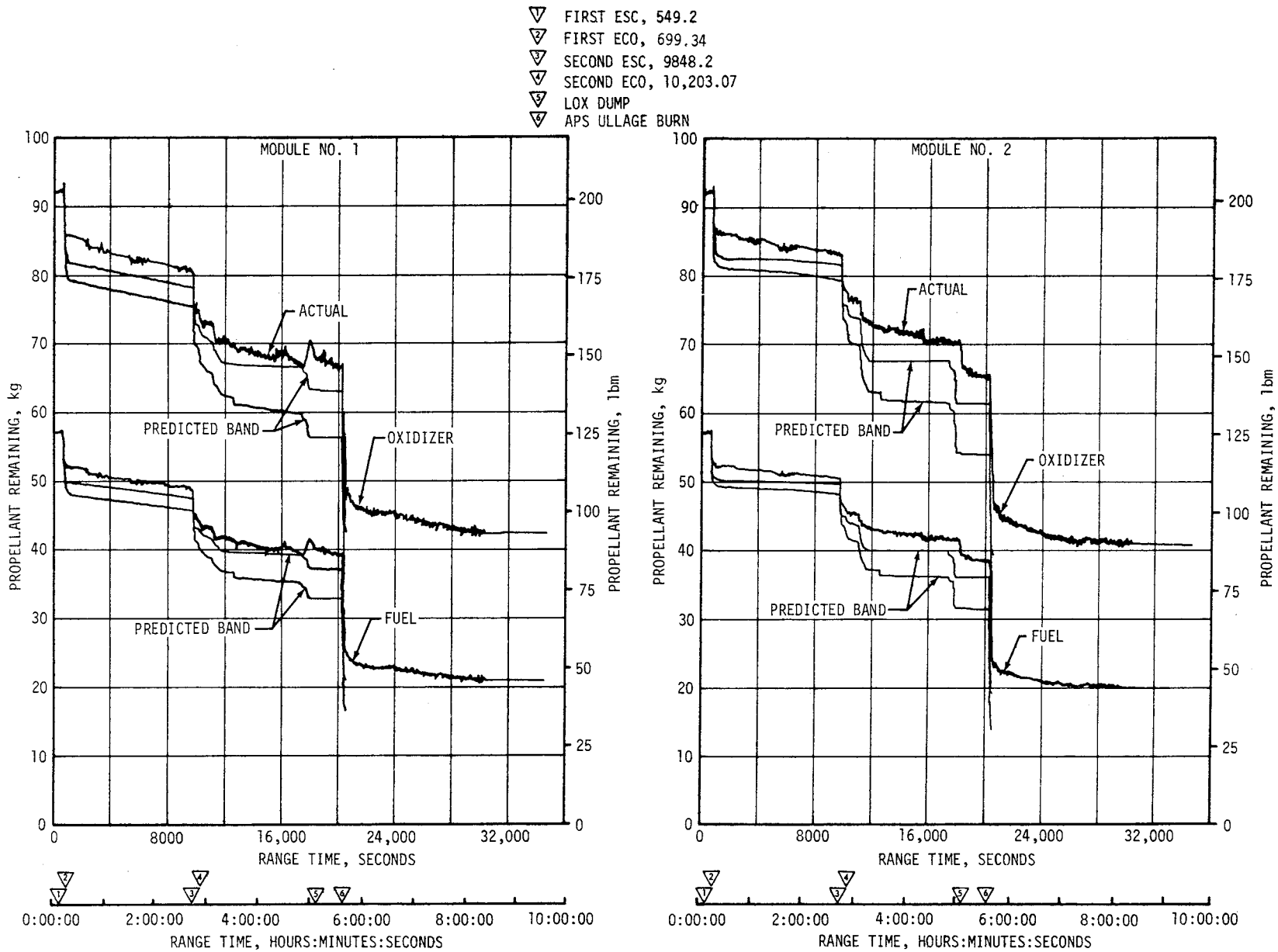

Figure 7-17. S-IVB APS Propellants Remaining Versus Range Time, Module No. 1 and Module No. 2

Table 7-5. S-IVB APS Propellant Consumption

TIME PERIOD	MODULE AT POSITION I				MODULE AT POSITION III			
	OXIDIZER		FUEL		OXIDIZER		FUEL	
	KG	(LBM)	KG	(LBM)	KG	(LBM)	KG	(LBM)
Initial Load	92.16	(203.00)	57.20	(126.00)	92.08	(203.00)	57.20	(126.00)
First Burn (Roll Control)	0.43	(0.95)	0.35	(0.76)	0.43	(0.95)	0.33	(0.72)
ECO to End of First APS Ullaging	7.30	(16.07)	5.52	(12.18)	7.27	(16.02)	5.53	(12.17)
End of First Ullage Burn to Start of T_6	4.48	(9.88)	2.77	(6.11)	2.38	(5.24)	1.48	(3.27)
T_6 to Start of Second Ullage	0.83	(1.83)	0.52	(1.15)	0.12	(0.26)	0.07	(0.16)
Second Ullage Burn	6.12	(13.50)	4.80	(10.58)	5.57	(12.27)	4.34	(9.57)
Second Burn (Roll Control)	0.59	(1.29)	0.38	(0.84)	0.11	(0.25)	0.07	(0.16)
ECO to LOX Dump	4.03	(8.88)	2.52	(5.55)	7.55	(16.64)	4.72	(10.41)
LOX Dump	1.27	(2.80)	0.79	(1.74)	3.18	(7.00)	1.98	(4.37)
LOX Dump to Third Ullage Burn	1.78	(3.92)	1.11	(2.45)	1.45	(3.20)	0.91	(2.00)
Third Ullage Burn	18.06	(39.82)	14.45	(31.85)	19.09	(42.09)	15.09	(33.27)
Third Ullage Burn to Loss of Data	4.60	(10.14)	2.97	(6.55)	4.27	(9.42)	2.67	(5.89)
Total Usage	49.52	(109.08)	36.16	(79.72)	51.41	(113.34)	37.19	(81.99)

7.13 S-IVB ORBITAL SAFING OPERATIONS

7.13.1 Fuel Tank Safing

The LH_2 tank was satisfactorily safed using three programed vent cycles utilizing both the Non Propulsive Vent (NPV) and CVS as indicated in Figure 7-18. The LH_2 tank ullage pressure during safing is shown in Figure 7-9. At second ECO, the LH_2 tank ullage pressure was 22.4 N/cm^2 (32.4 psia) and after three vents had decayed to approximately zero. The mass of GH_2 and LH_2 vented agrees well with the 1174 kilograms (2589 lbm) of liquid residual and pressurant in the tank at the end of powered flight.

7.13.2 LOX Tank Dump and Safing

Immediately following second burn cutoff, a programed 150-second vent cycle reduced LOX tank ullage pressure from 27.2 to 13.0 N/cm^2 (39.4 to 18.9 psia) as shown in Figure 7-13. Data levels were as expected with 32 kilograms (71 lbm) of helium and 50 kilograms (110 lbm) of GOX being vented overboard. As indicated in Figure 7-13, the ullage pressure then increased due to self-pressurization and sloshing to 16.6 N/cm^2 (24.1 psia) at initiation of LOX dump.

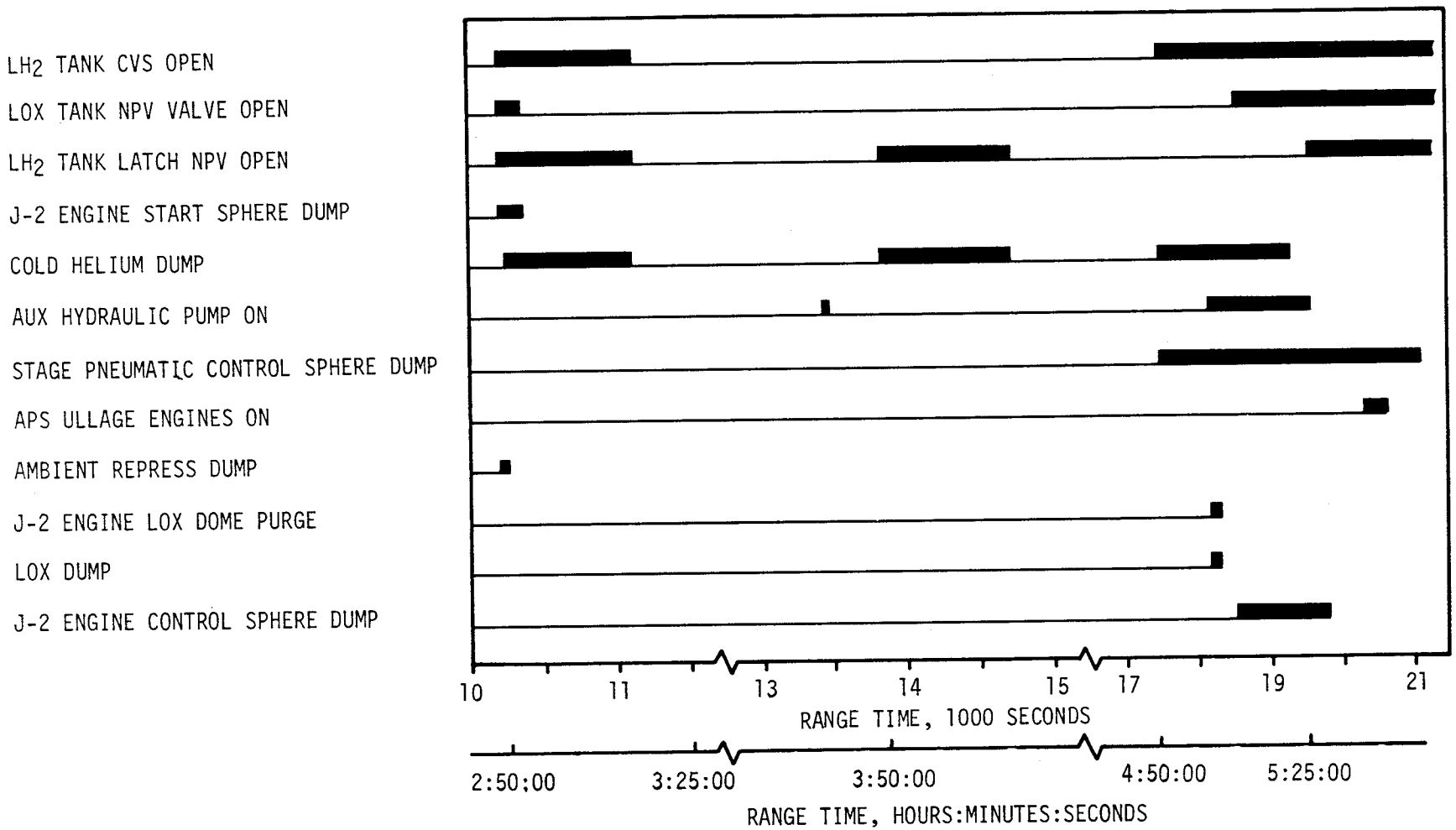

Figure 7-18. S-IVB LOX Dump and Orbital Safing Sequence

The 108-second LOX tank dump was initiated at 18,187.6 seconds and was satisfactorily accomplished. A steady-state liquid flow of 0.024 m^3/s (380.6 gpm) was reached within 50 seconds.

Approximately 79 seconds after dump initiation, the measured LOX flowrate showed a sudden increase indicating that gas ingestion had begun. Shortly thereafter, the LOX ullage pressure began decreasing at a greater rate. Calculations indicate the LOX residual, approximately 921 kilograms (2030 lbm), was essentially dumped within 100 seconds. Ullage gases continued to be dumped until the programed termination. The tank pressure had decayed to 15.4 N/cm^2 (22.4 psig) at this time.

LOX dump ended at 18,295.8 seconds as scheduled by closure of the Main Oxidizer Valve (MOV). A steady-state LOX dump thrust of 4003 Newtons (900 lbf) was obtained. The total impulse before MOV closure was 318,048 N-s (71,500 lbf-s), resulting in a calculated velocity increase of 17 m/s (55.8 ft/s). Figure 7-19 shows the LOX flowrate during dump and the mass of liquid and gas in the oxidizer tank. This figure also shows LOX ullage pressure and the LOX dump thrust produced. The predicted curves provided for the LOX flowrate and dump thrust correspond to the quantity of LOX dumped and the actual ullage pressure.

At 195 seconds after the end of LOX dump the LOX NPV valve was opened for the duration of the mission. LOX tank ullage pressure decayed from 15.5 N/cm^2 (22.5 psia) at 18,490.8 seconds to zero pressure at approximately 24,000 seconds.

7.13.3 Cold Helium Dump

Cold helium was dumped through the $O2/H_2$ burner LH_2 heating coils and into the LH_2 tank, and overboard through the tank vents.

Three separate programed dumps totaling 3537 seconds were made starting at 10,264 seconds, as shown in Figure 7-16. During these periods, the pressure decayed from 365 to 17 N/cm^2 (530 to 25 psia). Approximately 73.9 kilograms (163 lbm) of helium were dumped overboard.

7.13.4 Ambient Helium Dump

The ambient helium in the LOX and LH_2 repress spheres was dumped through the fuel tank. The 60-second dump was commanded on at 10,204.8 seconds and started at 10,221.6 seconds when the LH_2 tank pressure switch dropped out and allowed the repress valve to open. The pressure in the fuel repress spheres decayed from 2124 to 579 N/cm^2 (3080 to 840 psia) and 15.6 kilograms (34.4 lbm) of helium were dumped.

7.13.5 Stage Pneumatic Control Sphere Safing

The stage pneumatic control sphere was safed by initiating the J-2 engine pump purge and flowing helium overboard through the pump seal cavities.

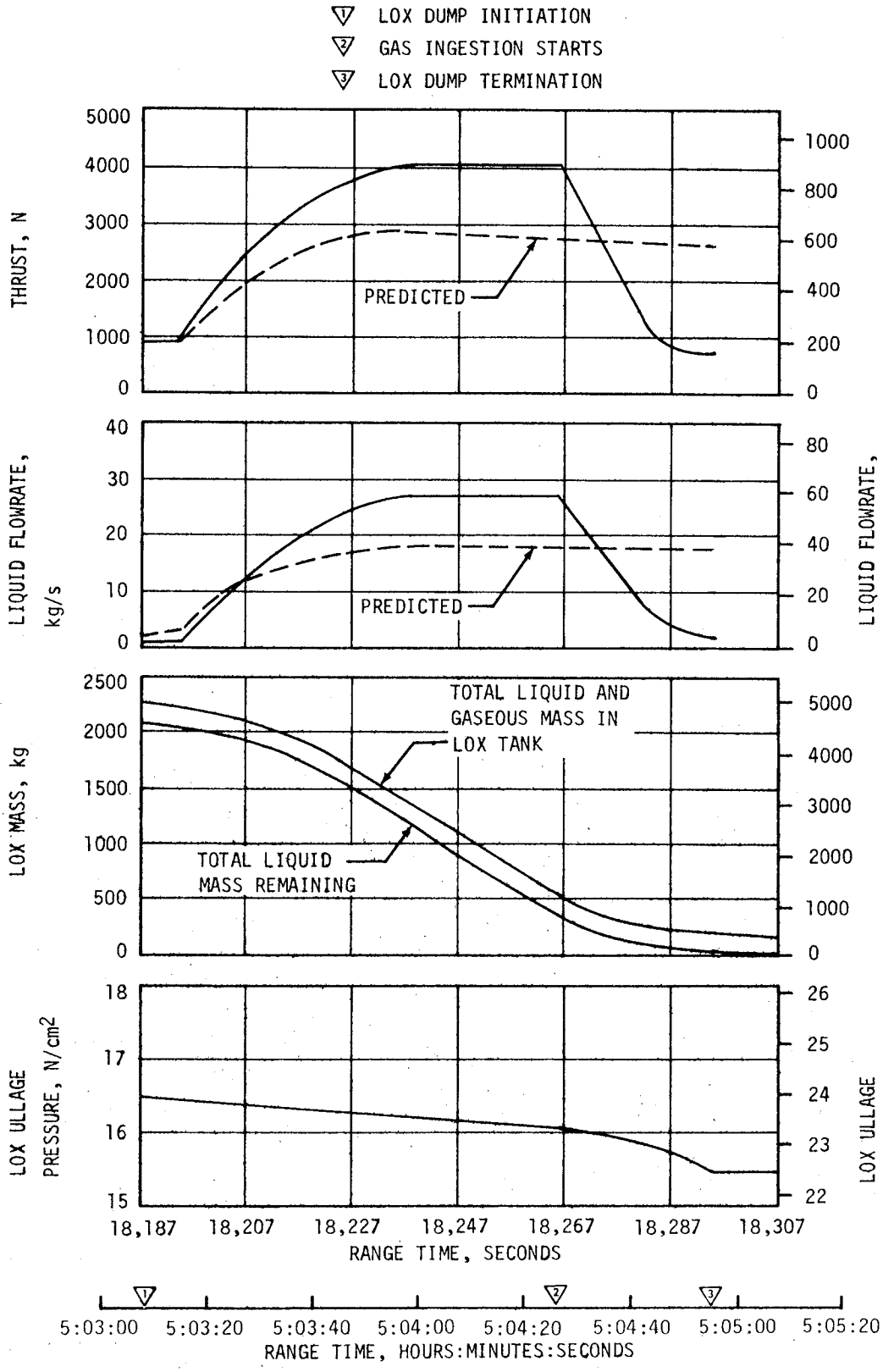

Figure 7-19. S-IVB LOX Dump

The safing period of 3600 seconds satisfactorily reduced the potential energy in the spheres.

7.13.6 Engine Start Sphere Safing

The engine start sphere was safed during an approximately 148-second period starting at 10,206.3 seconds. Safing was accomplished by opening the sphere vent valve. Pressure was decreased from 776 N/cm^2 (1125 psia) to zero with 1.78 kilograms (3.93 lbm) of hydrogen being vented.

7.13.7 Engine Control Sphere Safing

The engine control sphere safing began at 18,505 seconds. The helium control solenoid was energized to flow helium overboard through the engine purge system. The pressure decayed from 1379 to 103.4 N/cm^2 (2000 to 150 psia) and 0.680 kilogram (1.50 lbm) of helium was vented during the 1300-second safing period.

SECTION 8

HYDRAULIC SYSTEMS

8.1 SUMMARY

The stage hydraulic systems performed satisfactorily on the S-IC, S-II, and first burn and coast phase of the S-IVB stage. During this period all parameters were within specification limits.

The S-IVB hydraulic system pressure exceeded the upper limit by 0.6 percent just after second burn ignition and remained at this level until 202 seconds into the burn. At this time a step decrease in system pressure to a normal operating level occurred. The pressure remained at this level for the remainder of the burn. Other than this minor deviation system performance was nominal and no other problems were noted.

The manufacturer of the S-IVB engine driven hydraulic pump states that the pump has an output pressure "drift-up" characteristic that could account for this excess pressure. The abrupt pressure changes noted during the burn are probably due to frictional hysteresis within the engine driven pump pressure/flow-regulating mechanism. The pump manufacturer does not consider this condition to indicate impending malfunction of the engine driven pump.

8.2 S-IC HYDRAULIC SYSTEM

The performance of the S-IC hydraulic system was satisfactory. All servoactuator supply pressures, and return pressures and temperatures were within required limits.

8.3 S-II HYDRAULIC SYSTEM

System steady-state supply pressures during flight ranged from 2400 to 2468 N/cm^2 (3480 to 3580 psia) with steady-state reservoir pressures ranging from 63 to 70 N/cm^2 (92 to 101 psia). These pressures were well within the predicted ranges of 2275 to 2620 N/cm^2 (3300 to 3800 psia) and 54 to 72 N/cm^2 (78 to 105 psia), respectively. Reservoir volumes at Engine Cutoff (ECO) ranged from 16 to 21 percent, well within the predicted range of 12 to 34 percent. Reservoir fluid temperatures at ECO

ranged from 304 to 319°K (88 to 115°F) compared to a predicted 300 to 328°K (80 to 130°F). The reservoir fluid temperatures and rate of increase of these temperatures compared well with predicted values.

Throughout the flight, all servoactuators responded to commands with good precision. The maximum difference between actuator command and position was 0.2 degree. Forces acting on the actuators were well below a predicted maximum of 84,516 Newtons (19,000 lbf). The maximum force in tension was 32,027 Newtons (7200 lbf) acting on the pitch actuator of engine No. 1. The maximum force in compression was 35,586 Newtons (8000 lbf) acting on the pitch actuator of engine No. 1.

8.4 S-IVB HYDRAULIC SYSTEM

The S-IVB hydraulic system performance was nominal during S-IC/S-II boost and S-IVB first burn. The supply pressure was nearly constant at 2503 N/cm^2 (3630 psia) as compared to an allowable of 2425 to 2527 N/cm^2 (3515 to 3665 psia). System flow requirement was provided by the engine driven hydraulic pump during first burn as indicated by a rise in system pressure after ignition and an auxiliary pump motor current draw of 19.5 amperes. Power extraction by the engine driven pump during burn was 3.64 kw (4.88 horsepower).

Engine deflections were nominal during first burn.

During orbital coast, two hydraulic system thermal cycles of 48 seconds duration were programed to start at 3300 and 6100 seconds.

The auxiliary hydraulic pump was turned on at 9497.2 seconds during second burn prestart preparations. System operation was normal with output pressure at 2487 N/cm^2 (3610 psia) as shown in Figure 8-1. After second ESC at 9848.2 seconds, as the engine driven pump commenced operation, the system pressure increased to 2542 N/cm^2 (3688 psia) which exceeded the upper limit of 2526 N/cm^2 (3665 psia) by 0.6 percent. At 10,050 seconds system pressure dropped below the upper limit to 2505 N/cm^2 (3632 psia) and remained steady until 10,233.1 seconds when the auxiliary pump was turned off. At 10,050 seconds, as the system pressure dropped, the auxiliary pump motor current increased from 20 to 30 amperes indicating that the auxiliary pump assumed an increased share of the hydraulic load. System temperatures, actuator positions and auxiliary pump current loads were normal during the burn and therefore this slight excess in system pressure did not appear to cause any problems.

The pump manufacturer states that the engine driven hydraulic pump has a "drift-up" characteristic which, when combined with uncompensated thermal expansion in the pump compensator mechanism, makes a rise in output pressure during second burn highly likely. It should be noted that the predicted upper limit of output pressure does not make allowance for this pressure increase. The excessive system pressure after S-IVB second

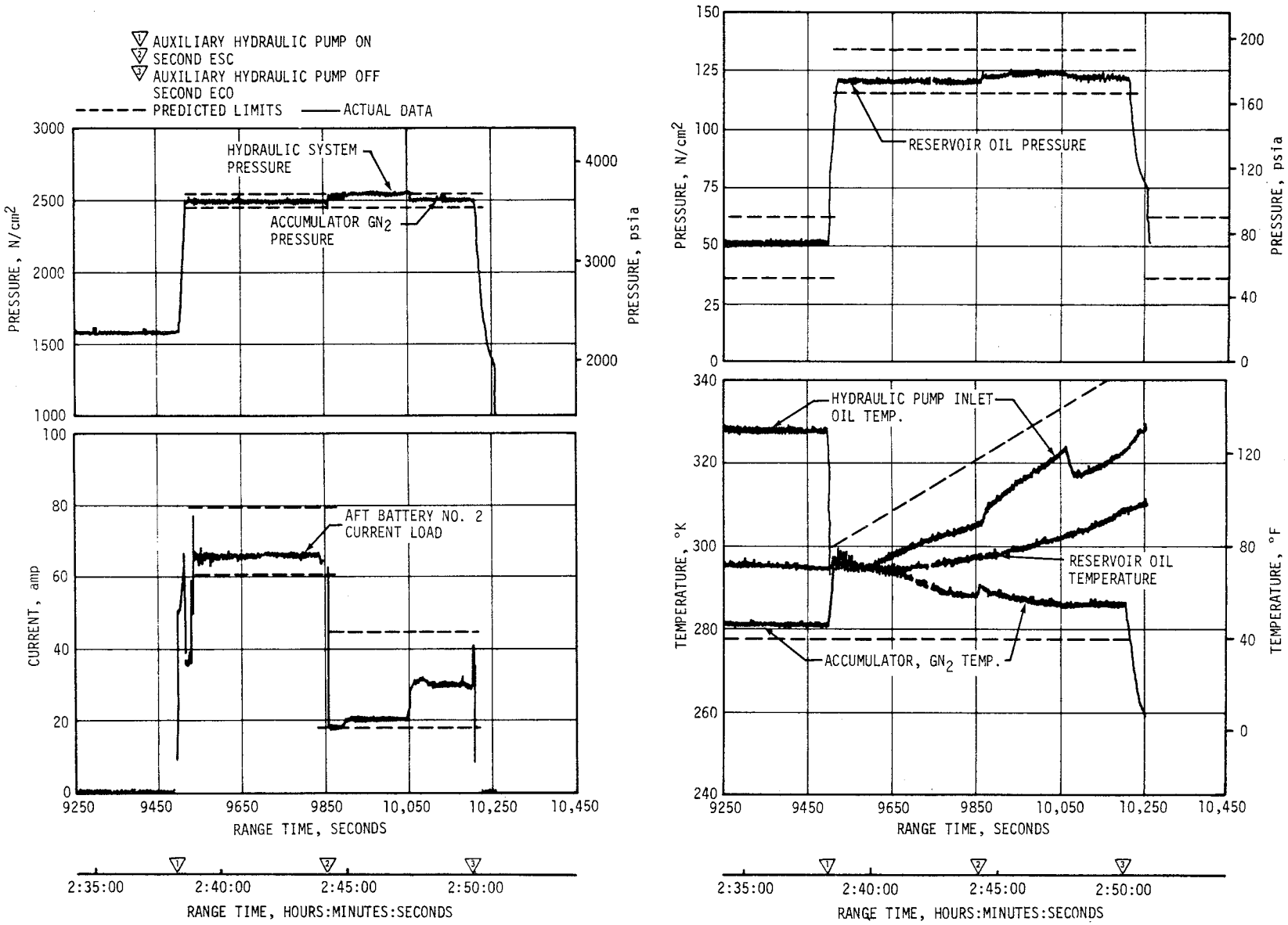

Figure 8-1. S-IVB Hydraulic System - Second Burn

start is probably due to this effect. The abrupt changes noted during the burn could be due to frictional hysteresis in the pressure/flow-regulating mechanism shown schematically in Figure 8-2. The pump response to a slowly changing demand would then consist of small step changes in output pressure.

The pump manufacturer indicates that the frictional hysteresis may be due to "silting" or entrapment of particulate matter in the small clearance between the compensator spool and sleeve. These components have a lap fit with a clearance of 0.00076 to 0.0010 centimeter (0.0003 to 0.0004 in.) whereas the circulating fluid has nominal 15 micron (0.00059 in.) filtration. This added friction would increase the required force on the spool before a response could occur. It should be noted however, that the existence of silting is not necessary to explain this high friction. The extremely small clearance of the lapped fit between the spool and sleeve, possibly modified by normal wear in proportion to pump life, could be a sufficient explanation. In any case, the pump manufacturer considers that this condition does not indicate impending malfunction of the engine driven pump.

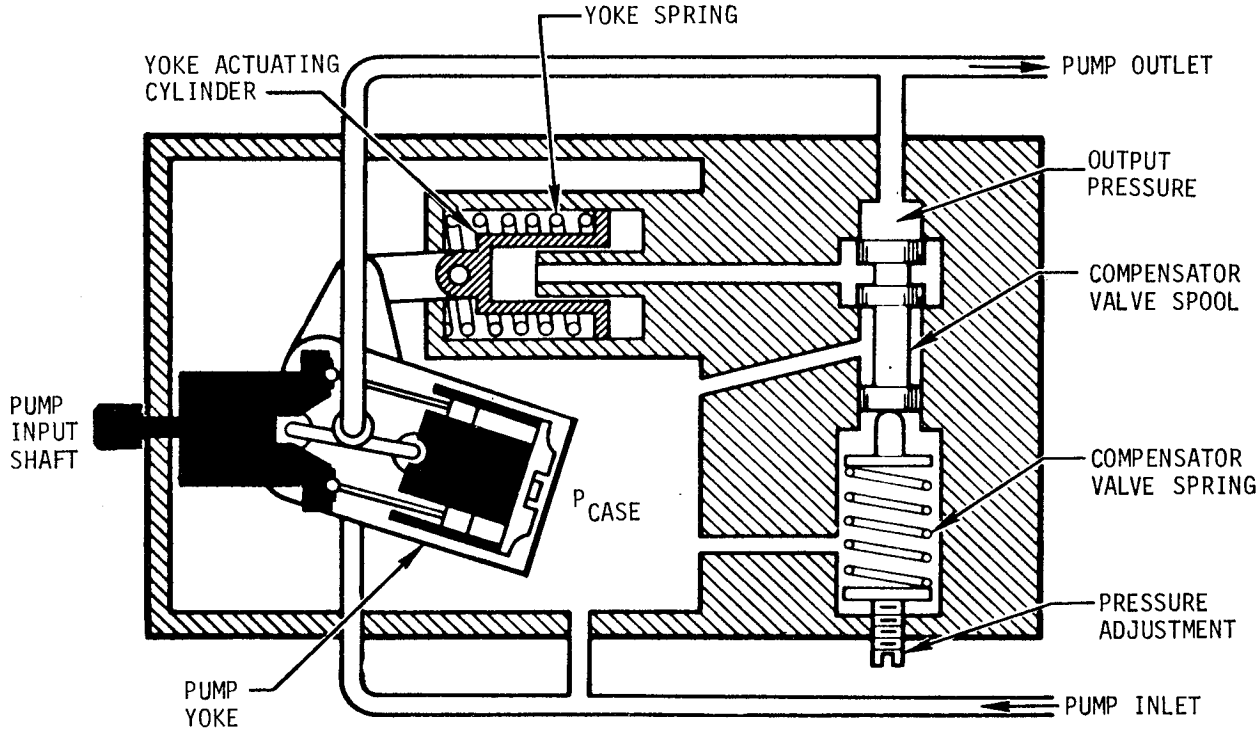

Figure 8-2. S-IVB Engine Driven Hydraulic Pump Schematic

SECTION 9

STRUCTURES

9.1 SUMMARY

The structural loads and dynamic environments experienced by the AS-506 launch vehicle were well within the vehicle structural capability. The longitudinal loads experienced during flight were nominal. The maximum bending moment condition, 3.75 x 10^6 N-m (33.2 x 10^6 lbf-in.), was experienced at 91.5 seconds and was lower than that experienced on any previous flights. The maximum longitudinal loads on the S-IC thrust structure, fuel tank, and intertank were experienced at 135.2 seconds, Center Engine Cutoff (CECO). On all the vehicle structure above the intertank, the maximum longitudinal loads were experienced at 161.6 seconds, Outboard Engine Cutoff (OECO), at the maximum longitudinal acceleration of 3.94 g.

During the S-IC boost phase, low-level (±0.07 g) 4.8-hertz longitudinal oscillations were detected in the Instrument Unit (IU) and peaked at approximately 107 seconds. These oscillations occurred in the first vehicle mode. Except for AS-502, the amplitudes of the oscillations were slightly higher than those observed on other previous flights.

The S-IVB gimbal block longitudinal measurement recorded a small (±0.037 g at 15.5 hertz) oscillation buildup at 252 seconds (S-II boost phase). Similar oscillations were experienced on the AS-505 flight.

Low-frequency longitudinal oscillations similar to those experienced on the AS-505 flight occurred during AS-506 S-IVB first and second burns. The AS-506 first burn peak amplitude (±0.07 g at 19 hertz) was about 20 percent of the AS-505 peak amplitude (±0.3 g at 19 hertz). The second burn oscillations peaked at approximately ±0.12 g (13 hertz) at 10,172 seconds.

9.2 TOTAL VEHICLE STRUCTURES EVALUATION

9.2.1 Longitudinal Loads

The AS-506 vehicle liftoff occurred nominally at a steady-state acceleration of approximately 1.2 g. Transients due to thrust buildup and release resulted in a ±0.13 g maximum longitudinal dynamic acceleration measured

at the IU. The slow-release rod forces measured during liftoff are presented in Figure 9-1.

The longitudinal loads that existed at the time of maximum aerodynamic loading (91.5 seconds) are shown in Figure 9-2. The steady-state longitudinal acceleration was 2.34 g, and the corresponding axial loads experienced were nominal.

As shown in Figure 9-2, the maximum longitudinal loads imposed on the S-IC thrust structure, fuel tank, and intertank occurred at 135.2 seconds (CECO) at a longitudinal acceleration of 3.71 g. The maximum longitudinal loads imposed on all vehicle structure above the S-IC intertank occurred at 161.6 seconds (OECO) at an acceleration of 3.94 g.

9.2.2 Bending Moments

The lateral loads experienced during thrust buildup and release were much lower than design because of the low-level winds experienced during launch. The wind speed at launch was 3.3 m/s (6.4 knots) at the 18.3-meter (60-ft) level. The comparable launch vehicle and spacecraft redline winds were 18.9 m/s (36.8 knots) and 15.4 m/s (30 knots), respectively.

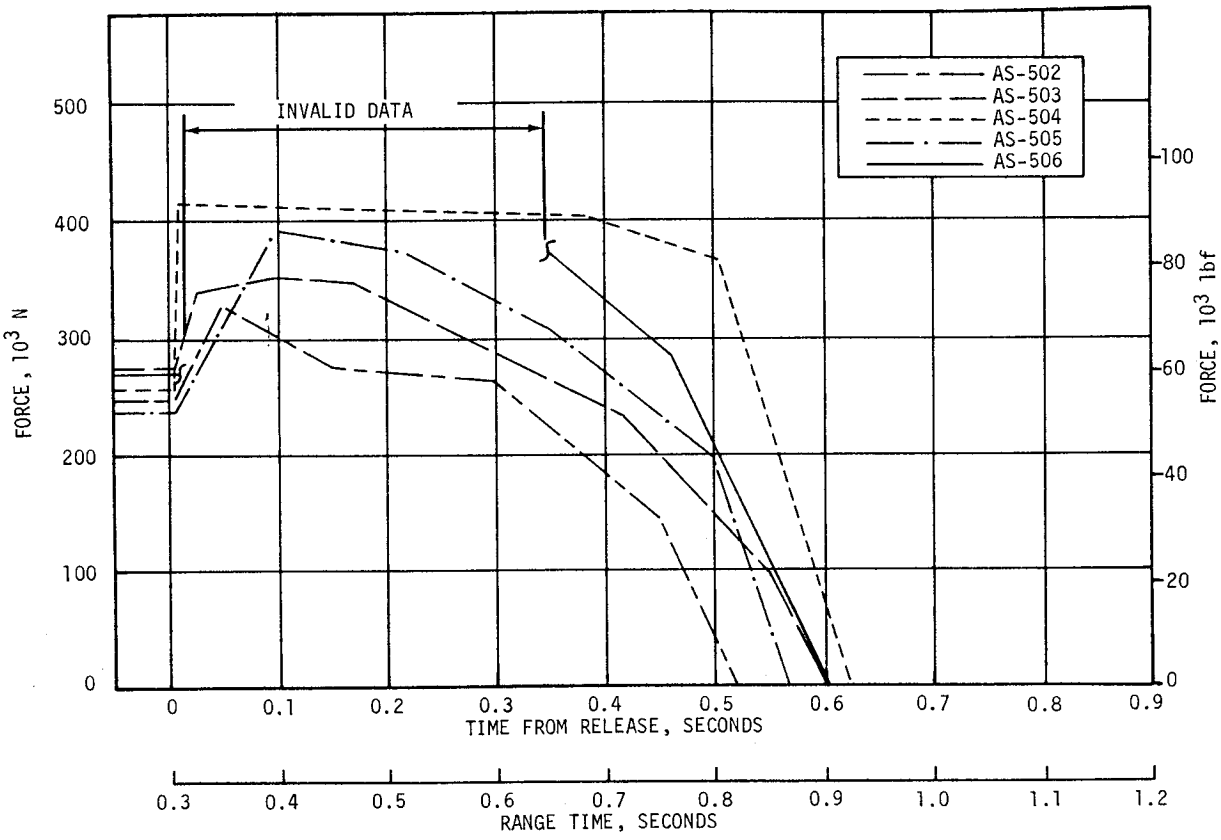

Figure 9-1. Release Rod Force Time History Comparison

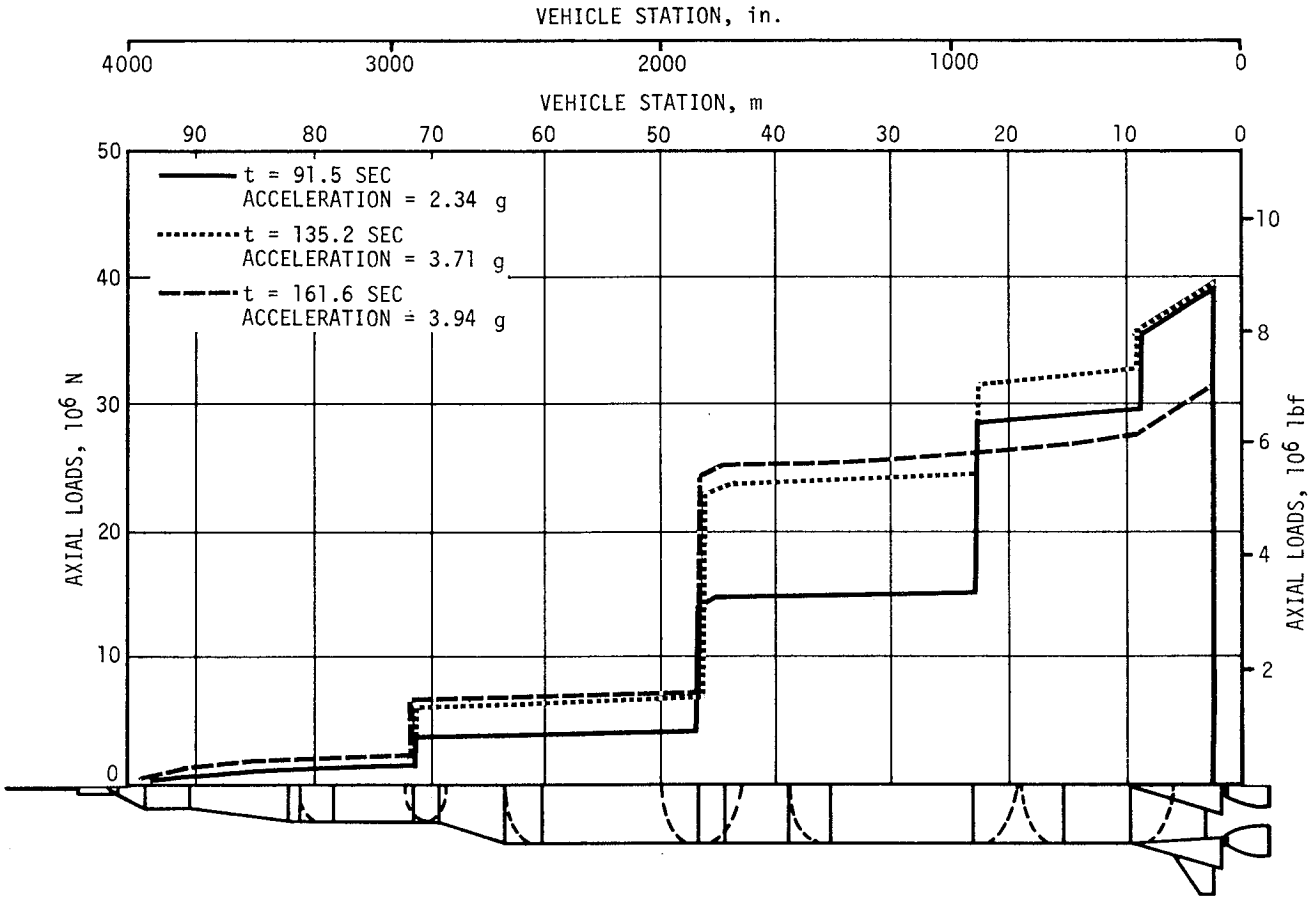

Figure 9-2. Longitudinal Load at Maximum Bending Moment, CECO and OECO

The inflight winds that existed during the maximum dynamic pressure phase of the flight were low, 9.6 m/s (18.7 knots), at the 11.4-kilometer (37,400 ft) level and were increasing steadily at higher altitudes, as shown in Figure A-1. The maximum bending moments on AS-506 were less than the bending moments experienced on any previous Saturn V vehicle, less than 15 percent of design criteria. As shown in Figure 9-3, the maximum bending moment of 3.75 x 10^6 N-m (33.2 x 10^6 lbf-in.) was imposed on the S-IC LOX tank at 91.5 seconds. Bending moment computations are based upon measured inflight parameters such as thrust, gimbal angle, angle-of-attack, dynamic pressure, and accelerations.

9.2.3 Vehicle Dynamic Characteristics

9.2.3.1 Longitudinal Dynamic Characteristics. The predicted first longitudinal mode frequencies were present throughout the AS-506 S-IC boost phase. As shown in Figure 9-4, the measured frequencies agree well with the analytical predictions. The frequencies are determined by spectral analysis using 5-second time slices.

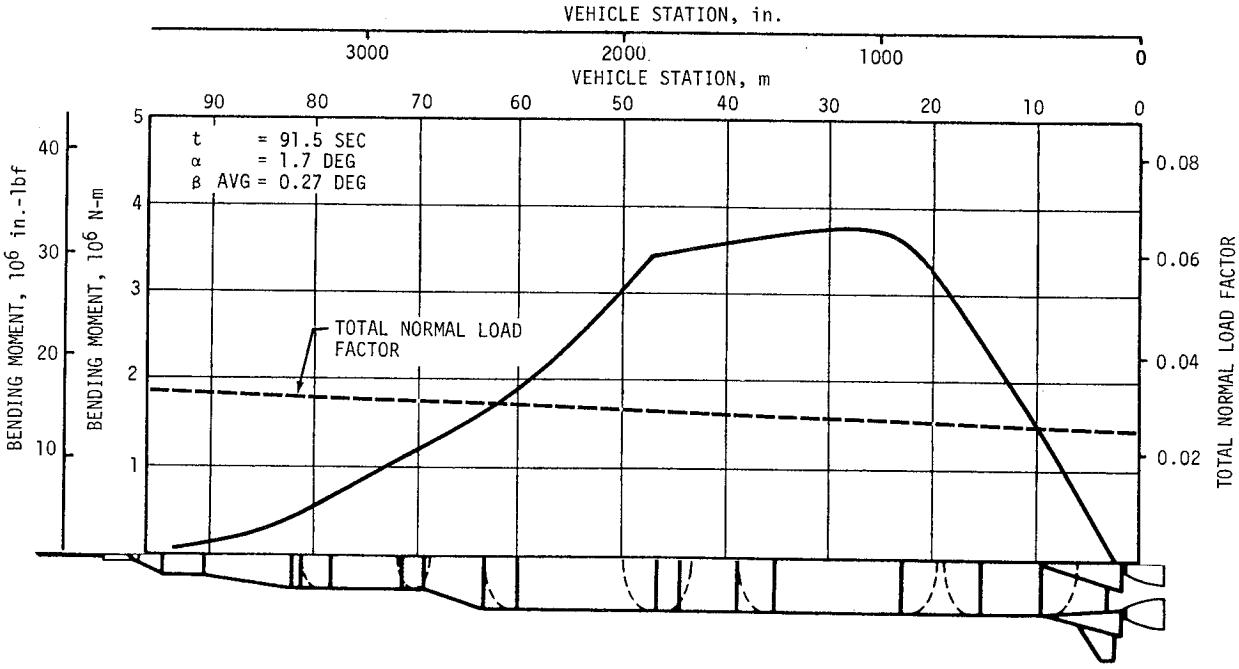

Figure 9-3. Maximum Bending Moment Near Max Q

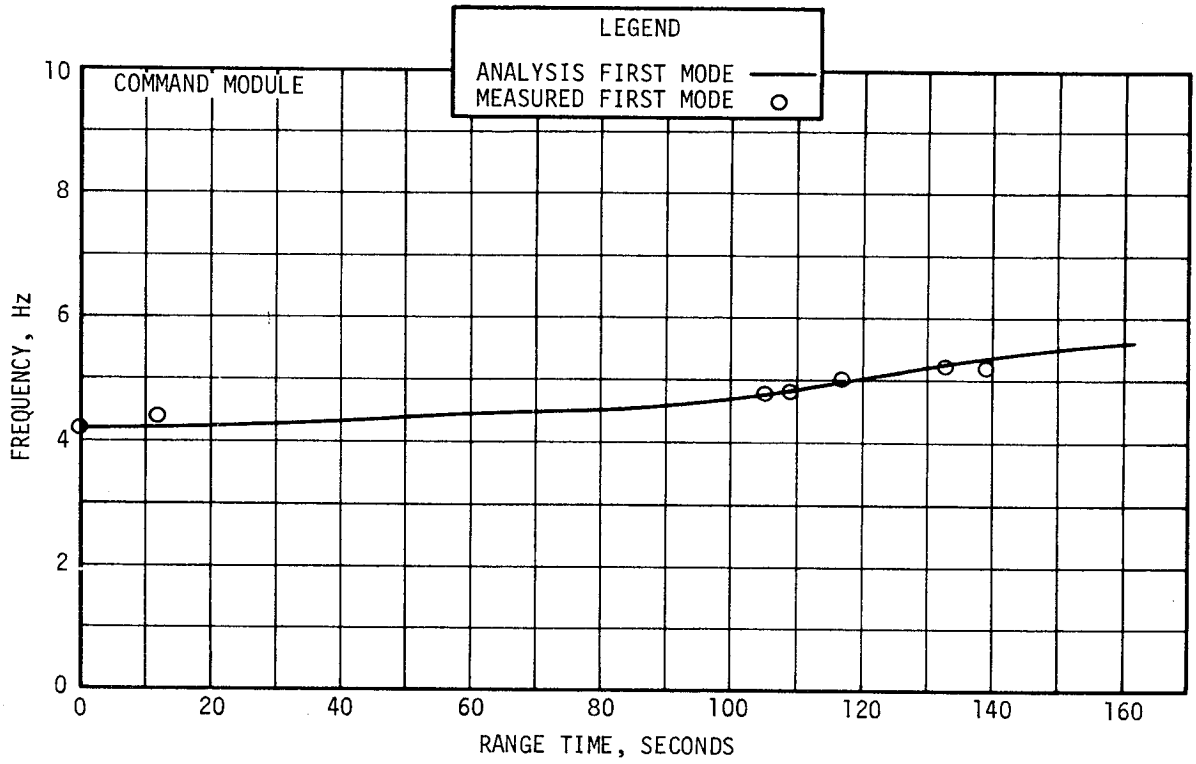

Figure 9-4. First Longitudinal Modal Frequencies During S-IC Powered Flight

The S-IC CECO and OECO transient responses measured at the Command Module (CM) and the IU are shown in Figure 9-5. The decay of the CECO amplitudes is comparable to previous flights, indicating that the vehicle damping in the first mode is similar. Peak amplitudes of first mode oscillations versus body station for the 135- to 138-second time slice are shown in Figure 9-6. The amplitudes of several measurements on AS-504, AS-505, and AS-506 are shown in this figure as well as a fit of the predicted first vehicle longitudinal mode through the data points.

The most significant vehicle responses during the S-IC stage boost phase were detected by the IU longitudinal (A2-603) measurements and the S-IC intertank longitudinal (A1-118) measurements. As shown in Figure 9-7, oscillations (4.7 to 5.2 hertz) began at approximately 102 seconds, peaked at 107 seconds, and damped by 125 seconds. The peak amplitude measured at the IU was ±0.07 g at 4.8 hertz. Except for AS-502, oscillations in the same frequency band, but at lower amplitudes, have been observed on other previous flights with an amplitude of ±0.05 g measured on AS-505 at 115 seconds. F-1 engine chamber pressures in the 4- to 5-hertz region were below the 0.4 N/cm^2 (0.5 psi) noise floor. The observed oscillations were a response of the first longitudinal mode to flight environmental excitations. POGO did not occur during S-IC boost.

During the S-II stage boost phase, a small response buildup was observed by the S-IVB stage gimbal block longitudinal accelerometer (A12-403) at 252 seconds. The AS-506 amplitude peaked at ±0.037 g at 15.5 hertz, as shown in Figure 9-8. A similar response was observed during the AS-505 flight, ±0.035 g (15 to 16 hertz), at 293 seconds. The S-II crossbeam amplitude on AS-505 was ±1.0 g. The crossbeam on AS-506 was not instrumented; however, since the AS-506 oscillations also occur in the high-gain S-II crossbeam mode (15 to 16 hertz), the AS-506 crossbeam response is estimated to have been ±1 g (15.5 hertz), which is well below the design limits.

Low-frequency longitudinal oscillations similar to those experienced on AS-505 occurred during AS-506 S-IVB first and second burns. As shown in Figure 9-9, the AS-506 first burn oscillation frequency ranges were identical (17 to 20 hertz); however, the AS-506 peak amplitude (±0.07 g) was about 20 percent of the AS-505 peak amplitude (±0.3 g) at 19 hertz. The AS-506 oscillations were intermittent, recurring at lower amplitudes throughout the remainder of first burn. The LOX suction line inlet measurement reached a maximum of ±0.12 g and showed similar intermittent responses throughout first burn, as shown in Figure 9-10. The data of Figure 9-11 show that the AS-505 and AS-506 peak amplitudes, determined by spectral analysis using 2-second time slices, occurred at the same frequency and near the same time during flight.

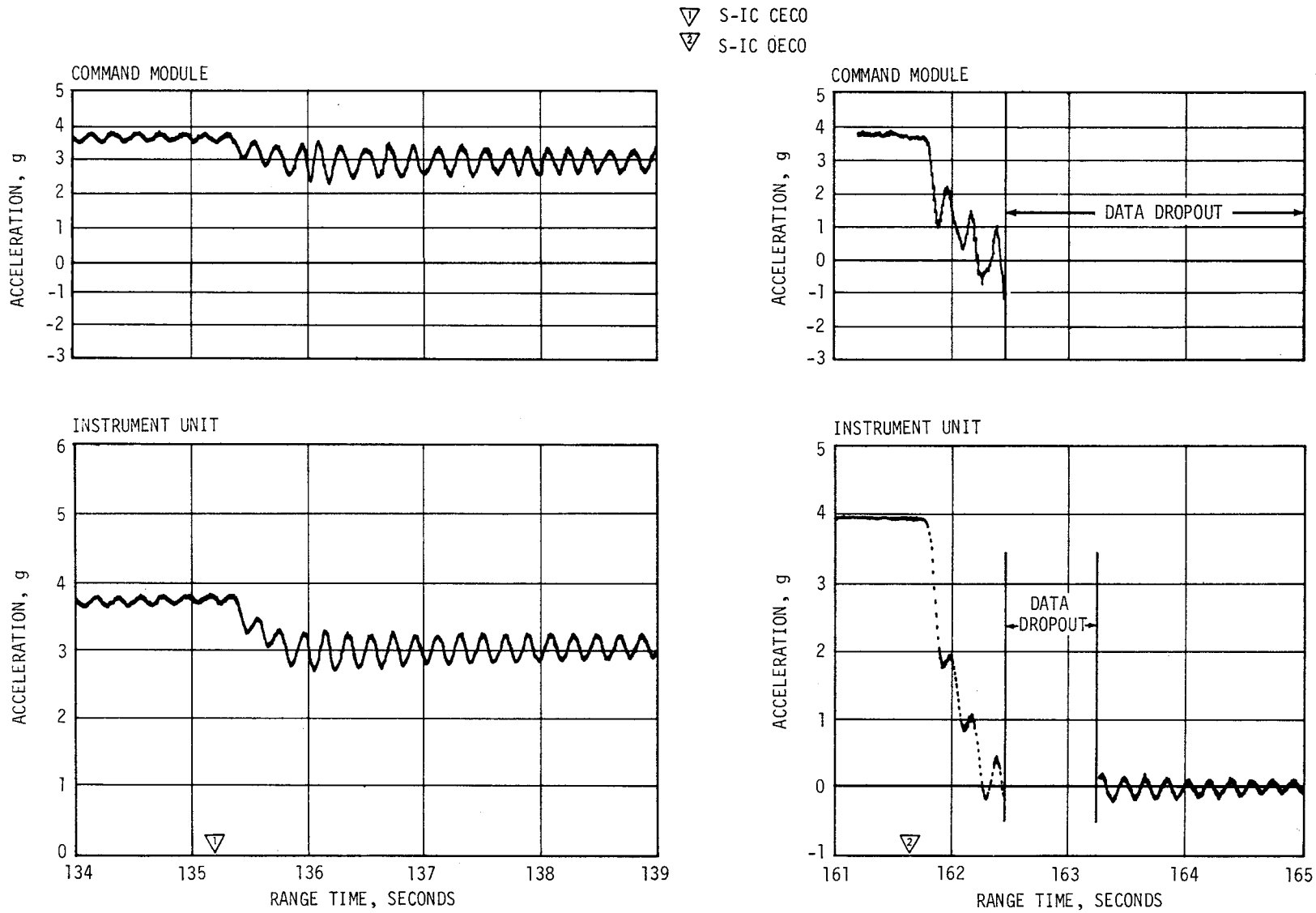

Figure 9-5. Longitudinal Acceleration at CM and IU

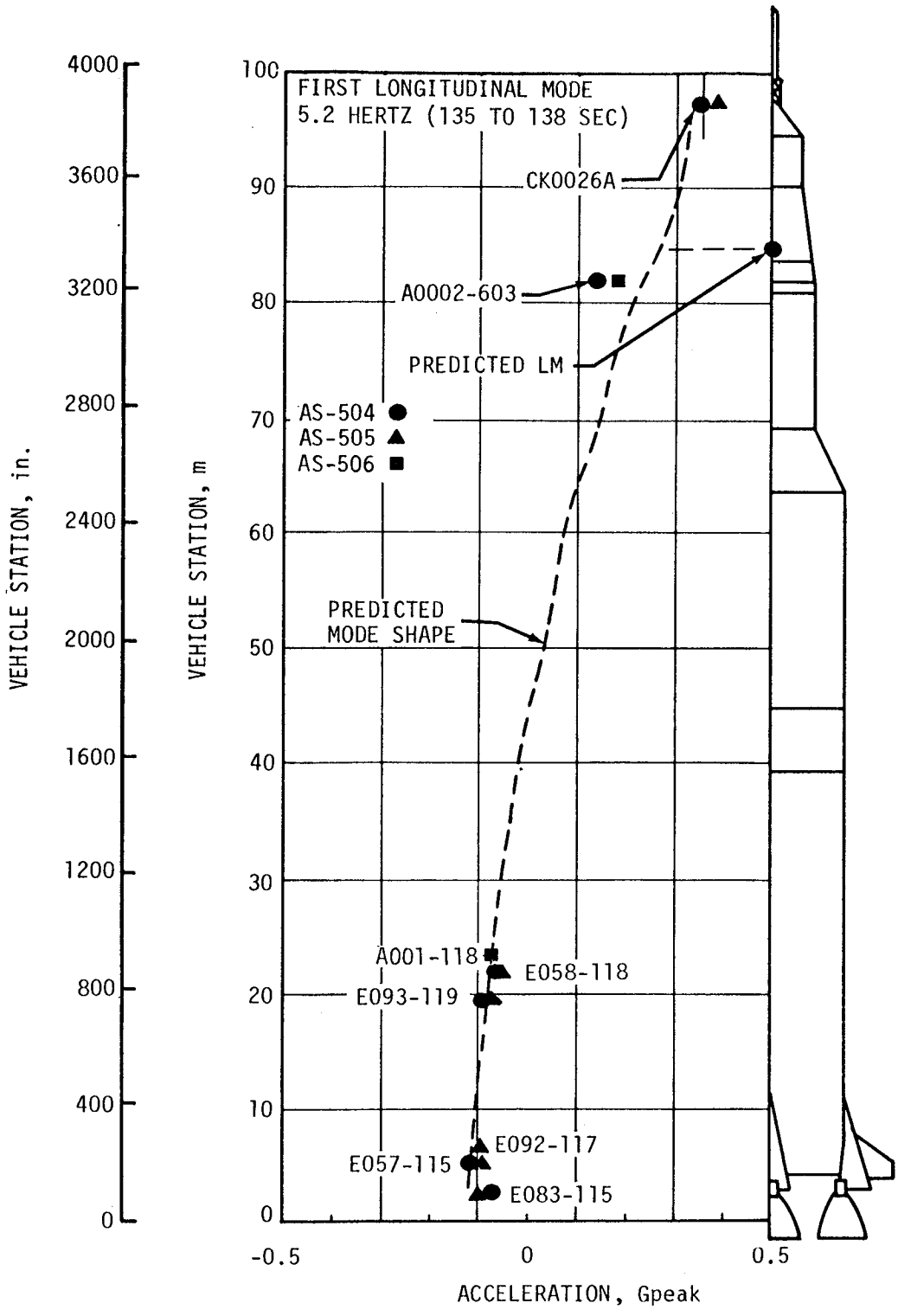

Figure 9-6. Peak Amplitudes of Vehicle First Longitudinal Mode for AS-504, AS-505, and AS-506

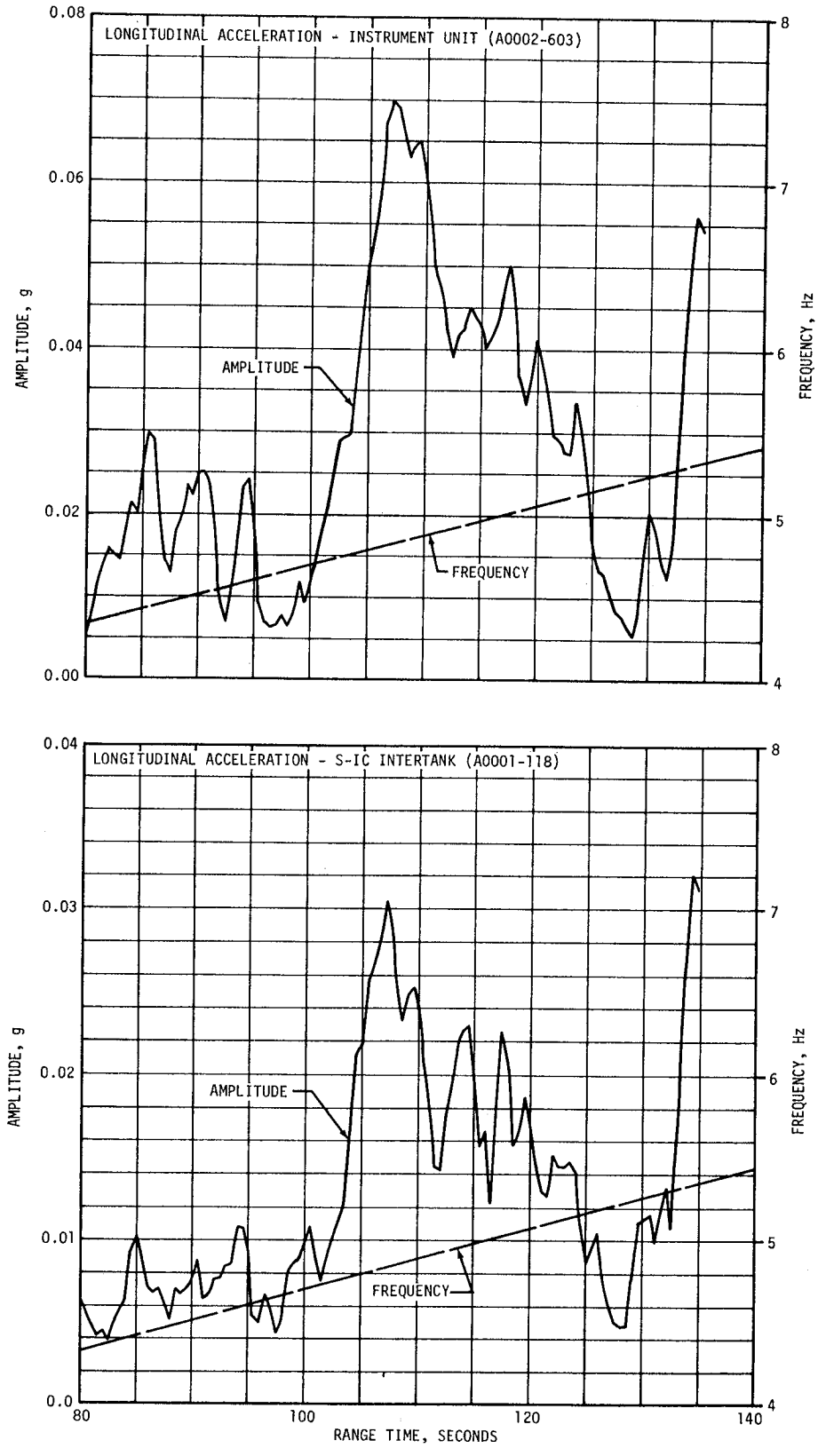

Figure 9-7. Frequency and Amplitude of Longitudinal Oscillations During S-IC Boost

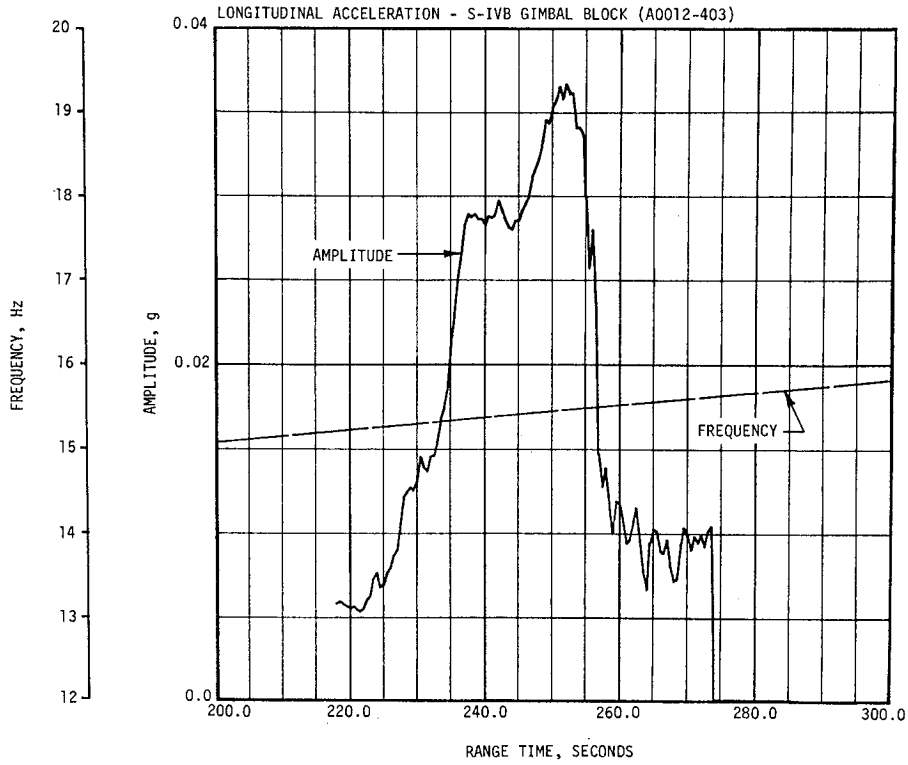

Figure 9-8. Amplitude and Frequency of Longitudinal Oscillations During S-II Stage Boost

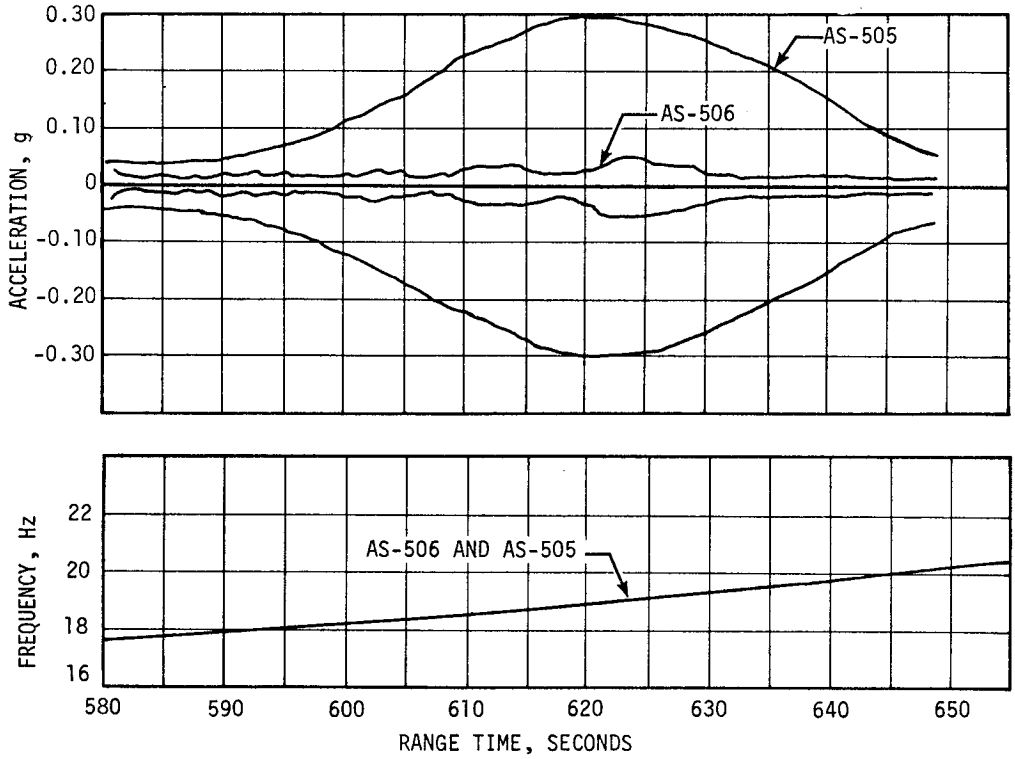

Figure 9-9. S-IVB AS-506 and AS-505 17- to 20-Hertz Oscillations Comparison

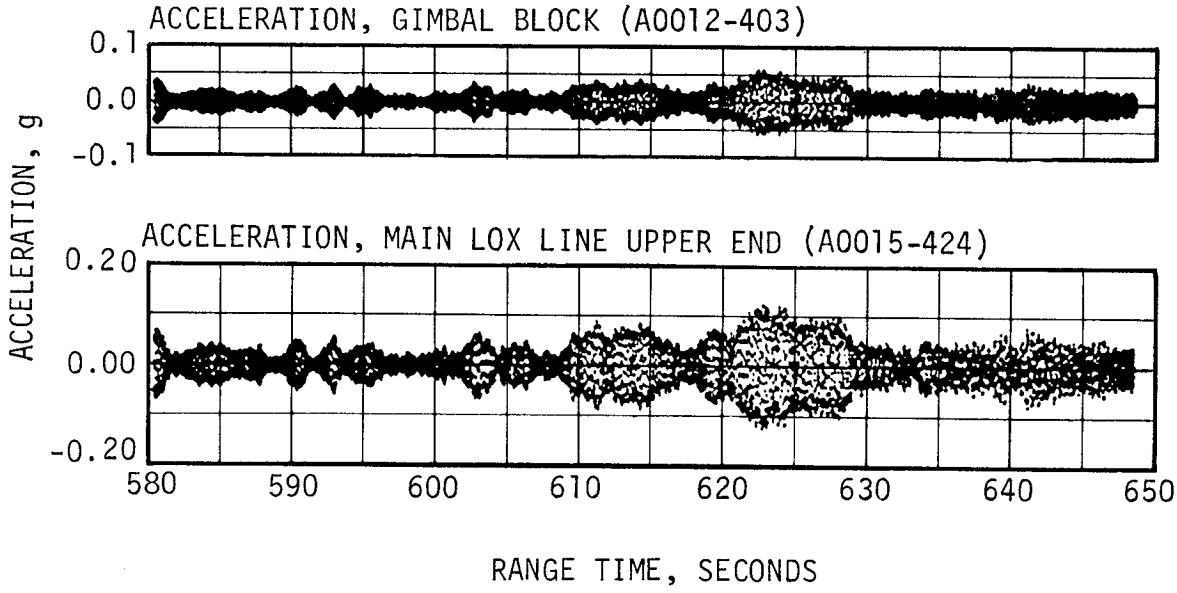

Figure 9-10. AS-506 S-IVB First Burn Maximum Response

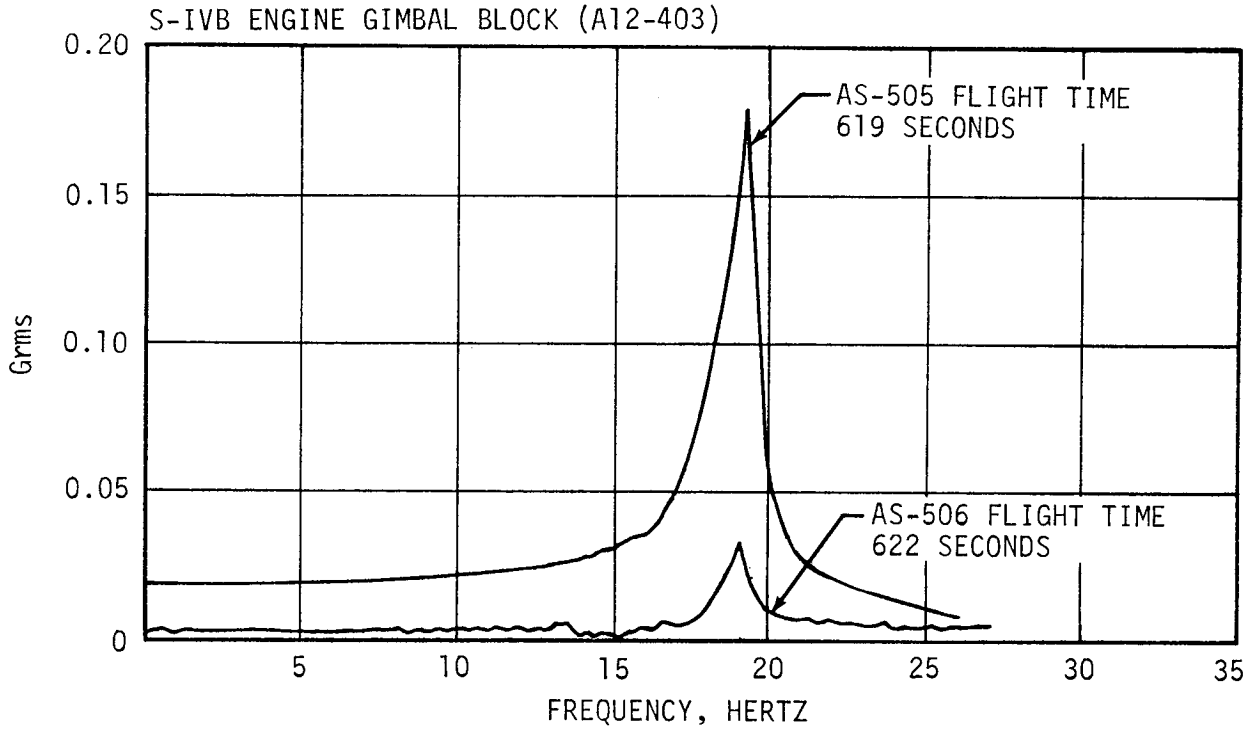

Figure 9-11. AS-506 and AS-505 First Burn Response

During S-IVB second burn, small longitudinal oscillations began on the engine gimbal pad (A12-403) at about 10,164 seconds and peaked (±0.12 g) at 10,172 seconds at the first longitudinal mode frequency of 13 hertz. These oscillations were damped out by 10,184 seconds. Similar 13- to 16-hertz oscillations occurred on AS-505 and other previous flights at approximately the same levels and range time.

The chamber pressure responses were in the noise floor in the 17- to 20-hertz region during first burn and the 13- to 16-hertz region during second burn. The LOX pump inlet and discharge pressure measurements showed insignificantly low amplitudes throughout both S-IVB burns as did the longitudinal accelerometers in the IU and CM.

The data show typical buildup and decay periods of low-level oscillations without indications of propulsion/structural coupling. Since these oscillations have been observed on previous flights, it is assumed that they are characteristic of the stage and could be expected on future flights.

The 45-hertz oscillations that occurred just after the LH_2 step pressurization event on AS-505 were not detected on AS-506. The AS-506 Non Propulsive Vent (NPV) pressures showed very small, ±0.35 N/cm^2 (±0.5 psia), pressure oscillations after step pressurization, as shown in Figure 9-12. The IU yaw

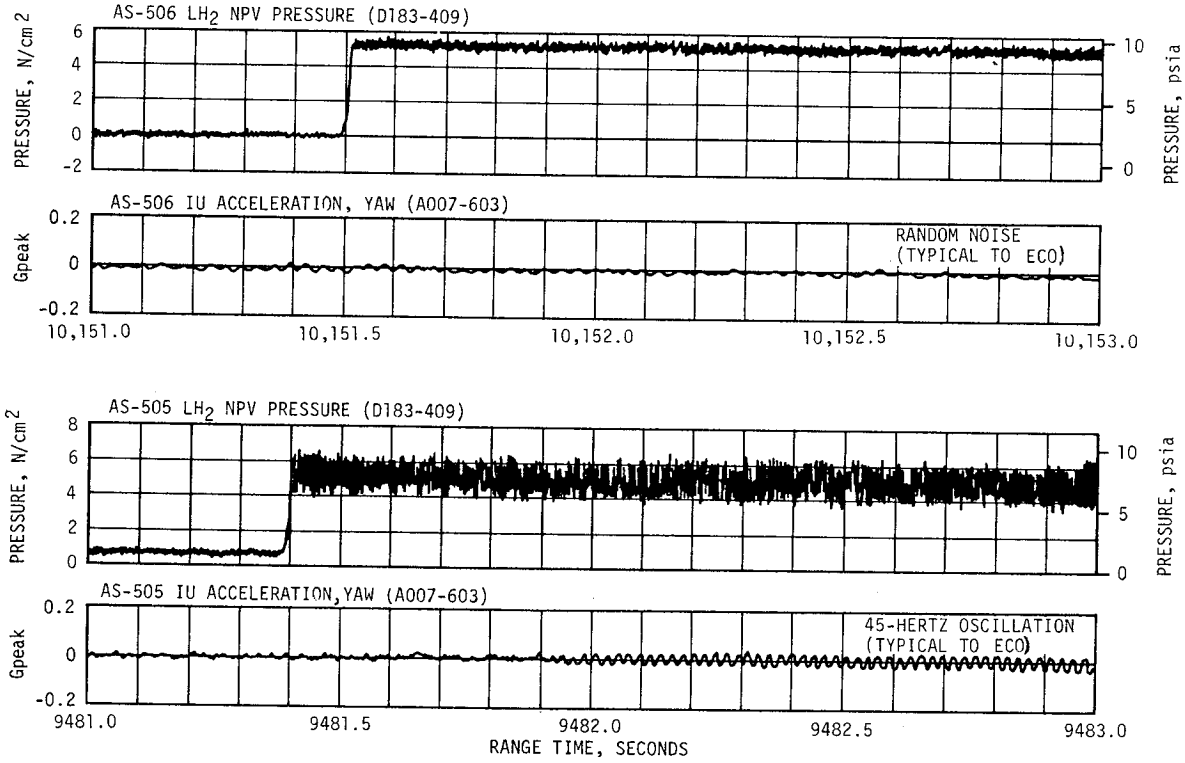

Figure 9-12. Comparison of 45-Hertz Oscillations During AS-505 and AS-506 Second Burn

acceleration measurement (A7-603) showed no response to these small pressure oscillations. In sharp contrast to this condition were the relatively large, ±1.4 N/cm^2 (±2 psia), NPV pressure oscillations observed on the AS-505 flight and the resulting 45-hertz vibration indicated by the A7-603 measurement. Therefore, it is assumed that the 45-hertz vibration did not occur on the AS-506 flight.

9.2.3.2 Lateral Dynamic Characteristics. Oscillations in the first four modes were detectable throughout S-IC powered flight. Spectral analyses were performed to determine modal frequencies using 5-second time slices. The frequencies of these oscillations agreed well with the analytical predictions, as shown in Figure 9-13.

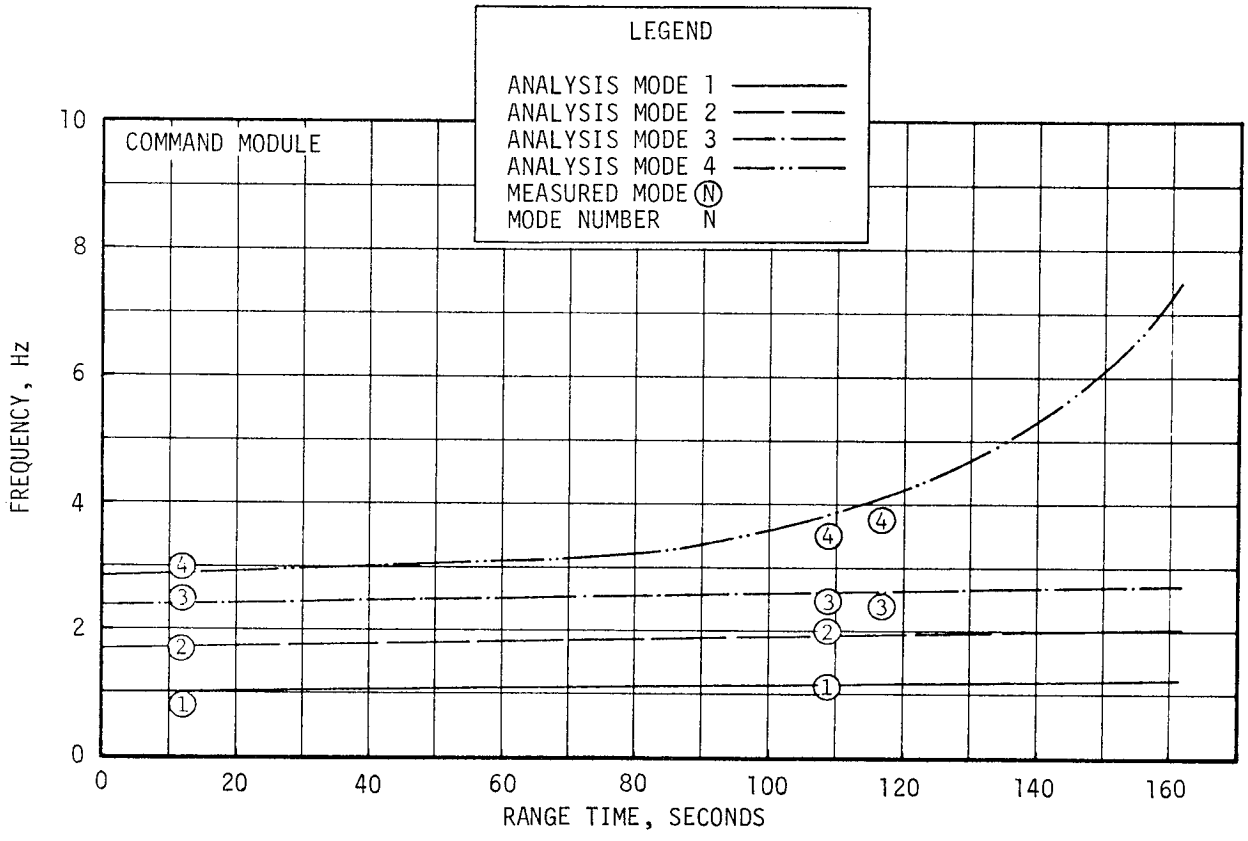

Figure 9-13. AS-506 Lateral Analysis/Measured Modal Frequency Correlation

SECTION 10

GUIDANCE AND NAVIGATION

10.1 SUMMARY

10.1.1 Flight Program

The guidance and navigation system performed satisfactorily at all times for which data are presently available. The parking orbit and translunar injection parameters are well within tolerance. The S-IVB LOX dump, LH_2 vent, and Auxiliary Propulsion System (APS) ullage burn resulted in a heliocentric orbit of the S-IVB/IU as planned.

The actual S-II Engine Mixture Ratio (EMR) shift occurred approximately 9.5 seconds later than indicated by the final stage propulsion prediction. About 4 seconds of this deviation was attributed to the change in Launch Vehicle Digital Computer (LVDC) nominal characteristic velocity presetting predictions and variation in actual from predicted flight performance. Approximately 5.5 seconds of the deviation are attributed to improper scaling in the flight program calculation of characteristic velocity.

10.1.2 Instrument Unit Components

The LVDC, the Launch Vehicle Data Adapter (LVDA), and the ST-124M-3 inertial platform functioned satisfactorily. The platform-measured crossrange velocity ($\dot{Y}$) exhibited a negative shift of approximately 1.8 m/s (5.9 ft/s) at 3.3 seconds after liftoff. The probable cause was the Y accelerometer head momentarily contacting an internal mechanical stop. Although this had negligible effect on the launch vehicle, investigation to determine the cause of the velocity shift is continuing.

10.2 GUIDANCE COMPARISONS

The postflight guidance error analysis was based on comparisons of the ST-124M-3 platform measured velocities with the postflight trajectory established from external tracking data. No precision tracking data were available for trajectory construction; therefore, hardware error analysis was limited to gross errors. The comparisons made and reported herein are referenced to the AS-506 final (14 day) postflight trajectory. The boost-to-parking orbit portion of the trajectory was a composite fit of C-Band radar data. The second burn trajectory consists of ST-124M-3 measured velocities constrained to orbital solutions.

Figure 10-1 presents the comparisons of the platform measured velocities with corresponding values from the postflight trajectory. A positive difference indicated trajectory data greater than the platform measurement. The velocity differences at S-IVB first Engine Cutoff (ECO) were 1.52 m/s (4.99 ft/s), 1.73 m/s (5.68 ft/s), and 0.54 m/s (1.77 ft/s) for vertical, crossrange, and downrange velocity, respectively. Although the differences at S-IVB cutoff are relatively small, the difference profiles do not reflect characteristic trends relative to platform system errors. These trends were not shown because of the difficulty in constructing a boost trajectory without precision tracking.

At approximately 3.3 seconds after liftoff, the crossrange velocity changed -1.8 m/s (-5.9 ft/s) from one computer cycle to the next and appeared to settle down with a bias in the accumulator. The comparisons with the postflight trajectory do not show this bias since the telemetered velocities were smoothed and used to initialize the trajectory program. A comparison of the crossrange velocities ($\dot{Y}$) with the LVDC and Operational Trajectory (OT) during the first 20 seconds of flight indicates a bias of about 1.2 m/s (3.9 ft/s). A more detailed discussion of this velocity change is given in paragraph 10.4.7.

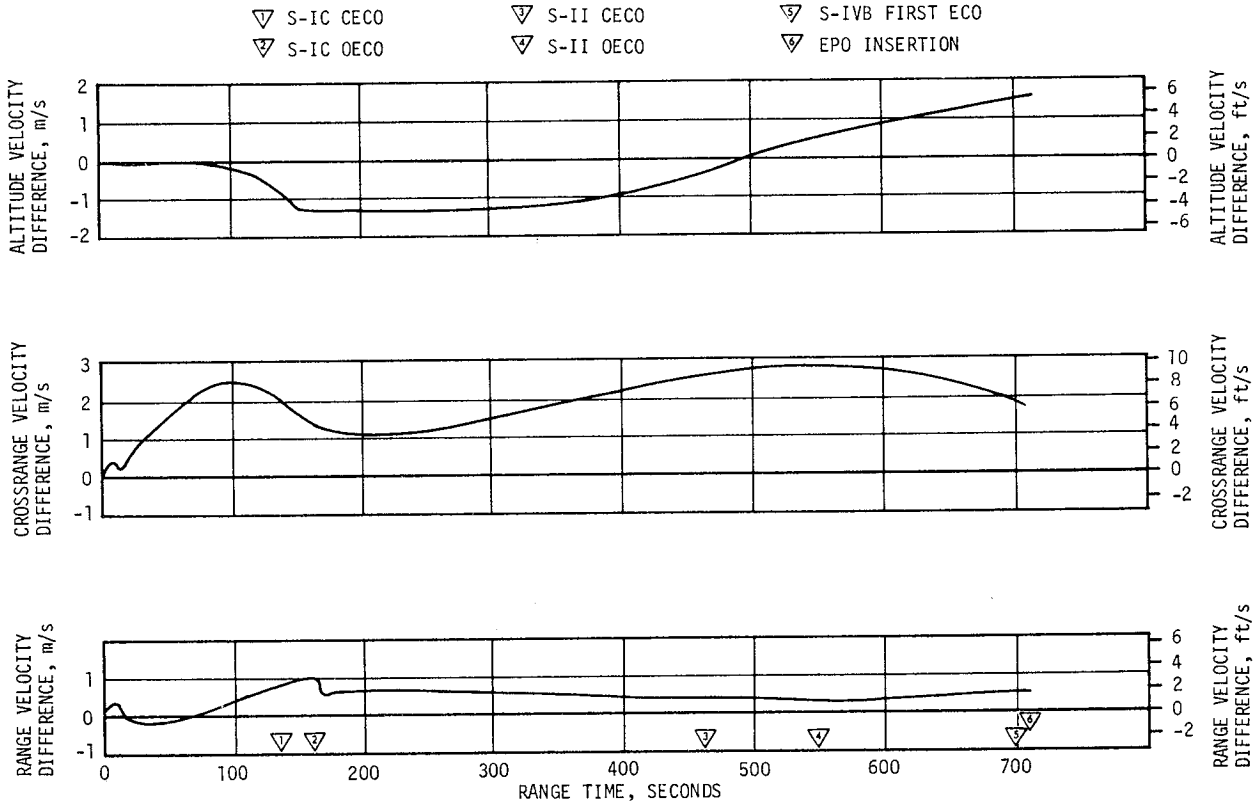

Figure 10-1. Trajectory and ST-124M-3 Platform Velocity Comparison (Trajectory Minus Guidance)

The platform velocity comparisons shown for the second S-IVB burn in Figure 10-2 reflect differences in LVDC and postflight orbital solution state vectors. The second burn portion of the postflight trajectory was constructed by initializing to parking orbit solution and constraining the telemetered platform velocities to a state vector after Translunar Injection (TLI). Some portion of the velocity differences might be attributed to platform misalignment due to drift. However, the differences build up to a maximum and then reverse slope indicating compensating drifts. The accelerations in the pitch plane were positive for the entire second burn, and the crossrange acceleration was less than -0.2 m/s (0.7 ft/s) for about 36 seconds after ignition and then went positive. If the velocity differences were assumed to be the result of platform errors, the curves would indicate g-sensitive drifts not compatible with the boost-to-parking orbit data where much higher accelerations were experienced. Work will be continued to resolve the state vector differences between the LVDC and orbital solutions.

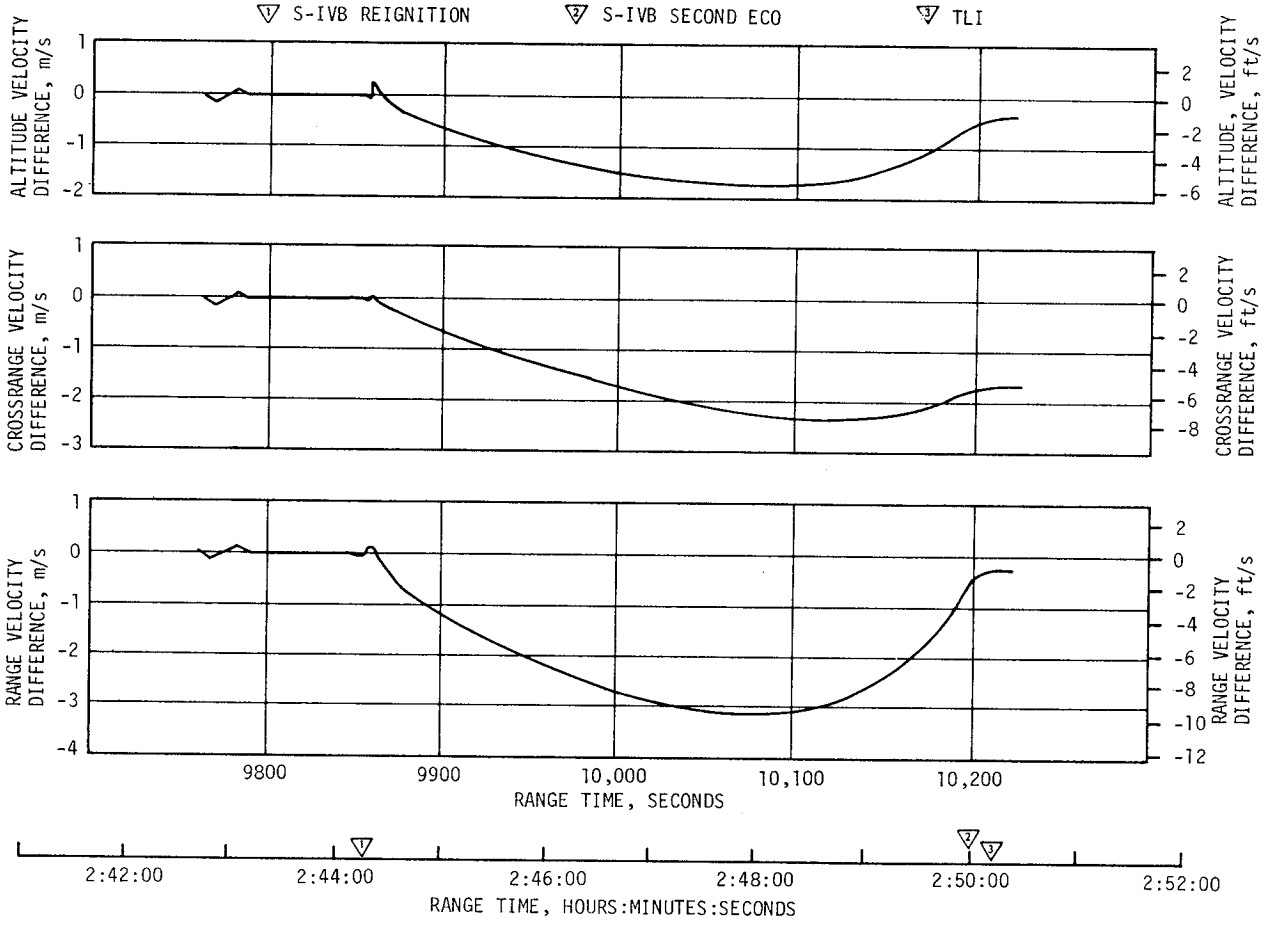

Figure 10-2. Trajectory and ST-124M-3 Platform Velocity Comparison Second S-IVB Burn (Trajectory Minus Guidance)

Velocities measured by the ST-124M-3 platform system at significant flight event times are shown in Table 10-1 along with corresponding values from both the observed postflight and operational trajectories. The differences between the telemetered velocities and the observed postflight trajectory values reflect some combination of small guidance hardware errors, tracking errors, and interpolation of data to specific event times. The differences between the telemetered and operational trajectory values reflect off-nominal flight conditions and vehicle performance.

Comparisons of navigation (PACSS 13 coordinate system) positions, velocities, and flight path angle at significant flight event times are presented in Table 10-2. The guidance (LVDC) and observed postflight trajectory values are in relatively good agreement for the boost-to-parking orbit burn mode. The initial error in crossrange velocity is reflected in the displacement. The component differences at Time Base 6 and at TLI are still under investigation. There appears to be a timing error of about 2.7 seconds between the orbital solutions and the LVDC. The component differences at parking orbit insertion, Time Base 6, and TLI are given in Table 10-3.

The ST-124M-3 platform measurements and the LVDC flight program were highly successful in guiding the AS-506 vehicle to near nominal end conditions. A minimum of corrections were required for the spacecraft to accomplish a near perfect mission.

10.2.1 Late S-II Stage EMR Shift

The S-II stage actual EMR shift occurred approximately 9.5 seconds later than indicated by the final stage propulsion prediction. About 4 seconds of this deviation was attributed to the change in IU LVDC nominal characteristic velocity presetting predictions and variation in actual from predicted flight performance.

About 5.5 seconds of the late EMR shift deviation was due to improper LVDC scaling. The EMR routine is entered when a time-to-go quantity T_{1i}, becomes zero or negative. The T_{1i} was larger than predicted because the calculated characteristic velocity, upon which T_{1i} is based, was smaller than predicted.

The S-II characteristic velocity calculated in the IU was incorrect due to an unfortunate combination of scaling situations in the LVDC flight program. These scaling errors caused the calculated S-II stage characteristic velocity (BNVC) to be low by approximately 91.7 m/s (300.9 ft/s) at the time EMR shift should have occurred. BNVC is calculated as follows:

$$DVC_i^2 = (\Delta\dot{X}^2 + \Delta\dot{Y}^2 + \Delta\dot{Z}^2)$$

$$\Delta BNVC = 1/2(DVC_{i-1} + DVC_i/DVC_{i-1})$$

$$BNVC_i = BNVC_{i-1} + \Delta BNVC$$

Table 10-1. Inertial Platform Velocity Comparisons

EVENTS	DATA SOURCE	VELOCITY M/S (FT/S)**		
		ALTITUDE ($\dot{X}_m$)	CROSSRANGE ($\dot{Y}_m$)	DOWN RANGE ($\dot{Z}_m$)
S-IC OECO	Guidance	2585.13 (8481.40)	1.50 (4.92)	2254.84 (7397.77)
	Postflight Trajectory	2583.28 (8475.33)	2.71 (8.89)	2255.10 (7398.62)
	Operational Trajectory	2600.23 (8530.94)	-5.34 (-17.52)	2239.23 (7346.56)
S-II OECO	Guidance	3430.03 (11,253.38)	-3.50 (-11.48)	6759.48 (22,176.77)
	Postflight Trajectory	3430.60 (11,255.25)	-0.96 (-3.15)	6759.88 (22,178.08)
	Operational Trajectory	3432.73 (11,262.24)	-1.10 (-3.61)	6784.83 (22,259.94)
First S-IVB ECO	Guidance	3190.55 (10,467.68)	1.50 (4.92)	7607.13 (24,957.78)
	Postflight Trajectory	3192.07 (10,472.67)	3.23 (10.60)	7607.67 (24,959.55)
	Operational Trajectory	3187.05 (10,456.20)	1.17 (3.84)	7606.29 (24,955.02)
Parking Orbit Insertion	Guidance	3189.85 (10,465.39)	1.50 (4.92)	7608.85 (24,963.42)
	Postflight Trajectory	3191.42 (10,470.54)	3.29 (10.79)	7609.49 (24,965.52)
	Operational Trajectory	3186.42 (10,454.13)	1.18 (3.87)	7607.85 (24,960.14)
Second S-IVB ECO*	Guidance	2677.57 (8784.68)	275.86 (905.05)	1656.05 (5433.23)
	Postflight Trajectory	2677.21 (8783.50)	274.00 (898.95)	1655.22 (5430.51)
	Operational Trajectory	2678.72 (8788.45)	276.23 (906.27)	1655.18 (5430.38)
Translunar Injection	Guidance	2680.70 (8794.95)	276.50 (907.15)	1658.50 (5441.27)
	Postflight Trajectory	2680.38 (8793.90)	274.79 (901.54)	1658.28 (5440.25)
	Operational Trajectory	2681.45 (8797.41)	276.77 (908.04)	1657.45 (5437.83)

*Second burn velocity data represent accumulated velocities from Time Base 6.

**PACSS 12 Coordinate System.

Table 10-2. Guidance Comparisons

EVENT	DATA SOURCE	POSITIONS (METERS) (FT)				VELOCITIES M/S (FT/S)				FLIGHT PATH ANGLE (DEG)
		X_S	Y_S	Z_S	R	$\dot{X}_S$	$\dot{Y}_S$	$\dot{Z}_S$	V_S	γ
S-IC OECO	Guidance	6,437,364 (21,119,961)	39,169 (128,507)	159,182 (522,251)	6,439,450 (21,126,804)	841.25 (2760.01)	121.94 (400.07)	2630.38 (8629.86)	2764.32 (9069.29)	19.1484
	Postflight Trajectory	6,437,247 (21,119,577)	39,441 (129,400)	159,164 (522,192)	6,439,335 (21,126,426)	839.62 (2754.66)	123.11 (403.90)	2630.64 (8630.71)	2764.13 (9068.67)	19.1143
	Operational Trajectory	6,437,901 (21,121,724)	38,968 (127,847)	157,586 (517,014)	6,439,948 (21,128,437)	861.66 (2826.97)	115.11 (377.66)	2614.93 (8579.17)	2755.64 (9040.81)	19.635
S-II OECO	Guidance	6,289,965 (20,636,368)	79,413 (260,541)	1,860,948 (6,105,471)	6,559,961 (21,522,182)	-1891.78 (-6206.63)	88.17 (289.27)	6651.61 (21,822.87)	6915.96 (22,690.16)	0.6139
	Postflight Trajectory	6,289,873 (20,636,067)	80,367 (263,670)	1,859,720 (6,101,444)	6,559,537 (21,520,790)	-1891.43 (-6205.48)	90.43 (296.69)	6651.87 (21,823.72)	6916.14 (22,690.75)	0.6075
	Operational Trajectory	6,283,160 (20,614,043)	79,489 (260,791)	1,884,673 (6,183,310)	6,560,214 (21,523,012)	-1917.77 (-6291.90)	90.69 (297.54)	6668.07 (21,876.87)	6938.96 (22,765.62)	0.661
First S-IVB ECO	Guidance	5,891,469 (19,328,968)	91,789 (301,144)	2,891,285 (9,485,842)	6,563,335 (21,533,251)	-3433.60 (-11,265.09)	76.86 (252.17)	6993.63 (22,944.98)	7791.43 (25,562.43)	-0.00148
	Postflight Trajectory	5,890,834 (19,326,885)	93,058 (305,310)	2,892,017 (9,488,245)	6,563,105 (21,532,498)	-3432.48 (-11,261.42)	78.03 (256.00)	6993.87 (22,945.77)	7791.17 (25,561.58)	0.01511
	Operational Trajectory	5,890,252 (19,324,973)	91,860 (301,377)	2,893,708 (9,493,791)	6,563,311 (21,533,172)	-3436.57 (-11,274.84)	76.94 (252.43)	6992.15 (22,940.12)	7791.41 (25,562.39)	-0.00220
Parking Orbit Insertion	Guidance	5,856,709 (19,214,926)	92,552 (303,647)	2,961,037 (9,714,687)	6,563,334 (21,533,247)	-3517.14 (-11,539.17)	75.69 (248.33)	6954.08 (22,815.22)	7793.28 (22,568.50)	-0.00064
	Postflight Trajectory	5,856,252 (19,213,427)	93,832 (307,846)	2,961,276 (9,715,472)	6,563,052 (21,532,323)	-3515.97 (-11,535.33)	76.90 (252.30)	6954.42 (22,816.34)	7793.07 (22,567.81)	0.01205
	Operational Trajectory	5,855,466 (19,210,845)	92,623 (303,882)	2,963,438 (9,722,567)	6,963,309 (21,533,166)	-3520.02 (-11,548.62)	75.77 (248.59)	6952.42 (22,809.78)	7793.10 (22,567.91)	-0.00142
Time Base 6	Guidance	-2,290,189 (-7,513,744)	-142,062 (-466,083)	-6,156,680 (-20,199,081)	6,570,377 (21,556,355)	7301.51 (23,955.09)	-26.14 (-85.76)	-2720.93 (-8926.94)	7792.02 (25,564.50)	0.03779
	Postflight Trajectory	-2,313,353 (-7,589,739)	-143,619 (-471,191)	-6,149,910 (-20,176,871)	6,572,186 (21,562,288)	7290.84 (23,920.08)	-26.54 (-87.07)	-2745.81 (-9008.56)	7790.80 (25,560.37)	0.02690
	Operational Trajectory	-2,322,832 (-7,620,838)	-142,124 (-466,286)	-6,148,429 (-20,172,011)	6,574,110 (21,568,603)	7284.60 (23,899.61)	-26.96 (-88.45)	-2756.71 (-9044.32)	7788.81 (25,553.84)	0.03622

Table 10-2. Guidance Comparisons (Continued)

EVENT	DATA SOURCE	POSITIONS (METERS) (FT)				VELOCITIES M/S (FT/S)				FLIGHT PATH ANGLE (DEG)
		X_S	Y_S	Z_S	R	$\dot{X}_S$	$\dot{Y}_S$	$\dot{Z}_S$	V_S	γ
Second S-IVB ECO	Guidance	4,836,744 (15,868,583)	-61,604 (-202,112)	-4,635,225 (-15,207,431)	6,699,493 (21,979,963)	8393.63 (27,538.16)	408.79 (1341.17)	6847.05 (22,464.07)	10,839.84 (35,563.78)	6.98785
	Postflight Trajectory	4,817,420 (15,805,184)	-63,231 (-207,451)	-4,653,785 (-15,268,322)	6,698,451 (21,976,545)	8412.93 (27,601.48)	408.40 (1339.90)	6825.11 (22,392.09)	10,840.96 (35,567.45)	6.91287
	Operational Trajectory	4,823,682 (15,825,729)	-61,683 (-202,371)	-4,651,489 (-15,260,971)	6,701,348 (21,986,049)	8409.82 (27,591.27)	408.93 (1341.63)	6825.36 (22,392.91)	10,838.72 (35,560.10)	6.959
Translunar Injection	Guidance	4,920,373 (16,142,956)	-57,507 (-188,670)	-4,566,438 (-14,981,750)	6,713,101 (22,024,610)	8332.21 (27,336.65)	410.24 (1345.93)	6910.34 (22,671.72)	10,832.68 (35,540.29)	7.44149
	Postflight Trajectory	4,901,502 (16,081,042)	-59,131 (-193,998)	-4,585,002 (-15,042,657)	6,711,964 (22,020,878)	8351.74 (27,400.72)	410.04 (1345.28)	6889.31 (22,602.72)	10,834.31 (35,545.64)	7.36695
	Operational Trajectory	4,907,485 (16,100,674)	-57,584 (-188,924)	-4,582,907 (-15,035,785)	6,714,891 (22,030,484)	8348.15 (27,388.94)	410.29 (1346.10)	6888.63 (22,600.49)	10,831.12 (35,535.17)	7.412

Table 10-3. Guidance Components Differences

PARAMETERS	OBSERVED TRAJECTORY LVDC	OPERATIONAL TRAJECTORY LVDC
PARKING ORBIT INSERTION		
$\Delta\dot{x}_S$ m/s (ft/s)	1.17 (3.84)	-4.05 (-13.29)
$\Delta\dot{y}_S$ m/s (ft/s)	1.21 (3.97)	0.08 (0.26)
$\Delta\dot{z}_S$ m/s (ft/s)	0.34 (1.12)	-1.66 (-5.45)
ΔV_S m/s (ft/s)	-0.21 (-0.69)	-0.18 (-0.59)
Δx_S m (ft)	-457 (-1499)	-1244 (-4081)
Δy m (ft)	1280 (4199)	72 (236)
Δz m (ft)	239 (784)	2402 (7880)
ΔR m (ft)	-282 (-925)	-25 (-82)
$\Delta\Theta$ deg	0.01269	-0.00098
TIME BASE 6		
Δx_S m/s (ft/s)	-10.67 (-35.01)	-16.91 (-55.48)
$\Delta\dot{y}_S$ m/s (ft/s)	-0.40 (-1.31)	-0.82 (-2.69)
$\Delta\dot{z}_S$ m/s (ft/s)	-24.88 (-81.63)	-35.78 (-117.39)
ΔV_S m/s (ft/s)	-1.26 (-4.13)	-3.25 (-10.66)
Δx_S m (ft)	-23,163 (-75,994)	-32,642 (-107,093)
Δy_S m (ft)	-1557 (-5108)	-62 (-203)
Δz_S m (ft)	6770 (22,210)	8251 (27,070)
ΔR m (ft)	1808 (5932)	3733 (12,247)
$\Delta\Theta$ deg	-0.01089	-0.00157
TRANSLUNAR INJECTION		
$\Delta\dot{x}_S$ m/s (ft/s)	19.53 (64.07)	15.94 (52.30)
$\Delta\dot{y}_S$ m/s (ft/s)	-0.20 (-0.66)	0.05 (0.16)
$\Delta\dot{z}_S$ m/s (ft/s)	-21.03 (-69.00)	-21.71 (-71.23)
ΔV_S m/s (ft/s)	1.63 (5.35)	-1.56 (-5.12)
Δx_S m (ft)	-18,871 (-61,913)	-12,888 (-42,283)
Δy_S m (ft)	-1624 (-5328)	-78 (-256)
Δz_S m (ft)	-18,564 (-60,906)	-16,470 (-54,035)
ΔR m (ft)	-1138 (-3734)	1790 (5873)
$\Delta\Theta$ deg	-0.07454	-0.03548

During the calculation of BNVC, DVC_i^2 lost significant information due to round off. The scaling factor required 28 bits of information. The LVDC maintains only 25 bits of information. The three least significant bits of information were lost by computer underflow. Another bit was lost due to the binary arithmetic and hardware algorithm for division. As a consequence, the apparent increase in BNVC per computer cycle was less than the actual increase in BNVC. The total S-II characteristic velocity error at the time of actual EMR shift was about 92.6 m/s (303.8 ft/s). The deviation in EMR shift time caused no performance perturbation. Figure 10-3 gives the differences between S-II stage correct BNVC values and those computed by the LVDC flight program. Investigation is being conducted to improve scaling in IU LVDC velocity calculations.

10.3 NAVIGATION AND GUIDANCE SCHEME EVALUATION

All analyzed guidance and navigation measurements indicated satisfactory performance throughout the flight. The active guidance phases start and stop times are given in Table 10-4. Included in this table are the start and stop times in the artificial tau phases and chi freezes. The rate-limited attitude commands shown in Figures 10-4 and 10-5 indicate near nominal performances.

The flight program routine causing S-II EMR shift to be commanded was entered later than predicted in the OT. This deviation is discussed in paragraph 10.2.1.

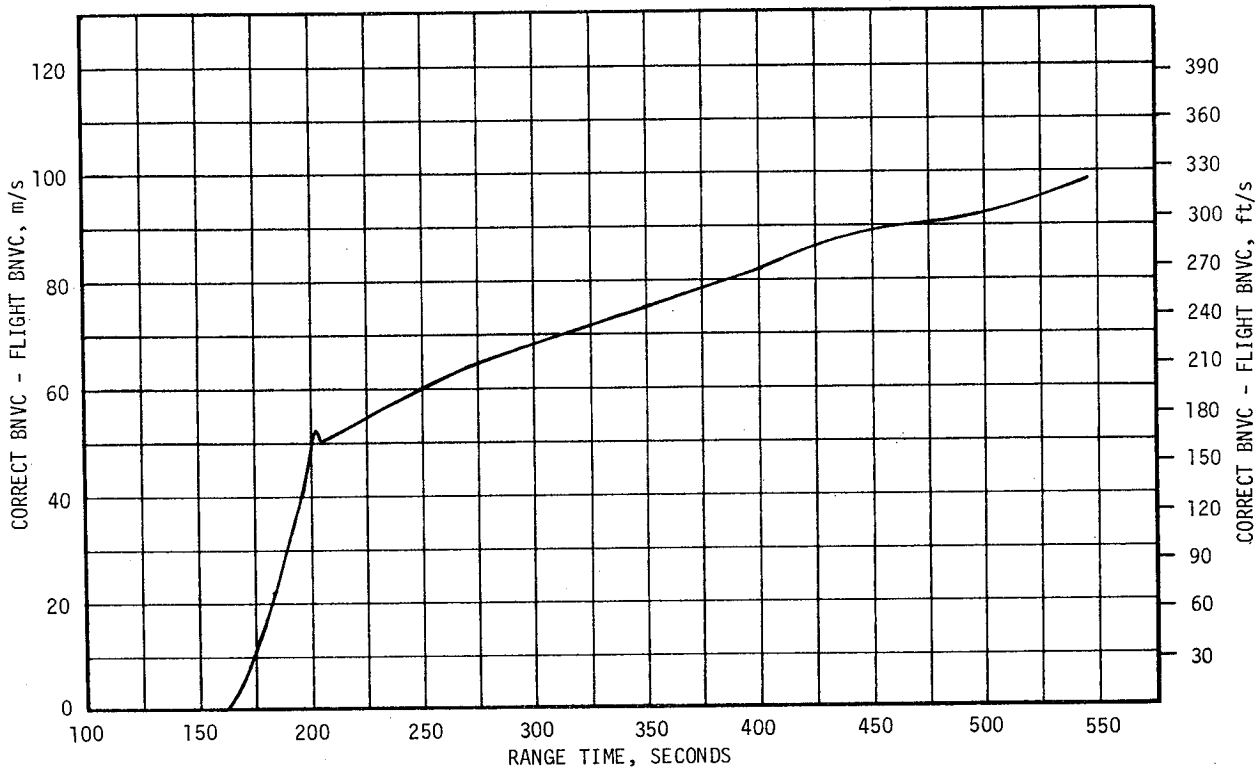

Figure 10-3. AS-506 Characteristic Velocity Error

Table 10-4. Start and Stop Times for IGM Guidance Commands

EVENT*	IGM PHASE (SEC)		ARTIFICIAL TAU (SEC)		STEERING MISALIGNMENT CORRECTION (SEC)		TERMINAL GUIDANCE (SEC)		CHI FREEZE (SEC)	
	Start	Stop	Start	Stop	Start	Stop	Start	Stop	Start	Stop
First Phase IGM	204.07	494.83			221.52	496.82				
Second Phase IGM	494.83	548.2	494.83	504.16	498.73	548.2				
Third Phase IGM	548.2	691.64	555.57	562.43	562.43	691.64	665.15	691.64	691.64	699.26**
Fourth Phase IGM	9862.51	9974.58			9872.87					
Fifth Phase IGM	9974.58	10,201.92	9974.58	9980.37		10,199.70	10,174.47	10,201.92	10,201.92	10,203.56**

* All times are for the start of the computation cycle in which the event occurred.

** Start orbital timeline.

Orbital guidance events were accomplished satisfactorily. All S-IVB stage first and second burn guidance parameters indicate satisfactory operation. The orbital insertion conditions after S-IVB first burn are given in Table 10-5. The TLI parameters after S-IVB second burn are given in Table 10-6.

10.4 GUIDANCE SYSTEM COMPONENT EVALUATION

10.4.1 LVDC Performance

The LVDC performed as predicted for the AS-506 mission. No valid error monitor word and no self-test error data have been observed that indicate any deviation from correct operation.

10.4.2 LVDA Performance

The LVDA performance was nominal. No valid error monitor words and no self-test error data indicating deviations from correct performance were observed.

10.4.3 Ladder Outputs

The ladder networks and converter amplifiers performed satisfactorily. No data have been observed that indicate an out-of-tolerance condition between Channel A and the reference channel converter-amplifiers.

10.4.4 Telemetry Outputs

Analysis of the available LVDA telemetry buffer and flight control computer attitude error plots indicated symmetry between the buffer outputs and the ladder outputs. The available LVDC power supply plots indicates satisfactory power supply performance. The H60-603 guidance computer telemetry was completely satisfactory.

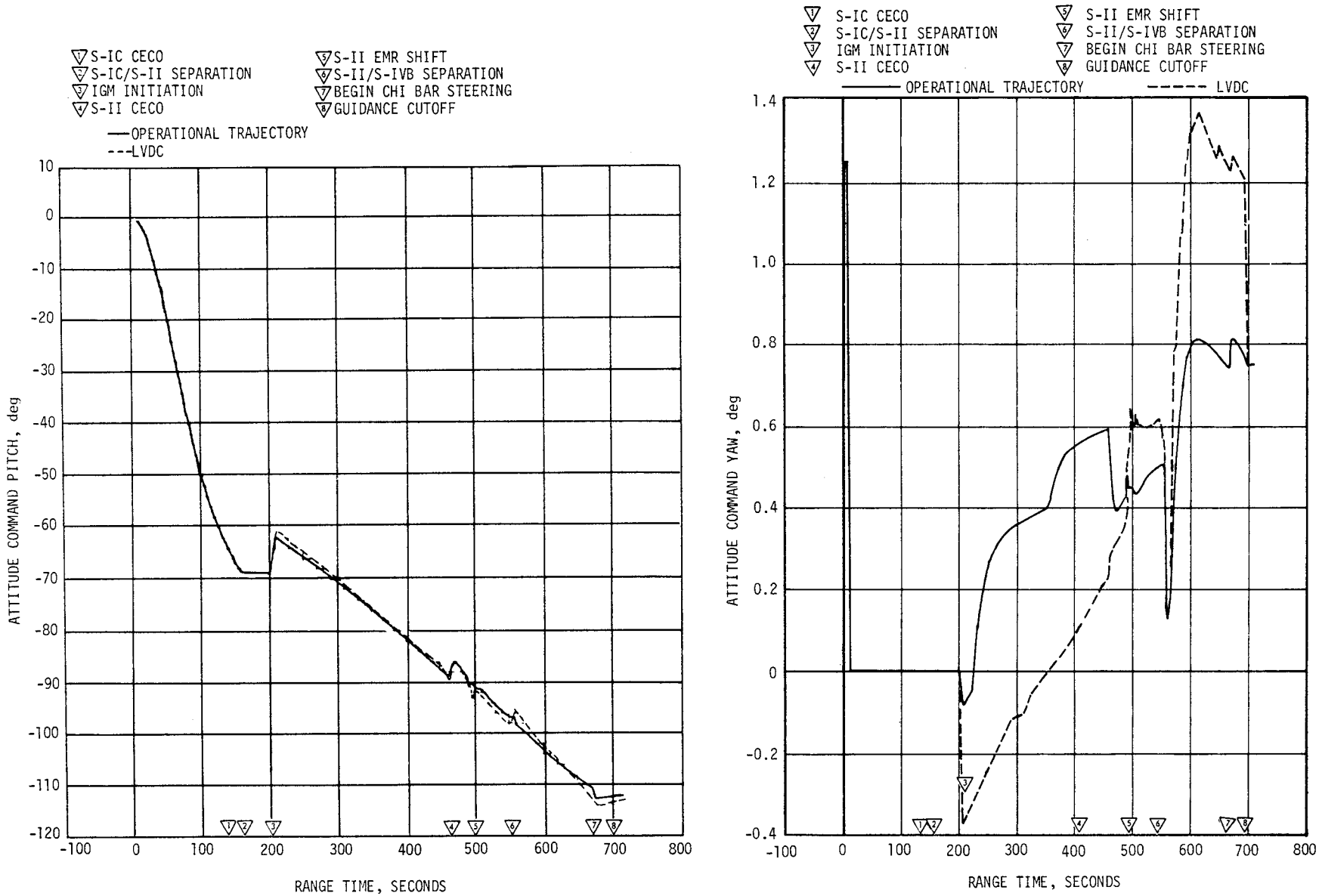

Figure 10-4. Attitude Commands During Active Guidance Period

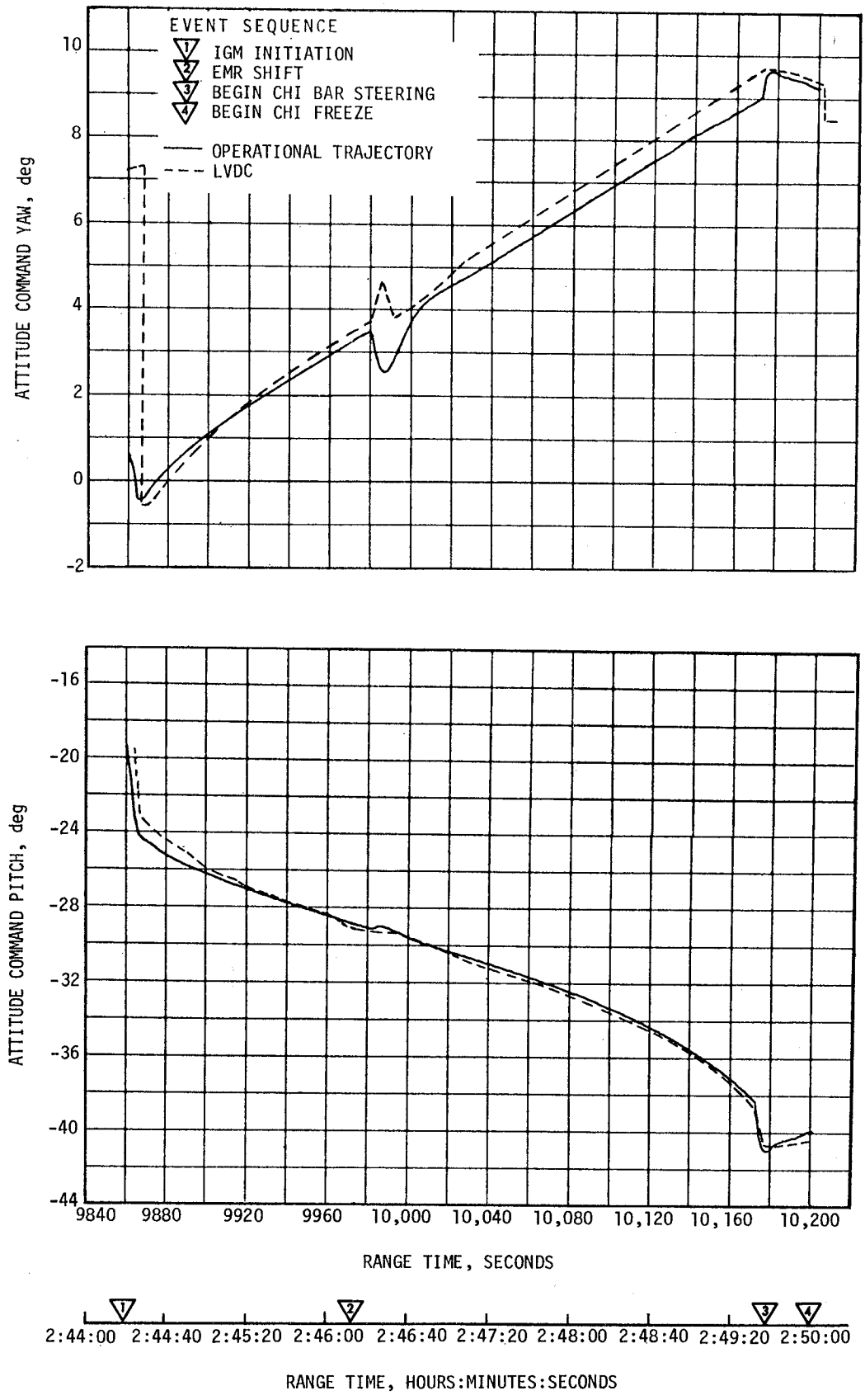

Figure 10-5. Attitude Angles During S-IVB Second Burn

Table 10-5. Parking Orbit Insertion Parameters

PARAMETER	OPERATIONAL TRAJECTORY	POSTFLIGHT TRAJECTORY	TRAJECTORY MINUS OT	LVDC	LVDC MINUS OT
Inertial Velocity m/s (ft/s)	7793.1 (25,567.9)	7793.1 (25,567.9)	0.0 (0.0)	7793.3 (25,568.5)	0.18 (0.6)
Flight Path Angle deg	-0.001	0.012	0.013	-0.0006	0.0004
Descending Node deg	123.100	123.088	-0.012	123.102	0.002
Inclination deg	32.531	32.521	-0.010	32.532	0.001
Eccentricity	0.00022	0.00021	-0.00001	0.00007	-0.00015

10.4.5 Discrete Outputs

No valid discrete output register words (tags 043 and 052) were observed to indicate guidance or simultaneous memory failure.

10.4.6 Switch Selector Functions

Switch selector data indicate that the LVDA switch selector functions were performed satisfactorily. No error monitor words were observed that indicate disagreement in the Triple Modular Redundant (TMR) switch selector register positions or in the switch selector feedback circuits. No mode code 24 words or switch selector feedback words were observed that indicated a switch selector feedback was in error. In addition, no indications were observed to suggest that the B channel input gates to the switch selector register positions were selected.

Table 10-6. Translunar Injection Parameters

PARAMETER	OPERATIONAL TRAJECTORY	POSTFLIGHT TRAJECTORY	TRAJECTORY MINUS OT	LVDC	LVDC MINUS OT
Inertial Velocity m/s (ft/s)	10,831.1 (35,535.1)	10,834.3 (35,545.6)	3.2 (10.5)	10,832.7 (35,540.4)	1.6 (5.3)
Descending Node deg	121.866	121.847	-0.019	121.855	-0.011
Inclination deg	31.379	31.383	0.004	31.382	0.003
Eccentricity	0.97667	0.97696	0.00029	0.97670	0.00003
C_3 m^2/s^2 (ft^2/s^2)	-1,408,484 (-15,160,796)	-1,391,607 (-14,979,133)	16,877 (181,633)	-1,406,545 (-15,139,924)	1939 (20,872)

10.4.7 ST-124M-3 Inertial Platform

The inertial platform system performed as designed. At 3.3 seconds after liftoff, the Y velocity (crossrange) exhibited a change of approximately -1.8 m/s (-5.9 ft/s). A lack of data prevents a precise determination of the cause; however, the probable cause was the Y accelerometer head momentarily contacting an internal mechanical stop. The forcing function was probably crossrange polarized 35 to 40 hertz vibrations, the natural frequency of the accelerometer servo loop.

The Y accelerometer head movement indicated significant incident vibrations. However, the measurement was sampled rather than continuous so the frequency and amplitude of the head motion cannot be readily defined.

The Y gyro was relatively unperturbed, but the X and Z gyros showed significant activity. This indicates a forcing function, probably vibration, mainly along the platform Y axis.

The body-mounted yaw accelerometer, A7-603, was oriented in the same direction as the Y accelerometer. It indicated a generally high random level of vibration which included significant amplitudes between 35 and 45 hertz. The amplitude is presently indeterminate because of telemetry channel and band width limitations.

The X, Y, and Z gyro servo loops for the stable element functioned as designed. The operational limits of the servo loops were not reached at anytime during the mission.

The inertial gimbal temperatures fell below specifications; however, there are no indications of degraded inertial performance. The temperature went below the minimum specification of 313.15°K (104.0°F) at 15,600 seconds, reaching 312.2°K (102.3°F) at approximately 20,800 seconds.

SECTION 11

CONTROL SYSTEM

11.1 SUMMARY

The AS-506 control system, which was essentially the same as that of AS-505, performed satisfactorily. The Flight Control Computer (FCC), Thrust Vector Control (TVC), and Auxiliary Propulsion System (APS) satisfied all requirements for vehicle attitude control during the flight. Bending and slosh dynamics were adequately stabilized. The prelaunch programed yaw, roll, and pitch maneuvers were properly executed during S-IC boost.

During the maximum dynamic pressure region of flight, the launch vehicle experienced winds that were less than 95-percentile July winds. The maximum average pitch and yaw engine deflections were the result of wind shears.

S-IC/S-II first and second plane separations were accomplished with no significant attitude deviations. At Iterative Guidance Mode (IGM) initiation, a pitch up transient occurred similar to that seen on previous flights. At S-II early Center Engine Cutoff (CECO), the guidance parameters were modified by the loss of thrust. There was a change in yaw attitude due to the slight thrust misalignment of the center engine. S-II/S-IVB separation occurred as expected and without producing any significant attitude deviations.

Satisfactory control of the vehicle was maintained during first and second S-IVB burns and during coast in Earth Parking Orbit (EPO). During the Command and Service Module (CSM) separation from the S-IVB/IU and during the Transposition, Docking and Ejection (TD&E) maneuver, the control system maintained the vehicle in a fixed inertial attitude to provide a stable docking platform. Following TD&E, S-IVB/IU attitude control was maintained during the maneuver to the slingshot attitude and during the LOX dump and LH_2 vent.

11.2 S-IC CONTROL SYSTEM EVALUATION

The AS-506 control system performed adequately during S-IC powered flight. The vehicle flew through winds which were less than 95 percentile for July in the maximum dynamic pressure region of flight. Less than 10 percent of the available engine deflection was used throughout flight (based on average engine gimbal angle). S-IC outboard engine cant was accomplished as planned.

All dynamics were within vehicle capability. In the region of high dynamic pressure, the maximum angles-of-attack were 1.6 degrees in pitch and 1.4 degrees in yaw. The maximum average pitch and yaw engine deflections were 0.2 degree and 0.3 degree, respectively, in the maximum dynamic pressure region. Both deflections were due to wind shears. The absence of any divergent bending or slosh frequencies in vehicle motion indicates that bending and slosh dynamics were adequately stabilized.

Vehicle attitude errors required to trim out the effects of thrust imbalance, thrust misalignment, and control system misalignments were within predicted envelopes. Vehicle dynamics prior to S-IC/S-II first-plane separation were within staging requirements.

11.2.1 Liftoff Clearances

The launch vehicle cleared the mobile launcher structure within the available clearance envelopes. Camera data showing liftoff motion were not available for the AS-506 flight, but simulations with flight data show that less than 15 percent of the available clearance was used. The ground wind was from the south with a magnitude of 3.3 m/s (6.4 knots) at the 18.3 m (60 ft) level.

The predicted and measured misalignments, slow release forces, winds, and the thrust-to-weight ratio are shown in Table 11-1.

11.2.2 S-IC Flight Dynamics

Maximum control parameters during S-IC burn are listed in Table 11-2. Pitch, yaw, and roll plane time histories during S-IC boost are shown in Figures 11-1, 11-2, and 11-3. Dynamics in the region between liftoff and 40 seconds result primarily from guidance commands. Between 40 and 110 seconds, maximum dynamics were caused by the pitch tilt program, wind magnitude, and wind shears. Dynamics from 110 seconds to S-IC/S-II separation were caused by high altitude winds, separated air flow aerodynamics, center engine shutdown, and tilt arrest. The transient at CECO indicates that the center engine cant was 0.2 degree in yaw and -0.06 degree in pitch.

At Outboard Engine Cutoff (OECO), the vehicle had attitude errors of -0.3, 0.1, and 0.0 degree in pitch, yaw, and roll, respectively. These errors are required to trim out the effects of thrust imbalance, offset Center of Gravity (CG), thrust vector misalignment, and control system misalignments. The maximum equivalent thrust misalignments were 0.11, -0.05 and -0.02 degree in pitch, yaw, and roll, respectively.

There was no significant sloshing observed. The engine response to the observed slosh frequencies showed that the slosh was well within the capabilities of the control system.

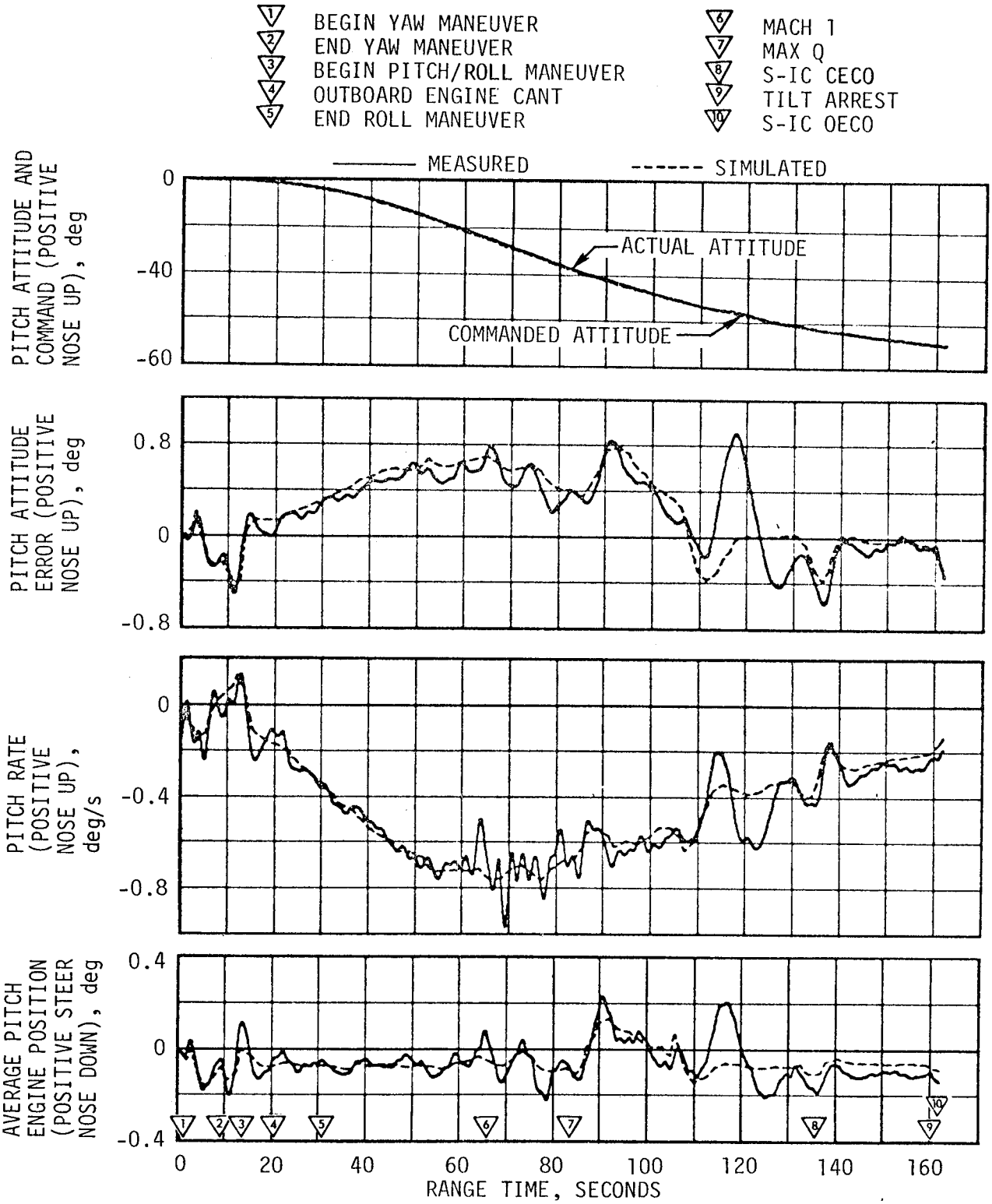

Figure 11-1. Pitch Plane Dynamics During S-IC Burn

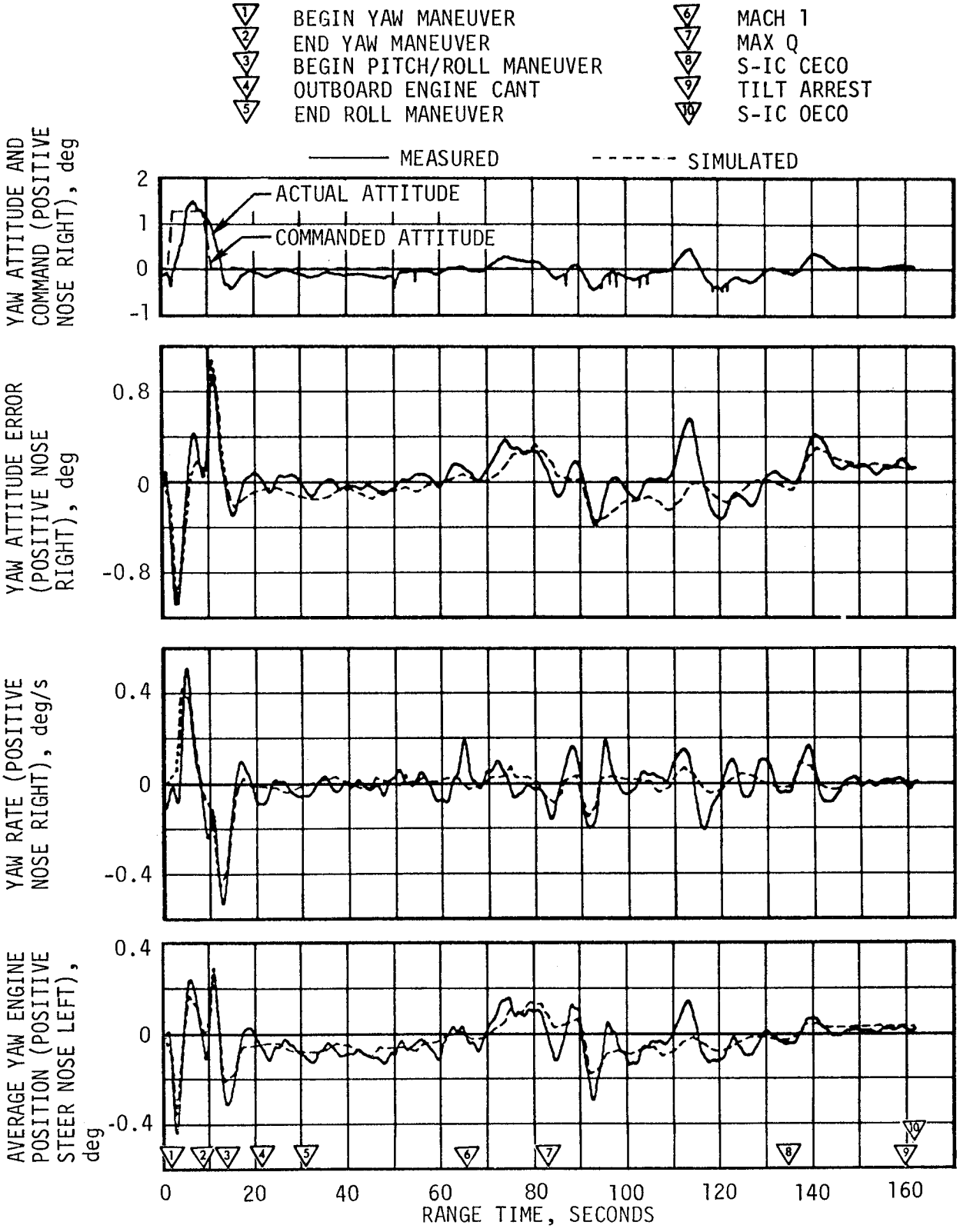

Figure 11-2. Yaw Plane Dynamics During S-IC Burn

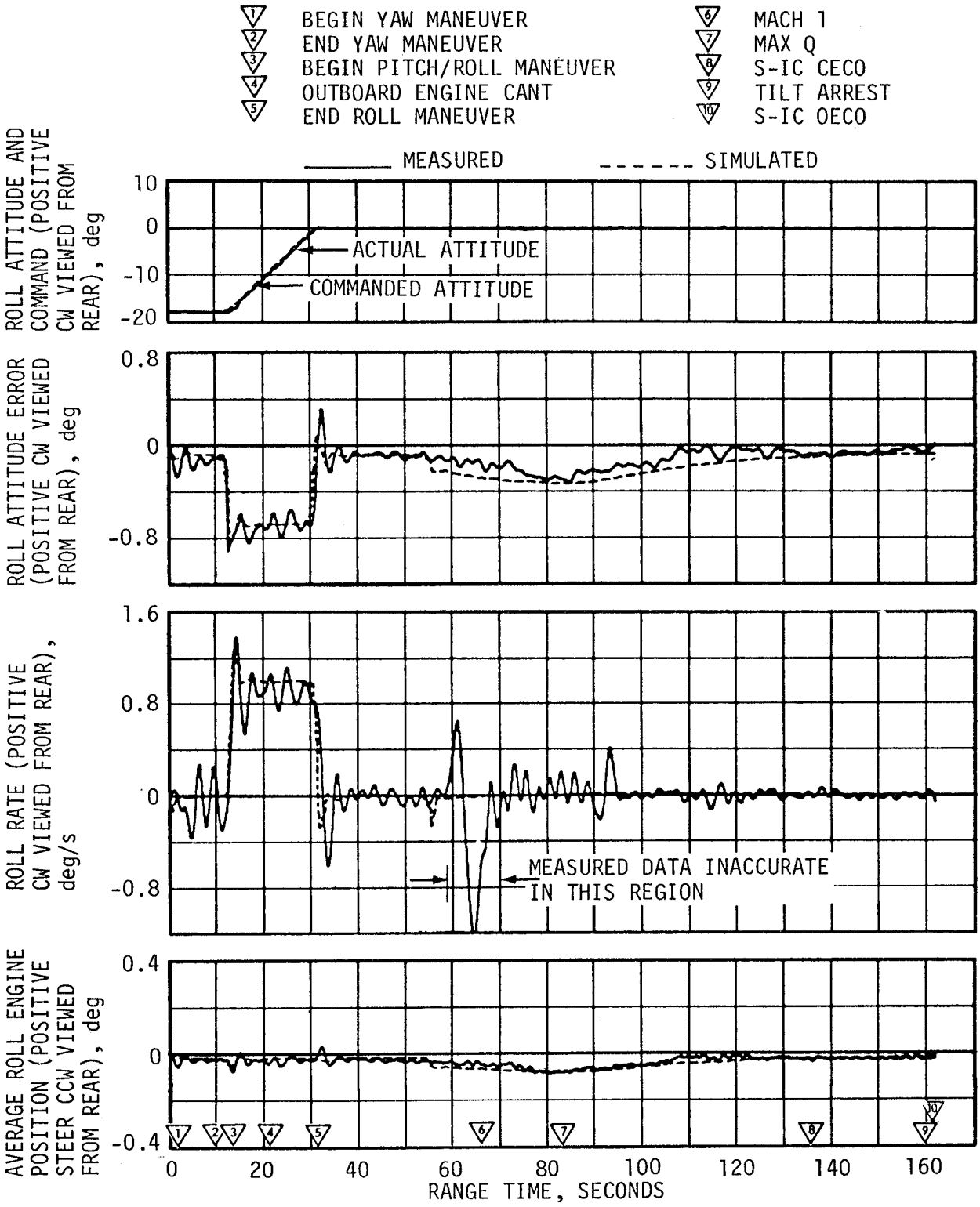

Figure 11-3. Roll Plane Dynamics During S-IC Burn

Table 11-1. AS-506 Misalignment and Liftoff Conditions Summary

	PREFLIGHT PREDICTED			LAUNCH		
	PITCH	YAW	ROLL	PITCH	YAW	ROLL
Thrust Misalignment deg*	±0.34	±0.34	±0.34	0.11	-0.05	-0.02
Center Engine Cant, deg	-	-	-	-0.06	0.2	-
Servo Amplifier Offset, deg/eng	±0.1	±0.1	±0.1	-	-	-
Vehicle Stacking & Pad Misalignment, deg	±0.29	±0.29	0.0	0.12	-0.06	0.0
Attitude Error at Holddown Arm Release, deg	-	-	-	0.06	-0.02	0.02
Peak Slow Release Force Per Rod, N (lbf)	415,000 (93,300)			400,000 (90,000) ***		
Wind	95 Percentile Envelope			3.3 m/s (6.4 Knots) At 18.3 Meters (60 Feet)		
Thrust to Weight Ratio	1.195			**		

*Thrust misalignment of 0.34 degree encompasses the center engine cant. A positive polarity was used to determine minimum fin tip/umbilical tower clearance. A negative polarity was used to determine vehicle/GSE clearances.

**Data not available for update.

*** Approximate data obtained during a data dropout period.

The normal accelerations observed during S-IC burn are shown in Figure 11-4. Pitch and yaw plane wind velocities and angles-of-attack are shown in Figure 11-5. The winds are shown both as determined from balloon and rocket measurements and as derived from the vehicle Q-ball.

11.3 S-II CONTROL SYSTEM EVALUATION

The S-II stage attitude control system performance was satisfactory. Analysis of the magnitude of modal components in the engine deflections revealed that vehicle structural bending and propellant sloshing had negligible effect on control system performance. The maximum values of pitch and yaw control parameters occurred in response to IGM Phase 1 initiation. The maximum values of roll control parameters occurred in

Table 11-2. Maximum Control Parameters During S-IC Burn

PARAMETERS	UNITS	PITCH PLANE		YAW PLANE		ROLL PLANE	
		MAGNITUDE	RANGE TIME (SEC)	MAGNITUDE	RANGE TIME (SEC)	MAGNITUDE	RANGE TIME (SEC)
Attitude Error	deg	0.83	117.4	-1.02	3.3	-0.92	13.8
Angular Rate	deg/s	-0.97	69.1	-0.53	12.6	1.38	14.4
Average Gimbal Angle	deg	0.23	90.6	-0.44	3.2	-0.09	80.9
Angle-of-Attack	deg	1.82	117.1	1.42	73.0	-	-
Angle-of-Attack/ Dynamic Pressure Product	deg-N/cm^2	4.93	91.4	4.50	73.0	-	-
Normal Acceleration	m/s^2	-0.331	95.5	0.306	63.9	-	-

response to S-IC/S-II separation disturbances. The control responses at other times were within expectations.

Between the events of S-IC OECO and initiation of IGM, the vehicle attitude commands were held constant. Significant events occurring during this interval were S-IC/S-II separation, S-II stage J-2 engine start, second plane separation, and Launch Escape Tower (LET) jettison. The attitude control dynamics throughout this interval indicated stable operation as shown in Figures 11-6 through 11-8. Steady-state attitudes were achieved within 20 seconds from S-IC/S-II separation. The maximum control parameter values for the period of S-II burn are shown in Table 11-3.

At IGM initiation, the TVC received FCC commands to pitch the vehicle up. During IGM, the vehicle pitched down at a constant commanded rate of approximately -0.1 deg/s. The transient magnitudes experienced at IGM initiation were similar to those of the AS-504 and AS-505 flights.

A steady-state pitch attitude error of approximately 0.15 degree resulted from thrust imbalance. Following CECO, a steady-state yaw attitude error of -0.3 degree occurred. Peak transient yaw attitude error after CECO was -0.5 degree at 464 seconds. This yaw error occurred in response to the loss of the compliance deflection of the center engine at cutoff. The center engine was not precanted to allow for compliance deflection. This compliance effect occurred in the yaw plane because of the location of the fixed links. Consequently, the outboard engines were deflected in yaw after CECO to compensate for the yaw attitude error and to stabilize the vehicle. The deflections of the outboard engines in pitch after CECO were the result of a pitch-up guidance command. This command was generated to compensate for the effects that loss of center engine thrust would have upon the flight trajectory.

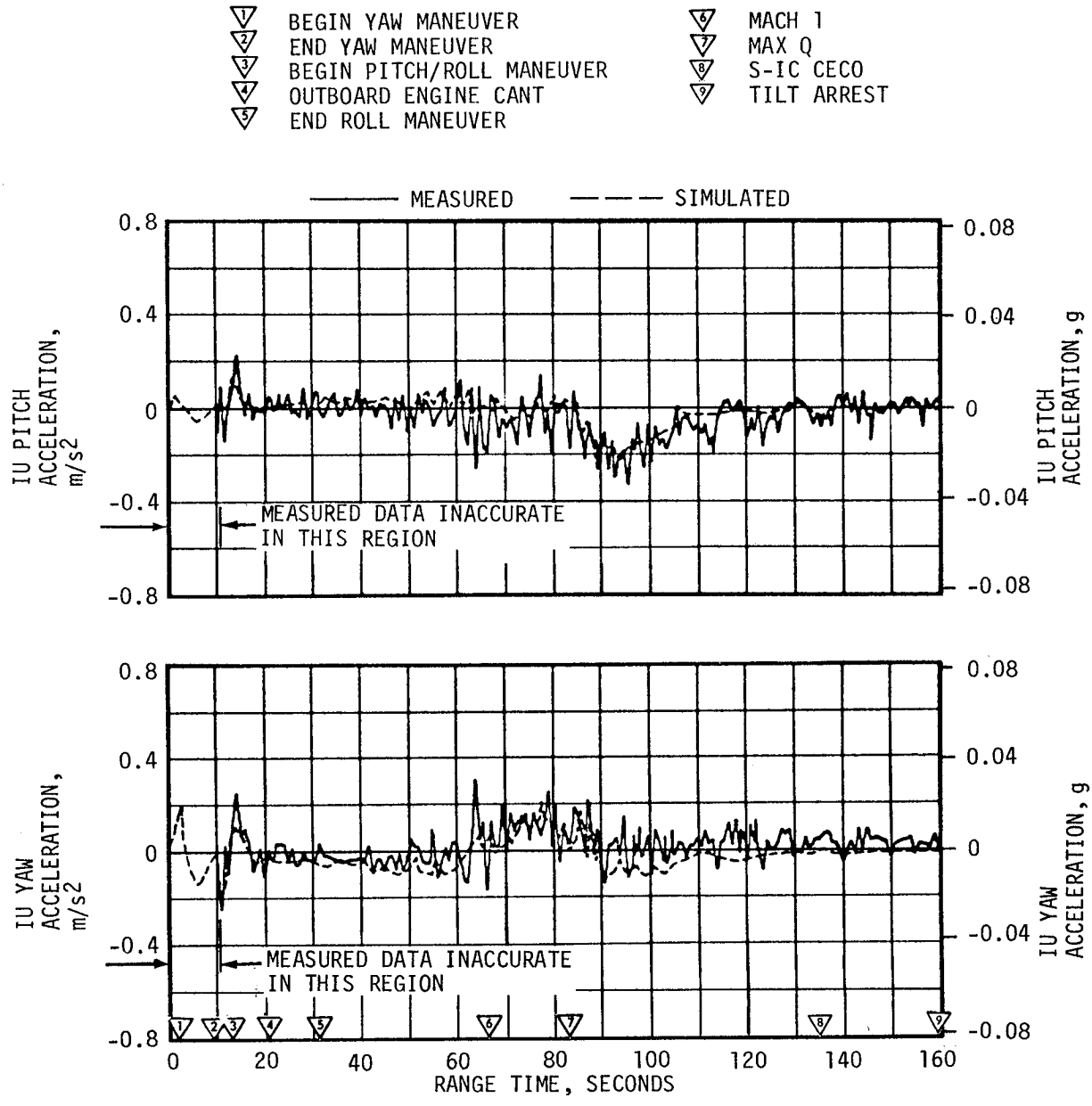

Figure 11-4. Normal Acceleration During S-IC Burn

Simulated and flight data for pitch, yaw, and roll plane dynamics are compared in Figures 11-6, 11-7 and 11-8, respectively. The major differences are as follows: Steady-state yaw attitude error caused by early CECO which reflects a lower compliance than predicted for the center engine; initial transients in the roll axis which could be attributed to uncertainties in thrust buildup of the J-2 engines; and steady-state attitude errors caused by engine location misalignments and thrust vector misalignments.

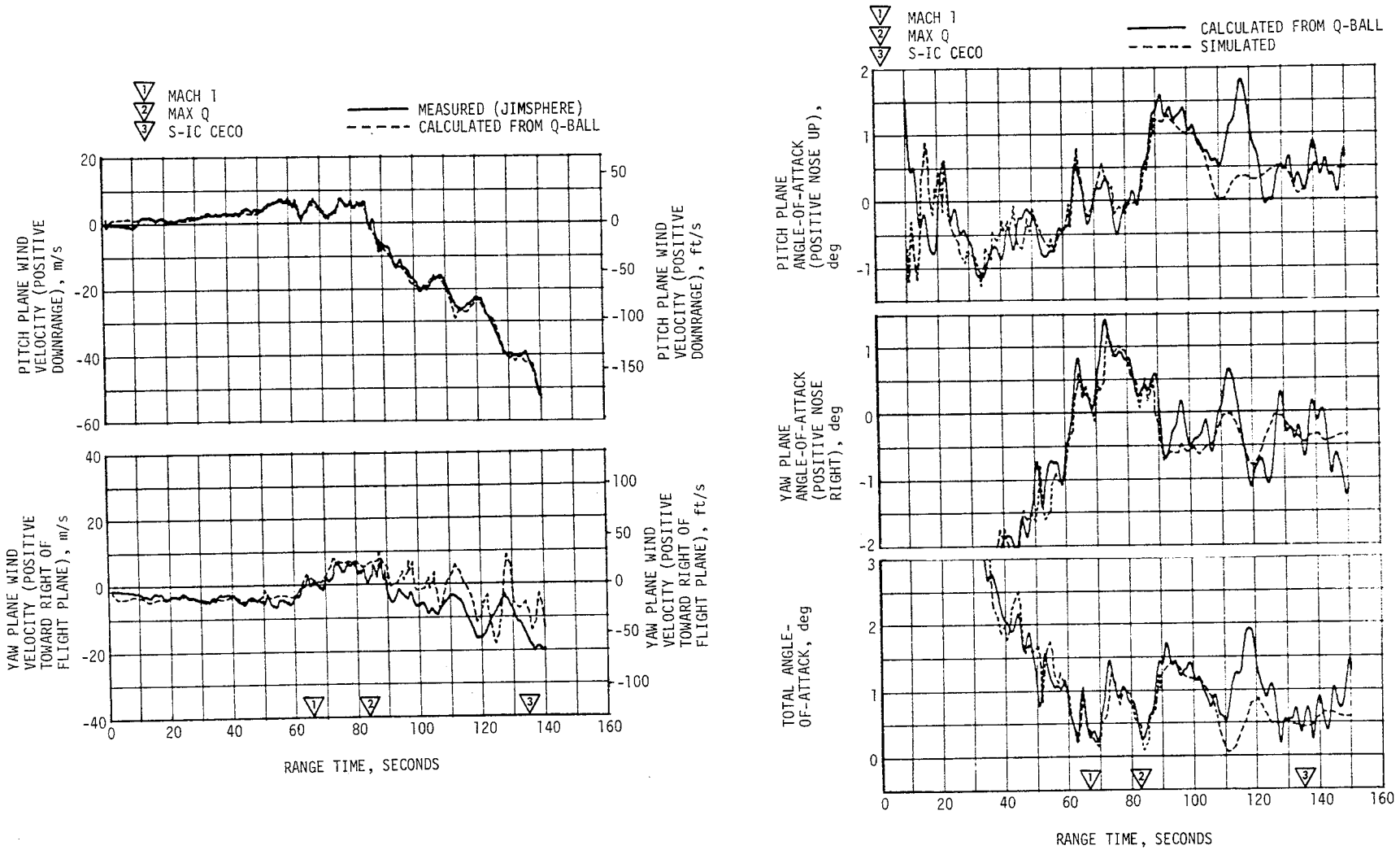

Figure 11-5. Pitch and Yaw Plane Wind Velocity and Free-Stream Angles-Of-Attack During S-IC Burn

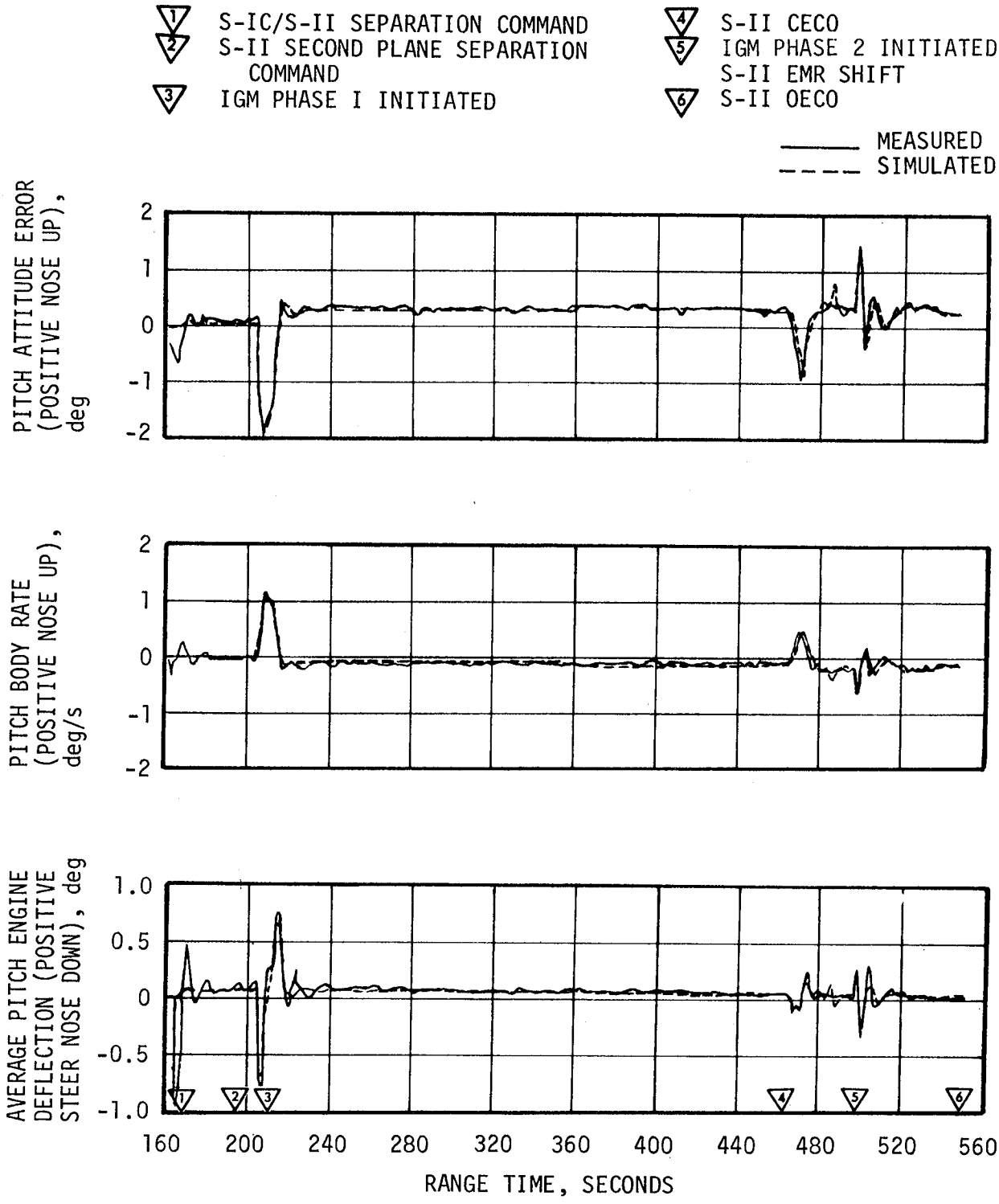

Figure 11-6. Pitch Plane Dynamics During S-II Burn

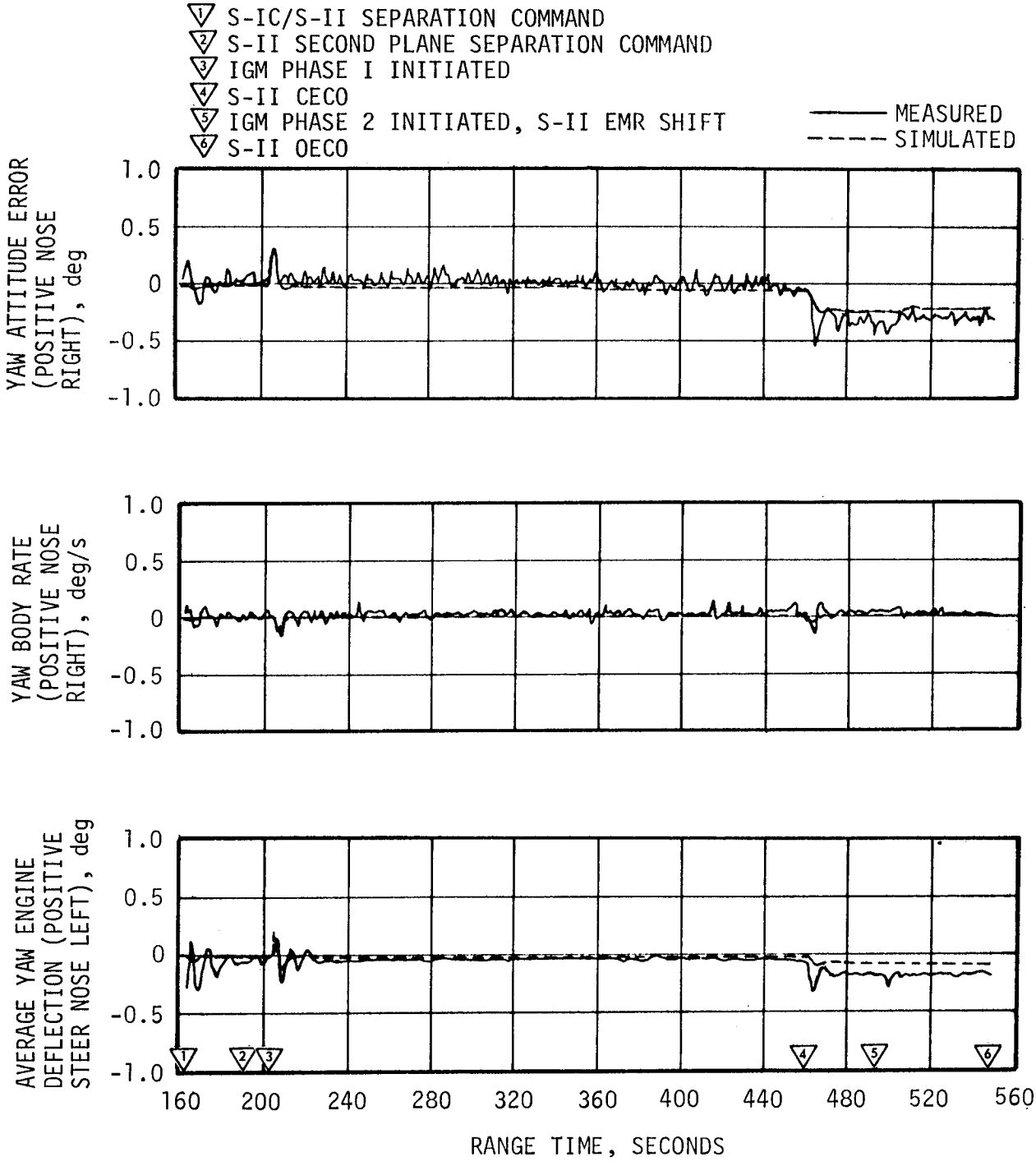

Figure 11-7. Yaw Plane Dynamics During S-II Burn

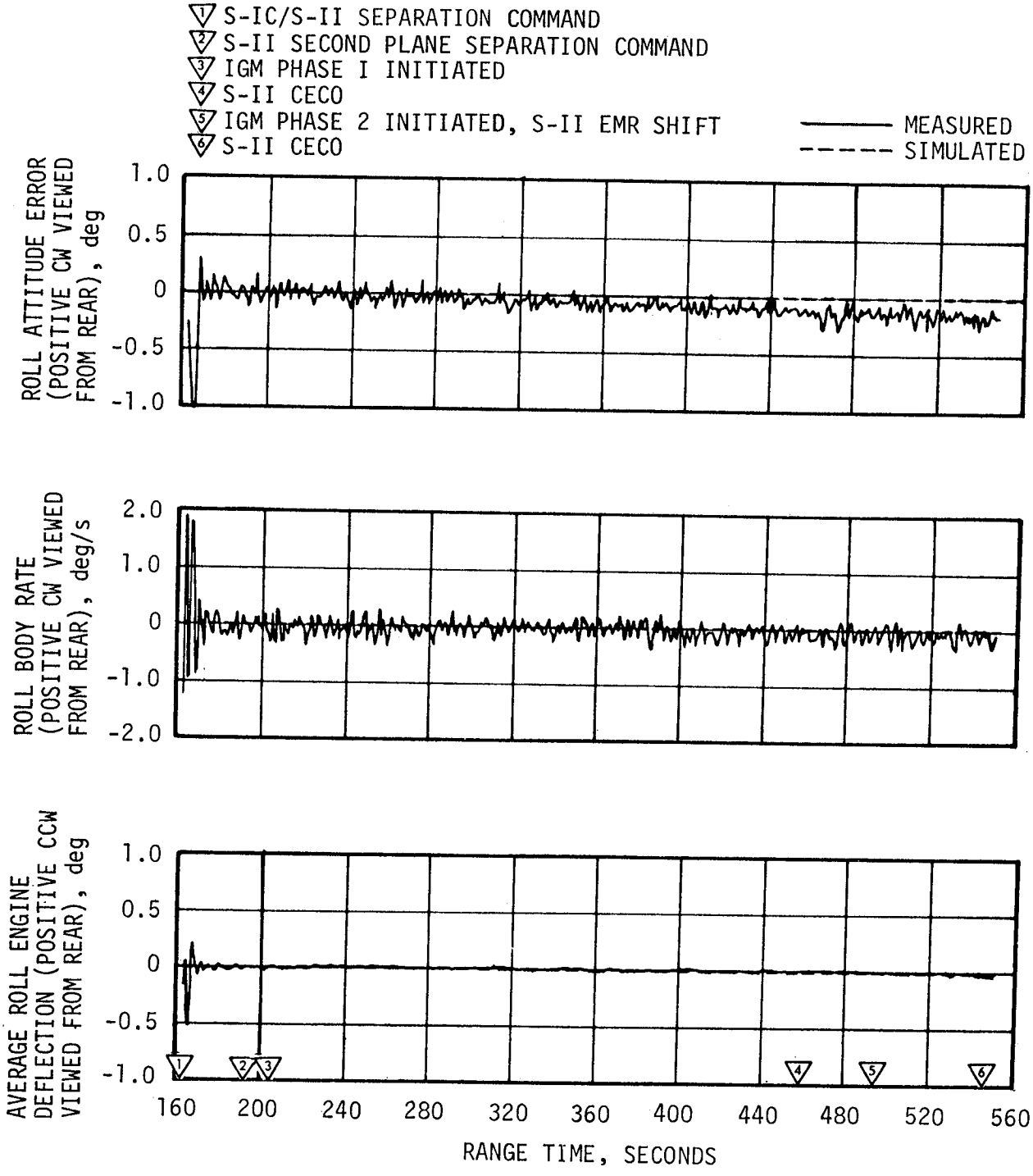

Figure 11-8. Roll Plane Dynamics During S-II Burn

Table 11-3. Maximum Control Parameters During S-II Burn

PARAMETERS	UNITS	PITCH PLANE		YAW PLANE		ROLL PLANE	
		MAGNITUDE	RANGE TIME (SEC)	MAGNITUDE	RANGE TIME (SEC)	MAGNITUDE	RANGE TIME (SEC)
Attitude Error	deg	-1.9	206.9	-0.54	464.8	-1.6	165.5
Angular Rate	deg/s	1.2	207.8	0.2	467.0	1.7	166.2
Average Gimbal Angle	deg	-0.9	165.3	-0.33	464.0	-0.54	165.3

11.4 S-IVB CONTROL SYSTEM EVALUATION

The S-IVB TVC system provided satisfactory pitch and yaw control during powered flight. The APS provided satisfactory roll control during first and second burns.

During S-IVB first and second burns, control system transients were experienced at S-II/S-IVB separation, guidance initiation, Engine Mixture Ratio (EMR) shift, chi bar guidance mode, and J-2 engine cutoff. These transients were expected and were within the capabilities of the control system.

11.4.1 Control System Evaluation During First Burn

The S-IVB first burn attitude control system response to guidance commands for pitch, yaw and roll are presented in Figures 11-9, 11-10 and 11-11, respectively. The maximum attitude errors and rates occurred at IGM and chi bar steering initiation. A summary of maximum values of the critical flight control parameters during S-IVB first burn is presented in Table 11-4.

The pitch and yaw effective thrust vector misalignments during first burn were 0.22 and -0.33 degree, respectively. A steady-state roll torque of 61.4 N-m (45.3 lbf-ft), counterclockwise looking forward, required roll APS firings during first burn. The steady-state roll torque experienced on previous flights has ranged between 27 N-m (20 lbf-ft) counterclockwise and 54.2 N-m (40.0 lbf-ft) clockwise.

11.4.2 Control System Evaluation During Parking Orbit

The coast attitude control system provided satisfactory orientation and stabilization of the S-IVB/CSM in parking orbit. The only maneuver during parking orbit was to align the vehicle with the local horizontal just after S-IVB first cutoff. Pitch axis control parameters during the maneuver to the local horizontal are indicated in Figure 11-12. The yaw and roll control parameters did not show significant transients and are not presented.

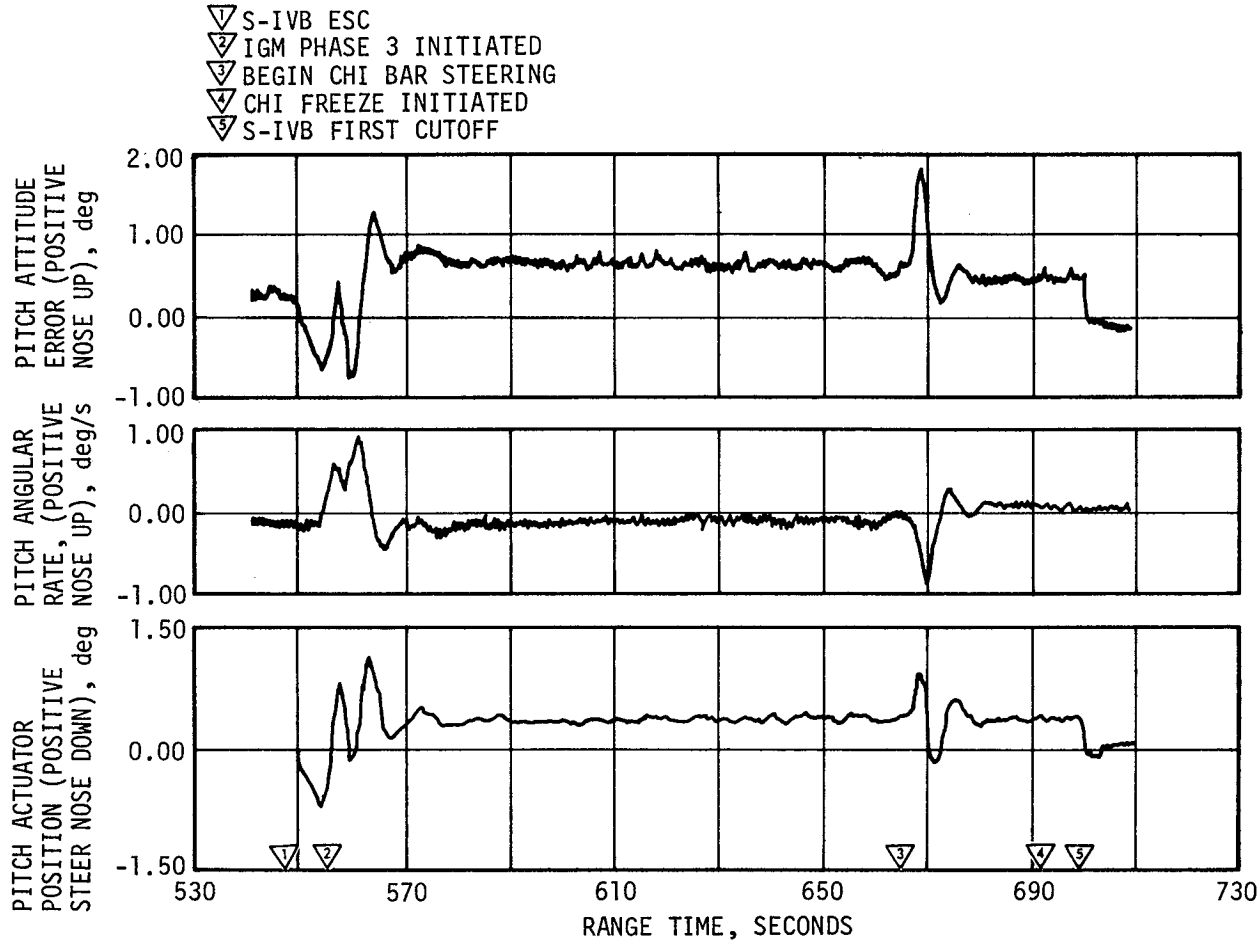

Figure 11-9. Pitch Plane Dynamics During S-IVB First Burn

11.4.3 Control System Evaluation During Second Burn

The S-IVB second burn attitude control system response to guidance commands for pitch, yaw and roll are presented in Figure 11-13, 11-14 and 11-15, respectively. The maximum attitude errors and rates occurred at guidance initiation and EMR shift. A summary of maximum values of the critical flight control parameters during S-IVB second burn is presented in Table 11-5.

The pitch and yaw effective thrust vector misalignments during second burn were approximately 0.25 and -0.35 degree, respectively. The steady-state roll torque during second burn ranged from 42.1 N-m (31.1 lbf-ft) at the low EMR to 52.3 N-m (38.6 lbf-ft) at the 5.0:1.0 EMR.

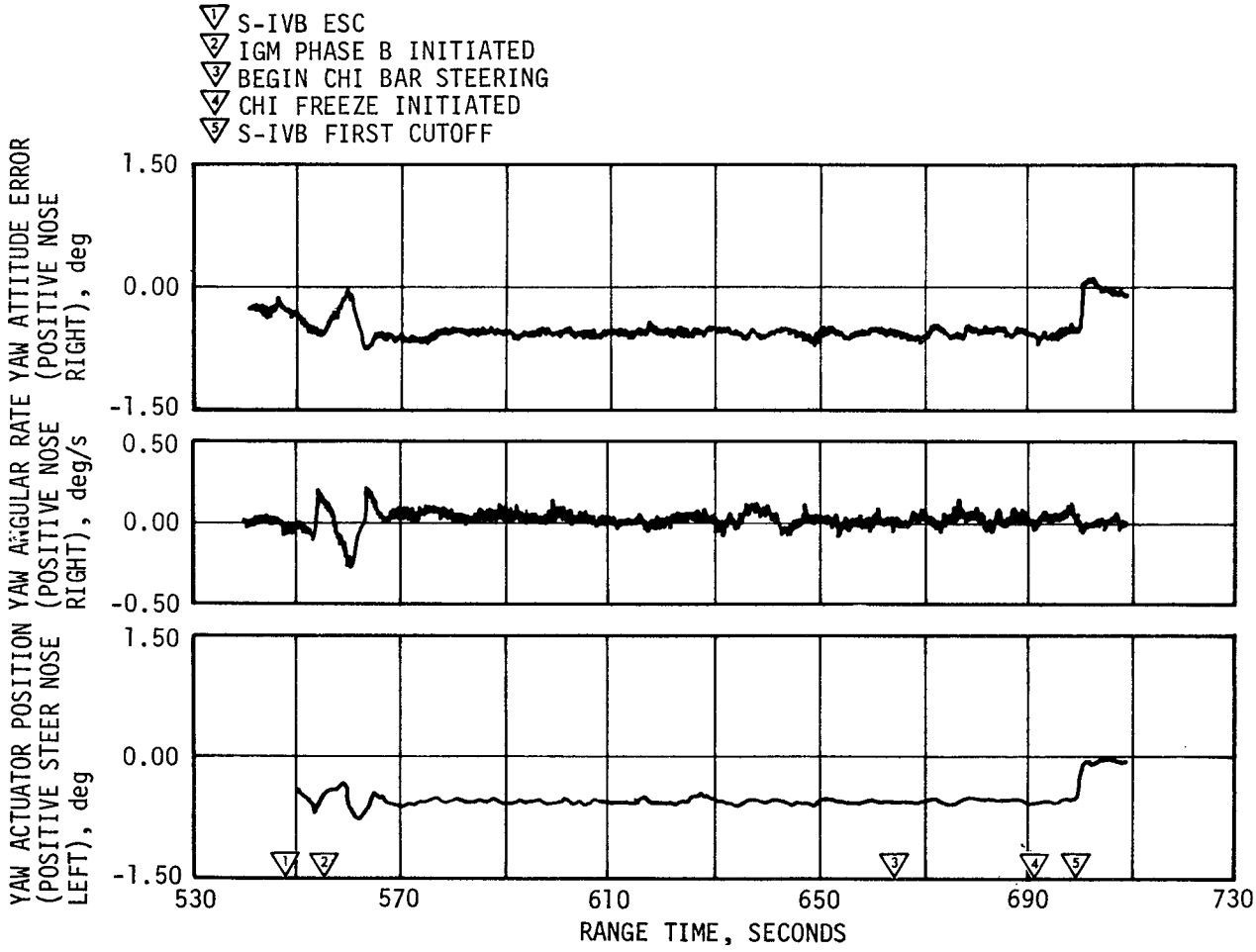

Figure 11-10. Yaw Plane Dynamics During S-IVB First Burn

11.4.4 Control System Evaluation After S-IVB Second Burn

The coast attitude control system provided satisfactory orientation and stabilization from S-IVB second cutoff through the last data available. The maneuver to the local horizontal just after second burn is shown in Figure 11-16 for pitch and yaw control. Attitude control parameters in pitch, yaw, and roll for the maneuver to the TD&E attitude are shown in Figure 11-17. The vehicle attitude was inertially fixed for CSM separation and the TD&E maneuver. Pitch, yaw, and roll control during the maneuver to slingshot attitude are shown in Figure 11-18. The magnitude of the maneuver to slingshot attitude per axis was approximately 36 degrees, 41 degrees, and 10 degrees in pitch, yaw and roll, respectively.

During the LOX dump the S-IVB/IU was controlled to the -1.0 degree attitude error limit in the pitch and yaw axis and approximately -0.4 degree in the roll axis. This performance was expected and as designed.

Table 11-4. Maximum Control Parameters During S-IVB First Burn

PARAMETERS	UNITS	PITCH PLANE		YAW PLANE		ROLL PLANE	
		MAGNITUDE	RANGE TIME (SEC)	MAGNITUDE	RANGE TIME (SEC)	MAGNITUDE	RANGE TIME (SEC)
Attitude Error	deg	+1.80	668.1	-0.77	562.7	-1.15	584.2
Angular Rate	deg/s	+0.90	560.1	-0.29	560.0	+0.10	554.3
Gimbal Angle	deg	+1.08	562.7	-0.79	561.5	--	--

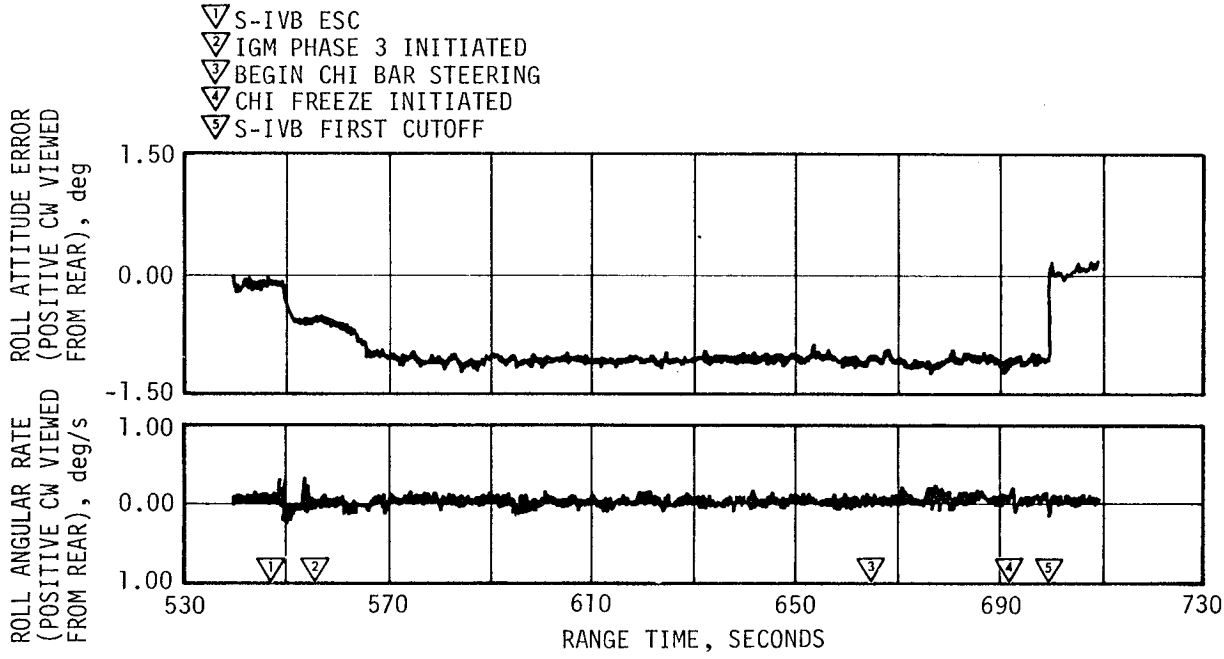

Figure 11-11. Roll Plane Dynamics During S-IVB First Burn

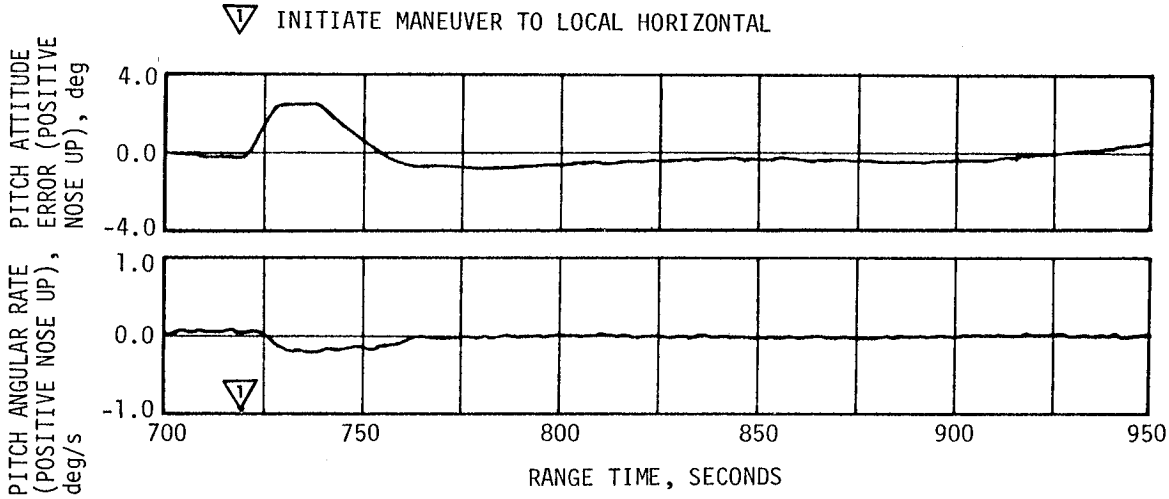

Figure 11-12. Pitch Plane Dynamics During Coast in Parking Orbit

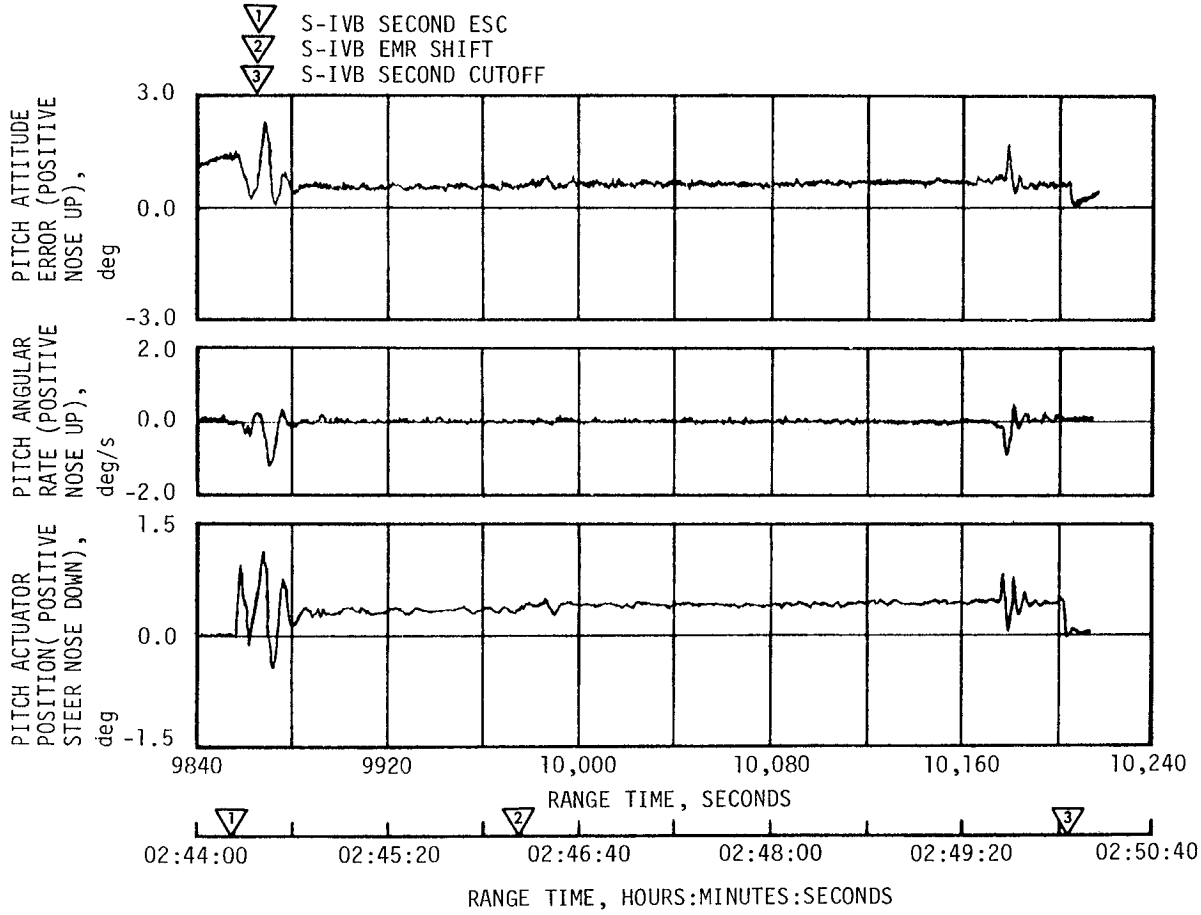

Figure 11-13. Pitch Plane Dynamics During S-IVB Second Burn

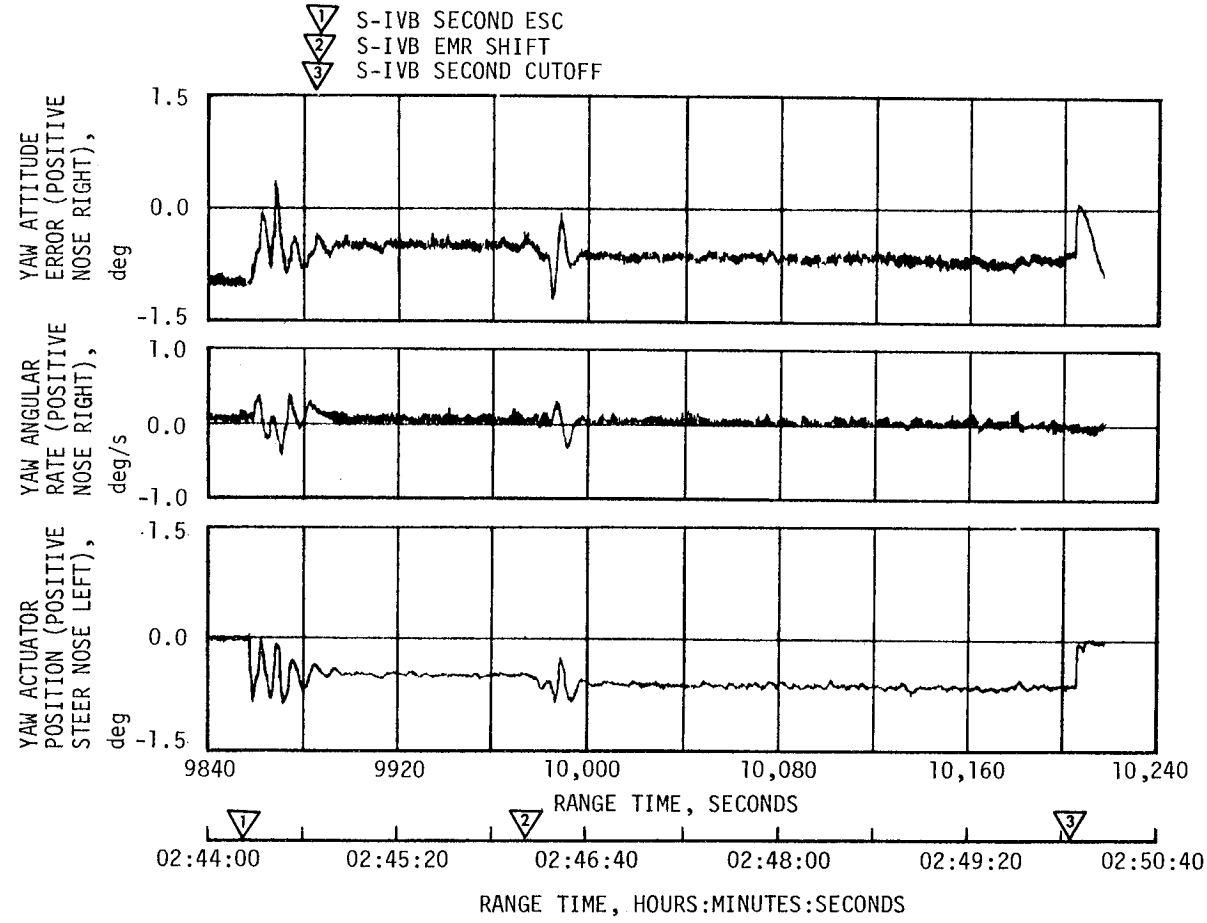

Figure 11-14. Yaw Plane Dynamics During S-IVB Second Burn

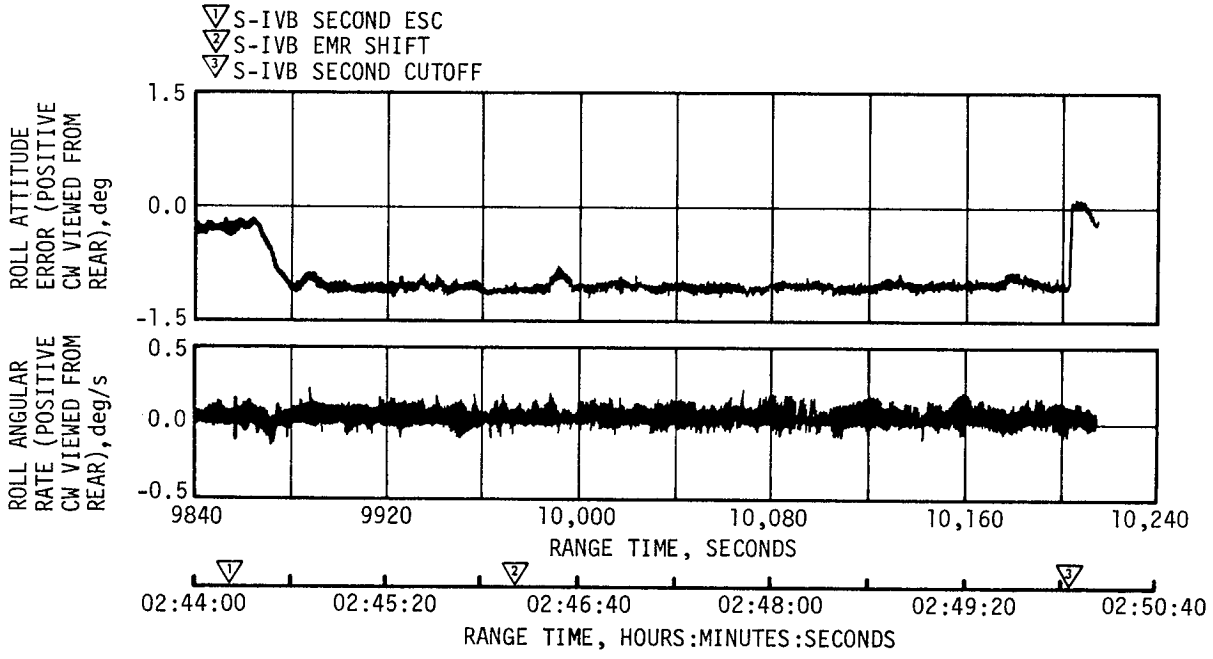

Figure 11-15. Roll Plane Dynamics During S-IVB Second Burn

Table 11-5. Maximum Control Parameters During S-IVB Second Burn

PARAMETERS	UNITS	PITCH PLANE		YAW PLANE		ROLL PLANE	
		MAGNITUDE	RANGE TIME (SEC)	MAGNITUDE	RANGE TIME (SEC)	MAGNITUDE	RANGE TIME (SEC)
Attitude Error	deg	2.3	9,867.9	-1.25	9,984.0	-1.09	9,910.0
Angular Rate	deg/s	-1.25	9,868.6	-0.50	9,869.0	0.175	9,857.2
Gimbal Angle	deg	1.16	9,867.5	-0.99	9,870.0	--	--

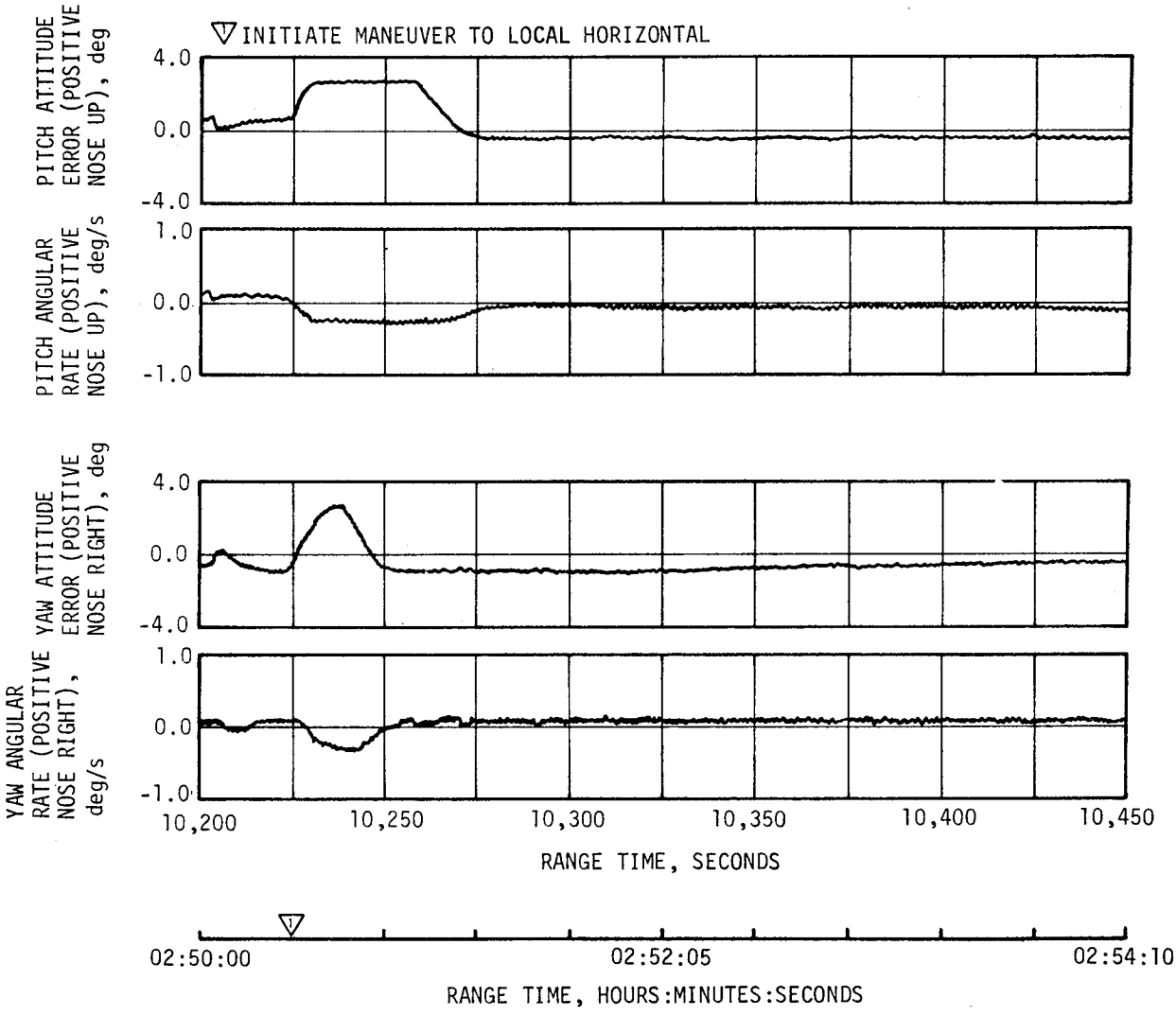

Figure 11-16. Pitch and Yaw Plane Dynamics Following Translunar Injection

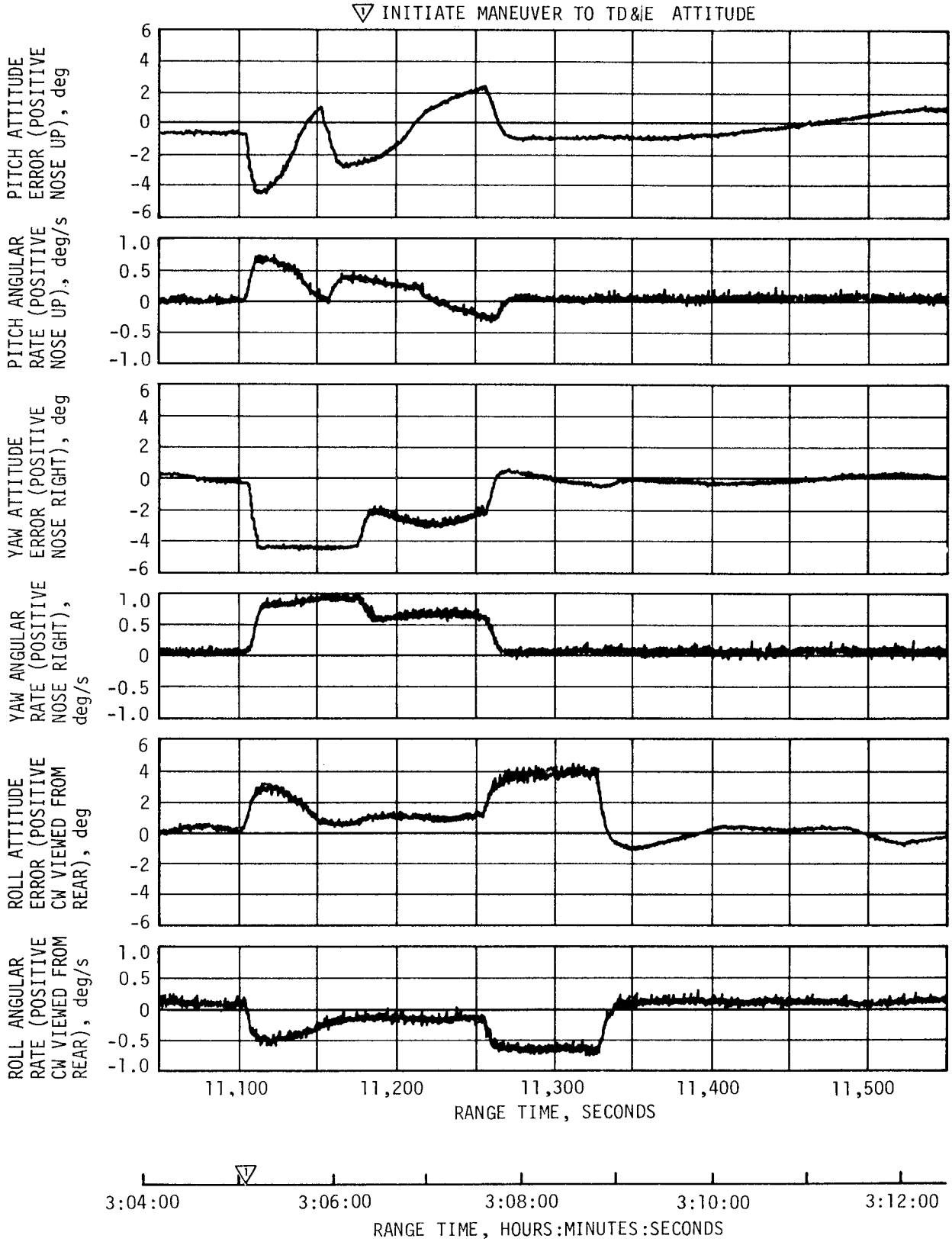

Figure 11-17. Pitch, Yaw and Roll Plane Dynamics During the Maneuver to TD&E Attitude

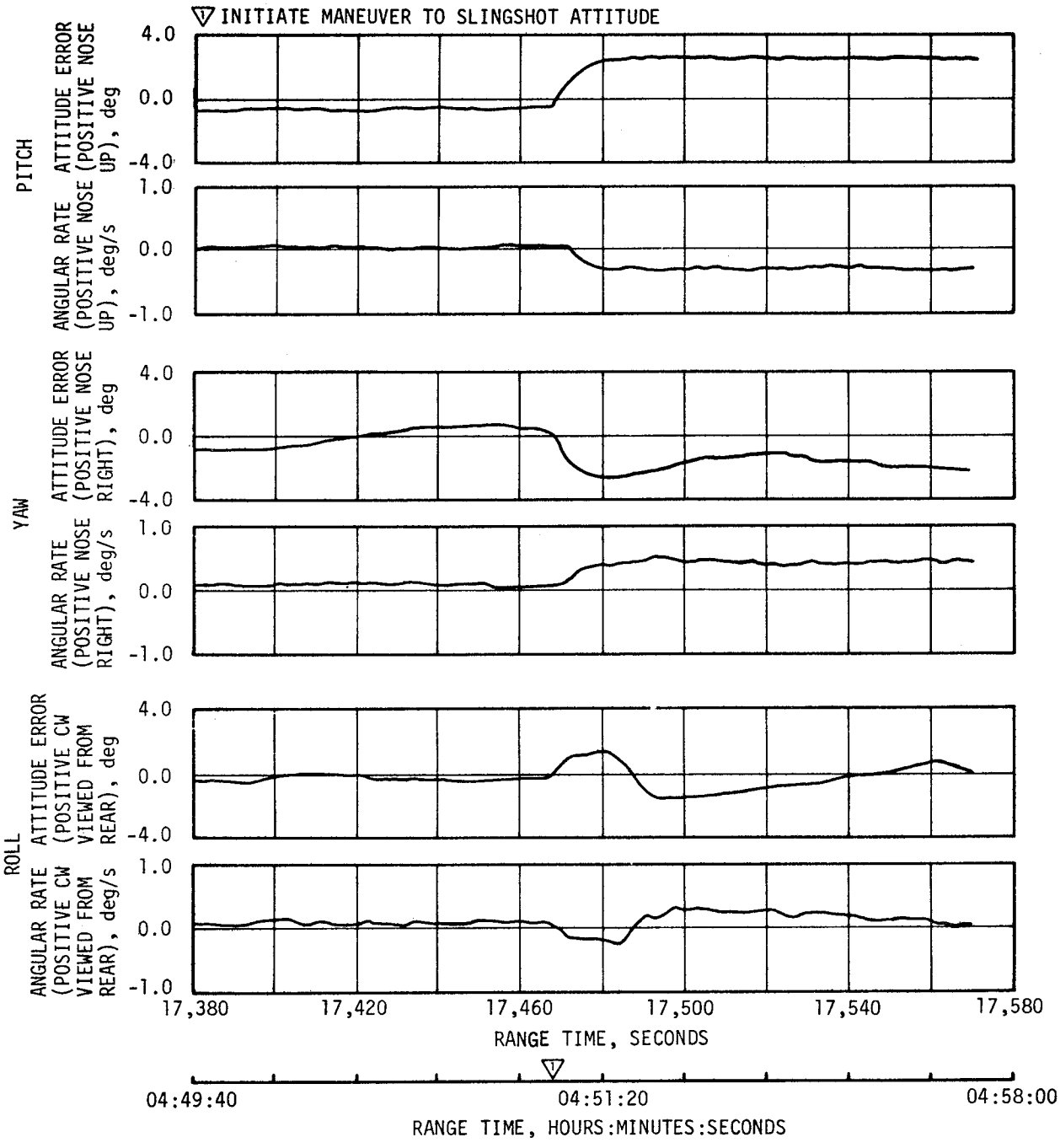

Figure 11-18. Pitch, Yaw and Roll Plane Dynamics During The Maneuver to Slingshot Attitude

SECTION 12

SEPARATION

12.1 SUMMARY

S-IC/S-II first plane separation was satisfactory. Related data indicate that the S-IC retromotors performed as expected. Similarly, S-II second plane separation and S-II/S-IVB separation were nominal. The S-II retromotors and S-IVB ullage motors performed as expected.

Command and Service Module (CSM) separation from the Launch Vehicle (LV) occurred as predicted during translunar coast. The Transposition, Docking, and Ejection (TD&E) maneuver occurred as expected. Attitude control of the LV was maintained during each separation sequence.

12.2 S-IC/S-II SEPARATION EVALUATION

S-IC/S-II separation and associated sequencing were accomplished as planned. Dynamic conditions at separation were within staging limits. Rate gyros and accelerometers located on the Instrument Unit (IU) showed no disturbances, indicating a clean severance of the stages. Data from the Exploding Bridge Wire (EBW) firing unit indicate that S-IC retromotor ignition was accomplished. The S-II ullage motors performed as predicted. Since there were no cameras on the S-II stage, calculated dynamics of the interstage and the S-II stage were used to determine if second plane separation was within the staging requirements.

12.3 S-II/S-IVB SEPARATION EVALUATION

The S-II retromotors and the S-IVB ullage motors performed satisfactorily and provided a nominal S-II/S-IVB separation. Dynamic conditions at separation were within staging limits with separation conditions similar to those observed on previous flights.

12.4 S-IVB/IU/LM/CSM SEPARATION EVALUATION

Separation of the CSM from the LV was accomplished as planned. There were no large control disturbances noted during the separation.

12.5 LUNAR MODULE DOCKING AND EJECTION EVALUATION

The attitude of the LV was adequately maintained during the docking of the CSM with the Lunar Module (LM). The CSM/LM was then successfully spring ejected from the LV. There were no significant control disturbances during the ejection.

SECTION 13

ELECTRICAL NETWORKS

13.1 SUMMARY

The AS-506 launch vehicle electrical systems performed satisfactorily throughout all phases of flight. Operation of the batteries, power supplies, inverters, Exploding Bridge Wire (EBW) firing units, switch selectors, and interconnecting cabling was normal.

13.2 S-IC STAGE ELECTRICAL SYSTEM

The voltage for Battery No. 1 (Operational) and Battery No. 2 (Instrumentation) remained within performance limits of 26.5 to 32.0 vdc during powered flight. Battery currents were near predicted and below the maximum limit of 64 amperes for both Battery No. 1 and Battery No. 2. Battery power consumption was well within the rated capacity of 640 ampere-minutes for both Battery No. 1 and Battery No. 2, as shown in Table 13-1.

The two measuring power supplies remained within the 5 ±0.05 vdc design limit during powered flight.

Table 13-1. S-IC Stage Battery Power Consumption

BATTERY	BUS DESIGNATION	RATED CAPACITY (AMP-MIN)	POWER CONSUMPTION*	
			AMP-MIN	PERCENT OF CAPACITY
Operational No. 1	1D10	640	29.6	4.6
Instrumentation No. 2	1D20	640	90.0	14.1

*Battery power consumptions were calculated from power transfer until S-IC/S-II separation.

All switch selector channels functioned correctly, and all outputs were issued within their required time limits in response to commands from the Instrument Unit (IU).

The separation and retromotor EBW firing units were armed and triggered as programed. Charging times and voltages were within the requirements of 1.5 seconds for maximum allowable charging time and 4.2 ±0.4 volts for the allowable voltage level.

The command destruct EBW firing units were in the required state of readiness if vehicle destruct became necessary.

13.3 S-II STAGE ELECTRICAL SYSTEM

All battery bus voltages remained within specified limits throughout the prelaunch and flight periods, and bus currents remained within required and predicted limits. Main bus current averaged 36 amperes during S-IC boost and varied from 49 to 57 amperes during S-II boost. Instrumentation bus current averaged 23 amperes during S-IC and S-II boost. Recirculation bus current averaged 97 amperes during S-IC boost, and ignition bus current averaged 31 amperes during the S-II ignition sequence. Battery power consumption was well within the rated capacities of the batteries as shown in Table 13-2.

Table 13-2. S-II Stage Battery Power Consumption

BATTERY	BUS DESIG-NATION	RATED CAPACITY (AMP-HR)	POWER CONSUMPTION*		TEMPERATURE	
			AMP-HR	PERCENT OF CAPACITY	MAX	MIN
Main	2D11	35	7.96	22.7	305.4°K (90.0°F)	299.8°K (80.0°F)
Instrumentation	2D21	35	3.80	10.9	301.5°K (83.0°F)	299.5°K (79.5°F)
Recirculation No. 1	2D51	30	5.68	18.9	302.9°K (85.5°F)	299.8°K (80.0°F)
Recirculation No. 2	2D51 and 2D61	30	5.73	19.1	307.6°K (94.0°F)	304.3°K (88.0°F)

*Power consumption calculated from -50 seconds.

The five temperature bridge power supplies and the three 5-vdc instrumentation power supplies all performed within acceptable limits. The five LH_2 recirculation inverters that furnish power to the recirculation pumps operated properly throughout the J-2 engine chilldown period.

All switch selector channels functioned correctly, and all outputs were issued within their required time limits in response to commands from the IU. Performance of the EBW circuitry for the separation system was satisfactory. Firing units charge and discharge responses were within predicted time and voltage limits. The command EBW firing units were in the required state of readiness if vehicle destruct became necessary.

13.4 S-IVB STAGE ELECTRICAL SYSTEM

The voltages, currents, and temperatures of the three 28-vdc and one 56-vdc batteries stayed well within acceptable limits as shown in Figures 13-1 through 13-4. Battery temperatures remained below the 322°K (120°F) limit during the powered portions of flight. (This limit does not apply after insertion into orbit.) The highest temperature of 316.5°K (110°F) was reached on Aft Battery No. 2, Unit 1, after S-IVB first burn cutoff. Battery power consumption is shown in Table 13-3.

All switch selector channels functioned correctly, and all outputs were issued within their required time limits in response to commands from the IU.

Table 13-3. S-IVB Stage Battery Power Consumption

BATTERY	RATED CAPACITY (AMP-HRS)*	POWER CONSUMPTION**	
		AMP-HRS	PERCENT OF CAPACITY
Forward No. 1	300.0	121.5	40.5
Forward No. 2	24.75	25.4	102.7
Aft No. 1	300.0	78.2	26.1
Aft No. 2	75.0	42.3	56.4

*Rated capacities are minimum guaranteed by vendor.
**Actual usage to 29,000 seconds (08:03:20) is based on flight data.

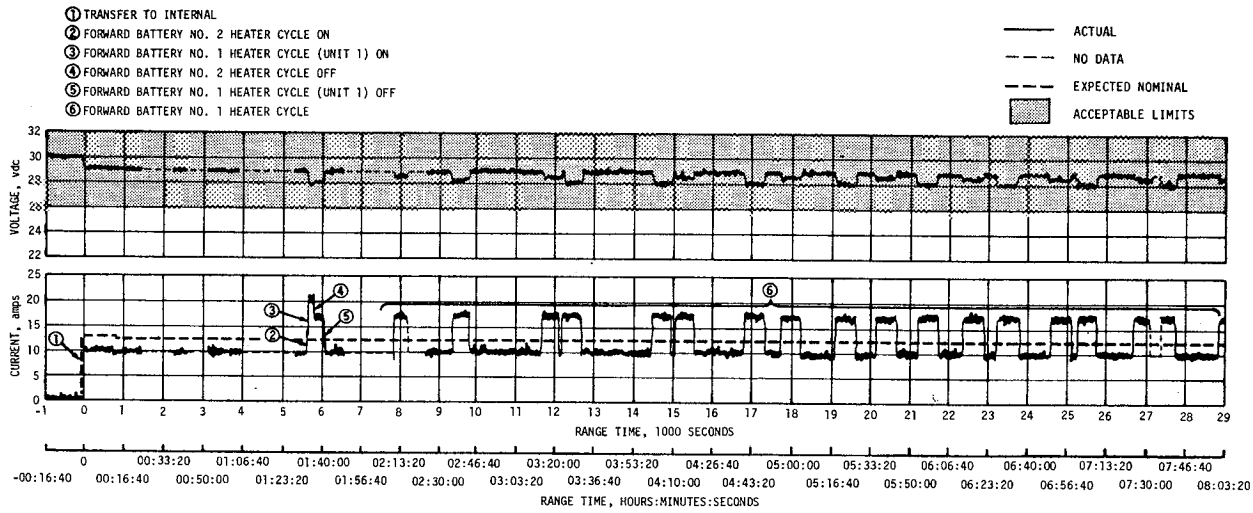

Figure 13-1. S-IVB Stage Forward Battery No. 1 Voltage and Current

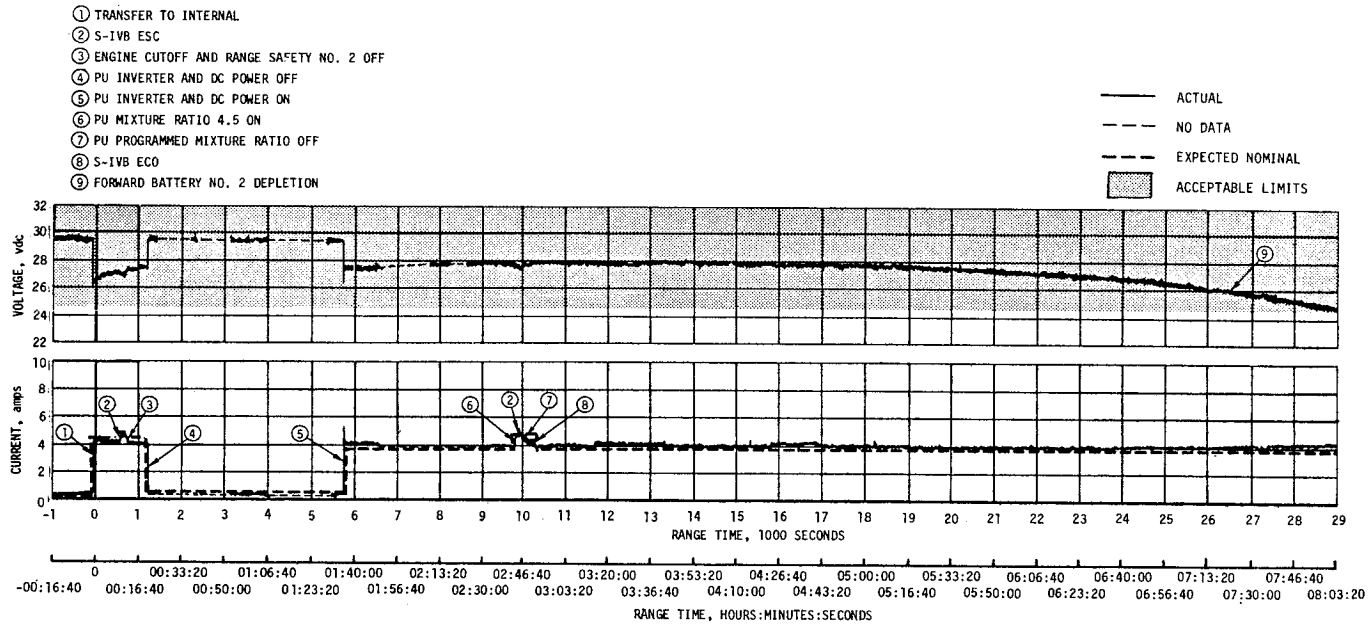

Figure 13-2. S-IVB Stage Forward Battery No. 2 Voltage and Current

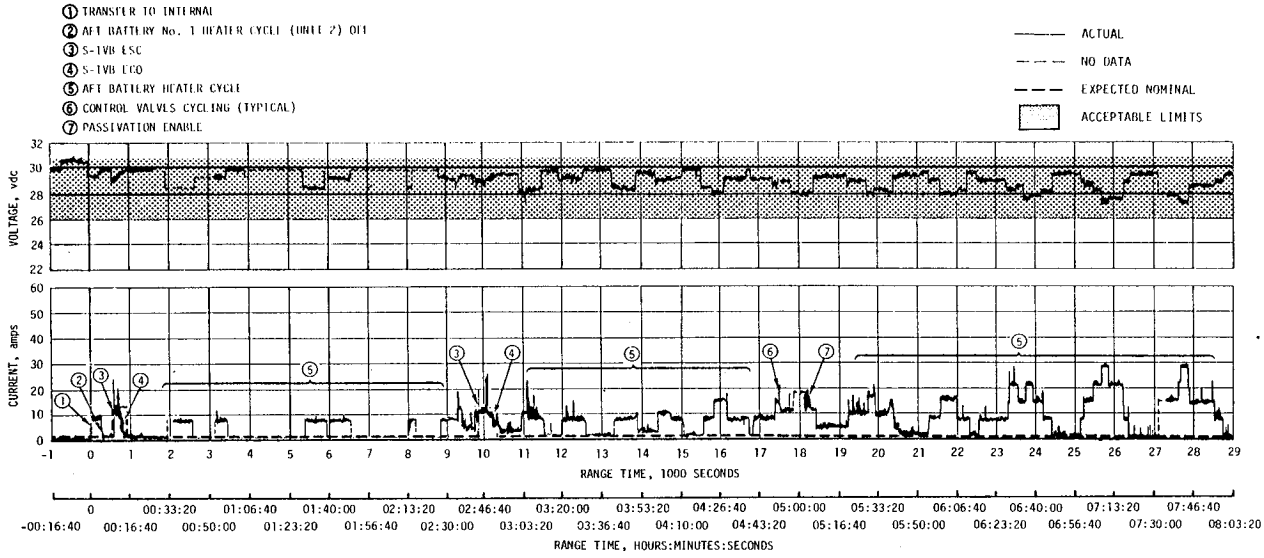

Figure 13-3. S-IVB Stage Aft Battery No. 1 Voltage and Current

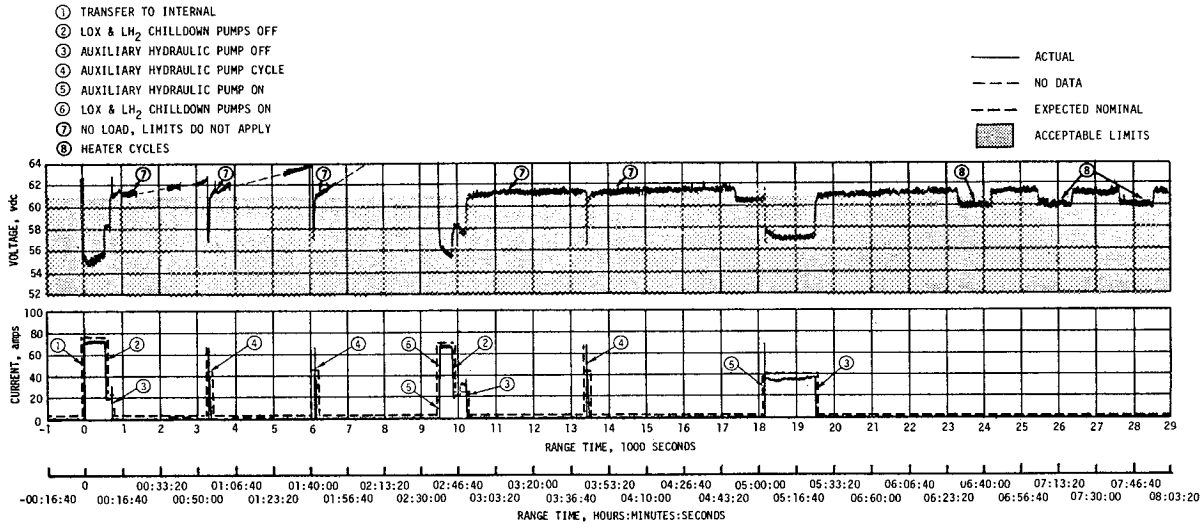

Figure 13-4. S-IVB Stage Aft Battery No. 2 Voltage and Current

The three 5-vdc and seven 20-vdc excitation modules all performed within acceptable limits. The LOX and LH_2 chilldown inverters that furnish power to the LOX and LH_2 recirculation pumps performed satisfactorily and met their load requirements.

Performance of the EBW circuitry for the separation system was satisfactory. Firing units charge and discharge responses were within predicted time and voltage limits. The command destruct EBW firing units were in the required state of readiness if vehicle destruct became necessary.

13.5 INSTRUMENT UNIT ELECTRICAL SYSTEM

All battery voltages and temperatures increased gradually from liftoff as expected. All battery voltages remained within normal limits. Battery currents remained normal during launch and coast periods of flight. Battery power consumption and estimated depletion times are shown in Table 13-4. Battery voltages, currents, and temperatures are shown in Figures 13-5 through 13-7.

The 56-vdc power supply maintained an output voltage of 55.7 to 56.6 vdc, well within the required tolerance of 56 ±2.5 vdc.

The 5-volt measuring power supply performed nominally, maintaining a constant voltage within specified tolerances.

Switch selector, electrical distributors, and network cabling performed nominally.

Table 13-4. IU Battery Power Consumption

BATTERY	RATED CAPACITY (AMP-HRS)	POWER CONSUMPTION*		ESTIMATED* LIFETIME (HOURS)
		AMP-HRS	PERCENT OF CAPACITY	
6D10	350	181.2	51.8	18.9
6D30	350	235.2	67.2	14.4
6D40	350	337.1	96.3	10.1

*Based on available flight data to 35,214 seconds (09:46:54).

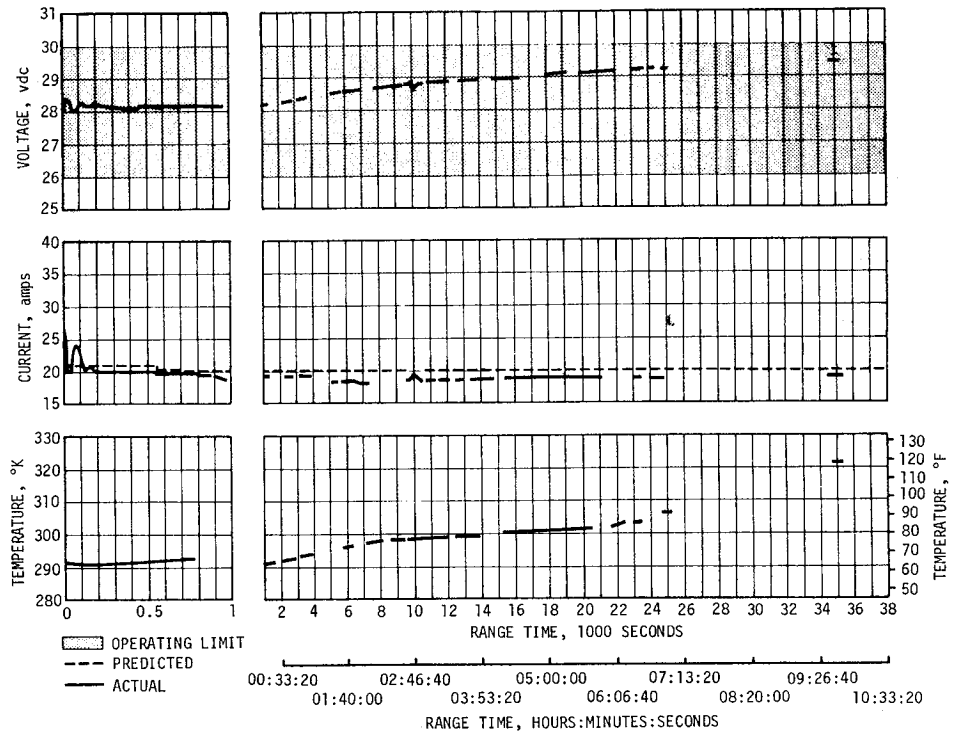

Figure 13-5. Battery 6D10 Voltage, Current, and Temperature

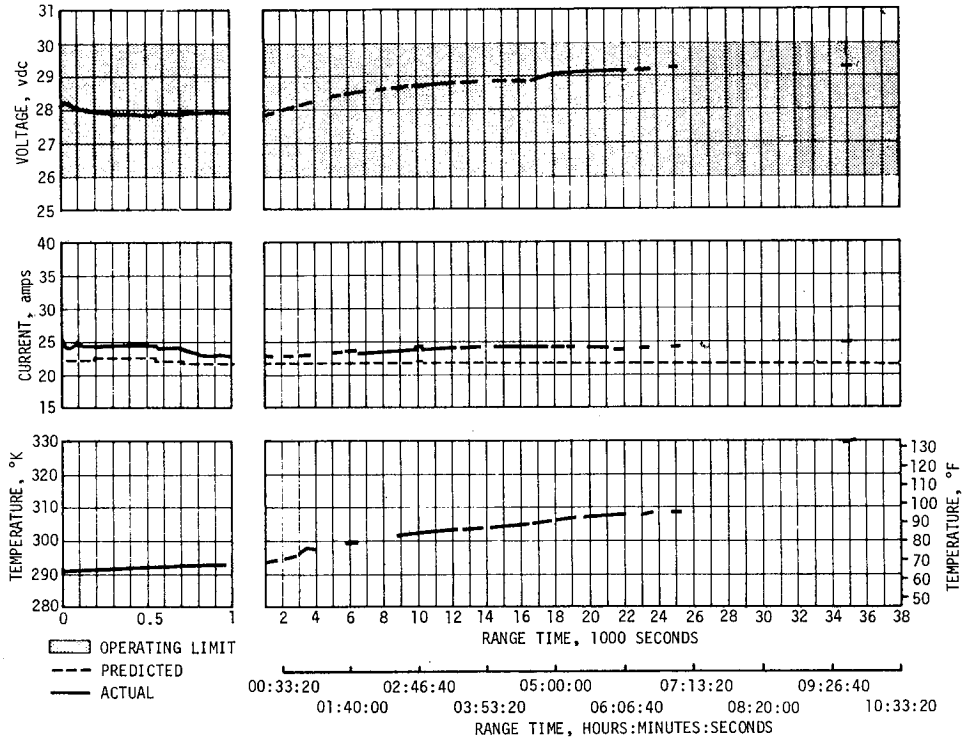

Figure 13-6. Battery 6D30 Voltage, Current, and Temperature

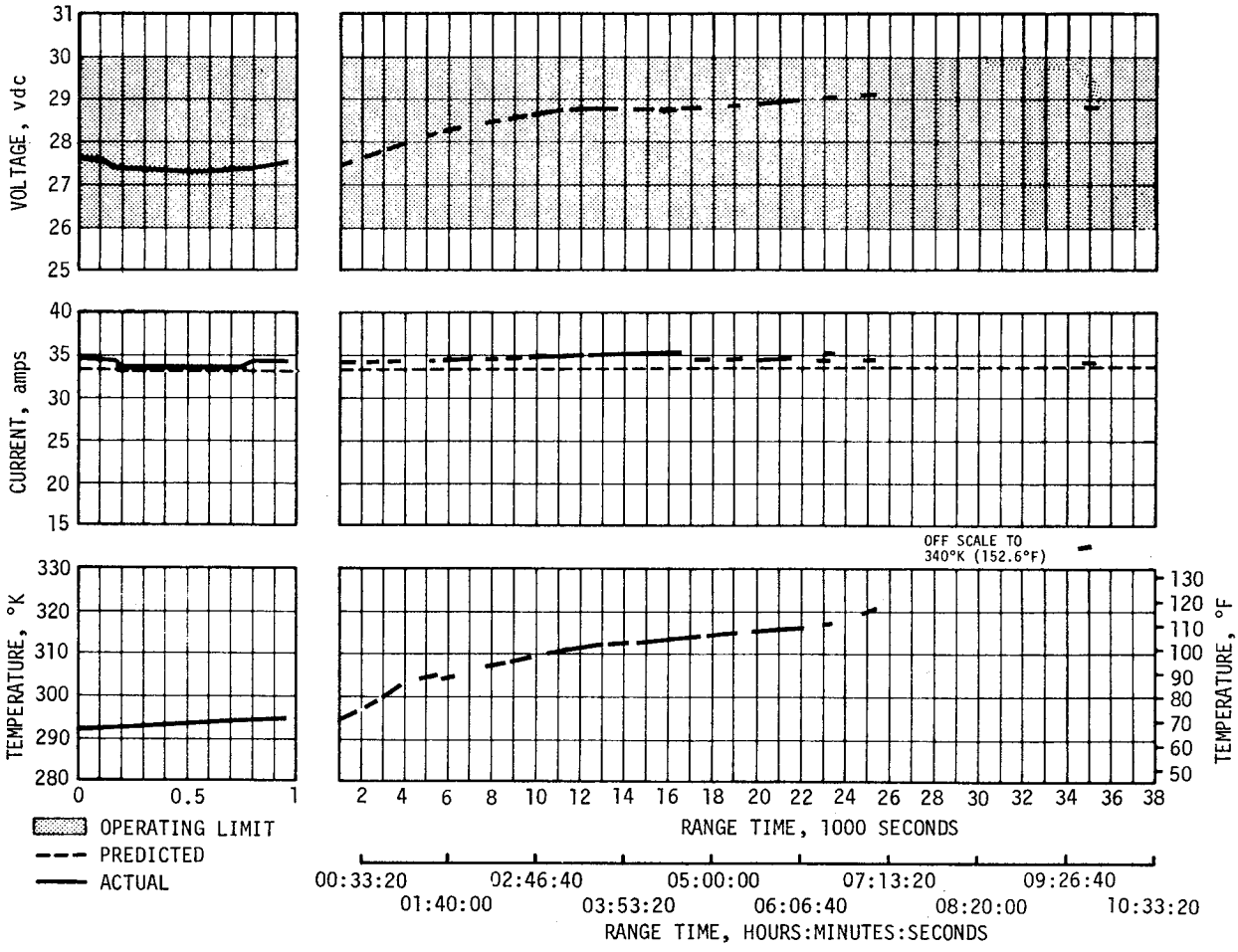

Figure 13-7. Battery 6D40 Voltage, Current, and Temperature

SECTION 14

RANGE SAFETY AND COMMAND SYSTEMS

14.1 SUMMARY

Data indicated that the redundant Secure Range Safety Command Systems (SRSCS) on the S-IC, S-II and S-IVB stages were ready to perform their functions properly on command if flight conditions during the launch phase had required vehicle destruct. The system properly safed the S-IVB SRSCS on a command transmitted from Bermuda (BDA). The performance of the Command and Communications System (CCS) in the Instrument Unit (IU) was satisfactory, except for the Radio Frequency (RF) problem noted in paragraph 19.4.3.2.

14.2 SECURE RANGE SAFETY COMMAND SYSTEMS

Telemetered data indicated that the command antennas, receivers/ decoders, Exploding Bridge Wire (EBW) networks, and destruct controllers on each powered stage functioned properly during flight and were in the required state of readiness if flight conditions during the launch phase had required vehicle destruct. Since no arm/cutoff or destruct commands were required, all data except receiver signal strength remained unchanged during the flight. Power to the system was cut off at 723.5 seconds by ground command from BDA, thereby deactivating (safing) the system. Both S-IVB stage systems, the only systems in operation at this time, responded properly to the safing command.

Radio Frequency (RF) performance aspects of the system are discussed in paragraph 19.4.3.1.

14.3 COMMAND AND COMMUNICATION SYSTEM

The command section of the CCS operated satisfactorily except for the RF problem noted in paragraph 19.4.3.2. Twenty commands were initiated by Mission Control Center - Houston (MCC-H) for transmission via the Goldstone (GDS) Wing Station, as shown in Table 14-1. The last 11 commands were initiated with the ground station in the Message Acceptance Pulse (MAP) override mode. The MAP override mode was necessary because the telemetry data was noisy and the Address Verification Pulses (AVP's) and Computer Reset Pulses (CRP's) could not be detected at the ground

station. A total of 50 command words were attempted by the GDS Wing Station.

The command at 19,033.7 seconds (05:17:13.7) to switch the CCS coaxial switch to the low-gain directional antenna position was unsuccessfully transmitted four times. The command was not received by the onboard equipment because the uplink subcarrier was not in lock. Upon completion of the automatic command cycle (the ground station is set up to automatically transmit the command word four times or until the AVP's and CRP's are received), a terminate command was issued to reset the command system and the switch command was again attempted at 19,062.3 seconds (05:17:42.3). During this second transmission, the ground computer failed to capture the AVP's and CRP's, resulting in the command being repeated three times. The verification pulses were missed because

Table 14-1. Command and Communication System GDS Commands History

RANGE TIME		COMMAND	NUMBER OF WORDS	REMARKS
SECONDS	HRS:MIN:SEC			
17,466.6	04:51:06.6	T_8 Initiated	1	Accepted
17,770.9	04:56:10.9	Begin Environmental Control System (ECS) Experiment	1	Accepted
18,502.2	05:08:22.2	Engine He Control Valve Enable	6	Accepted
19,033.7	05:17:13.7	Set Antenna Low Gain	4*	Uplink Subcarrier Out-of-Lock
19,051.9	05:17:31.9	Terminate	1	Accepted
19,062.3	05:17:42.3	Set Antenna Low Gain	4*	Accepted
27,367.7	07:36:07.7	Set Antenna High Gain	2*	Accepted
32,019.3	08:53:39.3	CCS Transponder Disable	4	Noisy Telemetry**
32,066.6	08:54:26.6	CCS Transponder Disable	4	Noisy Telemetry**
32,601.4	09:03:21.4	CCS Transponder Disable	3	Accepted (MAP Override)
32,669.5	09:04:29.5	CCS Transponder Enable	3	Accepted (MAP Override)
33,825.1	09:23:45.1	Set Antenna Omni	1	Accepted (MAP Override)
34,000.1	09:26:40.1	Set Antenna Low Gain	1	Accepted (MAP Override)
34,105.3	09:28:25.3	CCS Transponder Disable	3	Accepted (MAP Override)
34,160.0	09:29:20.0	CCS Transponder Enable	3	Not Transmitted by Ground Station
34,234.5	09:30:34.5	Set Antenna Omni	1	Acceptance Status Unknown (MAP Override)
34,312.0	09:31:52.0	Set Antenna High Gain	1	Acceptance Status Unknown (MAP Override)
34,419.9	09:33:39.9	Set Antenna Omni	1	Acceptance Status Unknown (MAP Override)
34,530.0	09:35:30.0	CCS Transponder Disable	3	Acceptance Status Unknown (MAP Override)
34,554.9	09:35:54.9	CCS Transponder Enable	3	Accepted (MAP Override)

*One word is normally required to switch antennas. These commands were repeated due to the uplink being out of lock or missed verification pulses at the ground station because of noisy telemetry.

**Only Mode Words Transmitted

of noisy telemetry due to low downlink signal strength. Acceptance of the command was verified by an increase in signal strength and by the antenna position measurement (K132-603) indicating the CCS coaxial switch was in the low-gain antenna position.

Noisy telemetry resulted in a repeated command at 27,367.7 seconds (07:36:07.7) to transfer the CCS coaxial switch to the high-gain antenna position. The command was repeated once before the ground computer detected the acceptance pulses and terminated transmission of the command.

Transmission of the CCS disable command was unsuccessful when attempted at both 32,019.3 seconds (08:53:39.3) and 32,066.6 seconds (08:54:26.6) due to noisy telemetry. The noise prevented the ground station from detecting the AVP's and CRP's. Therefore, acceptance of the mode word could not be verified. The mode word was transmitted eight times before the MAP override mode was selected and the complete command transmitted (one mode and two data words). The command was accepted on this third attempt at 32,601.4 seconds (09:03:21.4).

The command to enable the CCS at 34,160.0 seconds (09:29:20.0) was not transmitted by the ground station because the 70-kilohertz subcarrier was off. This meant that the CCS downlink was inhibited from 34,105.3 seconds (09:28:25.3) (CCS disable command) until the enable command transmitted at 34,554.9 seconds (09:35:54.9) was accepted. This mode was verified by the signal strength level during this period (see paragraph 19.4.3.2). Since the downlink was inhibited during this period, no AVP's and CRP's were received for the antenna switching commands and the disable command was not transmitted during this period.

The acceptance status of the commands transmitted during the period in which the CCS was inhibited is unknown except for the two commands to switch to the omni antennas. One or both of these commands, 34,234.5 seconds(09:30:34.5) and 34,419.9 seconds (09:33:39.9), were accepted by the onboard system because measurement K131-603 indicated the system was on the omni antennas when the downlink signal returned at 34,555 seconds (09:35:55).

SECTION 15

EMERGENCY DETECTION SYSTEM

15.1 SUMMARY

The performance of the AS-506 Emergency Detection System (EDS) was normal, and no abort limits were exceeded.

15.2 SYSTEM EVALUATION

15.2.1 General Performance

The AS-506 EDS configuration was the same as on AS-505. All launch vehicle EDS parameters remained well within acceptable limits during the AS-506 mission. EDS related sequential events and discrete indications occurred as expected.

15.2.2 Propulsion System Sensors

The performance of all thrust OK sensors, which monitor engine status, was nominal insofar as EDS operation was concerned. The associated voting logic was also nominal. S-II and S-IVB tank ullage pressures remained within the abort limits, and displays to the crew were normal.

15.2.3 Flight Dynamics and Control Sensors

As noted in Section 11, none of the triple redundant rate gyros gave any indication of angular overrate in the pitch, yaw, or roll axes. The maximum angular rates were well below the abort limits. The roll rate abort limit is 20 deg/s; a switch selector command deactivated the overrate automatic abort and changed the pitch and yaw rate abort settings from 4 deg/s to 9.2 deg/s at 134.8 seconds.

The maximum angle-of-attack dynamic pressure sensed by a redundant Q-ball mounted atop the escape tower was 0.28 N/cm^2 (0.4 psid) between 89 and 91 seconds. This pressure was only 12.5 percent of the EDS abort limit of 2.2 N/cm^2 (3.2 psid).

SECTION 16

VEHICLE PRESSURE ENVIRONMENT

16.1 SUMMARY

The S-IC stage base pressure environments were monitored by two heat shield differential pressure measurements. S-II stage base pressure environments were monitored by two absolute pressure measurements on the heat shield and one on the thrust cone. The flight data were generally in good agreement with the postflight predictions and compared well with previous flight data. The pressure environments were well below design levels.

There was no instrumentation provided on the AS-506 vehicle which would permit a direct evaluation of the surface and compartment pressure environments. One internal ambient pressure measurement located on the S-II forward skirt was used to calculate the pressure loading acting on that area and agreed with predictions and previous flight data.

16.2 BASE PRESSURES

16.2.1 S-IC Base Pressures

The S-IC stage base heat shield pressure loading was recorded by two differential pressure measurements. Both measurements show good agreement with previous flight data as shown in Figure 16-1. Pressure loading is the difference between internal and external pressures (Pint-Pbase) defined such that positive loading is in the burst direction. The heat shield loadings were well within the 1.4 N/cm^2 (2.0 psid) design pressure loading.

16.2.2 S-II Base Pressures

The S-II stage base heat shield and thrust cone pressure environment was recorded by two absolute pressure measurements on the heat shield and one absolute pressure measurement on the thrust cone.

Except for the absence of a more significant drop in measured aft face pressure at S-II Center Engine Cutoff (CECO), Figure 16-2 shows good agreement between the postflight predicted and AS-506 flight heat shield aft face static pressure history. It is seen that the AS-506 pressure falls within the AS-501 through AS-505 data band. The predicted pressure drop after S-II CECO is based on the computed total pressure loss resulting

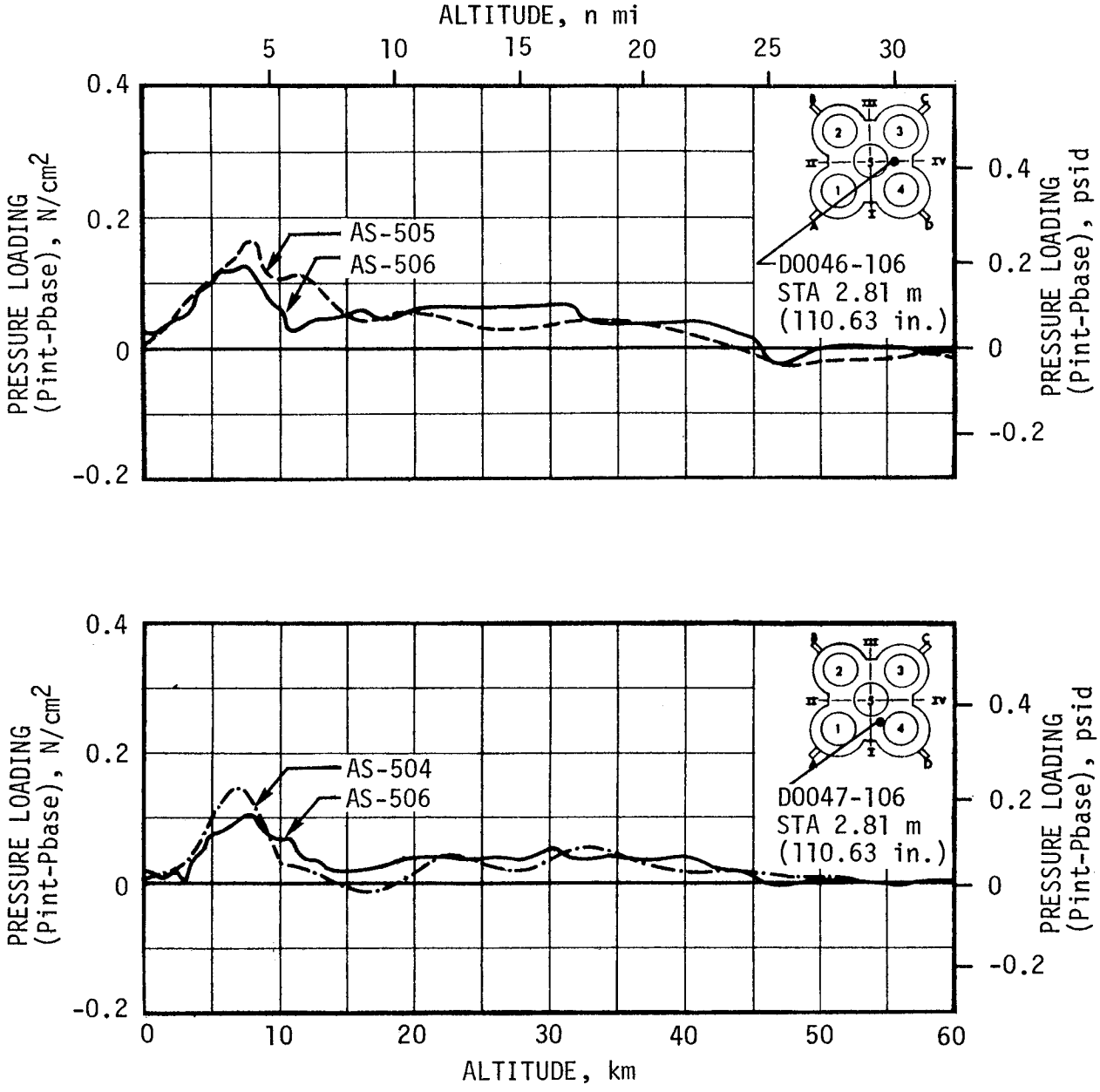

Figure 16-1. S-IC Base Heat Shield Pressure Loading

from the reverse flow passing through a shock wave above the nozzle lip of the inoperative center engine. Based on AS-505 flight data, a somewhat smaller but still measurable drop was expected for the D158-206 measurement. The further pressure reduction occurring after Engine Mixture Ratio (EMR) shift is predicted from the reduction of the maximum pressure in the J-2 engine exhaust plume interaction regions.

Figure 16-3 shows the static pressure variation with range time on the forward face of the base heat shield. It is seen that the AS-506 measured static pressure on the forward face of the heat shield, while within design limits, exceeds the postflight prediction and was

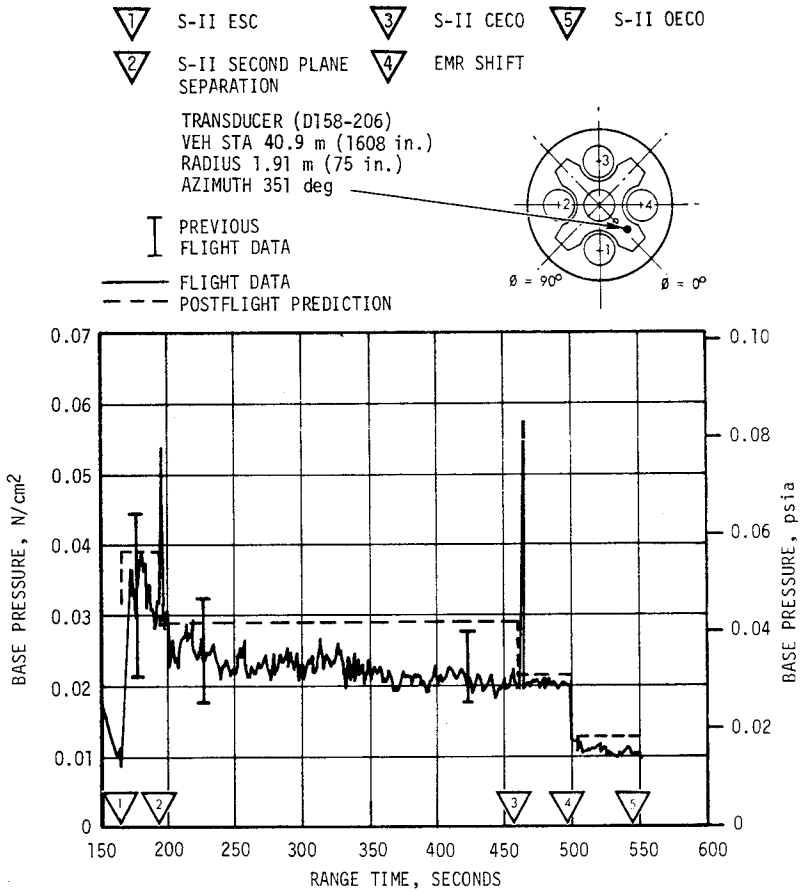

Figure 16-2. S-II Heat Shield Aft Face Pressure

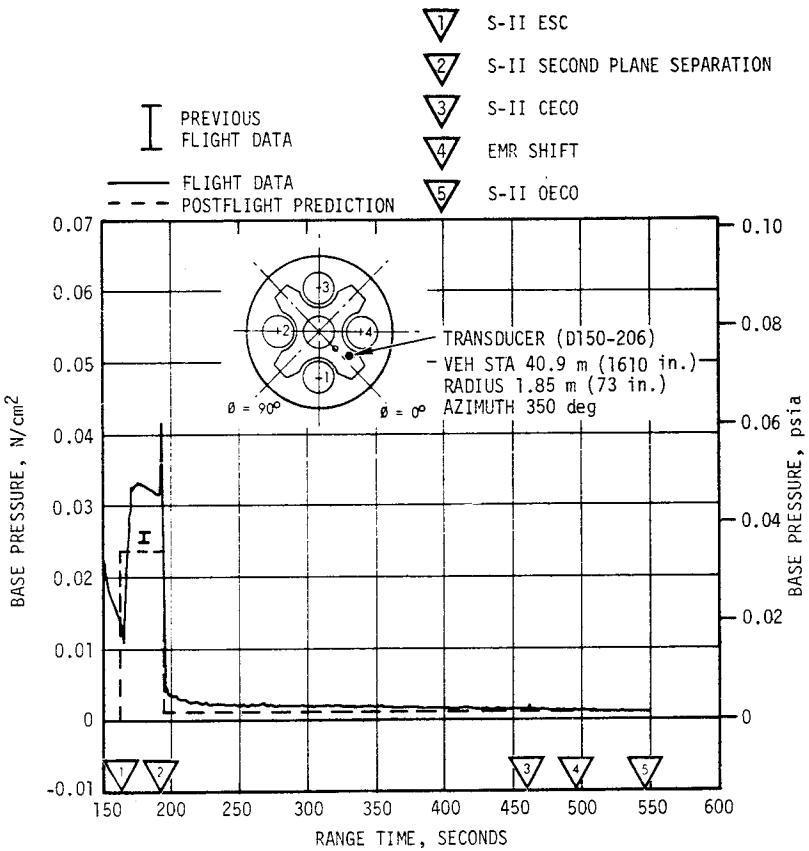

Figure 16-3. S-II Heat Shield Forward Face Pressure

approximately 30 percent higher than that measured during the AS-501 and AS-502 flights. No pressure measurement was available at this exact location during the AS-503 through AS-505 flights. This condition is believed to be a localized effect due to variable leakage through the J-2 engine nozzle flexible curtains.

Figure 16-4 shows the AS-506 static pressure variation on the thrust cone. The measured AS-506 thrust cone static pressures agreed well with predicted values and with previous flight data.

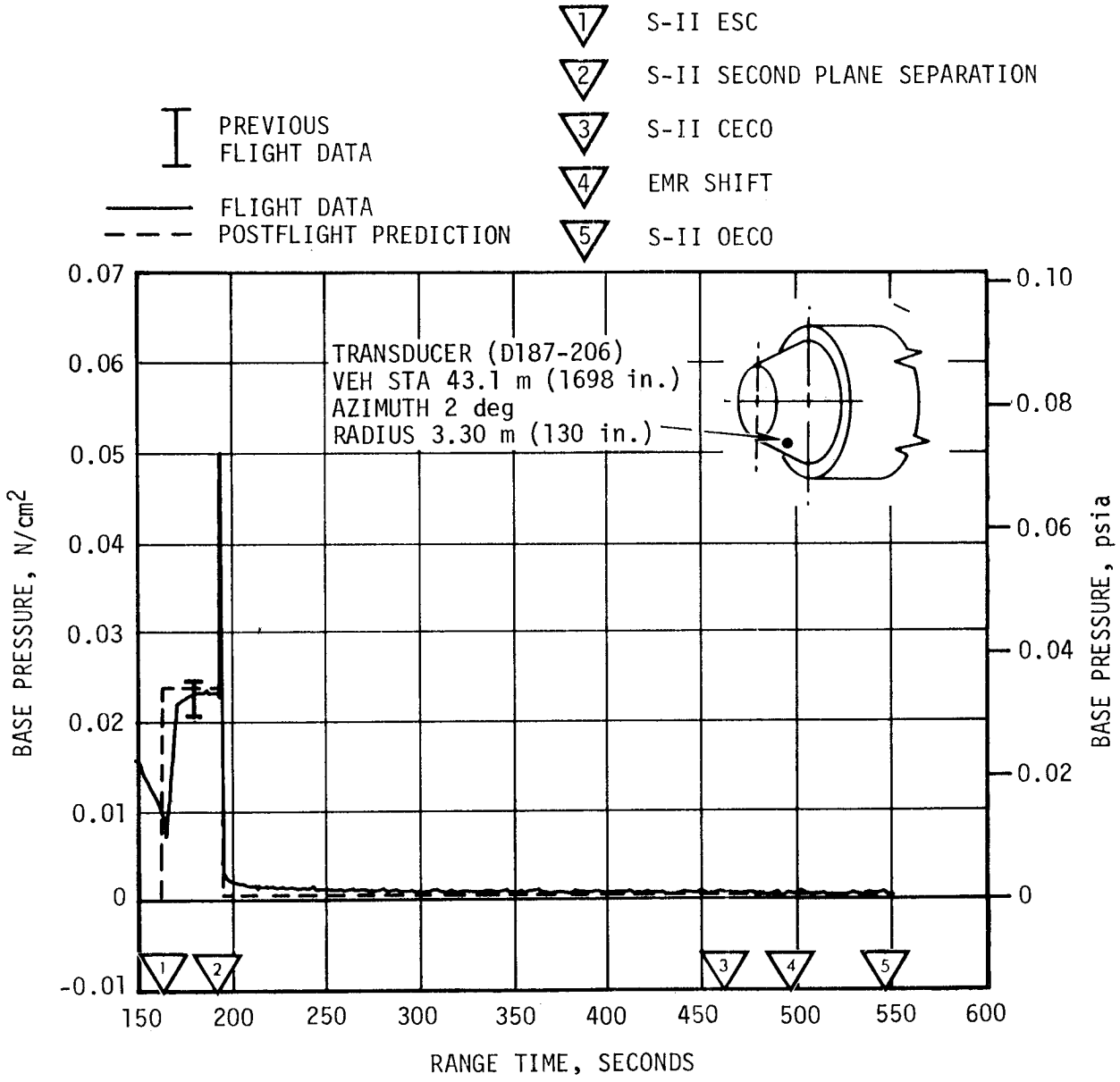

Figure 16-4. S-II Thrust Cone Pressure

16.3 SURFACE PRESSURE AND COMPARTMENT VENTING

16.3.1 S-IC Stage

There was no instrumentation on the S-IC stage for evaluation of the surface and compartment pressure environments.

16.3.2 S-II Stage

Other than the internal ambient pressure measurement (D163-219) located on the forward skirt, there was no instrumentation on the S-II stage for evaluation of the surface and compartment pressure environments. A calculated pressure loading (Pint-Pext) on the forward skirt was obtained by taking the difference between the predicted external pressure values and the internal pressure (assumed uniform), which was measured at vehicle longitudinal station 62.2 m (2449 in.) and peripheral angle of 191 degrees (see Figure 16-5). The AS-506 flight data (calculated) show the same trends and are in good agreement with the postflight predictions and previous flight data.

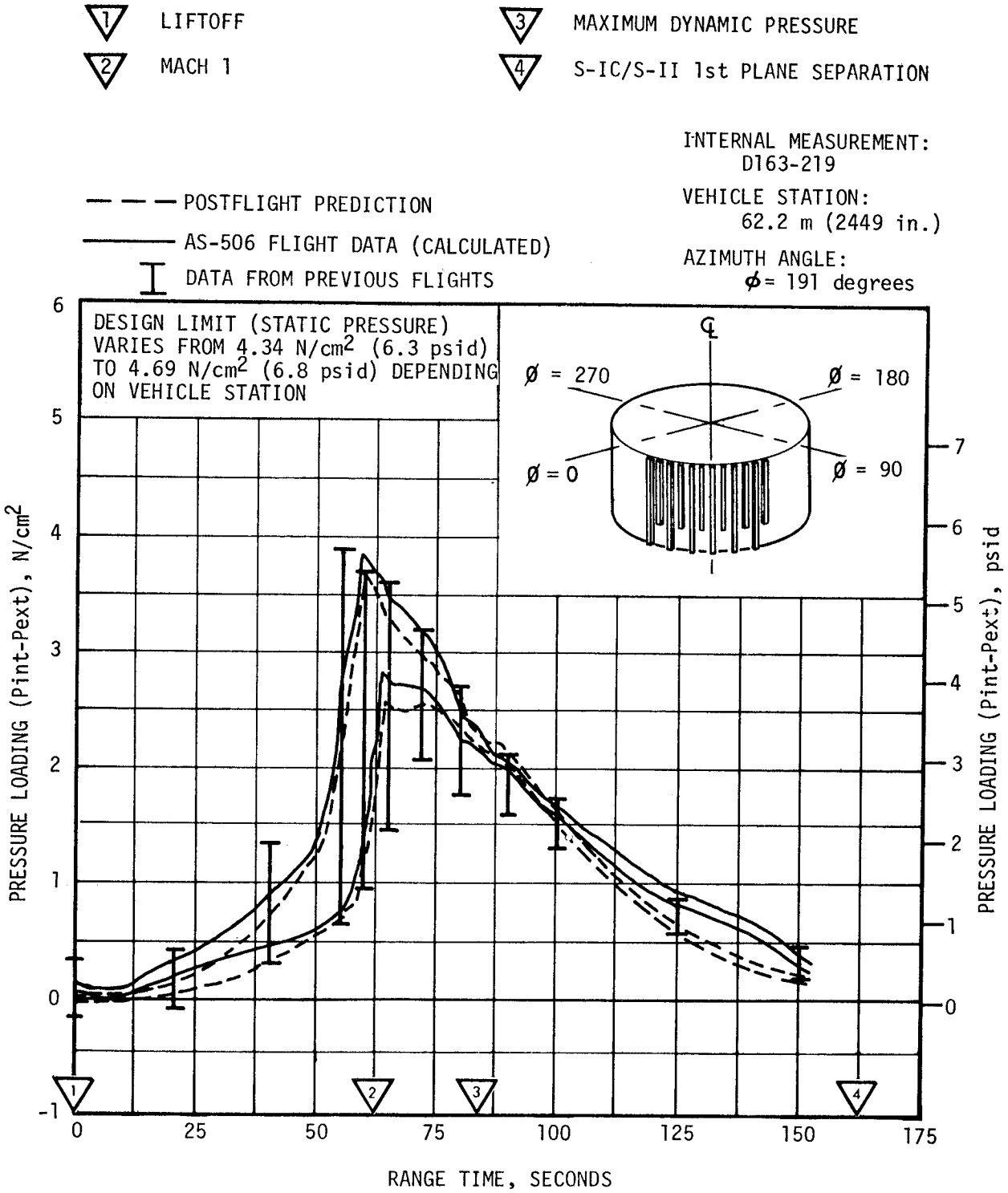

Figure 16-5. S-II Forward Skirt Pressure Loading

SECTION 17

VEHICLE THERMAL ENVIRONMENT

17.1 SUMMARY

The AS-506 S-IC base region thermal environments have similar magnitudes and trends as those measured during previous flights. Maximum values of total heating and gas temperature were recorded at approximately 20 kilometers (10.8 n mi) altitude with maximum values of 25 watt/cm^2 (22.2 Btu/ft^2-s) and 1200°K (1695°F), respectively.

In general, base thermal environments on the S-II stage were similar to those measured on previous flights and were well below design limits. However, the heat shield aft radiation heating rates were approximately 20 percent higher than the maximum values measured during previous flights.

Flow separation was observed (ALOTS film) to occur at approximately 116 seconds range time. Aerodynamic heating environments were not measured on AS-506.

17.2 S-IC BASE HEATING

Thermal environments in the base region of the S-IC stage were recorded by two total calorimeters and two gas temperature probes which were on the heat shield at the locations shown in Figure 17-1. Data from these instruments are compared with the AS-502 through AS-505 flight data band (Figures 17-2 and 17-3) and are shown versus altitude to minimize trajectory differences. AS-501 flight data, which showed less severity than subsequent flight data because of flow deflector effects, are not shown.

As shown in Figures 17-2 and 17-3, the AS-506 S-IC base heat shield thermal environments have similar magnitudes and trends as those measured during the previous flights. Maximum values of total heating and gas temperature data were recorded at approximately 20 kilometers (10.8 n mi) with maximum values of 25 watt/cm^2 (22.2 Btu/ft^2-s) and 1200°K (1695°F), respectively. Center Engine Cutoff (CECO) on AS-506 produced a spike in the data with a magnitude and duration similar to previous flight data at CECO. The AS-506 gas temperature data are similar to previous flight data. However the AS-506 and AS-505 gas temperature data do not show the decrease between 4 and 9 kilometers (2.2 and 4.9 n mi) which the AS-502 through AS-504 flight data indicated.

Ambient gas temperatures inside the engine cocoons remained within the band of previous flight data.

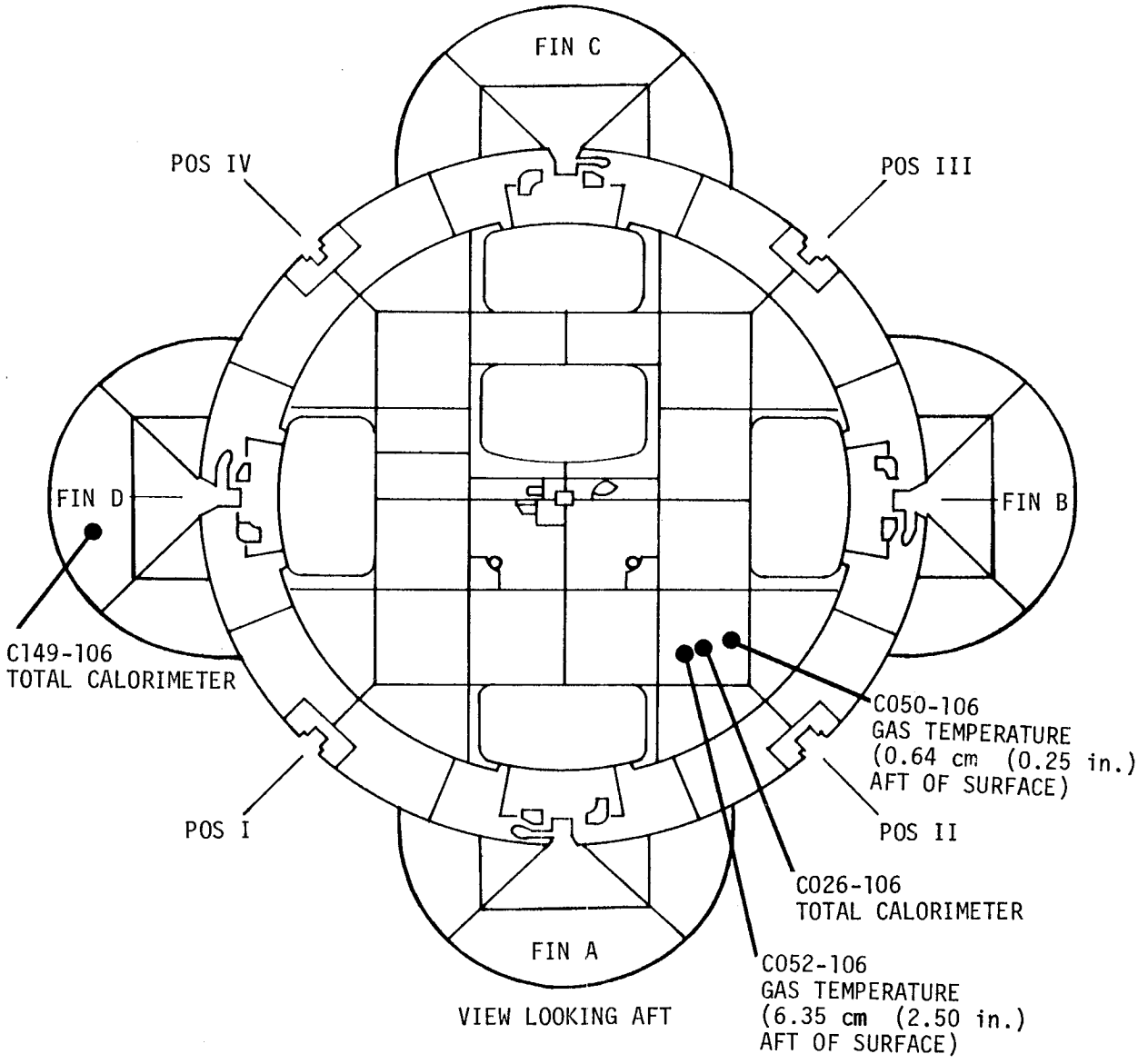

Figure 17-1. S-IC Base Heat Shield Measurement Locations

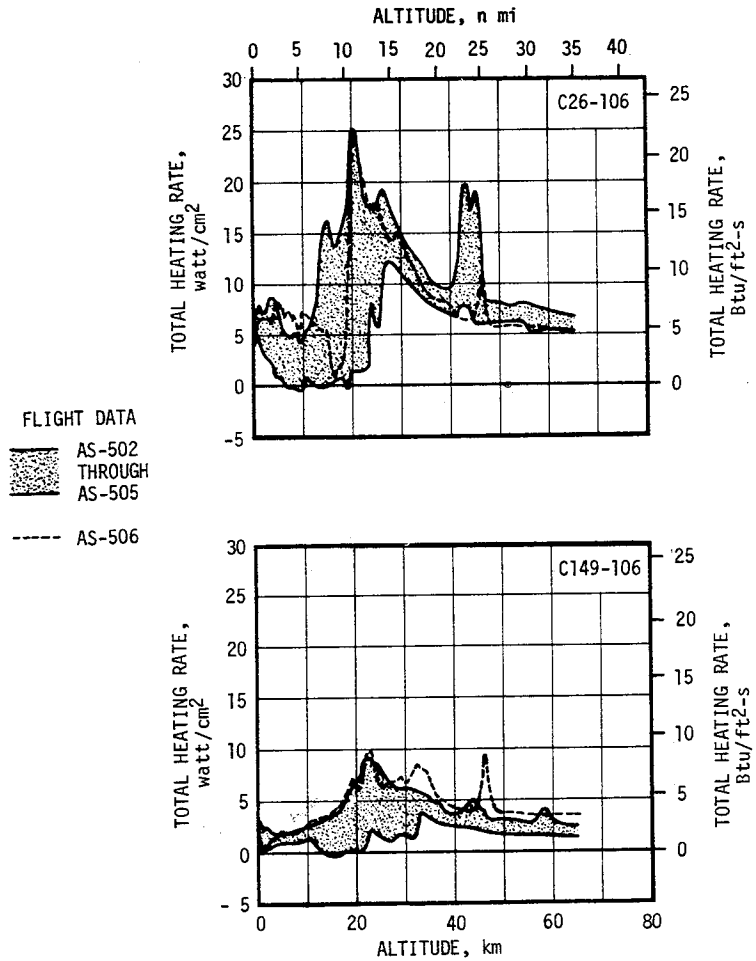

Figure 17-2. S-IC Base Heat Shield Total Heating Rate

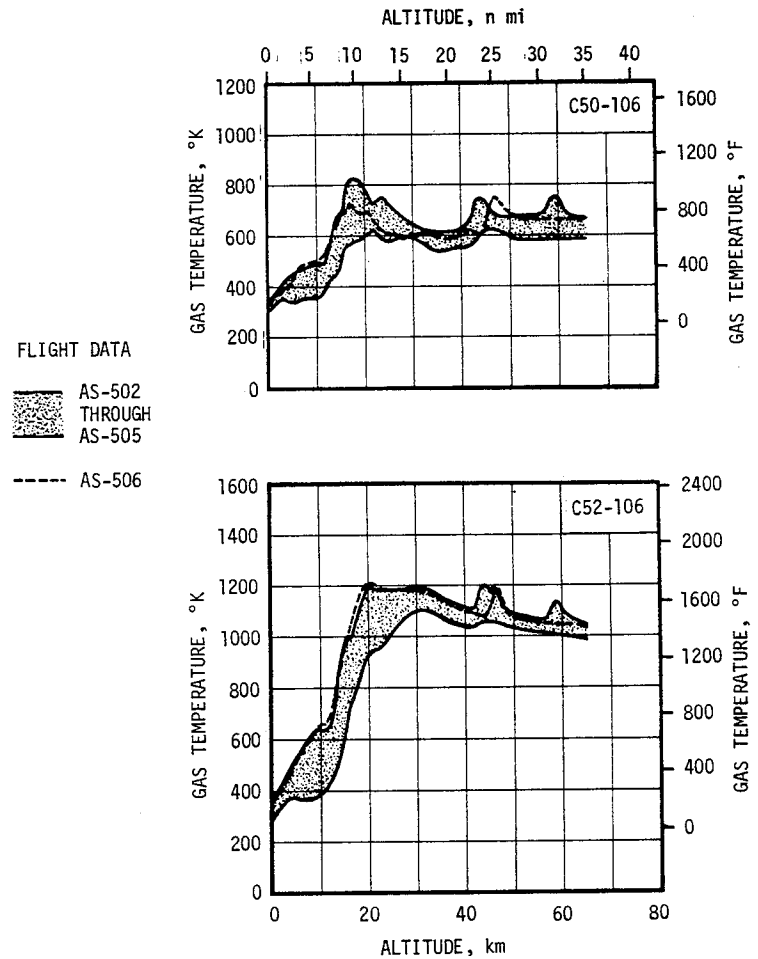

Figure 17-3. S-IC Base Heat Shield Gas Temperature

17.3 S-II BASE REGION ENVIRONMENT

The S-II base heat shield flight environments were, in general, in good agreement with previous flight data and were well below design limits. S-II heat shield aft face convective heating rates, aft radiation heating rates, and base gas temperatures are presented in Figures 17-4 through 17-6, along with previous flight data and postflight predictions. The postflight predicted heat shield convective heating rates are based on hot flow 1/25 scale S-II stage model test data. Postflight predictions for the other two figures were accomplished by the same analytical methods that have been described in previous flight evaluation reports.

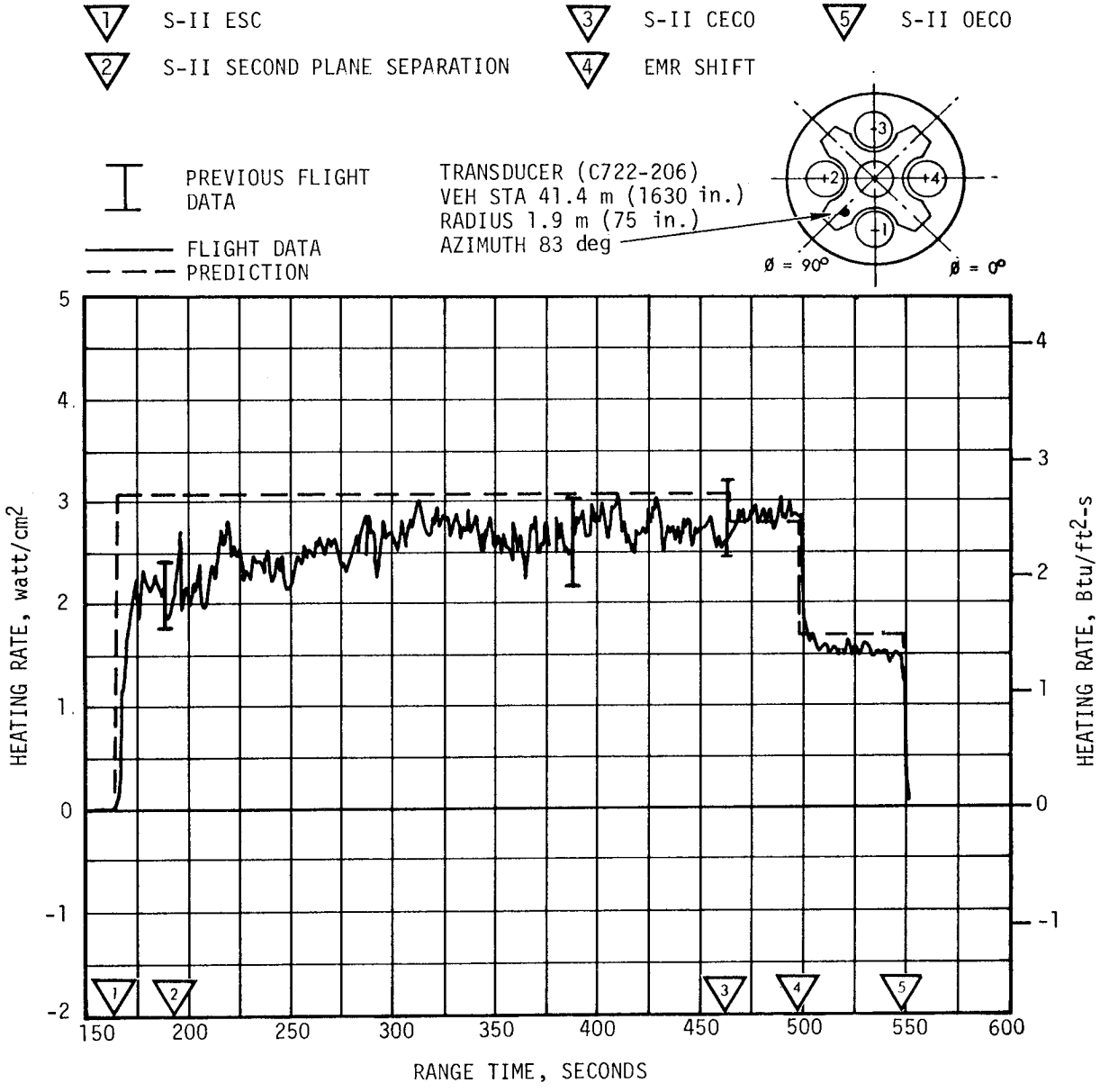

Figure 17-4. S-II Heat Shield Aft Face Heat Rate

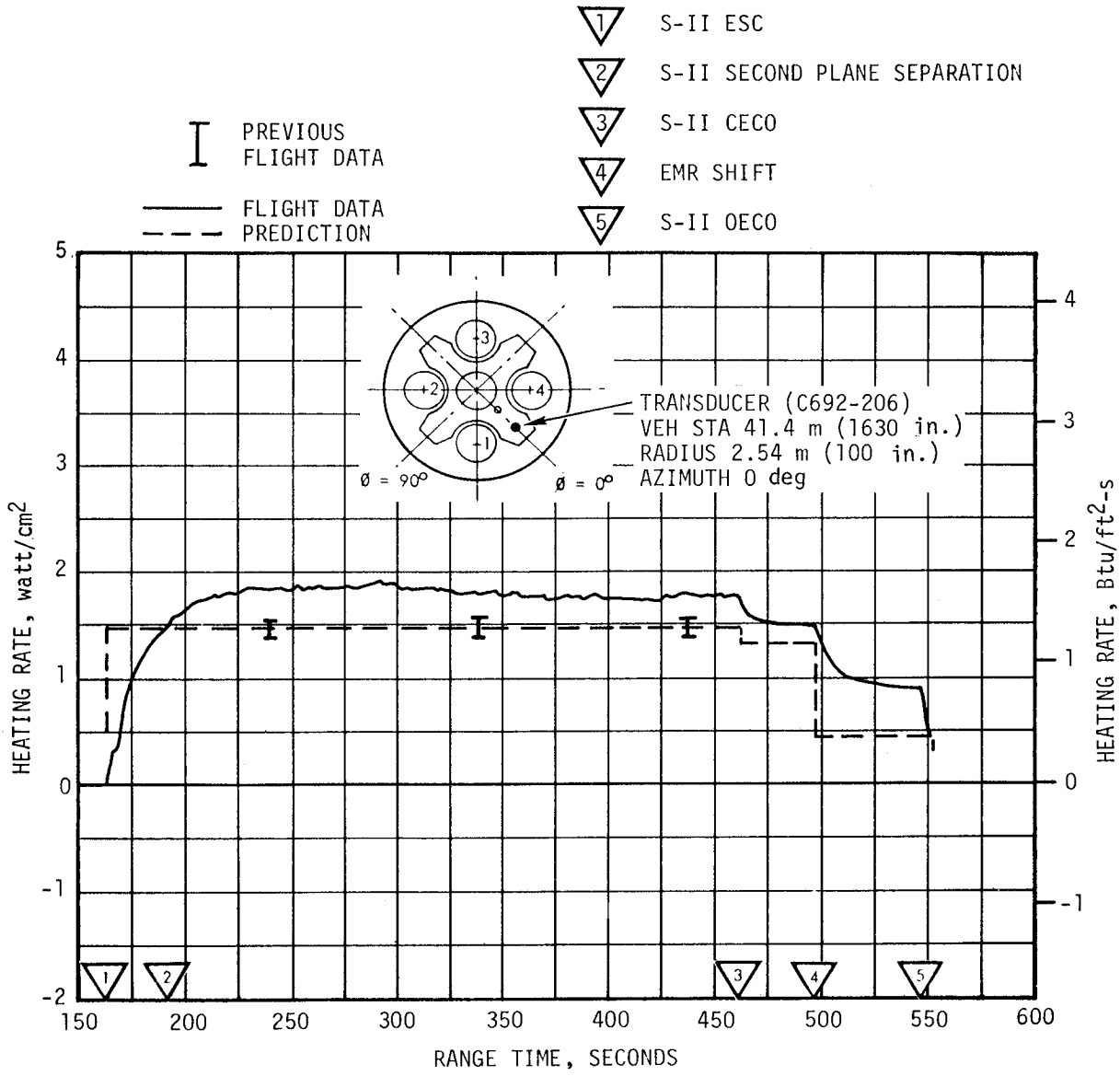

Figure 17-5. Heat Shield Aft Radiation Heat Rate

Figure 17-5 shows that the incident radiative heat flux during the AS-506 flight was greater than predicted and approximately 20 percent higher than the maximum values measured during flights AS-501 through AS-505. The most probable cause for this increase is engine misalignment or engine gimbaling, neither of which are accounted for in the postflight prediction of the incident radiative heat flux.

There were no measurements of structural temperatures made on the AS-506 S-II stage base heat shield. To evaluate the structural temperatures experienced on the aft surface of the heat shield, a maximum postflight

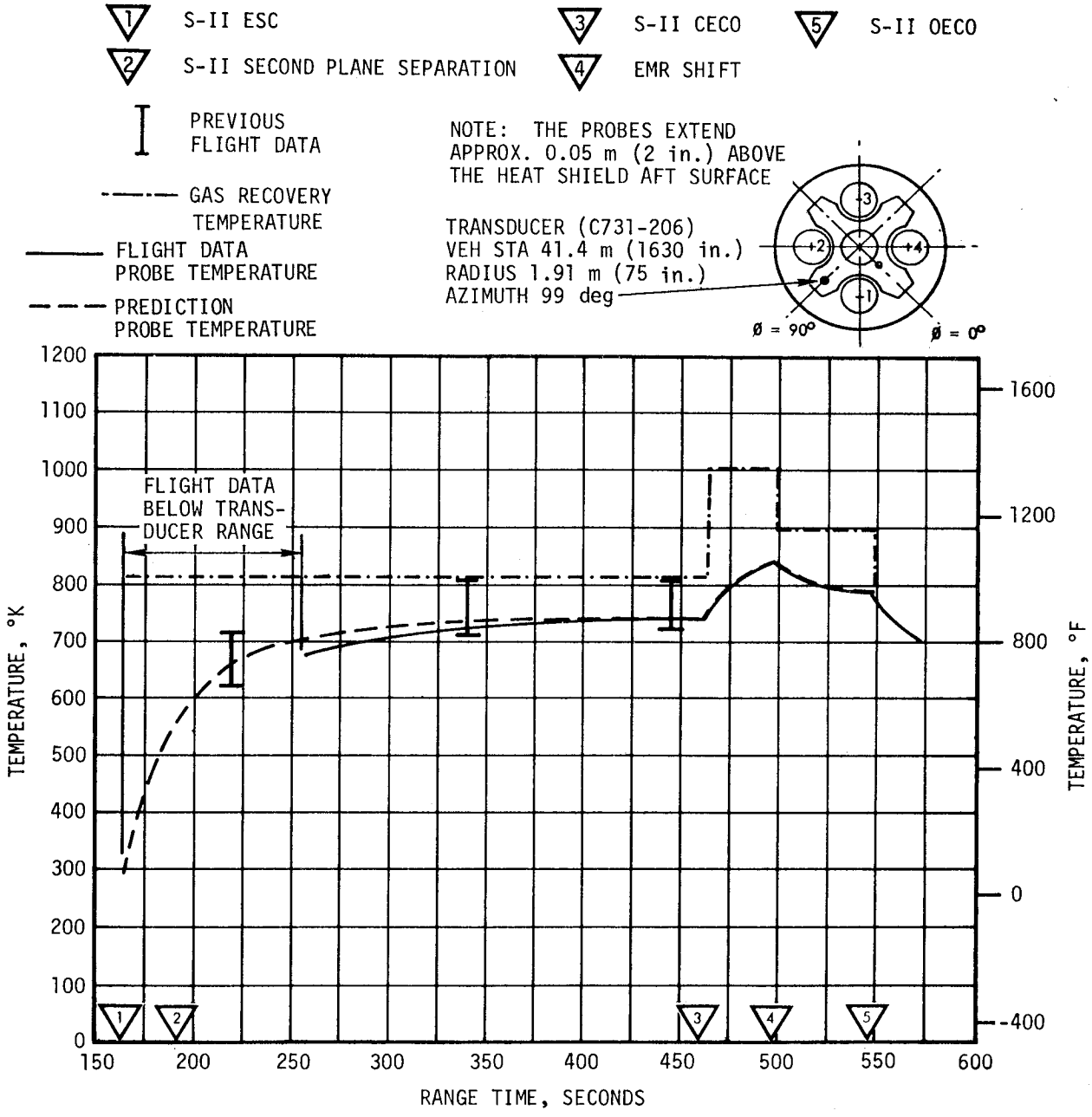

Figure 17-6. S-II Base Gas Temperature

predicted temperature was calculated for the aft surface using base heating rates predicted for the AS-506 flight. The predicted maximum postflight temperature was 818°K (1014°F) which compared favorably with maximum postflight temperatures predicted from previous flights, and was well below the maximum design temperatures of 1066°K (1460°F) for the no-engine-out case and 1116°K (1550°F) for the one control engine-out case.

The effectiveness of the heat shield and flexible curtains as a thermal protection system was again demonstrated on this flight as on previous flights by the relatively low temperatures recorded on the thrust cone forward surface. The AS-506 maximum measured thrust cone forward surface temperature was 266°K (20°F), essentially equal to that recorded during previous flights. The measured temperatures were well below design values and in good agreement with postflight predictions.

17.4 VEHICLE AEROHEATING THERMAL ENVIRONMENT

17.4.1 S-IC Stage Aeroheating Environment

The aerodynamic heating environments were not measured on the AS-506 S-IC stage. However, flow separation was measurable from flight optical data (ALOTS film) and was observed to occur at approximately the same time as on AS-505, 116 seconds as shown in Figure 17-7. The effects of CECO on the separated flow region during AS-506 flight were the same as observed on previous flights. It should be noted that at higher altitudes, the measured location of the forward point of flow separation is questionable because of loss of resolution in the flight optical data.

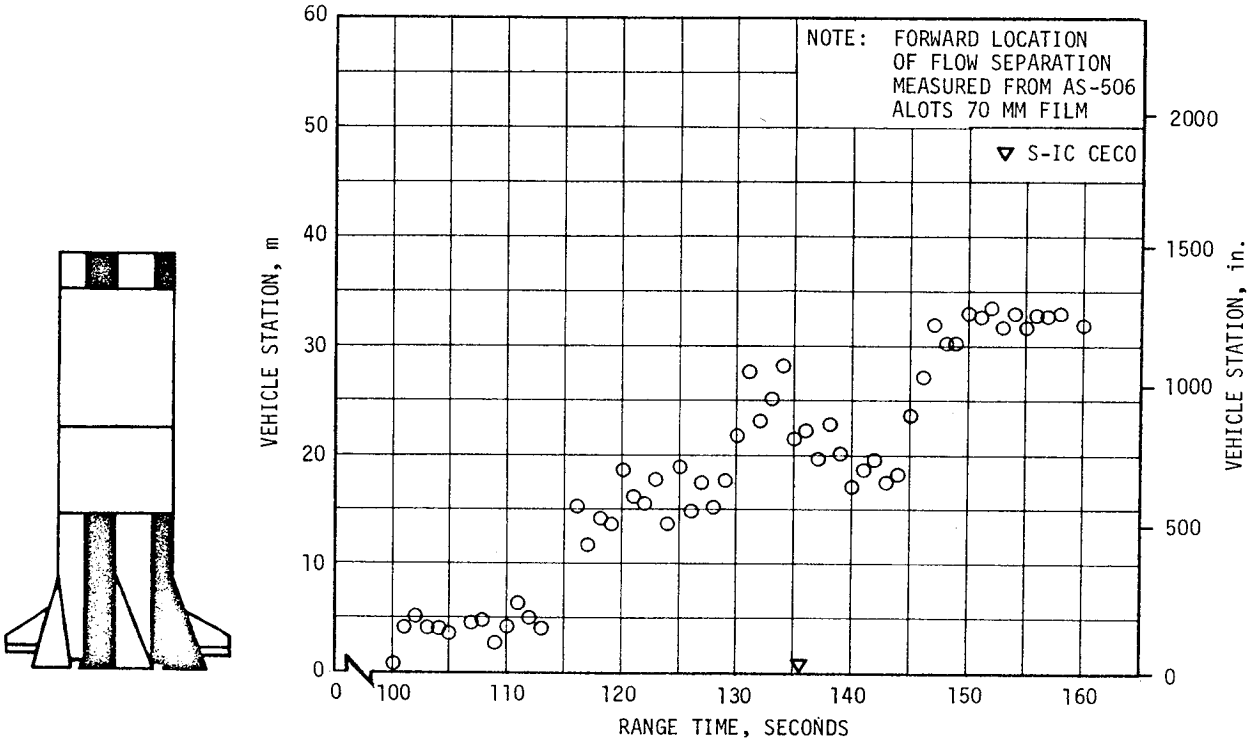

Figure 17-7. Forward Location of Separated Flow

17.4.2 S-II Stage Aeroheating Environment

There were no aerodynamic heating environments measured on the S-II stage; however, postflight predicted temperatures were determined based on the actual AS-506 trajectory and thermal models used in previous flight evaluations. All postflight predicted temperatures were well below the design limits and within the band of previous flight data.

SECTION 18

ENVIRONMENTAL CONTROL SYSTEM

18.1 SUMMARY

The S-IC canister conditioning system and the aft environmental conditioning system performed satisfactorily during the AS-506 countdown.

The S-II thermal control and compartment conditioning system apparently performed satisfactorily since the ambients external to the containers were nominal and there were no problems with the equipment in the containers.

The Instrument Unit (IU) Environmental Control System (ECS) exhibited overall satisfactory performance for the duration of the IU mission. Coolant temperatures, pressures, and flowrates were continuously maintained within required ranges and design limits. One deviation from specification was observed. The inertial platform gas bearing differential pressure drifted above the 10.7 N/cm^2 (15.5 psid) maximum to 11.2 N/cm^2 (16.3 psid). This drifting phenomenon also occurred on on AS-501, AS-503, and AS-504 and caused no detrimental effect on the mission.

18.2 S-IC ENVIRONMENTAL CONTROL

The ambient temperatures of the 4 canisters in the S-IC forward skirt compartment must be maintained at 300 ±11°K (80 ±20°F) during equipment operation prior to J-2 engine chilldown and 325 to 278°K (125 to 40°F) during J-2 engine chilldown. No canister conditioning is required after S-IC forward umbilical disconnect.

The canister conditioning system was supplied with air/GN_2 (gaseous nitrogen) at a flowrate of 17.24 kg/min (38 lbm/min) and a temperature of 299°K (79°F) through the S-IC forward lower umbilical and at a flowrate of 15.42 kg/min (34 lbm/min) and a temperature of 301°K (81°F) through the S-IC forward upper umbilical during AS-506 countdown prior to J-2 engine chilldown. During J-2 engine chilldown, the flowrate and temperature of the GN_2 supplied to the forward upper umbilical was increased to 18.82 kg/min (41.5 lbm/min) and 311°K (100°F), and the temperature of the GN_2 supplied to the forward lower umbilical was increased to 314°K (105°F). No instrumentation was installed in the canisters on AS-506; therefore,

no evaluation of the actual temperatures within the canisters was possible. No failure of any electrical/electronic equipment installed in the canisters was reported.

During J-2 engine chilldown, the thermal environment is at the most critical point. Within this period the ambient temperature in the forward skirt compartment dropped as shown in Figure 18-1. The lowest ambient temperature measured during AS-506 J-2 engine chilldown was 229°K (-48°F) at instrument location C206-120. During AS-506 flight, the lowest temperature recorded was 183°K (-130°F) at instrument location C206-120.

The design requirement for the aft compartment is that the ambient temperature for prelaunch be maintained at 300.0 ±8.3°K (80 ±15°F). Aft compartment prelaunch ambient temperatures are shown in Figure 18-2. The lowest prelaunch temperature recorded was 287°K (58°F) at instrument C107-115. This low temperature occurred prior to LOX loading and did not cause any problems. Aft compartment ambient temperatures for flight are also shown in Figure 18-2. The lowest temperature recorded was 285°K (54°F) at instrument C203-115.

18.3 S-II ENVIRONMENTAL CONTROL

The engine compartment conditioning system maintained the ambient and thrust cone surface temperature within design ranges throughout the launch countdown. The system also maintained an inert atmosphere within the compartment.

There were no thermal control container temperature measurements; however, since the ambients external to the containers were satisfactory and there were no problems with the equipment in the containers, it is assumed that the thermal control systems performed adequately. The ambient temperature near the forward system was 44.5 to 85°K (80 to 152°F) warmer than the extremes of past vehicles due to the increased effectiveness of the foam insulation used on the S-II-6 hydrogen tank forward bulkhead. Foam insulation reduced heat leakage from the engine compartment and resulted in more uniform temperatures from container to container.

18.4 IU ENVIRONMENTAL CONTROL

The IU ECS is composed of a Thermal Conditioning System (TCS) and a Gas Bearing Supply System (GBS). A preflight purge subsystem provided compartment conditioning prior to launch and maintained the compartment temperature within the required 290 to 296°K (63 to 73°F) range.

18.4.1 Thermal Conditioning System

Initial sublimator start-up and sublimator performance parameters during ascent are depicted in Figure 18-3. Immediately after liftoff, the Modulating Flow Control Valve (MFCV) began driving toward the full heatsink

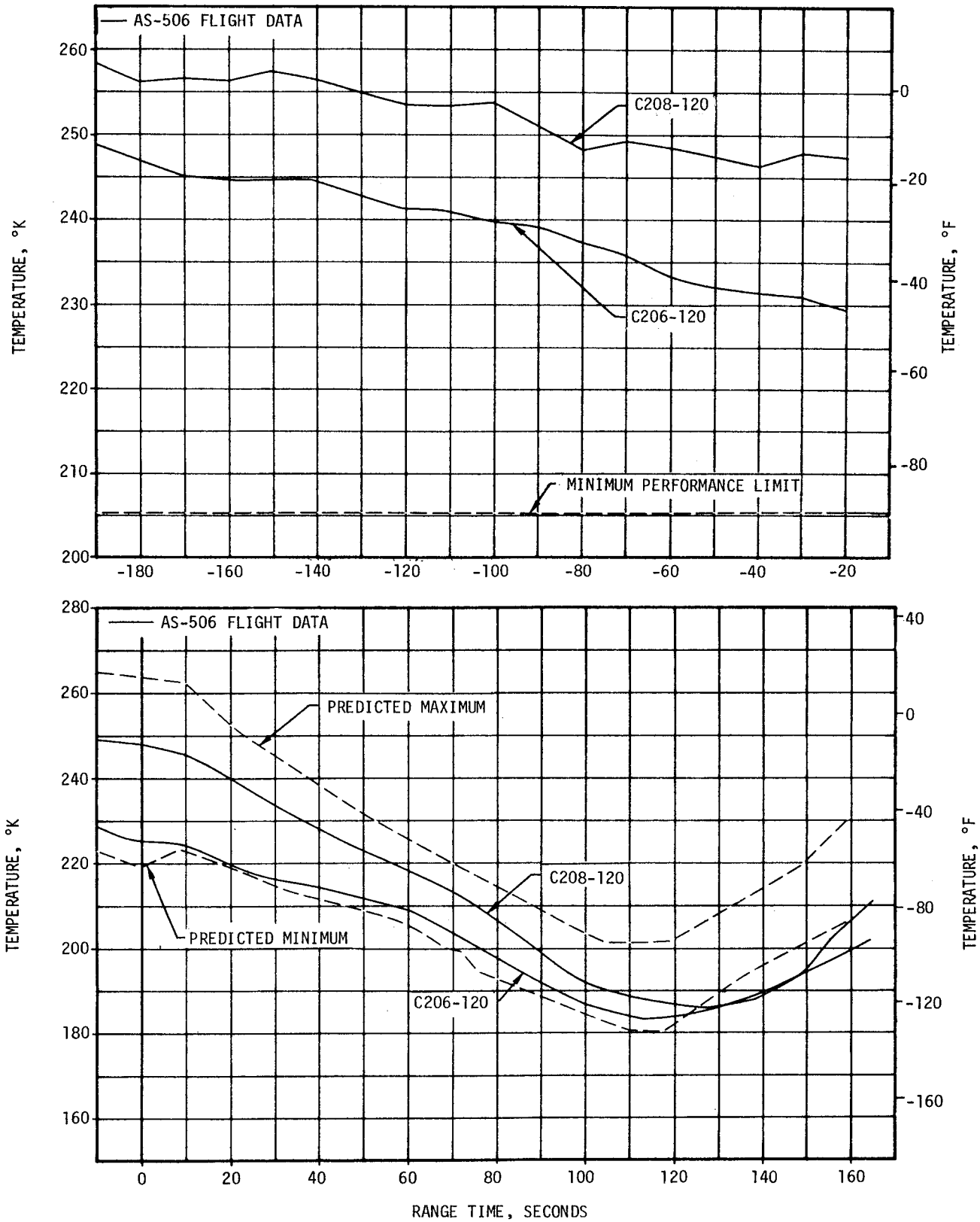

Figure 18-1. S-IC Forward Compartment Ambient Temperature

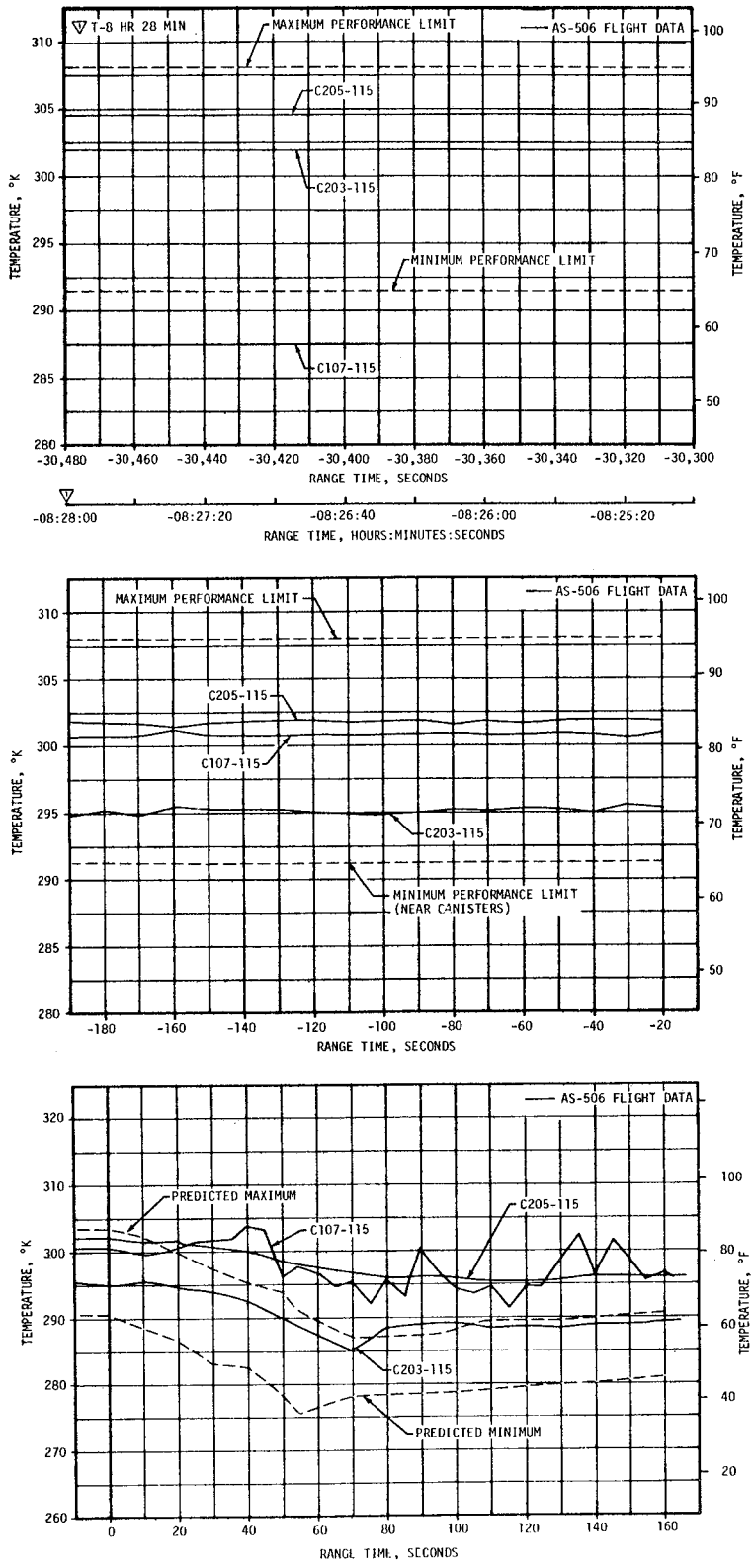

Figure 18-2. S-IC Aft Compartment Temperature

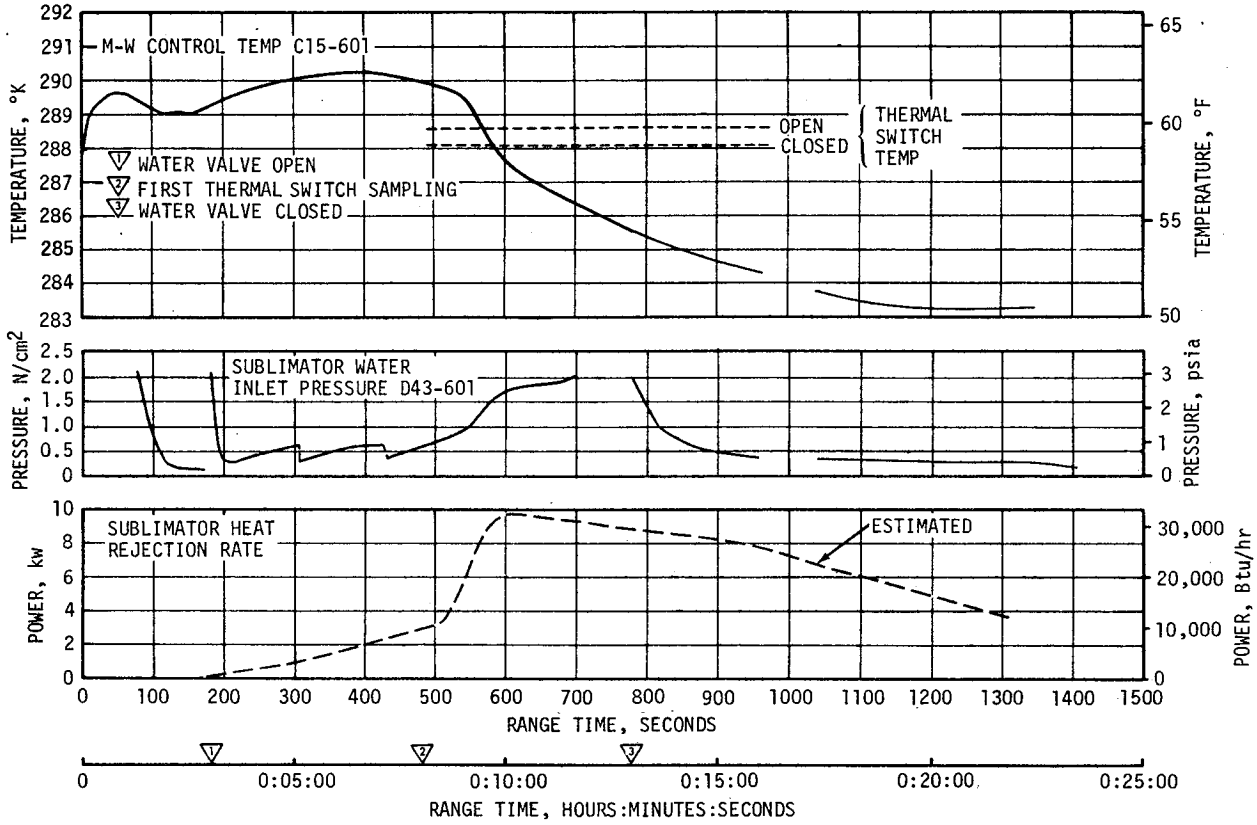

Figure 18-3. Sublimator Performance During Ascent

position which was reached at approximately 30 seconds. The water valve opened at 181 seconds allowing water to flow to the sublimator. Immediate cooling was evidenced by the rapid decline in the coolant fluid temperature. At the first thermal switch sampling, the coolant temperature was still above the actuation point and the water valve remained open. The second thermal switch sampling at approximately 780 seconds resulted in closing of the water supply valve.

Coolant flowrates and pressures were well within required ranges as indicated in Table 18-1.

An after mission experiment was performed in which the water supply valve logic was inhibited (valve closed) to determine the effect of loss of sublimator cooling. This was initiated approximately 5 hours after liftoff. The Methanol/Water (M/W) supply temperature exceeded the maximum scale range of 293°K (68°F) at about 23,200 seconds (Figure 18-4).

The TCS GN_2 sphere pressure decay which is indicative of GN_2 usage rate was as expected for the nominal case as shown in Figure 18-5.

Table 18-1. TCS Coolant Flowrates and Pressures

PARAMETER	REQUIREMENT	MINIMUM OBSERVED	MAXIMUM OBSERVED
IU Coolant Flowrate F9-602 m^3/hr (gpm)	2.18 (9.6)	2.20 (9.7)	2.27 (10.0)
S-IVB Coolant Flowrate F10-601 m^3/hr (gpm)	1.77 ±.09 (7.8 ±.4)	1.77 (7.8)	1.82 (8.2)
Pump Inlet Pressure D24-601 N/cm^2 (psia)	10.83 to 11.72 (15.7 to 17.0)	11.03 (16.0)	11.38 (16.5)
Pump Outlet Pressure D17-601 N/cm^2 (psia)	28.89 to 33.23 (41.9 to 48.2)	31.03 (45.0)	31.72 (46.0)

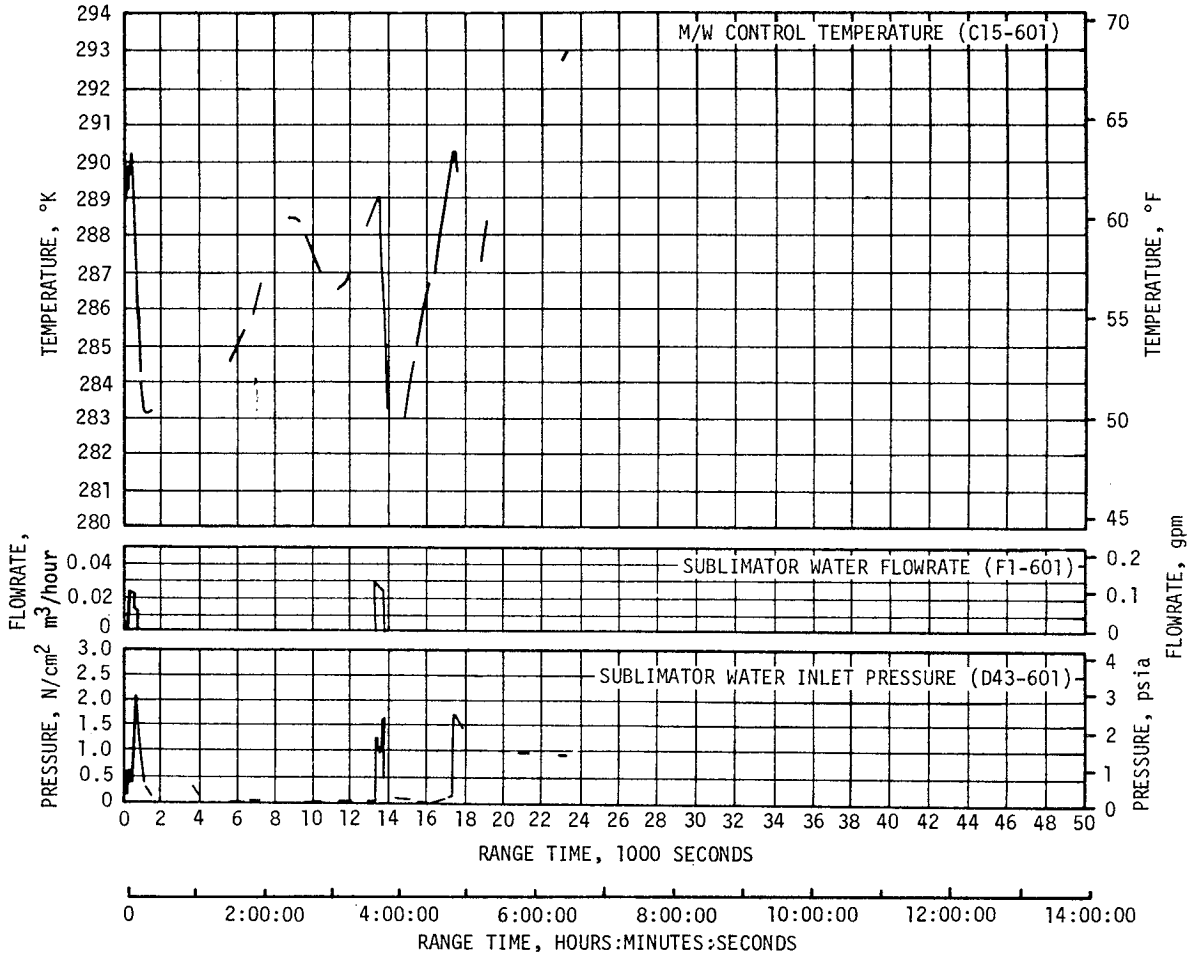

Figure 18-4. TCS Coolant Control Parameters

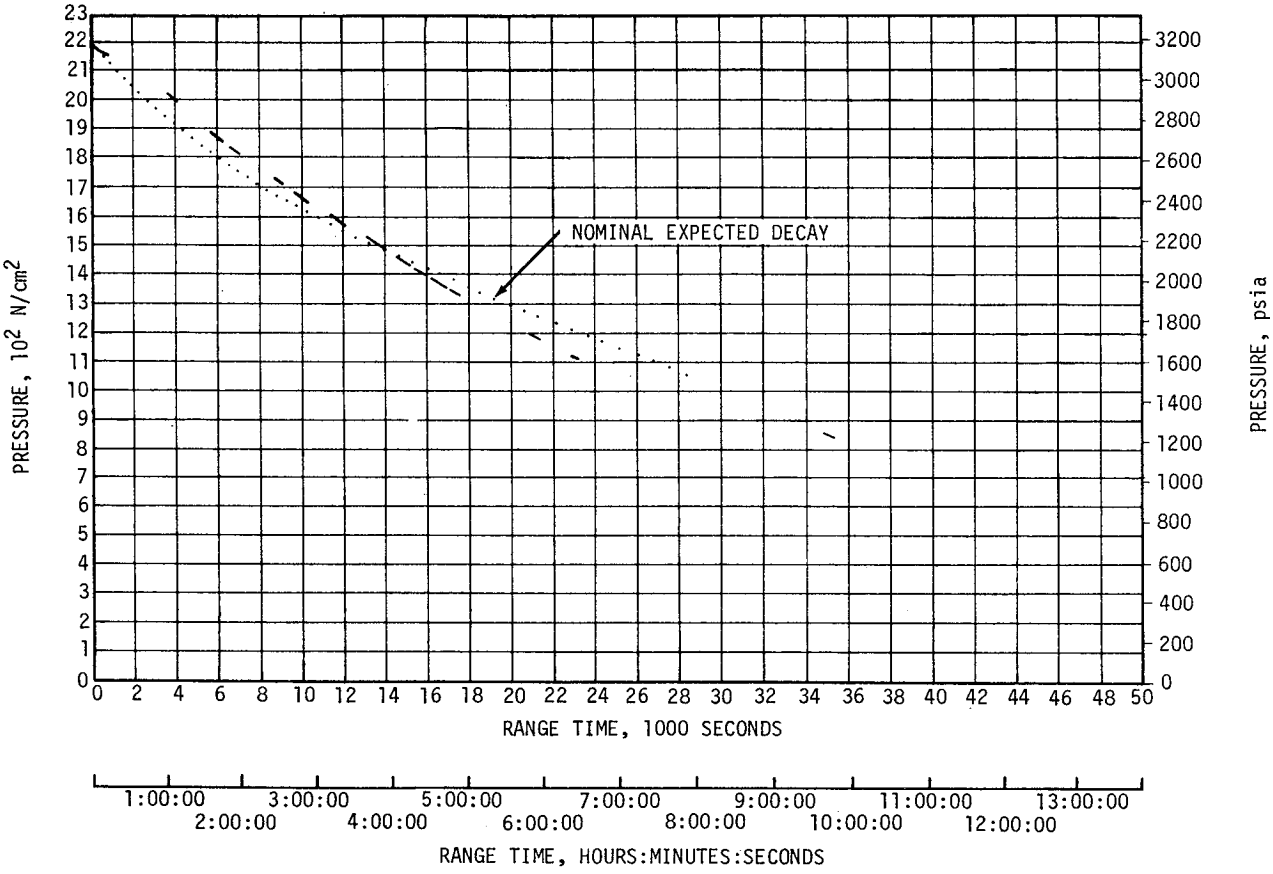

Figure 18-5. TCS GN_2 Sphere Pressure (D25-601)

All component temperatures remained within their expected ranges for the duration of the mission (Figure 18-6). The ST-124M internal gimbal (inertial) temperature (C34-603) went below operational temperature range 313°K (104°F) (marginal operation) at about 4 hours. Lower temperature operation was also observed on AS-504 and AS-505, and is due to a change in internal platform configuration (including axial blower) effective on AS-504 and subsequent. No degradation of platform performance has been noted. The component temperatures all climbed as expected during the ECS experiment and C34-603 went above its upper operating limit 319°K (115°F) at about 9 hours (Figure 18-6).

18.4.2 Gas Bearing Supply System

The GN_2 pressure differential across the ST-124M platform gas bearings drifted from an initial value of 10.48 N/cm^2 (15.2 psid) at liftoff to 11.24 N/cm^2 (16.3 psid) at 23,200 seconds (see Figure 18-7). The upper limit of the specification value 10.7 N/cm^2 (15.5 psid) was exceeded at about 2500 seconds. The phenomenon of upward drifting of the pressure differential has occurred on AS-501, AS-503, and AS-504 flights. Extensive analysis and laboratory testing has indicated that the pressure

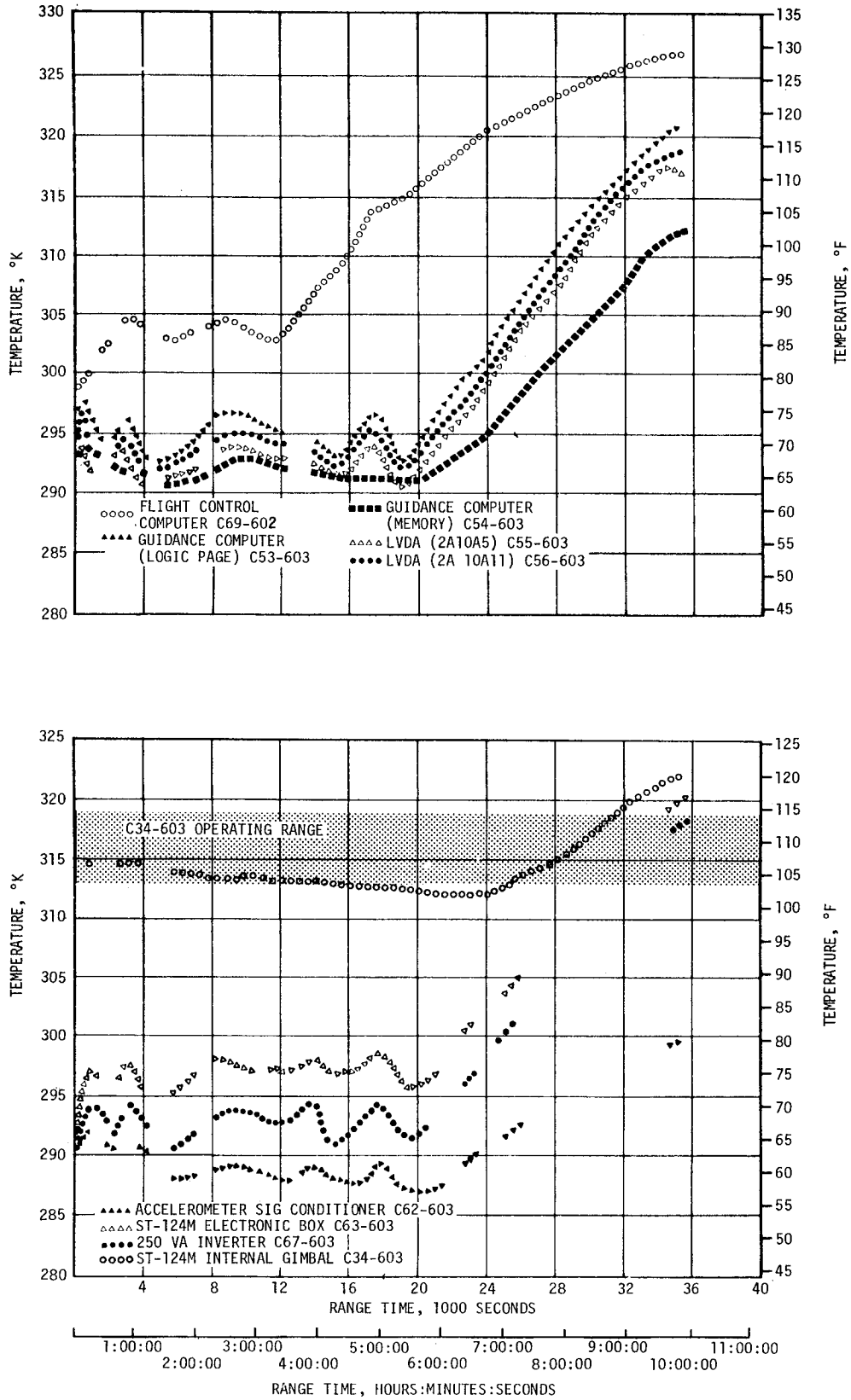

Figure 18-6. IU Selected Component Temperatures

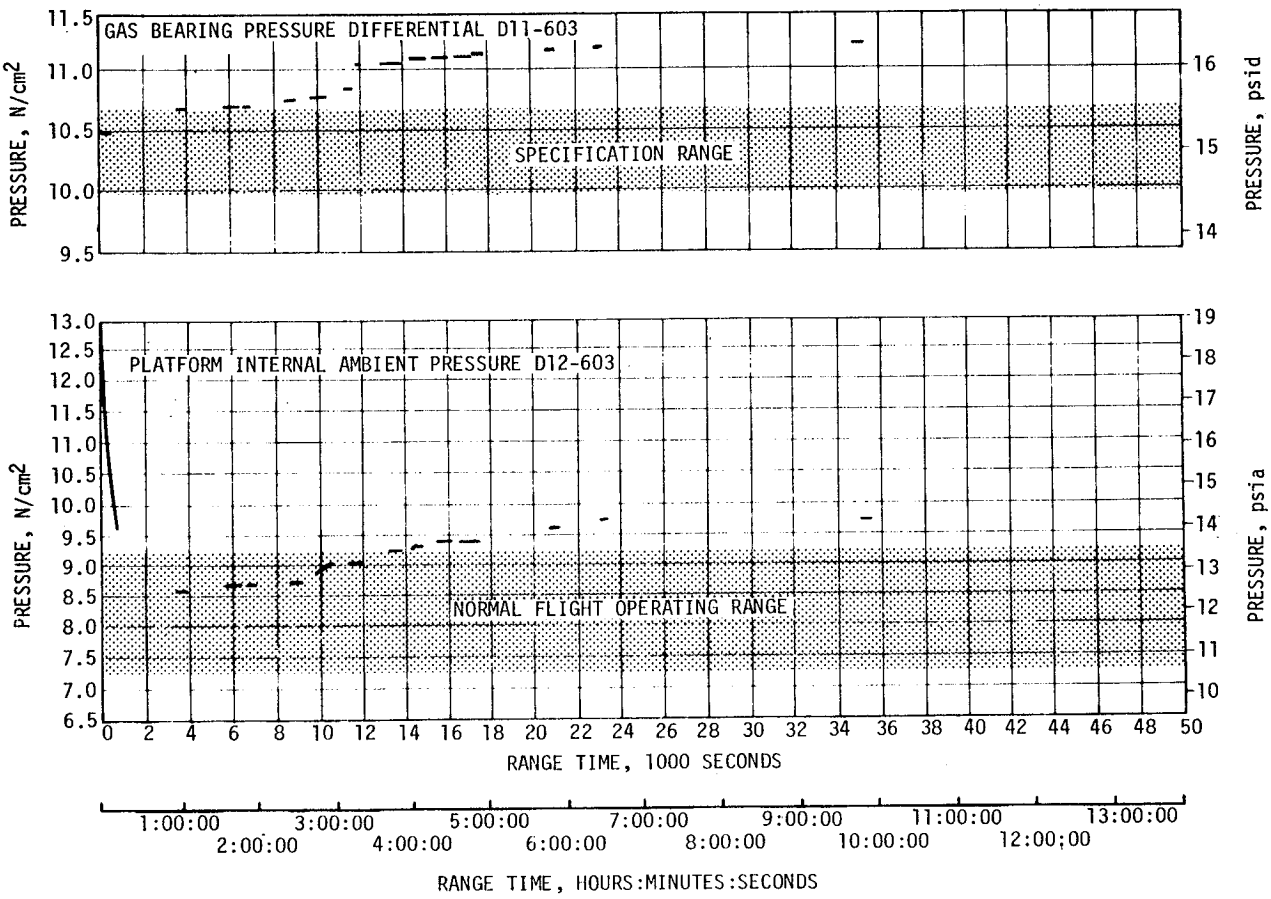

Figure 18-7. Inertial Platform GN_2 Pressures

differential discrepancy is a function of a number of variables acting simultaneously with no single controlling factor. Although the gas bearing pressure regulator as a component fulfills its functional requirements, variables are introduced at a systems level which cause the pressure differential drift.

The occurrence of a slightly higher pressure differential on previous flights has resulted in no discernible effect on platform operation. Vendor testing of the inertial platform at pressure differentials up to 13.8 N/cm^2 (20 psid) have resulted in no degradation in platform performance.

An engineering change proposal is being considered to change the upper limit of the specification to an acceptable value, which includes the tolerance buildup of the system variables.

The GBS sphere pressure decay shown in Figure 18-8 was as expected. This was an indication of normal GN_2 consumption.

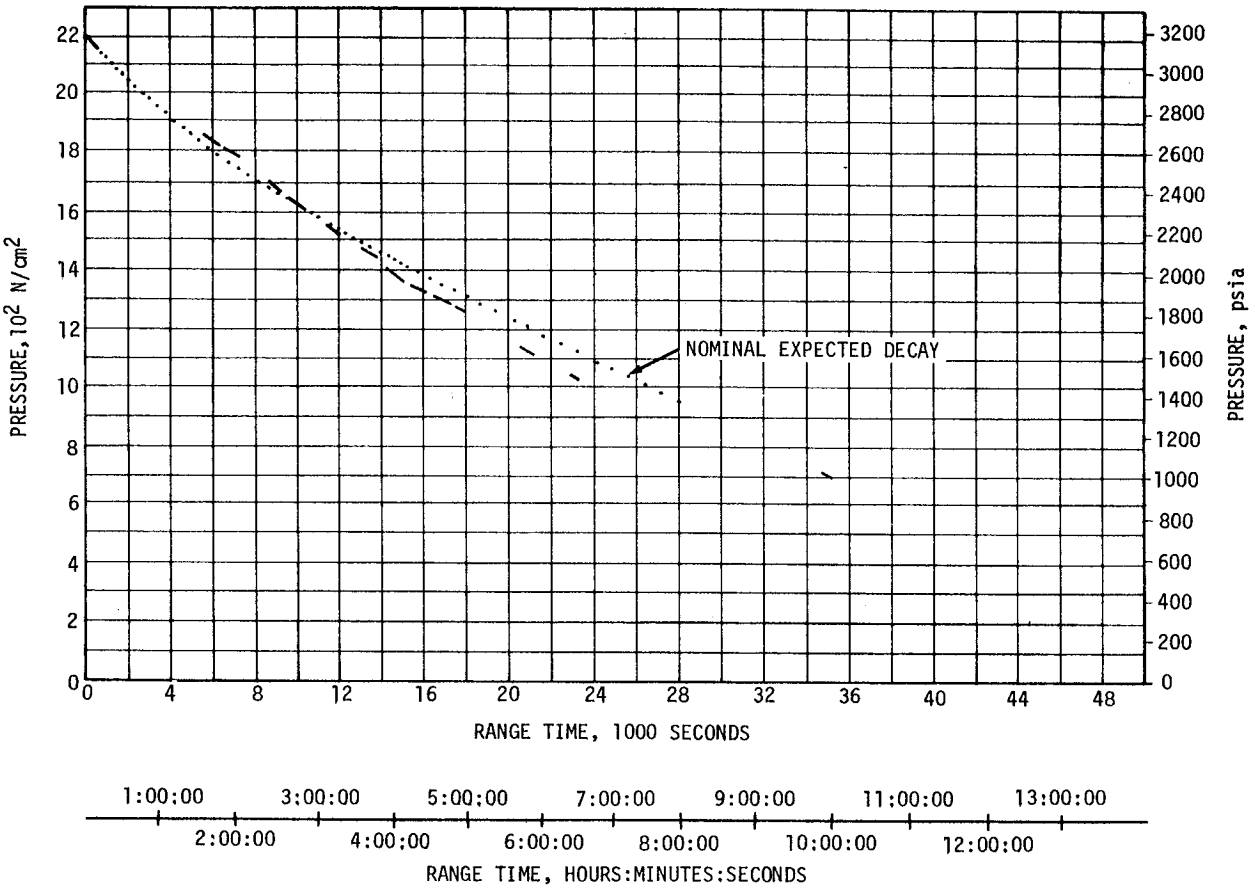

Figure 18-8. GBS GN_2 Sphere Pressure (D10-603)

SECTION 19

DATA SYSTEMS

19.1 SUMMARY

All elements of the data system performed satisfactorily except for a problem with the Command and Communications System (CCS) downlink during translunar coast.

Measurement performance was excellent, as evidenced by 99.9 percent reliability. This is the highest reliability attained on any Saturn V flight.

Telemetry performance was nominal, with the exception of a minor calibration deviation. Very High Frequency (VHF) telemetry Radio Frequency (RF) propagation was generally good, though the usual problems due to flame effects and staging were experienced. Usable VHF data were received to 17,800 seconds (04:56:40). Command systems RF performance for both the Secure Range Safety Command Systems (SRSCS) and CCS was nominal except for the CCS downlink problem noted. Usable CCS data were received to 35,214 seconds (09:46:54).

Goldstone (GDS) received CCS signal carrier to 35,779 seconds (09:56:19). Good tracking data were received from the C-Band radar, with Patrick Air Force Base (PAFB) indicating final Loss of Signal (LOS) at 42,912 seconds (11:55:12).

The 75 ground engineering cameras provided good data during the launch.

19.2 VEHICLE MEASUREMENT EVALUATION

The AS-506 launch vehicle had 1370 measurements scheduled for flight. Eight measurements were waived prior to the start of the automatic countdown sequence leaving 1362 measurements active for flight. Of the waived measurements, five provided valid data during the flight.

Table 19-1 presents a summary of measurement performance for the total vehicle and for each stage. Measurement performance was exceptionally good, as evidenced by 99.9 percent reliability, which is the highest attained on any Saturn V flight.

Table 19-1. AS-506 Measurement Summary

MEASUREMENTS CATEGORY	S-IC STAGE	S-II STAGE	S-IVB STAGE	INSTRUMENT UNIT	TOTAL VEHICLE
Scheduled	313	563	270	224	1370
Waived	3	4	1	0	8
Failures	0	2	0	0	2
Partial Failures	8	0	0	0	8
Reliability, Percent	100.0	99.6	100.0	100.0	99.9

Tables 19-2 and 19-3 tabulate by stage the waived measurements, totally failed and partially failed measurements. None of the listed failures had any significant impact on postflight evaluation.

19.3 AIRBORNE TELEMETRY SYSTEMS

Performance of the eight VHF telemetry links was generally satisfactory with the minor exceptions noted. A brief performance summary of these links is shown in Table 19-4.

There was a variation of approximately 17 counts in the 100 percent level of the inflight calibrations for the DP-1 telemetry link. This is equivalent to 85 millivolts as compared to 41 millivolts in the specifications. This type of variation is present in all other calibration levels to a lesser degree. The data indicate the variation is from the Model 301 or the Model 270 multiplexers and not the 5-volt measuring supply. This problem, which also occurred on AS-505, is being investigated.

Data degradation and dropouts were experienced at various times during boost as on previous flights due to attenuation of RF transmission, at these times, as discussed in paragraph 19.4.1.

Usable VHF telemetry data were received to 17,800 seconds (04:56:40) at Guaymas (GYM).

Performance of the CCS telemetry was generally satisfactory except for the period during translunar coast from 27,128 seconds (07:32:08) to 35,779 seconds (09:56:19). This problem is discussed in detail in paragraph 19.4.3.2. Usable CCS data were received at GDS to 35,214 seconds (09:46:54).

Table 19-2. AS-506 Flight Measurements Waived Prior to Launch

MEASUREMENT NUMBER	MEASUREMENT TITLE	NATURE OF FAILURE	REMARKS
		S-IC STAGE	
D004-102	Pressure, Fuel Pump Inlet 1	Transducer offset and not responsive to pressure	KSC Waiver I-B-506-3. Measurement provided valid data throughout powered flight
D119-102	Pressure Differential, Engine Gimbal System Filter Manifold	Transducer failure	KSC Waiver I-B-506-3
D119-103	Pressure Differential, Engine Gimbal System Filter Manifold	Transducer failure	KSC Waiver I-B-506-3
		S-II STAGE	
D008-201	E1 LOX Turbine Inlet Pressure	Transducer drift	Flight data usable
D104-201	Engine Hydraulic Reservoir Pressure	Noisy transducer	Flight data usable
D104-202	Engine Hydraulic Reservoir Pressure	Noisy transducer	Flight data usable
D104-203	Engine Hydraulic Reservoir Pressure	Noisy transducer	Flight data usable
		S-IVB STAGE	
C0005-405	Temp. - Cold He Sphere No. 3 Gas	Measurement failed off-scale low during LH_2 loading of CDDT.	It is suspected that a resistance dependent upon temperature was shunting the temperature sensor. This causes a lower than calibrated resistance of the probe to be seen by the bridge.

Table 19-3. AS-506 Measurement Malfunctions

MEASUREMENT NUMBER	MEASUREMENT TITLE	NATURE OF FAILURE	TIME OF FAILURE (RANGE TIME)	SATISFACTORY OPERATION	REMARKS
TOTAL MEASUREMENT FAILURES, S-II STAGE					
C003-205	E5 Fuel Turbine Inlet Temp.	Transducer opened	S-II ESC	0 second	
F001-204	E4 Main Fuel Flow	No data pulses during engine burn	Prior to launch	0 second	
PARTIAL MEASUREMENT FAILURES, S-IC STAGE					
C003-101	Temperature, Turbine Manifold	No data from 0 to 77 seconds	0 second	85 seconds	Probable cable problem
D007-101	Pressure, Fuel Pump Discharge 2	Data decreases after 135 seconds	135 seconds	135 seconds	Probable transducer malfunction
D007-102	Pressure, Fuel Pump Discharge 2	Data approximately 100 psi low from 105 to 120 seconds	105 seconds	148 seconds	Probable transducer malfunction
D007-105	Pressure, Fuel Pump Discharge 2	Data approximately 100 psi low from 85 to 100 seconds	85 seconds	148 seconds	Probable transducer malfunction
D016-104	Pressure, Engine Gimbal System Supply, Engine 4	Data approximately 100 psi high from 95 to 135 seconds	95 seconds	122 seconds	Probable transducer malfunction
D118-104	Pressure, Engine Gimbal System Return, Yaw Actuator	Data erratic subsequent to 140 seconds	140 seconds	140 seconds	Probable transducer malfunction
D144-119	Pressure, Helium Storage Tank	Data read low from 100 to 130 seconds	100 seconds	132 seconds	Cause unknown
K085-120	LOX Tank Vent Valve, Closed	Data noisy and erratic from ignition to 135 seconds	Ignition	27 seconds	Probable cable problem

Table 19-4. AS-506 Launch Vehicle Telemetry Links

LINK	FREQUENCY MHz	MODULATION	STAGE	FLIGHT PERIOD (RANGE TIME, SEC)	PERFORMANCE SUMMARY
AF-1 AP-1	256.2 244.3	FM/FM PCM/FM	S-IC S-IC	0-410 0-410	Satisfactory Data Dropouts Range Time (sec) — Duration (sec) 162.3 — 1.0 165.5 — 1.7
BF-1 BF-2 BP-1	241.5 234.0 248.6	FM/FM FM/FM PCM/FM	S-II S-II S-II	0-772 0-772 0-772	Satisfactory Data Dropouts Range Time (sec) — Duration (sec) 163.0 — 2.5 192.3 — 3.0
CP-1	258.5	PCM/FM	S-IVB	Flight Duration	Satisfactory Data Dropouts Range Time (sec) — Duration (sec) 162.4 — 1.0
DF-1 DP-1 DP-1B	250.7 245.3 2282.5	FM/FM PCM/FM PCM/FM	IU IU IU	Flight Duration Flight Duration 0-35,779	Satisfactory except for DP-1 calibration. Data Dropouts Range Time (sec) — Duration (sec) 162.9 (VHF) — 2.1 162.5 — 7.0 (DP-1B only) 193.5 — 8.0 (DP-1B only) 17,470 — See 19.4.3.2 (DP-1B only) 27,128 — See 19.4.3.2 (DP-1B only) 30,264 — See 19.4.3.2 (DP-1B only) 34,020 — See 19.4.3.2 (DP-1B only) 35,214 — See 19.4.3.2 (DP-1B only)

19.4 RF SYSTEMS EVALUATION

19.4.1 Telemetry System RF Propagation Evaluation

The performance of the eight VHF telemetry links was excellent and generally agreed with predictions. VHF telemetry links AF-2, AF-3, AS-1, AS-2, BF-3, BS-1, BS-2, CF-1 and CS-1 were deleted on AS-506.

Moderate to severe signal attenuation was experienced at various times during the boost due to main flame effects, S-IC/S-II and S-II/S-IVB staging, S-II ignition and S-II second plane separation. Magnitude of these effects was comparable to that experienced on previous flights. At S-IC/S-II staging, signal strength on all VHF telemetry links and on the CCS downlink dropped to threshold for approximately 2 and 7 seconds, respectively. Signal degradation due to S-II ignition and S-II flame effects was sufficient to cause loss of VHF telemetry data on the S-IC and S-II stages. CCS and S-II VHF data were lost during S-II second plane separation. In addition, there were intervals during the launch phase where some data were so degraded as to be unusable. Loss of these data, however, posed no problem since losses were of such short duration as to have little or no impact on flight analysis.

The performance of the S-IVB and IU telemetry systems was nominal during orbit, second burn and final coast, except for the CCS problem discussed in paragraph 19.4.3.2.

GYM reported VHF LOS at 17,800 seconds (04:56:40) and GDS reported CCS LOS at 35,779 seconds (09:56:19).

A summary of available VHF telemetry coverage showing Acquisition of Signal (AOS) and LOS for each station is shown in Figure 19-1.

19.4.2 Tracking Systems RF Propagation Evaluation

Analysis of data received to date indicates that the C-Band radar functioned satisfactorily during this flight, although several ground stations experienced some tracking problems.

The only problems reported during launch occurred at Cape Kennedy (CNV), Merritt Island Launch Area (MILA), and Grand Turk Island (GTK). All three stations lost track due to balance point shifts (erroneous pointing information caused by a sudden vehicle antenna null or a distorted beacon return). CNV and MILA went off track momentarily at 100 and 395 seconds, respectively. GTK had dropouts due to balance point shifts at 241 seconds (momentarily), from 535 to 538, from 555 to 570, from 572 to 580, from 594 to 599 and from 606 to 614 seconds. The highest elevation angle encountered by GTK during this period was 3 degrees. MILA went off track from 440 to 480 seconds due to interference from an electrical storm. Bermuda (BDA) did not report any problems during launch.

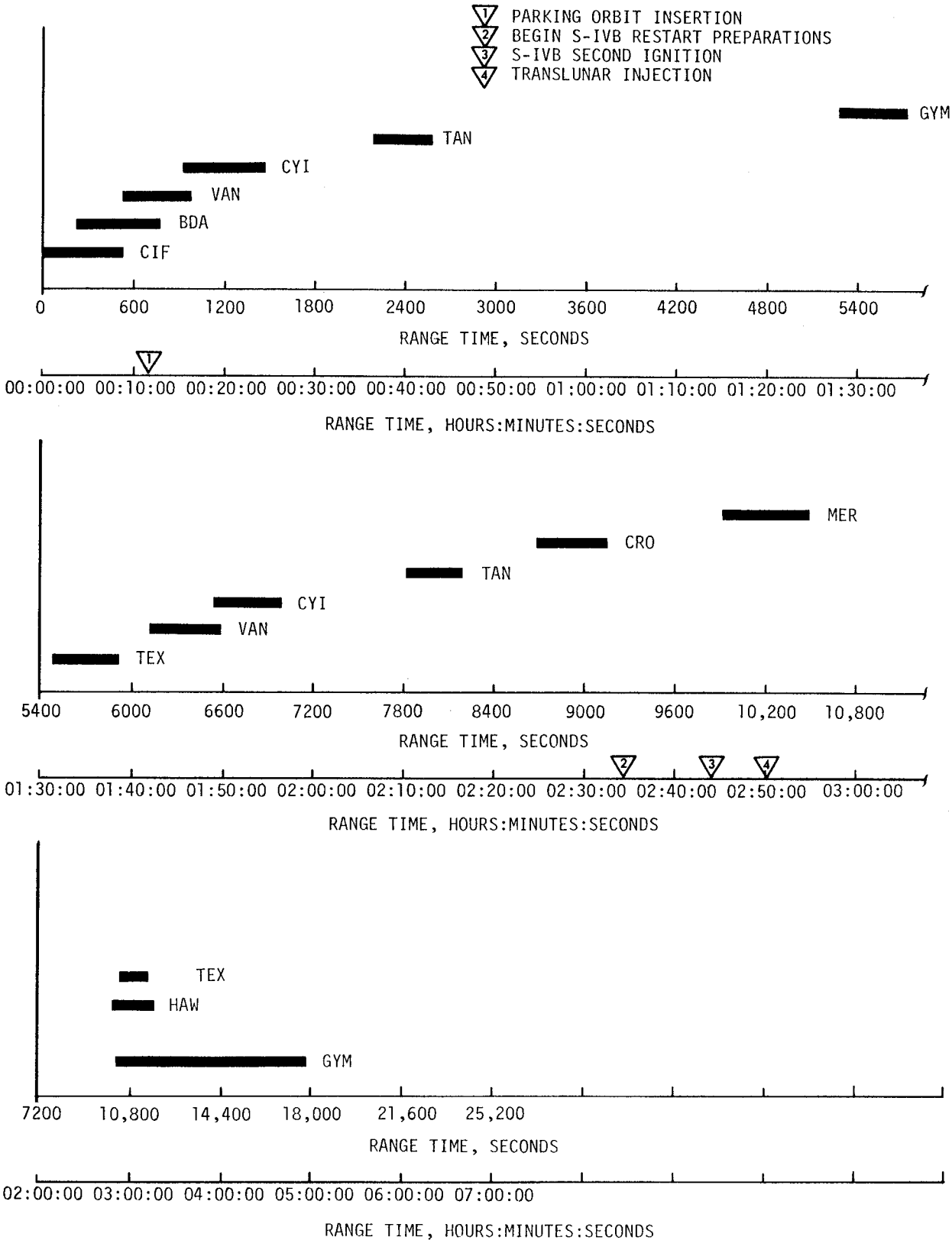

Figure 19-1. VHF Telemetry Coverage Summary

Problems experienced during earth orbit included tracking on a sidelobe by Vanguard (VAN) (revolution 2) and a phasing problem experienced by GTK (revolution 2). This type phasing problem is experienced when a ground station receives two closely spaced beacon returns; one generated as a result of its own interrogation and one resulting from the interrogation of the beacon by another ground station.

GTK lost track during translunar coast from 27,126 seconds (07:32:06) to 29,260 seconds (08:07:40) when attempting to phase away from the beacon return pulse of another ground station. PAFB indicated final LOS at 42,912 seconds (11:55:12).

A summary of available C-Band radar coverage showing AOS and LOS for each station is shown in Figure 19-2.

There is no mandatory tracking requirement of the CCS; however, the CCS transponder has turnaround ranging capabilities and provided a backup to the Command and Service Module (CSM) transponder used for tracking in case of failure or desire for a cross check. Since the same transponder is used for all CCS functions, discussion of the tracking performance of this system is included in the general discussion of the CCS RF evaluation.

19.4.3 Command Systems RF Evaluation

19.4.3.1 Secure Range Safety Command System. VHF telemetry measurements received by the ground stations from the S-IC, S-II and S-IVB stages indicated that the SRSCS RF subsystems functioned properly. CNV and BDA were the command stations used for this flight. The carrier signal at CNV was turned off at approximately 400 seconds. At BDA the carrier was turned on at approximately 375 seconds and turned off at approximately 750 seconds. A momentary dropout occurred at approximately 120 seconds when the command station switched transmitting antennas.

19.4.3.2 Command and Communications System. Available data indicated satisfactory CCS performance during boost and parking orbit with minor exceptions. Uplink and downlink dropouts occurred during S-IC/S-II staging and at S-II second plane separation. Dropouts at these times are expected. Performance during second burn and translunar injection was nominal.

Signal fluctuations were noted at HAW, GBM, GDS, and GYM from about 11,100 seconds (03:05:00) to 11,340 seconds (03:09:00) when the CSM was maneuvered to an inertial attitude. This inertial attitude was maintained during CSM separation, docking and Lunar Module (LM) ejection.

HAW lost track during translunar coast from 11,756 seconds (03:15:56) to 18,516 seconds (05:08:36) when the vehicle disappeared over the horizon.

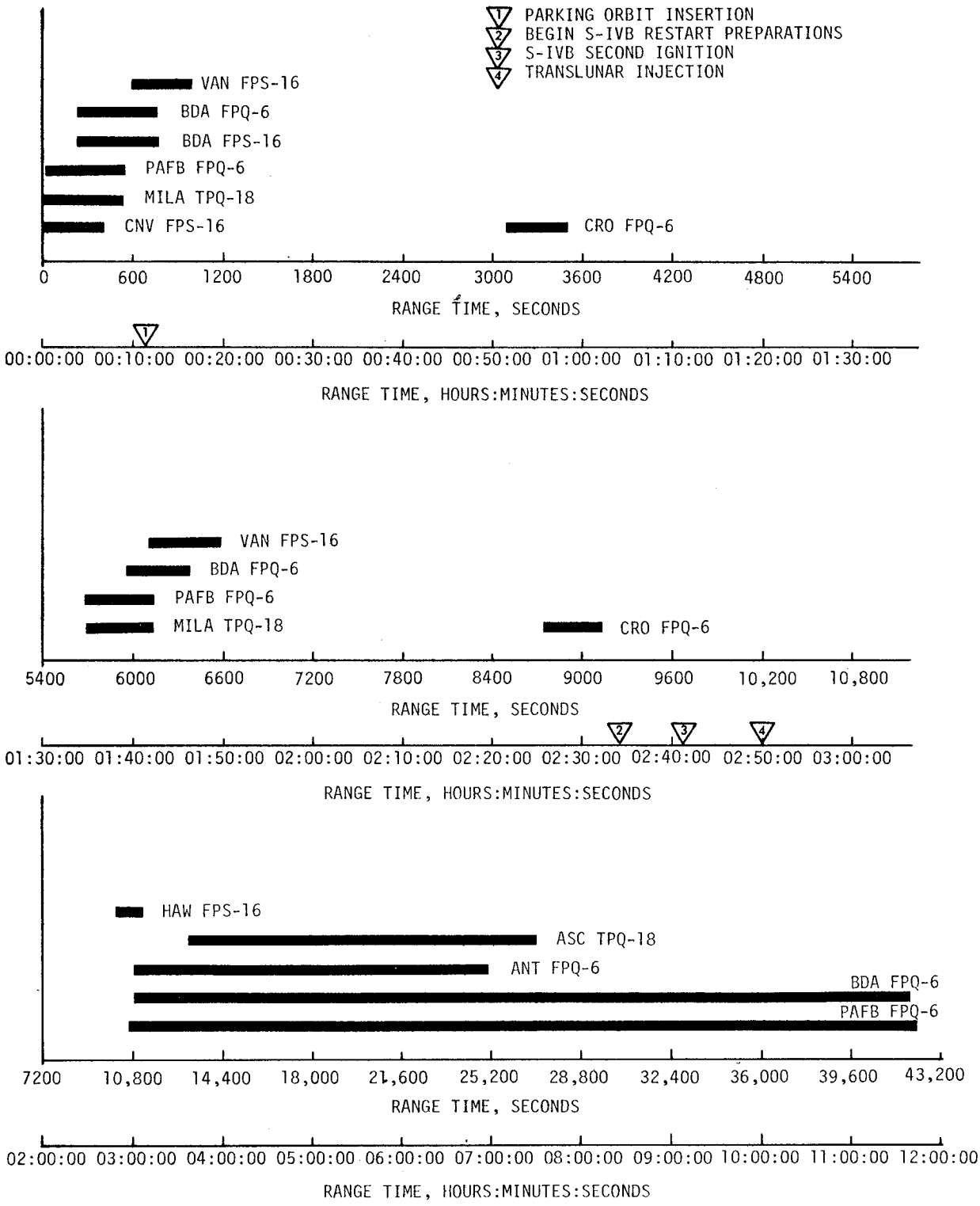

Figure 19-2. C-Band Radar Coverage Summary

A ground command was transmitted at 17,466.6 seconds (04:51:06.6) to initiate Time Base 8. The vehicle was placed in a slingshot attitude and the LOX dump followed. These events produced signal strength fluctuations from 17,470 seconds (04:51:10) to 19,060 seconds (05:17:40) at all stations tracking the CCS. The most severe fluctuations were experienced at GBM and resulted in 25 dropouts during this time period. These signal fluctuations were smooth and are believed to have been caused by changing vehicle antenna gains as the look angles to the ground stations varied with the changes in vehicle attitude (referenced to the ground station).

A sharp drop in downlink CCS signal was noted at HAW, GBM, GDS and GYM at 27,128 seconds (07:32:08). The onboard antenna system, which had been on the low gain since 19,034 seconds (05:17:14) was switched to the high gain mode at 27,368 seconds (07:36:08) to improve signal quality. Signal strength picked up and was maintained at a high level until 30,264 seconds (08:24:24) at which time the signal level again dropped. In an attempt to improve signal quality the CCS RF was switched OFF/ON two times and the CCS antennas were switched several times. However, signal level fluctuated intermittently at low levels until LOS at 35,779 (09:56:19). Figure 19-3 shows the fluctuations in signal level experienced at the HAW site. The GDS wing station experienced similar fluctuations at corresponding times as shown in Figure 19-4.

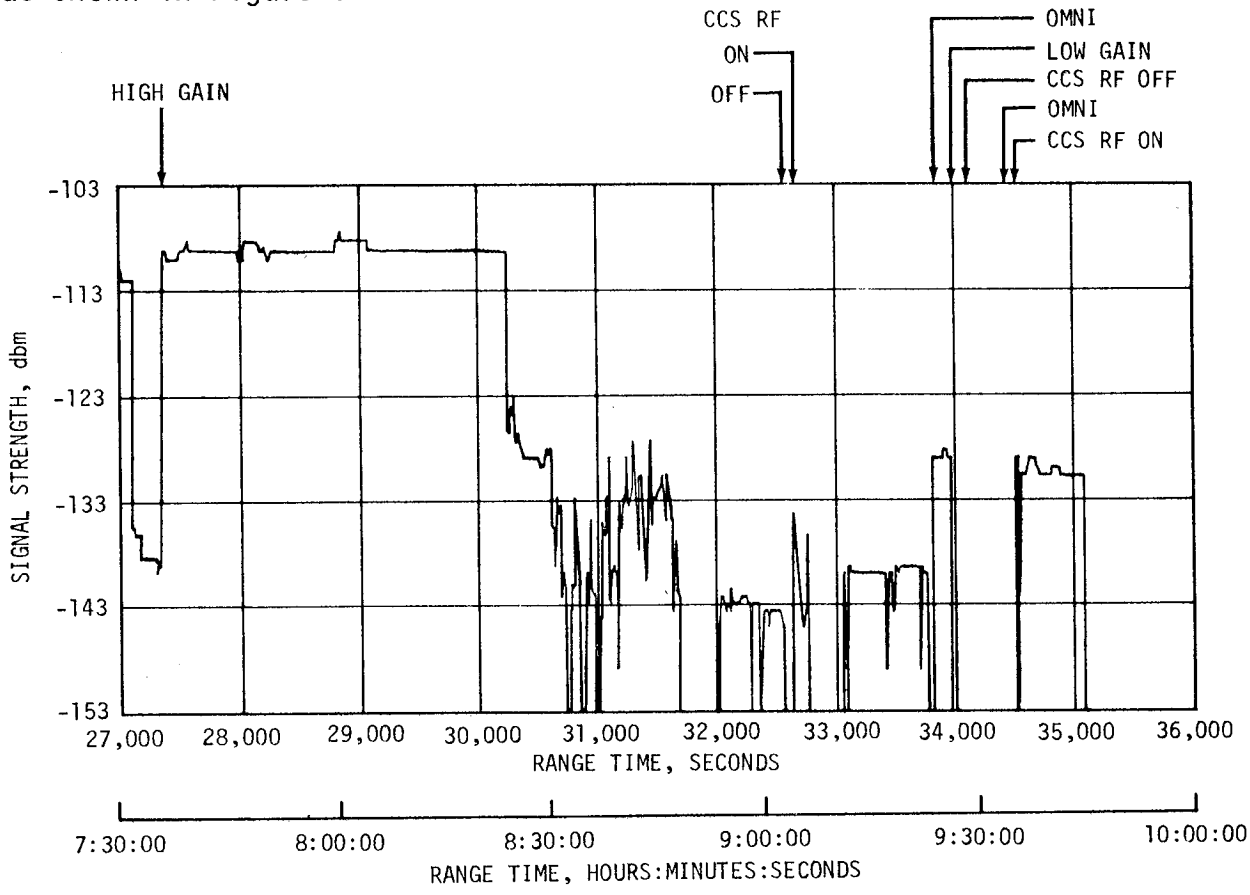

Figure 19-3. CCS Signal Strength Fluctuations at Hawaii

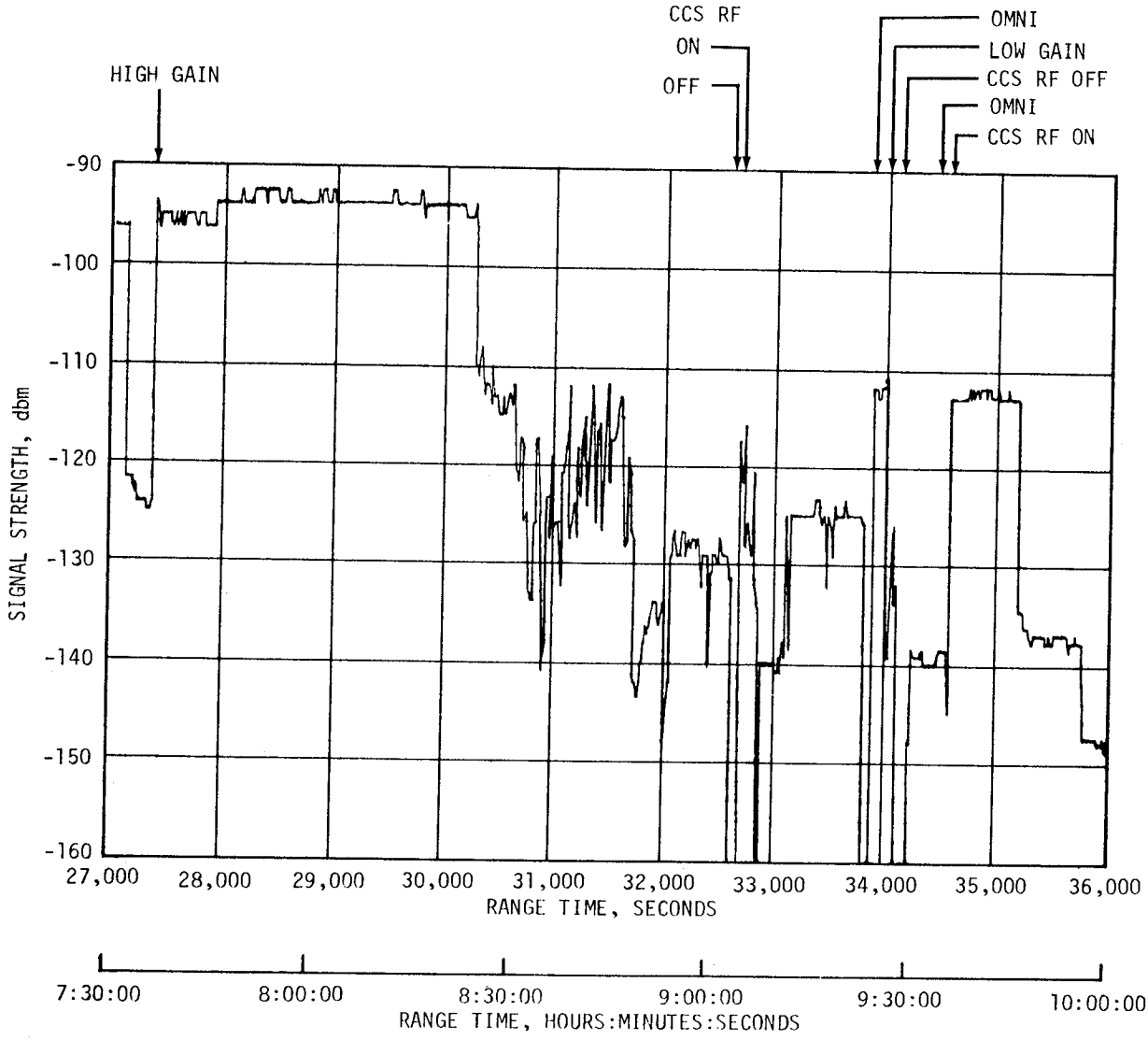

Figure 19-4. CCS Signal Strength Fluctuations at GDS Wing Station

The above indicates that the problem was present on low gain, high gain and omni antenna; therefore, it is concluded that the drop in signal level was caused by a malfunction of the CCS coaxial switch. On AS-505, a similar problem in the CCS antenna system occurred only while transmitting on the high gain or low gain antenna.

Test performed in IBM Report Number 69-223-0007 also concluded that the CCS coaxial switch (the only electromechanical component which is common to all CCS antennas) caused the failure. The general characteristics of the CCS operation, as observed on AS-505 and AS-506, was duplicated by a simulated leak in the hermetically sealed portion of the coaxial switch case. In addition, engineering tests have demonstrated that the coaxial switch will leak following vibration levels seen on AS-505 and AS-506.

Directional antenna tests did not duplicate the failure. Power amplifier tests showed a leak in the power amplifier would cause a total failure; this results in total loss of CCS downlink with no possible recovery.

Prior to any observed deficiencies in the flight operation of the CCS, incorporation of a new design coaxial switch was programed for AS-507 and subsequent vehicles. The new switch exhibits none of the general deficiencies of the earlier components and has shown no susceptibility to failure in simulated leak tests or at vibration levels in excess of the AS-505 or AS-506 vibration levels.

A summary of CCS coverage showing AOS and LOS for each station is shown in Figure 19-5.

19.5 OPTICAL INSTRUMENTATION

In general, ground camera coverage was very good. Seventy-five items were received from Kennedy Space Center (KSC) and evaluated. One camera jammed before acquiring requested data. Two cameras had bad tracking items, one camera had its field of view misoriented and one camera had no run. As a result of the 5 failures listed above, system efficiency was 94 percent. All Launch Umbilical Tower (LUT) cameras had erratic timing; therefore, all timing data were interpolated. Personnel at KSC have traced the timing problem to a loose connector at the base of the Launch Control Center (LCC).

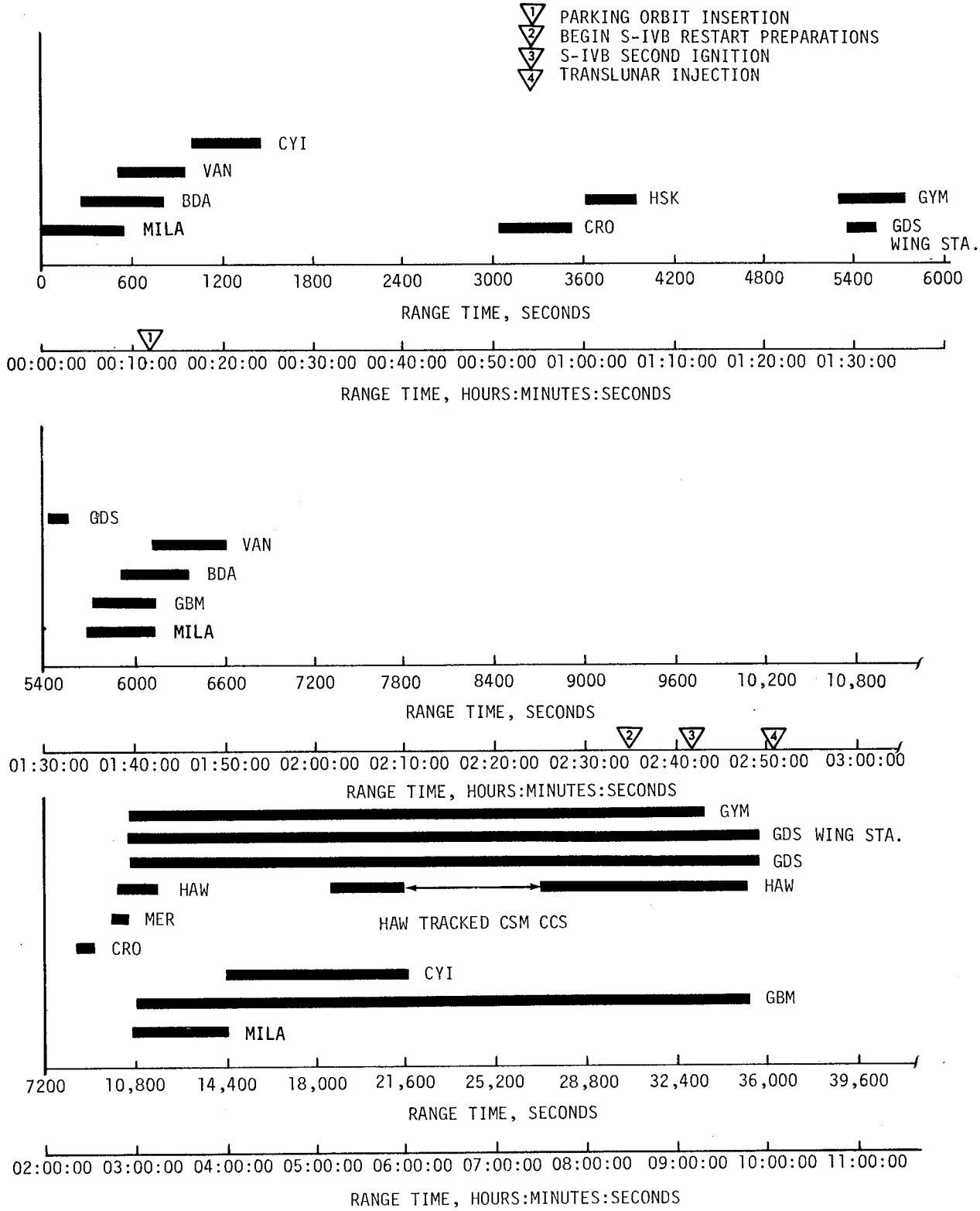

Figure 19-5. CCS Coverage Summary

SECTION 20

MASS CHARACTERISTICS

20.1 SUMMARY

Postflight analysis indicates that total vehicle mass was within 0.50 percent of the prediction from ground ignition through S-IVB stage final shutdown. This very small deviation signifies that the initial propellant loads and propellant utilization throughout vehicle operation were close to predicted.

20.2 MASS EVALUATION

Postflight mass characteristics are compared with the final predicted mass characteristics (MSFC Memorandum S&E-ASTN-SAE-69-M-70) and the final operational trajectory (MSFC Memorandum S&E-AERO-FMT-138-69).

The postflight mass characteristics were determined from an analysis of all available actual and reconstructed data from S-IC stage ignition through S-IVB stage second burn cutoff. Dry weights of the launch vehicle were based on actual stage weighings and evaluation of the weight and balance log books (MSFC Form 998). Propellant loading and utilization was evaluated from propulsion system performance reconstructions. Spacecraft data were obtained from the Manned Spacecraft Center (MSC).

Deviations from predicted in dry weights of the inert stages and the loaded spacecraft were all less than 0.75 percent which was well within the 3-sigma deviation limit.

During S-IC powered flight, mass of the total vehicle was determined to be 2906 kilograms (6407 lbm) or 0.09 percent lower than predicted at ignition, and 1366 kilograms (3011 lbm) or 0.16 percent lower at S-IC/S-II separation. These small deviations are attributed to less than predicted S-IC propellant load, S-IC dry stage mass, and mass of the upper staging. S-IC burn phase total vehicle mass is shown in Tables 20-1 and 20-2.

During S-II burn phase, the total vehicle mass varied from 898 kilograms (1981 lbm) or 0.13 percent lower than predicted at start command to 875 kilograms (1930 lbm) or 0.42 percent higher than predicted at S-II/S-IVB separation. Most of the initial deviation may be attributed to a less than predicted S-II propellant loading, and the deviation at separation

was due mainly to higher than predicted S-II propellant residuals. Total vehicle mass for the S-II burn phase is shown in Tables 20-3 and 20-4.

Total vehicle mass during both S-IVB burn phases, as shown in Tables 20-5 through 20-8, was within 0.45 percent of prediction. A deviation of 143 kilograms (317 lbm) or 0.09 percent at first start command was due mainly to a slight excess of S-IVB propellants. Lower than predicted propellant residuals at end of first burn resulted in a 607 kilogram (1340 lbm) or 0.44 percent deviation. Total vehicle mass at spacecraft separation was 832 kilograms (1834 lbm) or 4.62 percent less than predicted.

A summary of mass utilization and loss, actual and predicted, from S-IC stage ignition through completion of S-IVB second burn is presented in Table 20-9. A comparison of actual and predicted mass, center of gravity, and moment of inertia is shown in Table 20-10.

Table 20-1. Total Vehicle Mass - S-IC Burn Phase - Kilograms

EVENTS	GROUND IGNITION		HOLDDOWN ARM RELEASE		CENTER ENGINE CUTOFF		OUTBOARD ENGINE CUTOFF		S-IC/S-II SEPARATION	
	PRED	ACT	PRED	ACT	PRED	ACT	PRED	ACT	PRED	ACT
RANGE TIME--SEC	-6.40	-6.40	.30	.30	135.28	135.20	161.08	161.63	161.80	162.30
S-IC STAGE DRY	130975.	130422.	130975.	130422.	130975.	130422.	130975.	130422.	130975.	130422.
LOX IN TANK	1479418.	1478371.	1448229.	1446726.	190236.	194782.	1399.	1280.	931.	934.
LOX BELOW TANK	21000.	21108.	21737.	21868.	21720.	21851.	16778.	16761.	14663.	14717.
LOX ULLAGE GAS	187.	169.	207.	235.	2587.	2809.	3060.	3611.	3066.	3616.
RP1 IN TANK	642541.	642018.	632397.	631847.	91469.	93076.	8396.	8008.	7305.	6759.
RP1 BELOW TANK	4313.	4301.	5996.	5983.	5996.	5983.	5958.	5946.	5958.	5946.
RP1 ULLAGE GAS	35.	73.	35.	76.	211.	226.	240.	249.	241.	250.
N2 PURGE GAS	36.	36.	36.	36.	20.	20.	20.	20.	20.	20.
HELIUM IN BOTTLE	289.	289.	289.	286.	113.	136.	83.	112.	83.	112.
FROST	635.	635.	635.	635.	340.	340.	340.	340.	340.	340.
RETROMOTOR PROP	1027.	1027.	1027.	1027.	1027.	1027.	1027.	1027.	1027.	1027.
OTHER	239.	239.	239.	239.	239.	239.	239.	239.	239.	239.
TOTAL S-IC STAGE	2280695.	2278688.	2241801.	2239381.	444932.	450912.	168515.	168015.	164847.	164381.
TOTAL S-IC/S-II IS	5200.	5206.	5200.	5206.	5200.	5206.	5200.	5206.	5166.	5173.
TOTAL S-II STAGE	481003.	479964.	481003.	479964.	480745.	479706.	480745.	479706.	480745.	479706.
TOT S-II/S-IVB IS	3665.	3663.	3665.	3663.	3665.	3663.	3665.	3663.	3665.	3663.
TOTAL S-IVB STAGE	118911.	119119.	118911.	119119.	118820.	119029.	118820.	119029.	118820.	119029.
TOTAL INSTRU UNIT	1953.	1939.	1953.	1939.	1953.	1939.	1953.	1939.	1953.	1939.
TOTAL SPACECRAFT	49794.	49735.	49794.	49735.	49794.	49735.	49794.	49735.	49794.	49735.
TOTAL UPPER STAGE	660526.	659626.	660526.	659626.	660177.	659277.	660177.	659277.	660144.	659244.
TOTAL VEHICLE	2941221.	2938315.	2902328.	2899008.	1105110.	1110189.	828692.	827292.	824991.	823625.

Table 20-2. Total Vehicle Mass - S-IC Burn Phase - Pounds Mass

EVENTS	GROUND IGNITION		HOLDDOWN ARM RELEASE		CENTER ENGINE CUTOFF		OUTBOARD ENGINE CUTOFF		S-IC/S-II SEPARATION	
	PRED	ACT	PRED	ACT	PRED	ACT	PRED	ACT	PRED	ACT
RANGE TIME--SEC	-6.40	-6.40	.30	.30	135.28	135.20	161.08	161.63	161.80	162.30
S-IC STAGE DRY	288750.	287531.	288750.	287531.	288750.	287531.	288750.	287531.	288750.	287531.
LOX IN TANK	3261558.	3259250.	3192798.	3189486.	419398.	429420.	7084.	2821.	2051.	2059.
LOX BELOW TANK	46296.	46536.	47921.	48211.	47884.	48174.	36990.	36951.	32326.	32445.
LOX ULLAGE GAS	411.	372.	456.	518.	5703.	6193.	6745.	7960.	6759.	7973.
RP1 IN TANK	1416561.	1415408.	1394196.	1392984.	201655.	205198.	18509.	17655.	16105.	14900.
RP1 BELOW TANK	9509.	9481.	13219.	13191.	13219.	13191.	13136.	13108.	13136.	13108.
RP1 ULLAGE GAS	77.	161.	77.	168.	464.	498.	530.	550.	531.	551.
N2 PURGE GAS	80.	80.	80.	80.	43.	43.	43.	43.	43.	43.
HELIUM IN BOTTLE	636.	637.	636.	630.	249.	300.	183.	248.	182.	247.
FROST	1400.	1400.	1400.	1400.	750.	750.	750.	750.	750.	750.
RETROMOTOR PROP	2264.	2264.	2264.	2264.	2264.	2264.	2264.	2264.	2264.	2264.
OTHER	528.	528.	528.	528.	528.	528.	528.	528.	528.	528.
TOTAL S-IC STAGE	5028071.	5023648.	4942326.	4936991.	980908.	994090.	371512.	370409.	363426.	362399.
TOTAL S-IC/S-II IS	11463.	11477.	11463.	11477.	11463.	11477.	11463.	11477.	11390.	11404.
TOTAL S-II STAGE	1060431.	1058140.	1060431.	1058140.	1059861.	1057570.	1059861.	1057570.	1059861.	1057570.
TOT S-II/S-IVB IS	8081.	8076.	8081.	8076.	8081.	8076.	8081.	8076.	8081.	8076.
TOTAL S-IVB STAGE	262154.	262613.	262154.	262613.	261954.	262413.	261954.	262413.	261954.	262413.
TOTAL INSTRU UNIT	4306.	4275.	4306.	4275.	4306.	4275.	4306.	4275.	4306.	4275.
TOTAL SPACECRAFT	109777.	109646.	109777.	109646.	109777.	109646.	109777.	109646.	109777.	109646.
TOTAL UPPER STAGE	1456212.	1454227.	1456212.	1454227.	1455442.	1453457.	1455442.	1453457.	1455369.	1453384.
TOTAL VEHICLE	6484282.	6477875.	6398537.	6391218.	2436350.	2447547.	1826954.	1823866.	1818794.	1815783.

Table 20-3. Total Vehicle Mass - S-II Burn Phase - Kilograms

EVENTS	S-IC IGNITION		S-II IGNITION		S-II MAINSTAGE		S-II ENGINE CUTOFF		S-II/S-IVB SEPARATION	
	PRED	ACT	PRED	ACT	PRED	ACT	PRED	ACT	PRED	ACT
RANGE TIME--SEC	-6.40	-6.40	163.54	164.00	165.50	166.20	551.72	548.22	552.40	549.00
S-IC/S-II IS SMALL	814.	614.								
S-IC/S-II IS LARGE	3969.	3982.	3969.	3982.	3969.	3982.				
S-IC/S-II IS PROP	617.	610.	313.	309.	0.	0.				
TOTAL S-IC/S-II IS	5200.	5206.	4281.	4291.	3969.	3982.				
S-II STAGE DRY	36250.	36158.	36250.	36158.	36250.	36158.	36250.	36158.	36250.	36158.
LOX IN TANK	371672.	370778.	371672.	370778.	371220.	370325.	657.	816.	544.	730.
LOX BELOW TANK	737.	737.	737.	737.	800.	800.	787.	787.	787.	787.
LOX ULLAGE GAS	188.	188.	188.	188.	190.	191.	2337.	2335.	2340.	2335.
LH2 IN TANK	71668.	71615.	71660.	71608.	71449.	71396.	1966.	2572.	1916.	2531.
LH2 BELOW TANK	105.	105.	112.	112.	128.	128.	123.	123.	123.	123.
LH2 ULLAGE GAS	77.	77.	77.	77.	77.	78.	704.	735.	704.	735.
INSULATION PURGE	54.	54.								
FROST	204.	204.								
START TANK GAS	14.	14.	14.	14.	2.	2.	2.	2.	2.	2.
OTHER	34.	34.	34.	34.	34.	34.	34.	34.	34.	34.
TOTAL S-II STAGE	481003.	479964.	480745.	479706.	480151.	479112.	42862.	43564.	42702.	43436.
TOT S-II/S-IVB IS	3665.	3663.	3665.	3663.	3665.	3663.	3665.	3663.	3665.	3663.
TOTAL S-IVB STAGE	118911.	119119.	118820.	119029.	118820.	119029.	118820.	119029.	118818.	119026.
TOTAL INSTRU UNIT	1953.	1939.	1953.	1939.	1953.	1939.	1953.	1939.	1953.	1939.
TOTAL SPACECRAFT	49794.	49735.	49794.	49735.	49794.	49735.	45743.	45693.	45743.	45693.
TOTAL UPPER STAGE	174324.	174456.	174233.	174365.	174233.	174365.	170182.	170324.	170180.	170322.
TOTAL VEHICLE	660526.	659626.	659259.	658363.	658353.	657459.	213044.	213888.	212882.	213757.

Table 20-4. Total Vehicle Mass - S-II Burn Phase - Pounds Mass

EVENTS	S-IC IGNITION		S-II IGNITION		S-II MAINSTAGE		S-II ENGINE CUTOFF		S-II/S-IVB SEPARATION	
	PRED	ACT	PRED	ACT	PRED	ACT	PRED	ACT	PRED	ACT
RANGE TIME--SEC	-6.40	-6.40	163.54	164.00	165.50	166.20	551.72	548.22	552.40	549.00
S-IC/S-II IS SMALL	1353.	1353.								
S-IC/S-II IS LARGE	8750.	8779.	8750.	8779.	8750.	8779.				
S-IC/S-II IS PROP	1360.	1345.	689.	682.	0.	0.				
TOTAL S-IC/S-II IS	11463.	11477.	9439.	9461.	8750.	8779.				
S-II STAGE DRY	79918.	79714.	79918.	79714.	79918.	79714.	79918.	79714.	79918.	79714.
LOX IN TANK	819397.	817425.	819397.	817425.	818401.	816426.	1448.	1800.	1199.	1609.
LOX BELOW TANK	1625.	1625.	1625.	1625.	1764.	1764.	1736.	1736.	1736.	1736.
LOX ULLAGE GAS	415.	415.	415.	415.	419.	421.	5152.	5147.	5158.	5147.
LH2 IN TANK	158000.	157885.	157983.	157868.	157518.	157402.	4335.	5671.	4224.	5579.
LH2 BELOW TANK	231.	231.	248.	248.	282.	282.	272.	272.	272.	272.
LH2 ULLAGE GAS	169.	169.	169.	169.	170.	171.	1551.	1621.	1553.	1621.
INSULATION PURGE	120.	120.								
FROST	450.	450.								
START TANK GAS	30.	30.	30.	30.	5.	5.	5.	5.	5.	5.
OTHER	76.	76.	76.	76.	76.	76.	76.	76.	76.	76.
TOTAL S-II STAGE	1060431.	1058140.	1059861.	1057570.	1058552.	1056261.	94494.	96042.	94141.	95759.
TOT S-II/S-IVB IS	8081.	8076.	8081.	8076.	8081.	8076.	8081.	8076.	8081.	8076.
TOTAL S-IVB STAGE	262154.	262613.	261954.	262413.	261954.	262413.	261954.	262413.	261949.	262408.
TOTAL INSTRU UNIT	4306.	4275.	4306.	4275.	4306.	4275.	4306.	4275.	4306.	4275.
TOTAL SPACECRAFT	109777.	109646.	109777.	109646.	109777.	109646.	100847.	100736.	100847.	100736.
TOTAL UPPER STAGE	384318.	384610.	384118.	384410.	384118.	384410.	375188.	375500.	375183.	375495.
TOTAL VEHICLE	1456212.	1454227.	1453418.	1451441.	1451420.	1449450.	469682.	471542.	469324.	471254.

Table 20-5. Total Vehicle Mass - S-IVB First Burn Phase - Kilograms

EVENTS	S-IC IGNITION		S-IVB IGNITION		S-IVB MAINSTAGE		S-IVB ENGINE CUTOFF		S-IVB END DECAY	
	PRED	ACT	PRED	ACT	PRED	ACT	PRED	ACT	PRED	ACT
RANGE TIME--SEC	-6.40	-6.40	555.70	552.20	558.20	554.70	699.49	699.34	699.68	699.54
S-IVB STAGE DRY	11340.	11273.	11317.	11250.	11317.	11250.	11255.	11189.	11255.	11189.
LOX IN TANK	86934.	87149.	86934.	87149.	86773.	86993.	61359.	61120.	61327.	61052.
LOX BELOW TANK	166.	166.	166.	166.	180.	180.	180.	180.	180.	180.
LOX ULLAGE GAS	17.	16.	17.	16.	22.	17.	105.	67.	105.	67.
LH2 IN TANK	19709.	19758.	19705.	19731.	19649.	19708.	14530.	14369.	14516.	14356.
LH2 BELOW TANK	22.	22.	26.	26.	26.	26.	26.	26.	26.	26.
LH2 ULLAGE GAS	20.	19.	20.	19.	20.	20.	65.	52.	66.	52.
ULLAGE MOTOR PROP	54.	54.	10.	10.	1.	1.	1.	1.	1.	1.
APS PROPELLANT	286.	298.	286.	298.	286.	298.	285.	297.	285.	297.
HELIUM IN BOTTLES	200.	200.	200.	200.	199.	200.	178.	176.	178.	176.
START TANK GAS	2.	2.	2.	2.	0.	0.	3.	3.	3.	3.
FROST	136.	136.	45.	45.	45.	45.	45.	45.	45.	45.
OTHER	25.	25.	25.	25.	25.	25.	25.	25.	25.	25.
TOTAL S-IVB STAGE	118911.	119119.	118754.	118939.	118544.	118764.	88058.	87550.	88013.	87469.
TOTAL INSTRU UNIT	1953.	1939.	1953.	1939.	1953.	1939.	1953.	1939.	1953.	1939.
TOTAL SPACECRAFT	45743.	45693.	45743.	45693.	45743.	45693.	45743.	45693.	45743.	45693.
TOTAL UPPER STAGE	47697.	47632.	47697.	47632.	47697.	47632.	47697.	47632.	47697.	47632.
TOTAL VEHICLE	166608.	166751.	166450.	166571.	166240.	166396.	135755.	135182.	135709.	135102.

Table 20-6. Total Vehicle Mass - S-IVB First Burn Phase - Pounds Mass

EVENTS	S-IC IGNITION		S-IVB IGNITION		S-IVB MAINSTAGE		S-IVB ENGINE CUTOFF		S-IVB END DECAY	
	PRED	ACT	PRED	ACT	PRED	ACT	PRED	ACT	PRED	ACT
RANGE TIME--SEC	-6.40	-6.40	555.70	552.20	558.20	554.70	699.49	699.34	699.68	699.54
S-IVB STAGE DRY	25000.	24852.	24949.	24801.	24949.	24801.	24814.	24667.	24814.	24667.
LOX IN TANK	191656.	192130.	191656.	192130.	191302.	191787.	135273.	134747.	135203.	134597.
LOX BELOW TANK	367.	367.	367.	367.	397.	397.	397.	397.	397.	397.
LOX ULLAGE GAS	38.	36.	38.	36.	49.	38.	231.	147.	232.	147.
LH2 IN TANK	43452.	43560.	43442.	43499.	43318.	43449.	32033.	31678.	32002.	31649.
LH2 BELOW TANK	48.	48.	58.	58.	58.	58.	58.	58.	58.	58.
LH2 ULLAGE GAS	43.	41.	43.	42.	44.	44.	144.	114.	145.	115.
ULLAGE MOTOR PROP	118.	118.	22.	22.	0.	0.	0.	0.	0.	0.
APS PROPELLANT	630.	658.	630.	658.	630.	658.	628.	655.	628.	655.
HELIUM IN BOTTLES	441.	442.	441.	442.	439.	441.	393.	389.	392.	389.
START TANK GAS	5.	5.	5.	5.	1.	1.	7.	7.	7.	7.
FROST	300.	300.	100.	100.	100.	100.	100.	100.	100.	100.
OTHER	56.	56.	56.	56.	56.	56.	56.	56.	56.	56.
TOTAL S-IVB STAGE	262154.	262613.	261807.	262216.	261344.	261830.	194135.	193015.	194035.	192837.
TOTAL INSTRU UNIT	4306.	4275.	4306.	4275.	4306.	4275.	4306.	4275.	4306.	4275.
TOTAL SPACECRAFT	100847.	100736.	100847.	100736.	100847.	100736.	100847.	100736.	100847.	100736.
TOTAL UPPER STAGE	105153.	105011.	105153.	105011.	105153.	105011.	105153.	105011.	105153.	105011.
TOTAL VEHICLE	367307.	367624.	366960.	367227.	366497.	366841.	299288.	298026.	299188.	297848.

Table 20-7. Total Vehicle Mass - S-IVB Second Burn Phase - Kilograms

EVENTS	S-IVB IGNITION		S-IVB MAINSTAGE		S-IVB ENGINE CUTOFF		S-IVB END DECAY		SPACECRAFT SEPARATION	
	PRED	ACT	PRED	ACT	PRED	ACT	PRED	ACT	PRED	ACT
RANGE TIME--SEC	9855.50	9856.20	9858.00	9858.70	10204.06	10203.07	10204.27	10203.27	15004.40	15423.00
S-IVB STAGE DRY	11255.	11189.	11255.	11189.	11255.	11189.	11255.	11189.	11255.	11189.
LOX IN TANK	61240.	60985.	61074.	60857.	2191.	2308.	2160.	2247.	2160.	2224.
LOX BELOW TANK	166.	166.	180.	180.	180.	180.	180.	180.	166.	166.
LOX ULLAGE GAS	170.	126.	174.	128.	280.	205.	280.	205.	280.	124.
LH2 IN TANK	13257.	13275.	13192.	13224.	900.	944.	886.	932.	886.	391.
LH2 BELOW TANK	26.	26.	26.	26.	26.	26.	26.	26.	22.	22.
LH2 ULLAGE GAS	196.	167.	197.	170.	331.	286.	331.	286.	331.	156.
ULLAGE MOTOR PROP	0.	0.	0.	0.	0.	0.	0.	0.	0.	0.
APS PROPELLANT	183.	246.	183.	246.	179.	237.	179.	237.	144.	222.
HELIUM IN BOTTLES	145.	160.	145.	159.	83.	108.	83.	108.	83.	17.
START TANK GAS	2.	2.	0.	0.	3.	3.	3.	3.	3.	0.
FROST	45.	45.	45.	45.	45.	45.	45.	45.	45.	45.
OTHER	25.	25.	25.	25.	25.	25.	25.	25.	25.	25.
TOTAL S-IVB STAGE	86711.	86414.	86497.	86251.	15500.	15557.	15454.	15483.	15401.	14583.
TOTAL INSTRU UNIT	1953.	1939.	1953.	1939.	1953.	1939.	1953.	1939.	1953.	1939.
TOTAL SPACECRAFT	45743.	45693.	45743.	45693.	45743.	45693.	45743.	45693.	626.	626.
TOTAL UPPER STAGE	47697.	47632.	47697.	47632.	47697.	47632.	47697.	47632.	2579.	2565.
TOTAL VEHICLE	134408.	134046.	134194.	133883.	63196.	63189.	63151.	63116.	17980.	17148.

Table 20-8. Total Vehicle Mass - S-IVB Second Burn Phase - Pounds Mass

EVENTS	S-IVB IGNITION		S-IVB MAINSTAGE		S-IVB ENGINE CUTOFF		S-IVB END DECAY		SPACECRAFT SEPARATION	
	PRED	ACT	PRED	ACT	PRED	ACT	PRED	ACT	PRED	ACT
RANGE TIME--SEC	9855.50	9856.20	9858.00	9858.70	10204.06	10203.07	10204.27	10203.27	15004.40	15423.00
S-IVB STAGE DRY	24814.	24667.	24814.	24667.	24814.	24667.	24814.	24667.	24814.	24667.
LOX IN TANK	135010.	134450.	134645.	134166.	4831.	5089.	4762.	4953.	4762.	4902.
LOX BELOW TANK	367.	367.	397.	397.	397.	397.	397.	397.	367.	367.
LOX ULLAGE GAS	374.	278.	383.	283.	617.	453.	617.	453.	617.	274.
LH2 IN TANK	29226.	29266.	29082.	29155.	1985.	2081.	1954.	2054.	1954.	863.
LH2 BELOW TANK	58.	58.	58.	58.	58.	58.	58.	58.	48.	48.
LH2 ULLAGE GAS	433.	368.	434.	375.	729.	631.	729.	631.	729.	345.
ULLAGE MOTOR PROP	0.	0.	0.	0.	0.	0.	0.	0.	0.	0.
APS PROPELLANT	403.	542.	403.	542.	395.	522.	395.	522.	318.	490.
HELIUM IN BOTTLES	319.	353.	319.	350.	182.	237.	182.	237.	182.	38.
START TANK GAS	5.	5.	1.	1.	7.	7.	7.	7.	7.	0.
FROST	100.	100.	100.	100.	100.	100.	100.	100.	100.	100.
OTHER	56.	56.	56.	56.	56.	56.	56.	56.	56.	56.
TOTAL S-IVB STAGE	191165.	190510.	190693.	190150.	34171.	34298.	34070.	34135.	33953.	32150.
TOTAL INSTRU UNIT	4306.	4275.	4306.	4275.	4306.	4275.	4306.	4275.	4306.	4275.
TOTAL SPACECRAFT	100847.	100736.	100847.	100736.	100847.	100736.	100847.	100736.	1380.	1380.
TOTAL UPPER STAGE	105153.	105011.	105153.	105011.	105153.	105011.	105153.	105011.	5686.	5655.
TOTAL VEHICLE	296318.	295521.	295846.	295161.	139324.	139309.	139223.	139146.	39639.	37805.

Table 20-9. Flight Sequence Mass Summary

MASS HISTORY	PREDICTED KG	PREDICTED LBM	ACTUAL KG	ACTUAL LBM
S-IC STAGE, TOTAL	2280695.	5028071.	2278688.	5023648.
S-IC/S-II INTERSTAGE,TOTAL	5200.	11463.	5206.	11477.
S-II STAGE, TOTAL	481003.	1060431.	479964.	1058140.
S-II/SIIVB INTERSTAGE	3665.	8081.	3663.	8076.
S-IVB STAGE, TOTAL	118911.	262154.	119119.	262613.
INSTRUMENT UNIT	1953.	4306.	1939.	4275.
SPACECRAFT INCLUDING LES	49794.	109777.	49735.	109646.
1ST FLT STG AT IGN	2941221.	6484282.	2938315.	6477875.
S-IC THRUST BUILDUP	-38893.	-85745.	-39307.	-86657.
1ST FLT STG HOLDDWN ARM REL	2902328.	6398537.	2899008.	6391218.
S-IC FROST	-295.	-650.	-295.	-650.
S-IC MAINSTAGE PROPELLANT	-2071872.	-4567697.	-2069957.	-4563474.
S-IC N2 PURGE	-17.	-37.	-17.	-37.
S-IC INBD ENGINE T.D. PROP	-917.	-2022.	-908.	-2003.
S-IC INBD ENG EXPENDED PROP	-185.	-408.	-190.	-418.
S-II INSULATION PURGE GAS	-54.	-120.	-54.	-120.
S-II FROST	-204.	-450.	-204.	-450.
S-IVB FROST	-91.	-200.	-91.	-200.
1ST FLT STAGE AT S-IC OECOS	828692.	1826954.	827292.	1823866.
S-IC OTBD ENGINE T.D. PROP	-3668.	-8087.	-3634.	-8011.
S-IC/S-II ULLAGE RKT PROP	-33.	-73.	-33.	-73.
1ST FLT STAGE AT SIC/SII SEP	824991.	1818794.	823625.	1815783.
S-IC STAGE AT SEPARATION	-164847.	-363426.	-164381.	-362399.
S-IC/S-II INTERSTAGE SMALL	-614.	-1353.	-614.	-1353.
S-IC/S-II ULLAGE RKT PROP	-83.	-184.	-83.	-184.
2ND FLT STAGE AT S-II SSC	659447.	1453832.	658547.	1451847.
S-II FUEL LEAD	3.	3.	3.	3.
S-IC/S-II ULLAGE RKT PROP	-188.	-414.	-184.	-406.
2ND FLT STAGE AT S-II IGN	659259.	1453418.	658363.	1451441.
S-II T.B. PROPELLANT	-582.	-1283.	-582.	-1284.
S-II START TANK	-11.	-25.	-11.	-25.
S-IC/S-II ULLAGE RKT PROP	-313.	-689.	-309.	-682.
2ND FLT STAGE AT MAINSTAGE	658353.	1451420.	657459.	1449450.
S-II MAINSTAGE + VENTING	-437232.	-963932.	-435499.	-960110.
LAUNCH ESCAPE SYSTEM	-4051.	-8930.	-4042.	-8910.
S-IC/S-II INTERSTAGE LARGE	-3969.	-8750.	-3982.	-8779.
S-II T.D. PROPELLANT	-57.	-126.	-49.	-109.
2ND FLT STAGE AT S-II C.O.S.	213044.	469682.	213888.	471542.
S-II T.D. PROPELLANT	-160.	-353.	-128.	-283.
S-IVB ULLAGE PROPELLANT	-2.	-5.	-2.	-5.
2ND FLT STG AT SII/SIVB SEP	212882.	469324.	213757.	471254.
S-II STAGE AT SEPARATION	-42702.	-94141.	-43436.	-95759.
S-II/S-IVB INTERSTAGE-DRY	-3185.	-7021.	-3180.	-7010.
S-II/S-IVB IS PROP	-481.	-1060.	-484.	-1066.
S-IVB AFT FRAME	-22.	-48.	-22.	-48.
S-IVB ULLAGE PROPELLANT	-1.	-3.	-1.	-3.
S-IVB DET PACKAGE	-1.	-3.	-1.	-3.

Table 20-9. Flight Sequence Mass Summary (Continued)

MASS HISTORY	PREDICTED KG	PREDICTED LBM	ACTUAL KG	ACTUAL LBM
3RD FLT STG AT 1ST SSC	166490.	367048.	166634.	367365.
S-IVB ULLAGE PROPELLANT	-40.	-88.	-40.	-88.
S-IVB FUEL LEAD LOSS	-0.	-0.	-23.	-50.
3RD FLT STG AT 1ST SIVB IGN	166450.	366960.	166571.	367227.
S-IVB ULLAGE PROPELLANT	-10.	-22.	-10.	-22.
S-IVB START TANK	-2.	-4.	-2.	-4.
S-IVB T.B. PROPELLANT	-198.	-437.	-163.	-360.
3RD FLT STG AT MAINSTAGE	166240.	366497.	166396.	366841.
S-IVB ULLAGE ROCKET CASES	-61.	-135.	-61.	-134.
S-IVB MAINSTAGE PROP	-30424.	-67073.	-31152.	-68678.
S-IVB APS PROPELLANT	-1.	-2.	-1.	-3.
3RD FLT STG AT 1ST SIVB COS	135755.	299288.	135182.	298026.
S-IVB T.D. PROPELLANT	-45.	-99.	-81.	-178.
3RD FLT STG AT END 1ST TD	135709.	299188.	135102.	297848.
S-IVB ENG PROP EXPENDED	-18.	-40.	-18.	-40.
S-IVB FUEL TANK LOSS	-1151.	-2538.	-972.	-2143.
S-IVB LOX TANK LOSS	-20.	-44.	-4.	-8.
S-IVB APS PROPELLANT	-102.	-225.	-51.	-113.
S-IVB START TANK	-1.	-2.	-1.	-2.
S-IVB O2/H2 BURNER	-7.	-16.	-7.	-16.
3RD FLT STG AT 2ND SSC	134410.	296323.	134048.	295526.
S-IVB FUEL LEAD LOSS	-2.	-5.	-2.	-5.
3RD FLT STG AT 2ND SIVB IGN	134408.	296318.	134046.	295521.
S-IVB START TANK	-2.	-4.	-2.	-4.
S-IVB T.B. PROPELLANT	-212.	-468.	-161.	-356.
3RD FLT STG AT MAINSTAGE	134194.	295846.	133883.	295161.
S-IVB MAINSTAGE PROP	-70994.	-156514.	-70684.	-155832.
S-IVB APS PROPELLANT	-4.	-8.	-9.	-20.
3RD FLT STG AT 2ND SIVB COS	63196.	139324.	63189.	139309.
S-IVB T.D. PROPELLANT	-45.	-100.	-74.	-163.
3RD FLT STG AT END 2ND TD	63151.	139223.	63116.	139146.
JETTISON SLA	-1166.	-2570.	-1166.	-2571.
COMMAND SERVICE MODULE	-28839.	-63579.	-28806.	-63507.
S-IVB STAGE LOSS	-53.	-117.	-559.	-1232.
START OF TRANS/DOCKING	33093.	72957.	32584.	71836.
COMMAND SERVICE MODULE	28839.	63579.	28806.	63507.
S-IVB STAGE LOSS	0.	0.	-0.	-1.
END OF TRANS/DOCKING	61932.	136536.	61390.	135342.
COMMAND SERVICE MODULE	-28839.	-63579.	-28806.	-63507.
LUNAR MODULE	-15113.	-33318.	-15095.	-33278.
S-IVB STAGE LOSS	0.	0.	-341.	-752.
LAUNCH VEH AT S/C SEPARATION	17980.	39639.	17148.	37805.
SPACECRAFT NOT SEPARATED	-626.	-1380.	-626.	-1380.
INSTRUMENT UNIT	-1953.	-4306.	-1939.	-4275.
S-IVB STAGE AT SEPARATION	-15401.	-33953.	-14583.	-32150.

Table 20-10. Mass Characteristics Comparison

EVENT		MASS		LONGITUDINAL C.G. (X STA.)		RADIAL C.G.		ROLL MOMENT OF INERTIA		PITCH MOMENT OF INERTIA		YAW MOMENT OF INERTIA	
		KILO POUNDS	O/O DEV.	METERS INCHES	DELTA	METERS INCHES	DELTA	KG-M2 X10-6	O/O DEV.	KG-M2 X10-6	O/O DEV.	KG-M2 X10-6	O/O DEV.
S-IC STAGE DRY	PRED	130975. 288750.		9.368 368.8		.0580 2.2847		2.602		16.648		16.566	
	ACTUAL	130422. 287531.	-.42	9.368 368.8	.000 .00	.0580 2.2847	.0000 .0000	2.591	-.42	16.578	-.42	16.496	-.42
S-IC/S-II INTER-STAGE, TOTAL	PRED	5262. 11600.		41.623 1638.7		.1546 6.0877		.134		.081		.081	
	ACTUAL	5255. 11585.	-.12	41.626 1638.8	.003 .10	.1563 6.1555	.0017 .0678	.134	-.12	.080	-.12	.081	-.12
S-II STAGE, DRY	PRED	36251. 79918.		48.115 1894.3		.1875 7.3824		.600		2.027		2.038	
	ACTUAL	36158. 79714.	-.25	48.064 1892.3	-.051 -2.00	.1875 7.3824	.0000 .0000	.597	-.50	1.997	-1.47	2.009	-1.40
S-II/S-IVB INTER-STAGE, TOTAL	PRED	3666. 8081.		65.860 2592.9		.0573 2.2561		.065		.043		.044	
	ACTUAL	3650. 8045.	-.44	65.936 2595.9	.076 3.00	.0598 2.3537	.0025 .0976	.065	-.44	.043	-.44	.044	-.44
S-IVB STAGE, DRY	PRED	11340. 25000.		72.560 2856.7		.2194 8.6377		.082		.298		.298	
	ACTUAL	11273. 24852.	-.59	72.560 2856.7	.000 .00	.2194 8.6377	.0000 .0000	.081	-.59	.296	-.59	.296	-.59
VEHICLE INSTRUMENT UNIT	PRED	1954. 4306.		82.415 3244.7		.3576 14.0801		.019		.010		.009	
	ACTUAL	1940. 4275.	-.71	82.415 3244.7	.000 .0014	.3570 .0545	-.0007 -.0256	.019	-.71	.010	-.71	.009	-.71
SPACECRAFT, TOTAL	PRED	48731. 107433.		91.653 3608.4		.1085 4.2720		.090		1.552		1.555	
	ACTUAL	48626. 107200.	-.21	91.658 3608.6	.005 .20	.1099 4.3267	.0014 .0547	.088	-1.70	1.549	-.21	1.550	-.30

Table 20-10. Mass Characteristics Comparison (Continued)

EVENT		MASS		LONGITUDINAL C.G. (X STA.)		RADIAL C.G.		ROLL MOMENT OF INERTIA		PITCH MOMENT OF INERTIA		YAW MOMENT OF INERTIA	
		KILO POUNDS	O/O DEV.	METERS INCHES	DELTA	METERS INCHES	DELTA	KG-M2 X10-6	O/O DEV.	KG-M2 X10-6	O/O DEV.	KG-M2 X10-6	O/O DEV.
		2941220.		30.335		.0038							
	PRED	6484280.		1194.3		.1476		3.713		916.399		916.311	
1ST FLIGHT STAGE													
AT IGNITION		2938317.		30.332	-.003	.0038	.0000						
	ACTUAL	6477879.	-.09	1194.2	-.12	.1476	.0000	3.700	-.33	915.519	-.09	915.480	-.09
		2902327.		30.280		.0040							
1ST FLIGHT STAGE	PRED	6398535.		1192.1		.1565		3.715		915.181		915.093	
AT HOLDDOWN ARM													
RELEASE		2899010.		30.276	-.004	.0040	.0000						
	ACTUAL	6391222.	-.11	1192.0	-.16	.1565	.0000	3.703	-.33	914.293	-.09	914.254	-.09
		828693.		46.421		.0135							
1ST FLIGHT STAGE	PRED	1826954.		1827.6		.5331		3.700		442.012		441.928	
AT OUTBOARD ENGINE													
CUTOFF SIGNAL		827294.		46.453	.032	.0136	.0001						
	ACTUAL	1823870.	-.16	1828.9	1.27	.5371	.0040	3.689	-.31	440.511	-.33	440.475	-.32
		824992.		46.579		.0135							
	PRED	1818794.		1833.8		.5331		3.698		437.320		437.236	
1ST FLIGHT STAGE													
AT SEPARATION		823627.		46.612	.033	.0139	.0003						
	ACTUAL	1815786.	-.16	1835.1	1.31	.5463	.0132	3.686	-.31	435.728	-.36	435.692	-.35
		659447.		55.845		.0185							
2ND FLIGHT STAGE	PRED	1453831.		2198.6		.7303		.989		135.584		135.597	
AT START SEQUENCE													
COMMAND		658549.		55.854	.009	.0185	-.0000						
	ACTUAL	1451850.	-.13	2199.0	.36	.7301	-.0002	.985	-.37	135.506	-.05	135.520	-.05
		658354.		55.859		.0185							
	PRED	1451420.		2199.2		.7303		.977		135.462		135.475	
2ND FLIGHT STAGE													
AT MAINSTAGE		657461.		55.867	.008	.0185	-.0000						
	ACTUAL	1449453.	-.13	2199.5	.32	.7301	-.0002	.974	-.35	135.387	-.05	135.401	-.05
		213044.		71.099		.0549							
	PRED	469682.		2799.2		2.1602		.875		44.548		44.560	
2ND FLIGHT STAGE													
AT CUTOFF SIGNAL		213890.		71.014	-.085	.0546	-.0003						
	ACTUAL	471545.	.40	2795.8	-3.37	2.1502	-.0100	.871	-.43	44.932	.87	44.946	.87

Table 20-10. Mass Characteristics Comparison (Continued)

EVENT		MASS		LONGITUDINAL C.G. (X STA.)		RADIAL C.G.		ROLL MOMENT OF INERTIA		PITCH MOMENT OF INERTIA		YAW MOMENT OF INERTIA	
		KILO POUNDS	O/O DEV.	METERS INCHES	DELTA	METERS INCHES	DELTA	KG-M2 X10-6	O/O DEV.	KG-M2 X10-6	O/O DEV.	KG-M2 X10-6	O/O DEV.
2ND FLIGHT STAGE AT SEPARATION	PRED	212882.		71.118		.0549							
		469324.		2799.9		2.1602		.875		44.442		44.454	
	ACTUAL	213759.		71.029	-.090	.0546	-.0003						
		471257.	.42	2796.4	-3.52	2.1502	-.0100	.871	-.43	44.849	.92	44.862	.92
3RD FLIGHT STAGE AT 1ST START SEQUENCE COMMAND	PRED	166491.		77.138		.0382							
		367048.		3036.9		1.5059		.198		13.423		13.422	
	ACTUAL	166634.		77.130	-.008	.0386	.0003						
		367365.	.09	3036.6	-.31	1.5182	.0123	.198	.04	13.415	-.06	13.413	-.06
3RD FLIGHT STAGE AT 1ST IGNITION	PRED	166451.		77.132		.0382							
		366960.		3036.7		1.5059		.198		13.422		13.421	
	ACTUAL	166572.		77.124	-.009	.0386	.0003						
		367227.	.08	3036.4	-.34	1.5182	.0123	.198	.04	13.413	-.06	13.412	-.06
3RD FLIGHT STAGE AT 1ST MAINSTAGE	PRED	166241.		77.135		.0382							
		366497.		3036.8		1.5059		.198		13.420		13.419	
	ACTUAL	166397.		77.127	-.008	.0386	.0003						
		366841.	.10	3036.5	-.31	1.5182	.0123	.198	.04	13.412	-.05	13.411	-.05
3RD FLIGHT STAGE AT 1ST CUTOFF SIGNAL	PRED	135755.		78.041		.0466							
		299288.		3072.5		1.8334		.197		12.612		12.611	
	ACTUAL	135183.		78.046	.005	.0472	.0007						
		298026.	-.42	3072.7	.21	1.8593	.0259	.197	.02	12.594	-.14	12.592	-.15
3RD FLIGHT STAGE AT 1ST END THRUST DECAY, START COAST	PRED	135710.		78.042		.0466							
		299188.		3072.5		1.8334		.197		12.611		12.610	
	ACTUAL	135102.		78.050	.008	.0472	.0007						
		297848.	-.44	3072.9	.31	1.8593	.0259	.197	.02	12.591	-.16	12.589	-.16
3RD FLIGHT STAGE AT 2ND START SEQUENCE COMMAND	PRED	134410.		78.054		.0466							
		296323.		3073.0		1.8350		.195		12.606		12.606	
	ACTUAL	134049.		78.058	.004	.0474	.0007						
		295526.	-.26	3073.2	.16	1.8643	.0293	.196	.41	12.588	-.14	12.588	-.14

Table 20-10. Mass Characteristics Comparison (Continued)

EVENT		MASS		LONGITUDINAL C.G. (X STA.)		RADIAL C.G.		ROLL MOMENT OF INERTIA		PITCH MOMENT OF INERTIA		YAW MOMENT OF INERTIA	
		KILO POUNDS	O/O DEV.	METERS INCHES	DELTA	METERS INCHES	DELTA	KG-M2 X10-6	O/O DEV.	KG-M2 X10-6	O/O DEV.	KG-M2 X10-6	O/O DEV.
3RD FLIGHT STAGE AT 2ND IGNITION	PRED	134408. 296319.		78.053 3073.0		.0466 1.8350		.195		12.608		12.608	
	ACTUAL	134047. 295521.	-.26	78.057 3073.1	.004 .16	.0474 1.8643	.0007 .0293	.196	.41	12.591	-.13	12.590	-.14
3RD FLIGHT STAGE AT 2ND MAINSTAGE	PRED	134194. 295846.		78.060 3073.2		.0466 1.8350		.195		12.603		12.603	
	ACTUAL	133883. 295161.	-.23	78.062 3073.3	.002 .08	.0474 1.8643	.0007 .0293	.196	.41	12.587	-.17	12.587	-.13
3RD FLIGHT STAGE AT 2ND CUTOFF SIGNAL	PRED	63197. 139324.		85.770 3376.8		.0975 3.8394		.195		5.272		5.272	
	ACTUAL	63190. 139309.	-.01	85.712 3374.5	-.058 -2.29	.0989 3.8948	.0014 .0554	.195	.45	5.329	1.08	5.327	1.06
3RD FLIGHT STAGE AT 2ND END THRUST DECAY	PRED	63151. 139223.		85.781 3377.2		.0975 3.8394		.195		5.261		5.260	
	ACTUAL	63116. 139146.	-.05	85.731 3375.2	-.050 -1.98	.0989 3.8948	.0014 .0554	.195	.45	5.309	.93	5.308	.91
CSM SEPARATED	PRED	33093. 72957.		78.781 3101.6		.0825 3.2468		.139		1.687		1.684	
	ACTUAL	32585. 71836.	-1.53	78.799 3102.3	.017 .68	.0792 3.1164	-.0033 -.1304	.139	.16	1.686	-.01	1.682	-.10
CSM DOCKED	PRED	61932. 136536.		85.218 3355.1		.1292 5.0850		.186		4.719		4.715	
	ACTUAL	61391. 135342.	-.87	85.267 3357.0	.049 1.92	.1277 5.0293	-.0014 -.0557	.186	.30	4.691	-.59	4.686	-.61
SPACECRAFT SEPARATED	PRED	17980. 39639.		73.615 2898.2		.1517 5.9718		.109		.614		.611	
	ACTUAL	17149. 37805.	-4.62	73.573 2896.6	-.042 -1.66	.1456 5.7328	-.0061 -.2390	.109	.06	.609	-.81	.605	-1.08

SECTION 21

MISSION OBJECTIVES ACCOMPLISHMENT

Table 21-1 presents the MSFC Principal Detailed Objectives and Secondary Detailed Objectives as defined in the Saturn V Mission Implementation Plan, Mission G, Revision C. An assessment of the degree of accomplishment of each objective is shown. Discussion supporting the assessment can be found in the indicated sections of the Saturn V Launch Vehicle Flight Evaluation Report - AS-506, Apollo 11 Mission.

Table 21-1. Mission Objectives Accomplishment Summary

NO.	MSFC PRINCIPAL DETAILED OBJECTIVES (PDO) AND SECONDARY DETAILED OBJECTIVES (SDO)	DEGREE OF ACCOMPLISHMENT	DISCREPANCIES	PARAGRAPH IN WHICH DISCUSSED
1	Launch on variable 72 to 108-degree flight azimuth and insertion of S-IVB/IU/SC into a circular earth parking orbit (PDO).	Complete	None	4.1 4.3.1 4.3.2 11.4.2
2	Restart the S-IVB during either the second or third revolution and injection of the S-IVB/IU/SC onto the planned translunar trajectory (PDO).	Complete	None	4.1 4.3.3 7.6 10.3 11.4.4
3	Provide the required attitude control for the S-IVB/IU/SC during the Transposition, Docking, and Ejection (TD&E) maneuver (PDO).	Complete	None	4.1 4.3.4 10.3 11.4.4
4	Use residual S-IVB propellants and Auxiliary Propulsion System (APS), after final LV/SC separation, to safe the S-IVB and to minimize the possibility of the following, in order of priority: 1. S-IVB/IU recontact with SC 2. S-IVB/IU earth impact 3. S-IVB/IU lunar impact (SDO).	Complete	None	4.3.5 7.13 10.3 11.4.4

SECTION 22

FAILURES, ANOMALIES AND DEVIATIONS

22.1 SUMMARY

Evaluation of the launch vehicle performance during the AS-506 flight revealed no failures or anomalies and ten deviations. None of these deviations had an adverse effect on the mission.

22.2 SYSTEM FAILURES AND ANOMALIES

There were no failures or anomalies detected during the launch vehicle operational period of flight.

22.3 SYSTEM DEVIATIONS

Ten system deviations occurred, none of which had any significant effect on the flight or operation of the particular systems involved. Table 22-1 presents these deviations along with the corrective actions being considered and references to paragraphs containing additional discussion of the deviations.

Table 22-1. Summary of Deviations

VEHICLE SYSTEM	DEVIATION	PROBABLE CAUSE	CORRECTIVE ACTION BEING CONSIDERED	PARAGRAPH REFERENCE
S-IC Propulsion	Unexplained LOX suction duct pressure decay of engine No. 5 after Center Engine Cutoff (CECO).	Unknown.	None. Similar occurrences during AS-503, AS-504 and AS-505 with no effect on mission.	5.6
S-II Propulsion	J-2 engine No. 1 start tank pressure below pre-launch commit (-33 seconds) redline.	Lower than planned Ground Support Equipment (GSE) regulator setting.	Increase GSE regulator nominal setting and relax pre-launch commit redline to more closely approximate actual requirements.	3.6.2 6.2
S-II Propulsion	J-2 engine No. 2 helium tank pressure decay rate sharper than expected after Engine Start Command (ESC).	Leakage through engine helium regulator.	None. Decay rate returned to normal at 30 seconds after ESC.	6.2
S-IVB Hydraulics	1. S-IVB engine driven hydraulic pump system pressure drifted 16 N/cm^2 (23.2 psi) over the predicted upper limit of 2526 N/cm^2 (3665 psia) at 9848 seconds. 2. Later exhibited small but abrupt drop in pressure.	1. Inherent "drift-up" of pump plus uncompensated thermal expansion in compensator; neither of which was included in establishing the predicted upper limit. 2. Abrupt change could be due to frictional hysteresis in the pressure/flow regulating mechanism.	Under investigation.	8.4
S-IVB Propulsion	LOX tank pressure decayed approximately 5 percent below predicted minimum during coast in earth parking orbit.	1. Thermal collapse of ullage pressure. 2. LOX tank leakage.	None. Probably due to thermal collapse. Since LOX tank repressurization was well within design capabilities, this pressure decay was not considered a problem (even if second opportunity restart had been required).	7.10.2
S-IVB Structures	Low amplitude, 17 to 20 hertz longitudinal oscillations during first burn.	Similar to oscillations on AS-505, but only 20 percent of the amplitude. Data indicates typical buildup and decay periods of very mild oscillations without indications of propulsion/structural coupling.	None. While this is apparrently a phenomenon which is characteristic of the stage, changes in the engine or payload configuration would require a reassessment.	9.2.3.1
Instrument Unit (IU) Guidance	Delay of 6 seconds in IU command to shift S-II Engine Mixture Ratio (EMR).	Primarily due to improper scaling in IU LVDC velocity computations.	Improve scaling in IU LVDC velocity calculations.	6.5 10.2.1 10.3
IU/Gas Bearing Supply	Inertial platform gas bearing differential pressure drifted 0.54 N/cm^2 (0.8 psi) above specification at 23,200 seconds.	Inherent in the system late in the flight. Occurred on AS-502, AS-503, AS-504 and AS-506 and caused no problem.	Raise the maximum pressure differential spec. to an acceptable value. Ground tests indicate no performance deviations at 13.8 N/cm^2 (20 psi).	18.4.2
IU/ST-124 Inertial Platform	ST-124 platform crossrange velocity exhibited negative 1.8 m/s (5.9 ft/s) shift 3.3 seconds after liftoff.	Vibration caused the Y accelerometer to have a level shift or to touch a mechanical stop.	Under investigation, but had no effect on operation of launch vehicle.	10.2 10.4.7
IU/RF	Erratic signal strength at receiving station beginning at 27,128 seconds.	Malfunction of coaxial switch.	Coaxial switch has been replaced on AS-507 with new design.	19.4.3.2

SECTION 23

SPACECRAFT SUMMARY

The purpose of the Apollo 11 mission was to land men on the lunar surface and to return them safely. The crew was Neil A. Armstrong, Commander; Michael Collins, Command Module (CM) Pilot; and Edwin E. Aldrin, Jr., Lunar Module (LM) Pilot.

The space vehicle was launched from Kennedy Space Center (KSC), Florida, at 9:32:00 a.m. Eastern Daylight Time (EDT), July 16, 1969. The activities during earth orbit checkout, Translunar Injection (TLI), transposition and docking, spacecraft ejection, and translunar coast were similar to those of Apollo 10. Only one midcourse correction, performed at about 27 hours Ground Elapsed Time (GET), was required during translunar coast.

The spacecraft was inserted into lunar orbit at approximately 76 hours, and the circularization maneuver was performed two revolutions later. Initial checkout of LM systems was satisfactory, and after a planned rest period, the Commander and LM Pilot entered the LM to prepare for descent.

The two spacecraft were undocked at 100 hours, followed by separation of the Command and Service Modules (CSM) from the LM. Descent orbit insertion was performed at about 101.5 hours, and powered descent to the lunar surface began about 1 hour later. Operation of the guidance and descent propulsion systems was nominal. During the final 2.5 minutes of descent, the LM was maneuvered manually approximately 305 meters (1000 ft) downrange. The spacecraft landed in the Sea of Tranquility at 102:45:40. The landing coordinates were 0.647 degree north latitude and 23.505 degrees east longitude, based on identification of landmarks from the onboard sequence camera. During the first 2 hours on the surface, the two crewmen performed a postlanding checkout of all LM systems. Afterwards they ate their first meal on the moon and elected to perform the surface operations earlier than planned.

Considerable time was devoted to checkout and donning of the back-mounted portable life support and oxygen purge systems. The Commander egressed through the forward hatch and deployed an equipment module in the descent stage. A camera in this module provided live television coverage of the Commander descending the ladder to the surface, with first contact made

at 109:24:19 (10:56:19 p.m. EDT, July 20, 1969). The LM Pilot egressed soon thereafter, and both crewmen used the initial period on the surface to become acclimated to the reduced gravity and new surface conditions. A contingency sample was taken from the surface, and the television camera was deployed so that most of the LM was included in its view field. The crew took numerous photographs, erected a U.S. flag, and activated the scientific experiments, which included a solar wind detector, a passive seismometer, and a laser reflector. The LM Pilot spent considerable time evaluating his ability to operate and move about, and despite the limitations imposed by the pressurized suit, he was able to translate rapidly and with confidence. Approximately 24 kilograms (54 lbm) of bulk surface material were collected to be returned for analysis. The crew reentered the LM at 111:39:00, with surface exploration lasting 2 hours, 31 minutes.

Ascent preparation was conducted efficiently, and the ascent stage lifted off the surface at 124.5 hours. A nominal firing of the ascent engine placed the vehicle into an 83 by 17 kilometer (45 by 9 n mi) orbit. After a rendezvous sequence similar to that of Apollo 10, the two spacecraft were docked at 128 hours. Following transfer of the crew, the ascent stage was jettisoned, and the Command and Service Modules were prepared for transearth injection.

The return flight started with a 150-second firing of the service propulsion engine during the 31st lunar revolution at 135.5 hours. As in translunar flight, only one midcourse correction was required, and passive thermal control was exercised for most of transearth coast. The possibility of inclement weather necessitated moving the landing point 398 kilometers (215 n mi) downrange. The entry phase was normal, and the CM landed in the Pacific Ocean at 195:18:35. The landing coordinates, as determined from the onboard computer, were 13.3 degrees north latitude and 169.4 degrees west longitude.

After landing, the crew donned biological isolation garments and were retrieved by helicopter and taken to the primary recovery ship, USS Hornet. The crew then entered the Mobile Quarantine Facility, which arrived at the Lunar Receiving Laboratory in Houston on Sunday, July 27, 1969. The CM was taken aboard the Hornet about 3 hours after landing. The lunar samples arrived at the Receiving Laboratory the day after landing.

For further details on the spacecraft performance, refer to the Apollo 11 Mission Report published by NASA Manned Spacecraft Center at Houston, Texas.

APPENDIX A

ATMOSPHERE

A.1 SUMMARY

This appendix presents a summary of the atmospheric environment at launch time of the AS-506. The format of these data is similar to that presented on previous launches of Saturn vehicles to permit comparisons. Surface and upper winds, and thermodynamic data near the launch time are given.

A.2 GENERAL ATMOSPHERIC CONDITIONS AT LAUNCH TIME

A high pressure cell, in the Atlantic Ocean off the North Carolina coast, along with a weak trough of low pressure located in the northeastern Gulf of Mexico caused light southerly surface winds and brought moisture into the Cape Kennedy, Florida area, which contributed to the cloudy conditions and distant thunderstorms that were observed during launch.

A.3 SURFACE OBSERVATIONS AT LAUNCH TIME

At launch time, total sky cover was 9/10 with 1/10 cumulus at 0.7 kilometer (2400 ft), 2/10 altocumulus at 4.6 kilometers (15,000 ft) and 9/10 cirrostratus at an unknown altitude. Surface observations at launch time are summarized in Table A-1. Solar radiation data are given in Table A-2.

A.4 UPPER AIR MEASUREMENTS

Data were used from three of the upper air wind systems to compile the final meteorological tape. Table A-3 summarizes the data systems used.

A.4.1 Wind Speed

Wind speed was light in the lower levels. In the maximum dynamic pressure region a peak speed of 9.6 m/s (18.7 knots) was observed at 11.40 kilometers (37,400 ft). At higher altitudes the wind speed increased steadily, as shown in Figure A-1.

A.4.2 Wind Direction

The surface wind was from the south, but with altitude shifted clockwise through west, north and then stayed easterly above 16 kilometers (52,490 ft) altitude, as shown in Figure A-2.

Table A-1. Surface Observations at AS-506 Launch Time

LOCATION	TIME AFTER T-0 (MIN)	PRESSURE N/CM^2 (PSIA)	TEMPERATURE °K (°F)	DEW POINT °K (°F)	VISIBILITY KM (STAT MI)	AMOUNT (TENTHS)	SKY COVER TYPE	HEIGHT OF BASE	WIND	
									SPEED M/S (KNOTS)	DIR (DEG)
Kennedy Space Center, Station Merritt Island, Florida	0	10.203 (14.80)	302.6 (85.0)	297.0 (75.0)	16 (10)	1 2 9	Cumulus Alto-cumulus Cirro-stratus	700 (2400) 4600 (15,000) high	1.0 (2.0)	180
Cape Kennedy Rawinsonde Measurements	13	10.195 (14.79)	303.0 (85.6)	297.5 (75.7)	--	--	--	--	1.0 (2.0)	180
Pad 39A Lightpole SE 18.3 m * (60.0 ft)	0	--	--	--	--	--	--	--	3.3 (6.4)	175

*Above Natural Grade

A.4.3 Pitch Wind Component

The surface pitch wind speed component was a tail wind of 0.3 m/s (0.6 knots). A maximum tail wind of 7.6 m/s (14.8 knots) was observed at 11.18 kilometers (36,680 ft) altitude. Head winds were observed above 15.0 kilometers (49,210 ft) altitude. See Figure A-3.

A.4.4 Yaw Wind Component

The yaw wind speed component was a wind from the right at the surface to approximately 9.0 kilometers (29,530 ft) altitude. Winds from the left prevailed above this altitude to 16.3 kilometers (53,480 ft) with a peak yaw wind speed of 7.1 m/s (13.8 knots) at 12.1 kilometers (39,530 ft) altitude. Above 16.3 kilometers (53,480 ft) yaw winds were from the right. See Figure A-4.

A.4.5 Component Wind Shears

The largest component wind shear (Δh = 1000 m) in the altitude range of 8 to 16 kilometers (26,247 to 52,493 ft) was a pitch shear of 0.0077 sec^{-1} at 14.8 kilometers (48,490 ft). The largest yaw wind shear, in the lower levels, was 0.0056 sec^{-1} at 10.3 kilometers (33,790 ft). See Figure A-5.

Table A-2. Solar Radiation at AS-506 Launch Time, Launch Pad 39A

DATE	HOUR ENDING EST	TOTAL HORIZONTAL G-CAL/CM^2 (MIN)	NORMAL INCIDENT G-CAL/CM^2 (MIN)	DIFFUSE SKY G-CAL/CM^2 (MIN)
July 15, 1969	0600	0.00	0.00	0.00
	0700	0.11	0.03	0.10
	0800	0.15	0.02	0.14
	0900	0.21	0.02	0.20
	1000	0.41	0.03	0.39
	1100	0.57	0.03	0.54
	1200	0.78	0.12	0.66
	1300	1.17	0.44	0.74
	1400	0.89	0.29	0.62
	1500	0.39	0.02	0.37
	1600	0.33	0.01	0.32
	1700	0.43	0.06	0.40
	1800	0.30	0.10	0.27
	1900	0.07	0.00	0.07
	2000	0.01	0.00	0.01
July 16, 1969	0600	0.01	0.00	0.01
	0700	0.14	0.11	0.11
	0800	0.42	0.36	0.24
	0900	0.77	0.54	0.40
	1000	0.88	0.37	0.57
	1100	1.46	0.52	0.98

A.4.6 Extreme Wind Data in the High Dynamic Region

A summary of the maximum wind speeds and wind components is given in Table A-4. A summary of the extreme wind shear values is given in Table A-5.

A.5 THERMODYNAMIC DATA

Comparisons of the thermodynamic data taken at AS-506 launch time with the Patrick Reference Atmosphere, 1963 (PRA-63) for temperature, density, pressure, and Optical Index of Refraction are shown in Figures A-6 and A-7 and discussed in the following paragraphs.

A.5.1 Temperature

Atmospheric temperature deviations were small, being less than 3 percent deviation from the PRA-63. At most altitudes, the temperature was warmer than the PRA-63.

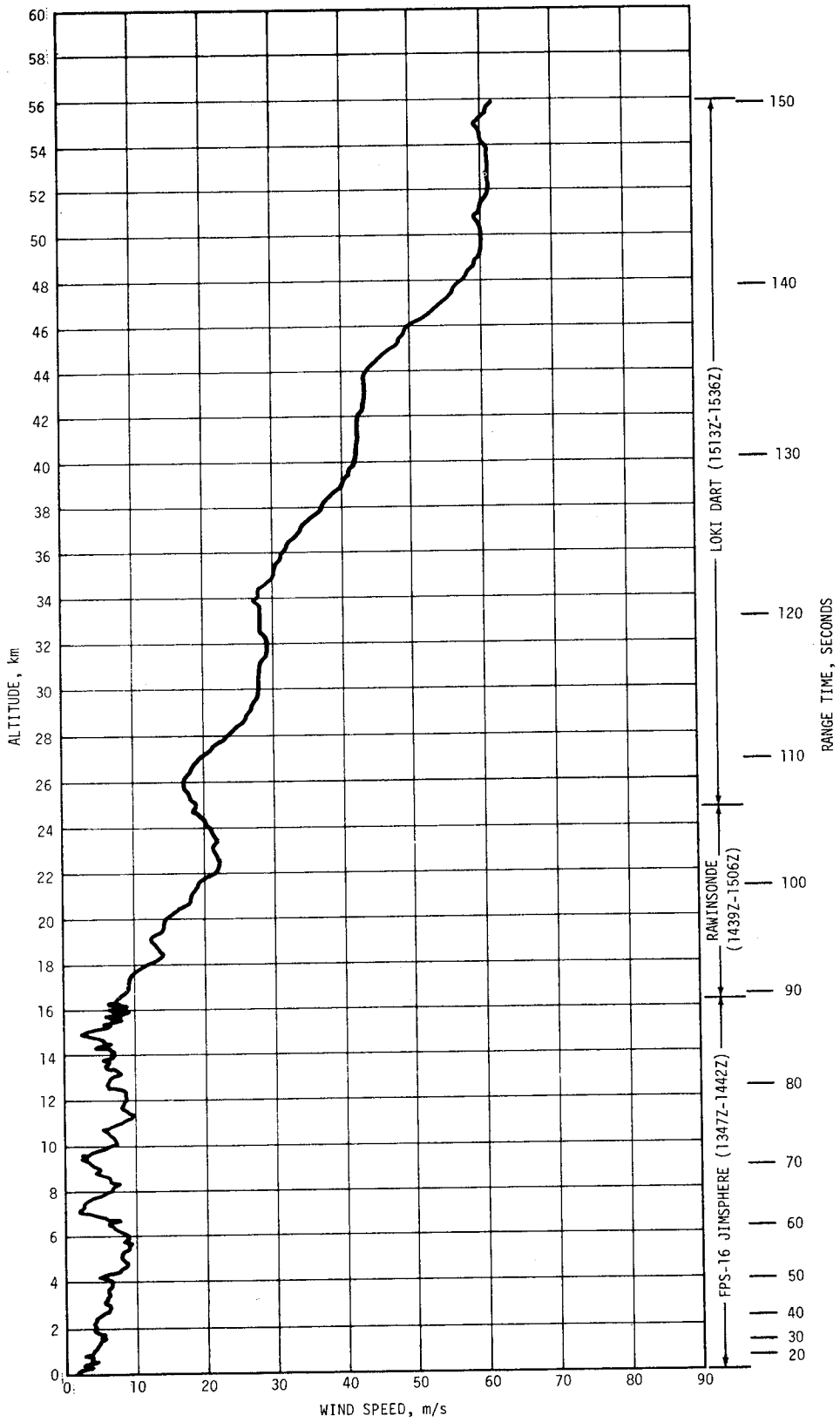

Figure A-1. Scalar Wind Speed at Launch Time of AS-506

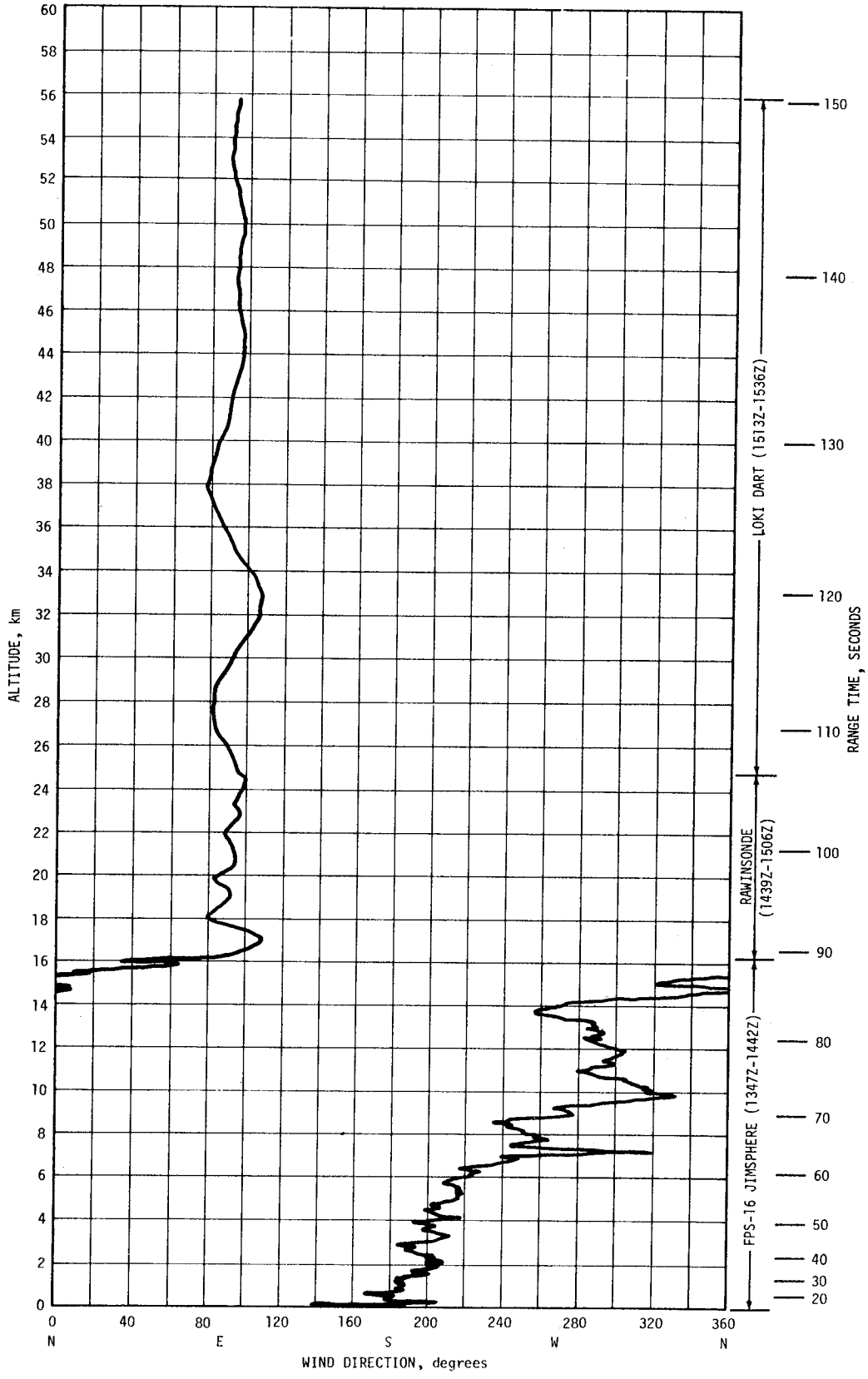

Figure A-2. Wind Direction at Launch Time of AS-506

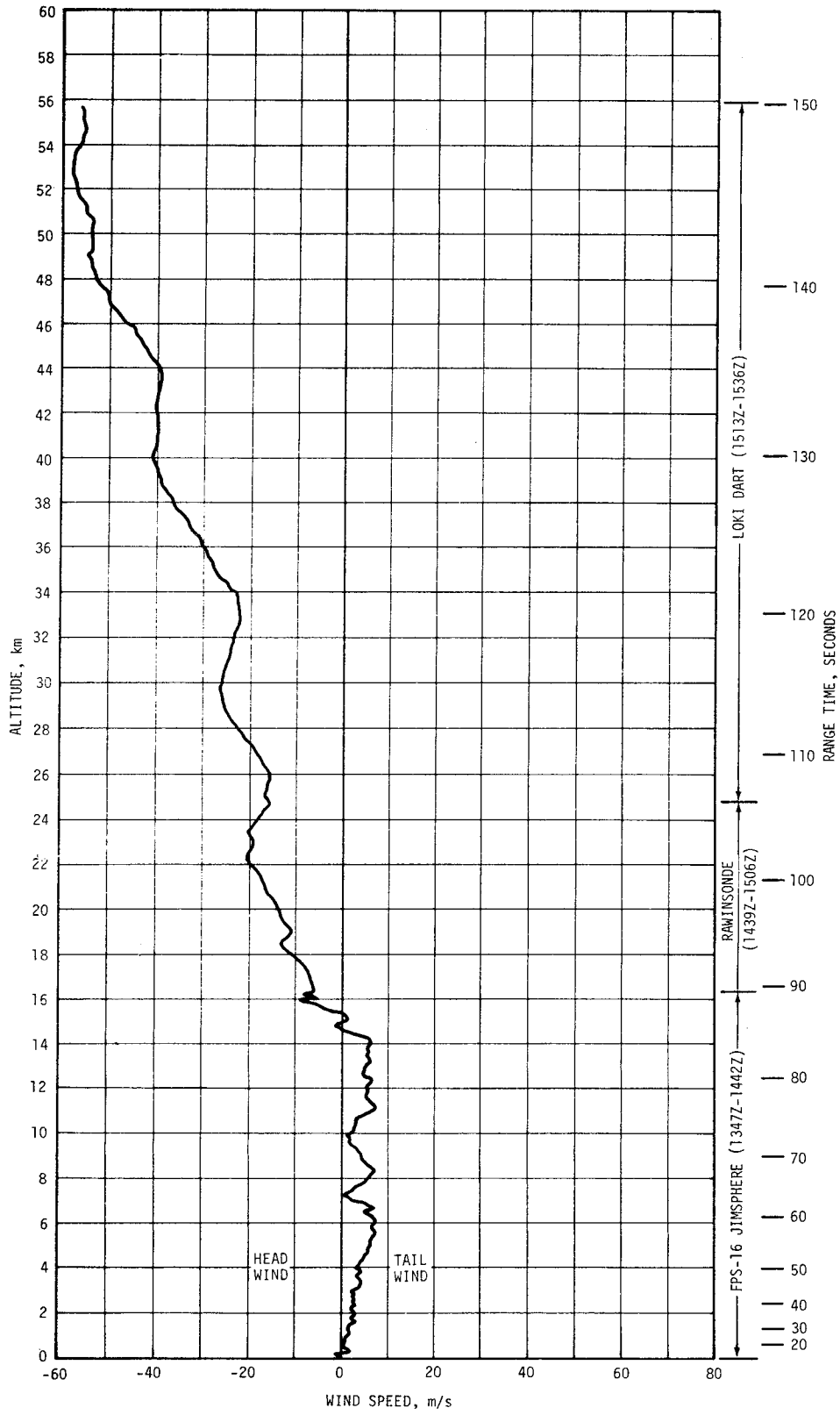

Figure A-3. Pitch Wind Speed Component (W_X) at Launch Time of AS-506

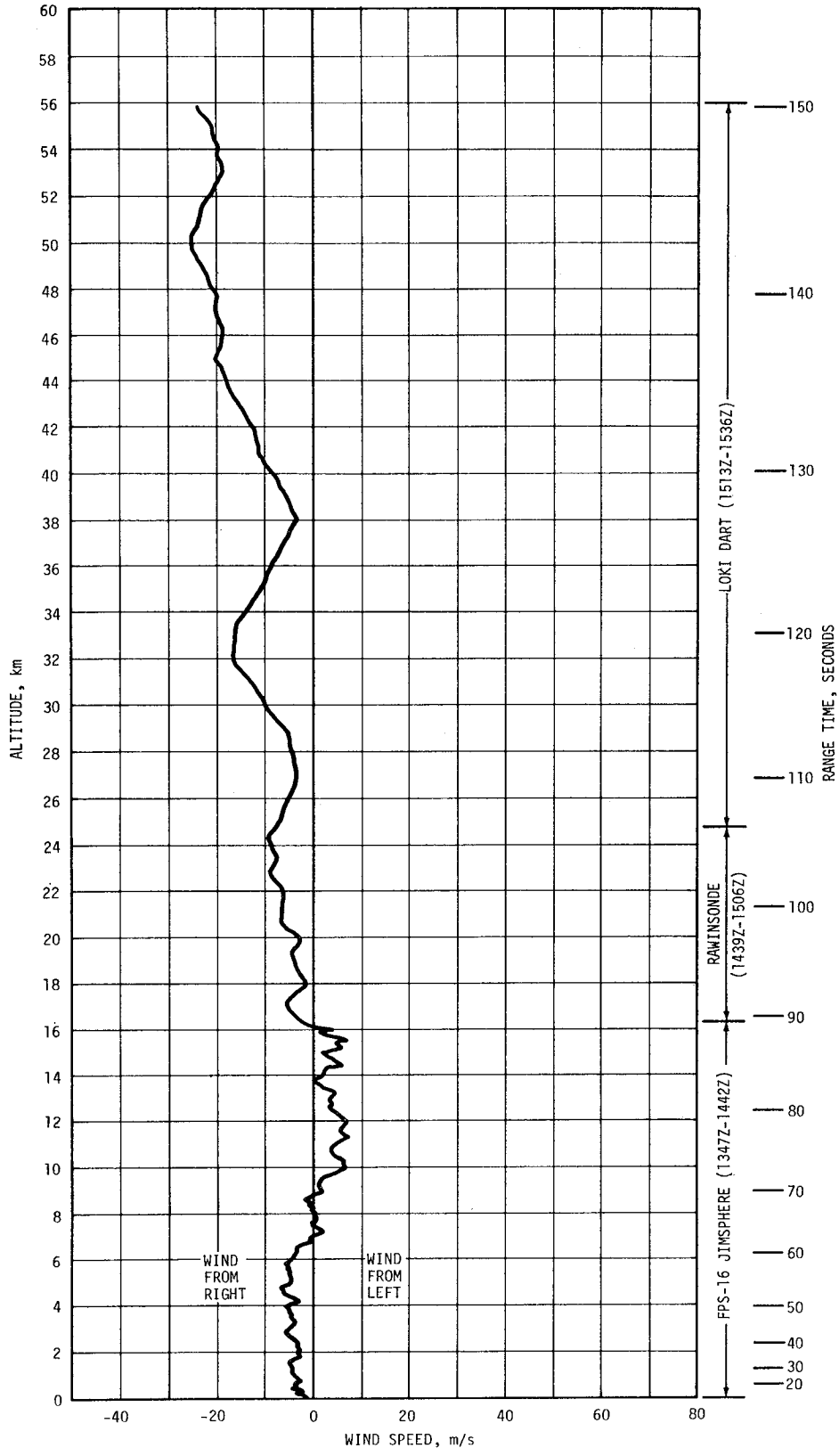

Figure A-4. Yaw Wind Speed Component (W_Z) at Launch Time of AS-506

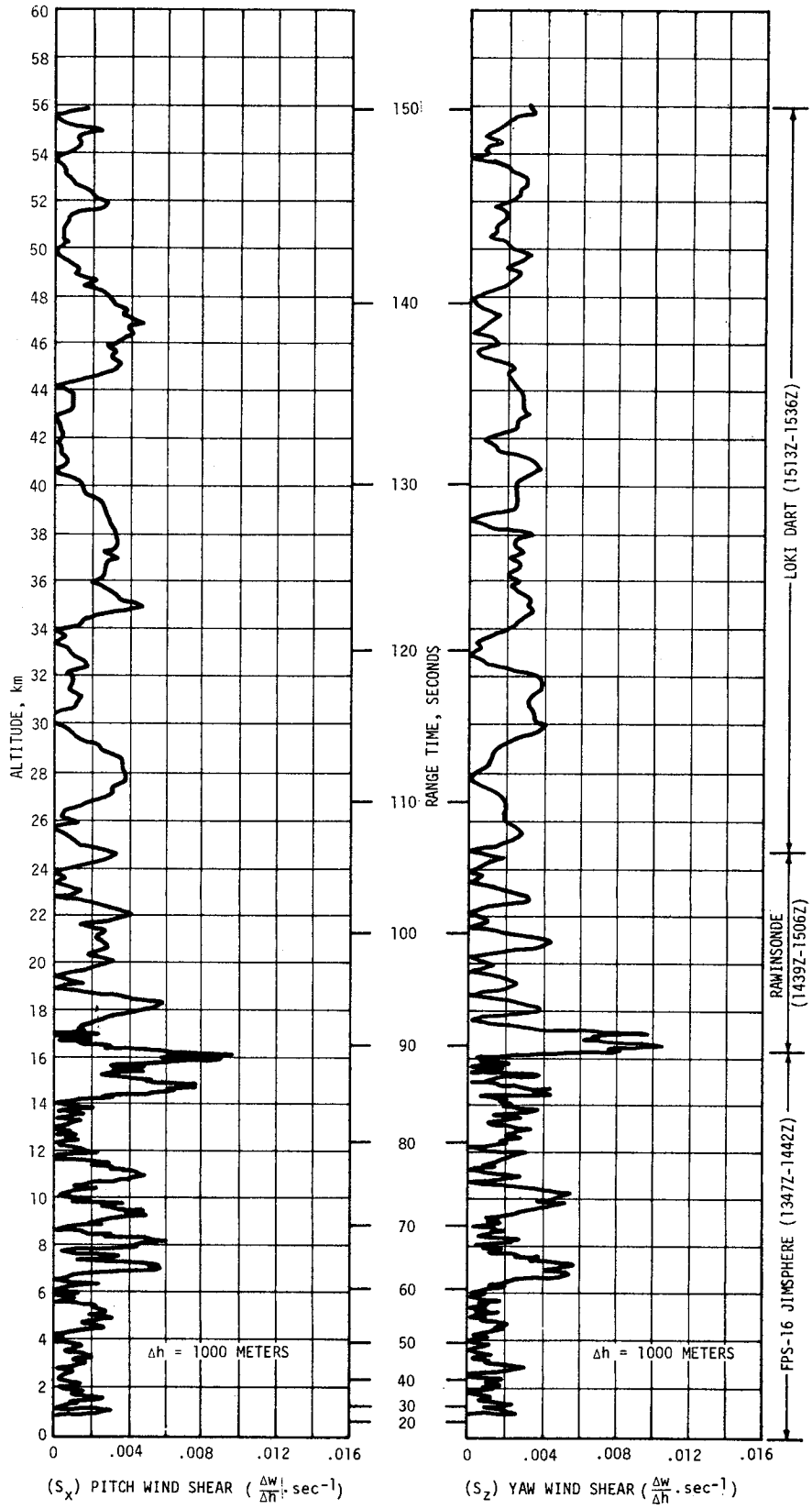

Figure A-5. Pitch (S_X) and Yaw (S_Z) Component Wind Shears At Launch Time of AS-506

Table A-3. Systems Used to Measure Upper Air Wind Data for AS-506

TYPE OF DATA	RELEASE TIME		PORTION OF DATA USED			
			START		END	
	TIME (UT)	TIME AFTER T-0 (MIN)	ALTITUDE M (FT)	TIME AFTER T-0 (MIN)	ALTITUDE M (FT)	TIME AFTER T-0 (MIN)
FPS-16 Jimsphere	1347	15	0	15	16,250 (53,310)	70
Rawinsonde	1345	13	16,500 (54,130)	67	24,750 (81,200)	94
Loki Dart	1512	100	56,000 (183,725)	101	25,000 (82,020)	124

Table A-4. Maximum Wind Speed in High Dynamic Pressure Region for Apollo/Saturn 501 through Apollo/Saturn 506 Vehicles

VEHICLE NUMBER	MAXIMUM WIND			MAXIMUM WIND COMPONENTS			
	SPEED M/S (KNOTS)	DIR (DEG)	ALT KM (FT)	PITCH (W_x) M/S (KNOTS)	ALT KM (FT)	YAW (W_z) M/S (KNOTS)	ALT KM (FT)
AS-501	26.0 (50.5)	273	11.50 (37,700)	24.3 (47.2)	11.50 (37,700)	12.9 (25.1)	9.00 (29,500)
AS-502	27.1 (52.7)	255	12.00 (42,600)	27.1 (52.7)	12.00 (42,600)	12.9 (25.1)	15.75 (51,700)
AS-503	34.8 (67.6)	284	15.22 (49,900)	31.2 (60.6)	15.10 (49,500)	22.6 (43.9)	15.80 (51,800)
AS-504	76.2 (148.1)	264	11.73 (38,480)	74.5 (144.8)	11.70 (38,390)	21.7 (42.2)	11.43 (37,500)
AS-505	42.5 (82.6)	270	14.18 (46,520)	40.8 (79.3)	13.80 (45,280)	18.7 (36.3)	14.85 (48,720)
AS-506	9.6 (18.7)	297	11.40 (37,400)	7.6 (14.8)	11.18 (36,680)	7.1 (13.8)	12.05 (39,530)

Table A-5. Extreme Wind Shear Values in the High Dynamic Pressure Region for Apollo/Saturn 501 through Apollo/Saturn 506 Vehicles

(Δh = 1000 m)				
VEHICLE NUMBER	PITCH PLANE		YAW PLANE	
	SHEAR (SEC^{-1})	ALTITUDE KM (FT)	SHEAR (SEC^{-1})	ALTITUDE KM (FT)
AS-501	0.0066	10.00 (32,800)	0.0067	10.00 (32,800)
AS-502	0.0125	14.90 (48,900)	0.0084	13.28 (43,500)
AS-503	0.0103	16.00 (52,500)	0.0157	15.78 (51,800)
AS-504	0.0248	15.15 (49,700)	0.0254	14.68 (48,160)
AS-505	0.0203	15.30 (50,200)	0.0125	15.53 (50,950)
AS-506	0.0077	14.78 (48,490)	0.0056	10.30 (33,790)

A.5.2 Atmospheric Pressure

Atmospheric pressure deviations remained greater than the PRA-63 values at all altitudes. Surface pressure was 0.2 percent greater than the PRA-63 and increased to a peak deviation of 9.0 percent at 44.0 kilometers (144,360 ft).

A.5.3 Atmospheric Density

Atmospheric density deviations were small, being less than 5 percent deviation from the PRA-63 from the surface to 29.8 kilometers (97,770 ft) altitude. Density deviations increased above this altitude and reached a peak of 10.3 percent at 46.0 kilometers (150,920 ft). Surface atmospheric density was -2.1 percent of the PRA-63 surface density.

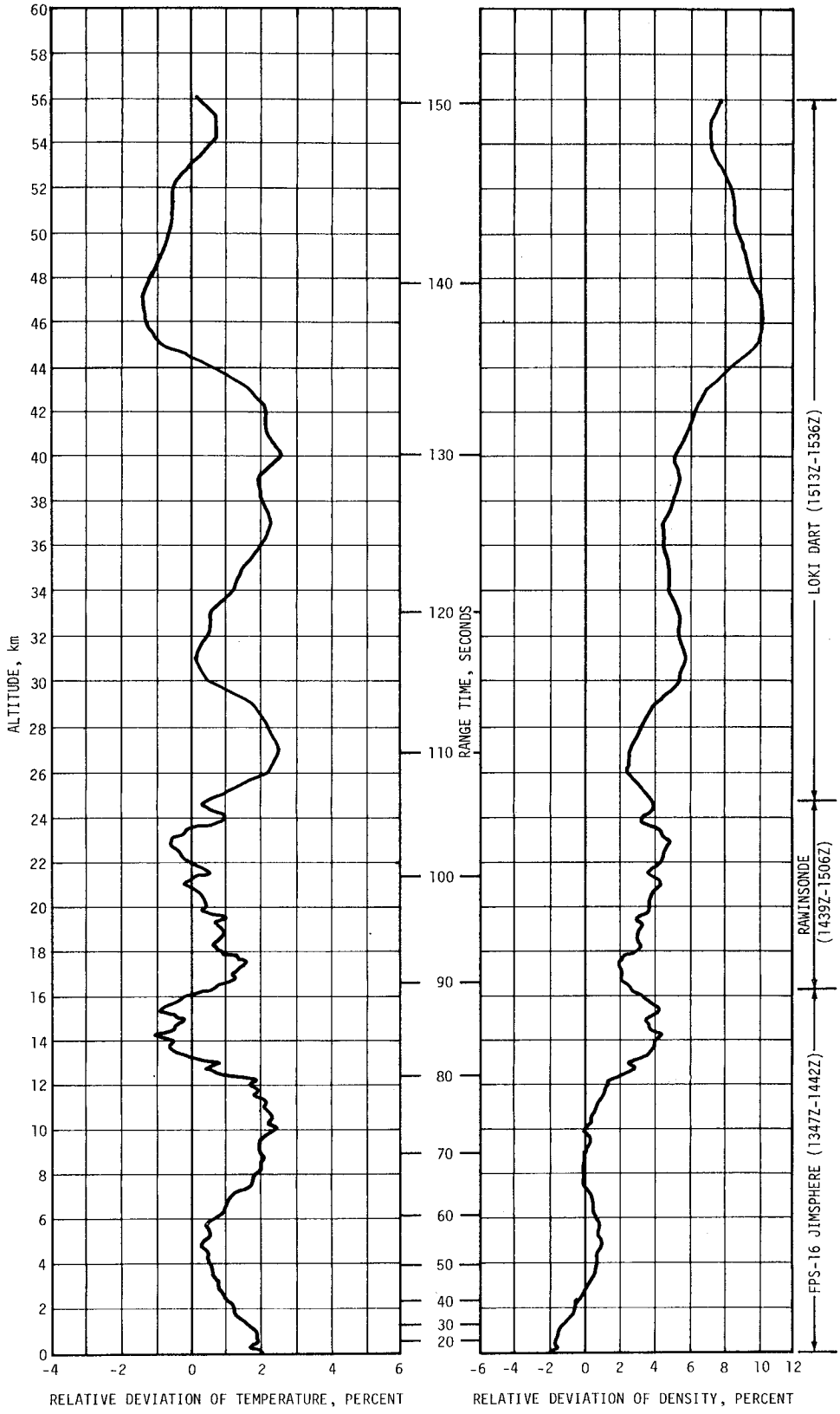

Figure A-6. Relative Deviation of Temperature and Density From the PRA-63 Reference Atmosphere, AS-506

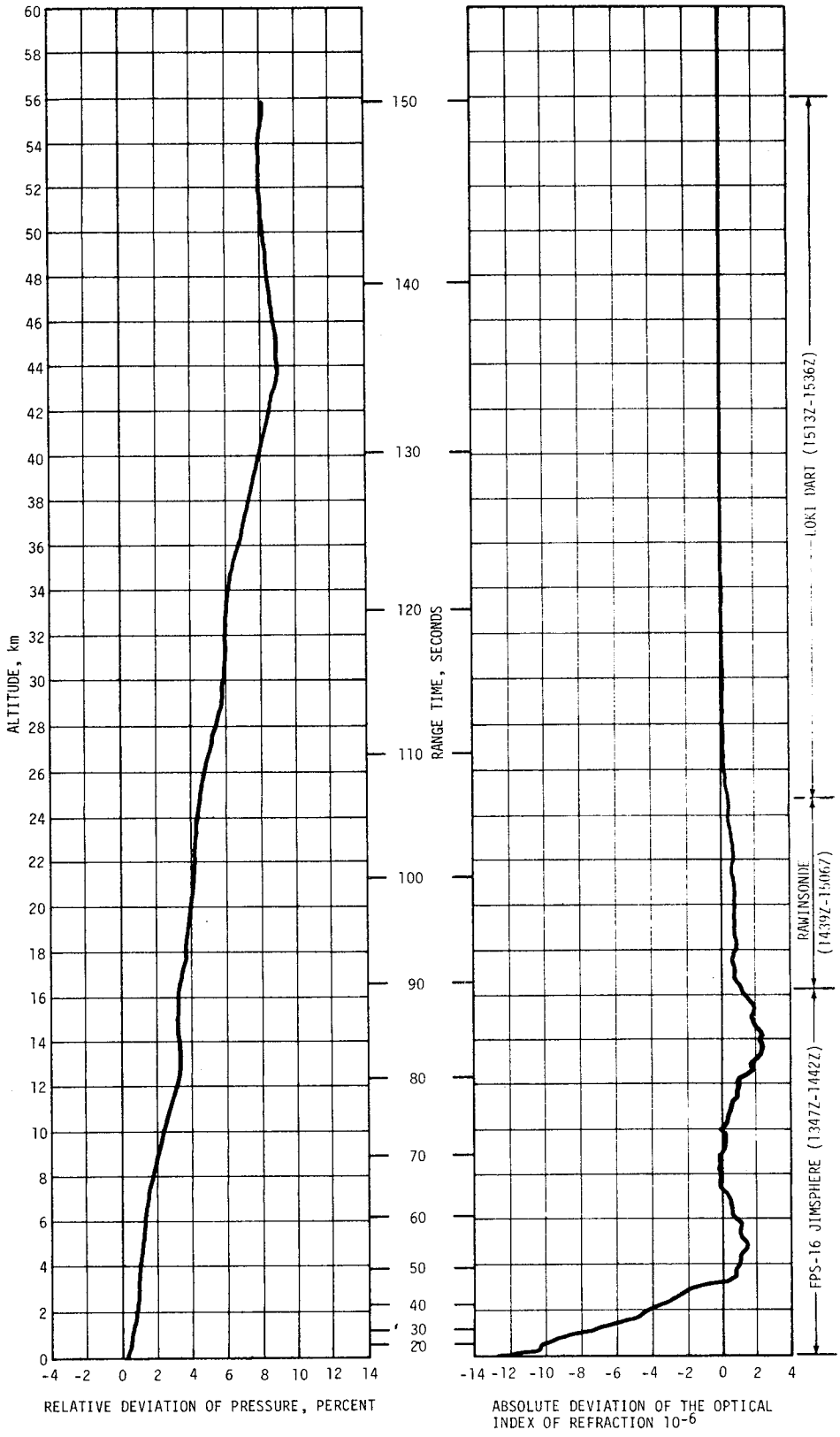

Figure A-7. Relative Deviation of Pressure and Absolute Deviation of the Index of Refraction From the PRA-63 Reference Atmosphere, AS-506

A.5.4 Optical Index of Refraction

At the surface, the Optical Index of Refraction was 12.9 x 10^{-6} units lower than the corresponding value of the PRA-63. The deviation became less negative with altitude, becoming a maximum positive deviation of 2.43 x 10^{-6} greater than the corresponding value of the PRA-63 at 14.3 kilometers (46,920 ft). Above this altitude the Optical Index of Refraction approximates the PRA-63 values.

A.6 COMPARISON OF SELECTED ATMOSPHERIC DATA FOR SATURN V LAUNCHES

A summary of the atmospheric data for each Saturn V launch is shown in Table A-6.

Table A-6. Selected Atmospheric Observations for Apollo/Saturn 501 Through Apollo/Saturn 506 Vehicle Launches at Kennedy Space Center, Florida

VEHICLE NUMBER	VEHICLE DATA			SURFACE DATA						INFLIGHT CONDITIONS		
	DATE	TIME NEAREST MINUTE	LAUNCH COMPLEX	PRESSURE N/CM^2	TEMPERATURE °C	RELATIVE HUMIDITY PERCENT	WIND* SPEED M/S	WIND* DIRECTION DEG	CLOUDS	MAXIMUM WIND IN 8-16 KM LAYER ALTITUDE KM	SPEED M/S	DIRECTION DEG
AS-501	9 Nov 67	0700 EST	39A	10.261	17.6	55	8.0	70	1/10 cumulus	11.50	26.0	273
AS-502	4 Apr 68	0600 EST	39A	10.200	20.9	83	5.4	132	5/10 stratocumulus	13.00	27.1	255
AS-503	21 Dec 68	0751 EST	39A	10.207	15.0	88	1.0	360	4/10 cirrus	15.22	34.8	284
AS-504	3 Mar 69	1100 EST	39A	10.095	19.6	61	6.9	160	10/10 stratocumulus	11.73	76.2	264
AS-505	18 May 69	1149 EDT	39B	10.190	26.7	75	8.2	125	4/10 cumulus, 2/10 altocumulus, 10/10 cirrus	14.18	42.5	270
AS-506	16 Jul 69	0932 EDT	39A	10.203	29.4	73	3.3	175	1/10 cumulus, 2/10 altocumulus, 9/10 cirrostratus	11.40	9.6	297

*Instantaneous readings from charts at T-0 from anemometers on launch pad at 18.3 m (60.0 ft) on launch complex 39 (A&B). Heights of anemometers are above natural grade.

APPENDIX B

AS-506 SIGNIFICANT CONFIGURATION CHANGES

B.1 INTRODUCTION

AS-506, sixth flight of the Saturn V series, was the fourth manned Apollo Saturn V vehicle. The AS-506 launch vehicle was configured the same as the AS-505 with significant exceptions as shown in Tables B-1 through B-4. The basic AS-506 Apollo 11 spacecraft structure and components were unchanged from the AS-504 Apollo 9 configuration except lunar module crew provisions were accompanied by portable life support systems and associated controls required to accommodate extra vehicular surface activity. The basic vehicle description is presented in Appendix B of the Saturn V Launch Vehicle Flight Evaluation Report AS-504, Apollo 9 Mission, MPR-SAT-FE-69-4.

Table B-1. S-IC Significant Configuration Changes

SYSTEM	CHANGE	REASON
Control Pressure	Deleted prevalve accumulator bottles.	Stage system tests have shown that the accumulator bottles are not required for satisfactory closure of prevalves.
Data	Measurements reduced from 669 to 313; deletions include all vibration and acoustic measurements.	R&D instrumentation which is no longer required.
	Deleted 3 PAM, 2 FM/FM, and 2 SS/FM systems.	Deletion of R&D instrumentation permitted reduction of telemetry system.
	Deleted airborne tape recorder.	R&D data recording system which is no longer required.
	Modified register switches card in telemetry PCM/DDAS assembly.	Improve reliability.
Electrical	Capacity of instrumentation battery 1D20 reduced.	Deletion of R&D instrumentation permitted use of lower capacity battery.

Table B-2. S-II Significant Configuration Changes

SYSTEM	CHANGE	REASON
Instrumentation	Reduction of measurement quantity from 1018 on S-II-5 to 563 on S-II-6 and subs.	Maturity of design, R&D instrumentation no longer required.
	Deleted 3 PAM, 1 FM/FM, and 2 SS/FM systems.	
	Deleted 2 airborne tape recorders.	
Thermal Control	Deleted electronic packages 206A84, 206A85, 208, 211, 212, 213 from aft skirt area and packages 222, 224, 227, and 228 from forward skirt area.	Instrumentation reduction.
Structures	Deleted 111-inch dollar weld doublers on aft LOX bulkhead.	Analysis and tests indicated the doublers not necessary.

Table B-3. S-IVB Significant Configuration Changes

SYSTEM	CHANGE	REASON
Instrumentation	Five S-IVB measurements are routed through the IU/FM/FM telemetry system. (Remaining measurements same as AS-504).	To better define the low frequency vibration which occurred on AS-505.
Propulsion	Addition of liner to LH_2 feed duct.	To eliminate flow resonance problems.
	O_2/H_2 injector change.	To eliminate possible burn through during flight operation.
	Addition of block point to shutoff valve of pneumatic power control module.	To prevent possible overheating of solenoid in secondary regulation mode (bang-bang).
	New configuration cold helium shutoff valves for cryogenic repress application.	To prevent main poppet seat distortion at low temperature.
	New configuration cold helium dump valve.	To prevent main poppet seat distortion at low temperature.
	Thermal protection - pneumatic shutoff valve solenoid.	High solenoid cold temperature in bang-bang mode of operation will reduce the solder strength.

Table B-4. IU Significant Configuration Changes

SYSTEM	CHANGE	REASON
Environmental Control	"Tee" section added to ends of air/GN_2 purge duct. "Tee" is capped on AS-506.	Provide capability for RTG fuel cask preflight thermal conditioning. Additional ducting, nozzle and brackets used on AS-505 not included on AS-506.
	Thermal switch settings were: Open at 288.8°K(60.1°F) Close at 288.2°K(59.0°F)	Settings determined from test data.
	Additional clamp added to IU air/GN_2 purge duct boot at the umbilical plate. Increased torque on clamps associated with the duct boot.	AS-505 preflight thermal conditioning to RTG was lost during countdown. Suspect area was the clamp at the inlet to the IU.
Instrumentation and Communication	Two acceleration and three pressure measurements added to the S-IVB are telemetered via IU FM/FM system. Added measurements: A12-403 Gimbal block longitudinal accelerometer A15-424 LOX feedline at Aft LOX dome accelerometer. D1-401 Thrust chamber pressure. D3-403 Oxidizer pump inlet pressure. D9-401 Oxidizer pump discharge pressure.	Low frequency structural vibrations monitored during the AS-506 flight.
Networks	Additional cables and modifications to the measuring distributor and F1 TM assembly.	Modifications required to add five measurements for the S-IVB.
Flight Program	Launch pad choice from target tape.	Pad choice can be loaded with targeting parameters from tape via the RCA-110A. Eliminates necessity for reassembly of flight program due to change of launch pad.
	Capability for detection of early S-IC engine out.	An S-IC engine out, formerly not detectable until 14 seconds after liftoff, can now be detected from 6 seconds after liftoff.
	Accelerometer zero test.	Adjusts the Sin D term for an early S-IC or S-II outboard engine out.
	Expanded S-II IGM guidance.	Automatically adjusts for wide variations in performance, for either high or low thrust levels. Has inherent capability to adjust guidance for multiple S-II engines out.
	Deletion of program recognition of critical pairs of switch selector commands.	The program will not prevent a time base update from altering the time separation between any pair of switch selector commands. It will be the responsibility of ground controllers to maintain such requirements if they exist.

Table B-4. IU Significant Configuration Changes (Continued)

SYSTEM	CHANGE	REASON
Flight Program (Cont'd)	Expanded data compression capability.	Maximum duration of data compression period extended from 50 to 95 minutes. Sample rate of Table 3 changed from 30 to 60 seconds. Maximum sample capacity of Table 2 increased from 31 to 59; Table 4 increased from 61 to 116.
	Deletion of LH_2 propellant dump.	The S-IVB residual LH_2 dump was deleted, since velocity change requirements could be satisfied otherwise.
	Selective telemetry calibration and dump.	Capability is provided to distinguish between "dump and calibrate" and "calibrate only" LVDC telemetry stations. Of the 14 LVDC telemetry stations on the mission, only Carnarvon, Hawaii, and Guaymas are compressed data dump stations.

MSFC—RSA, Ala

APPROVAL

SATURN V LAUNCH VEHICLE FLIGHT EVALUATION REPORT

AS-506, APOLLO 11 MISSION

By Saturn Flight Evaluation Working Group

The information in this report has been reviewed for security classification. Review of any information concerning Department of Defense or Atomic Energy Commission programs has been made by the MSFC Security Classification Officer. The highest classification has been determined to be unclassified.

Stanley L. Fragge
Security Classification Officer

This report has been reviewed and approved for technical accuracy.

George H. McKay, Jr.
Chairman, Saturn Flight Evaluation Working Group

for Herman K. Weidner
Director, Science and Engineering

Roy E. Godfrey
Saturn Program Manager

DISTRIBUTION:

MSFC:

Dr. von Braun, DIR
Mr. Shepherd, DIR
Dr. Rees, DEP-T
Mr. Gorman, DEP-M
Dr. Stuhlinger, ADIR-S

E

Mr. Maus, E-DIR
Mr. Smith, E-S

PA

Mr. Slattery, PA-DIR

PD

Dr. Lucas, PD-DIR
Mr. Williams, PD-DIR (2)
Mr. Driscoll, PD-DIR
Mr. Thomason, PD-DO-DIR
Mr. Goerner, PD-DO
Mr. Nicaise, PD-DO
Mr. Jean, PD-RV
Mr. Digesu, PD-DO-E
Mr. Palaoro, PD-SS
Mr. Blumrich, PD-DO-SL

PM

Mr. L. James, PM-DIR
Mr. Andressen, PM-PR-CM
Col. Teir, PM-SAT-IB-MGR
Mr. Huff, PM-SAT-E
Dr. Speer, PM-MO-MGR (4)
Mr. Belew, PM-AA-MGR
Mr. Brown, PM-EP-MGR
Mr. Smith, PM-EP-J
V. J. Norman, PM-MO
Mr. Stewart, PM-EP-F
Mr. Godfrey, PM-SAT-MGR
Mr. R. Smith, PM-SAT-MGR
Mr. Burns, PM-SAT-T
Mr. Bell, PM-SAT-E
Mr. Rowan, PM-SAT-E
Mr. Moody, PM-SAT-Q
Mr. Webb, PM-SAT-P
Mr. Urlaub, PM-SAT-S-IB/S-IC
Mr. Lahatte, PM-SAT-S-II
Mr. McCullough, PM-SAT-S-IVB
Mr. Duerr, PM-SAT-IU
Mr. Smith, PM-SAT-G
Col. Montgomery, PM-KM
Mr. Peters, PM-SAT-S-IVB
Mr. Weir, PM-SAT-IU
Mr. Ferrell, PM-EP-EJ
Dr. Constan, PM-MA-MGR
Mr. Riemer, PM-MA-QP
Mr. Balch, PM-MT-MGR
Mr. Auter, PM-MT-T
Mr. Sparks, PM-SAT-G
Mr. Ginn, PM-SAT-E
Mr. Haley, PM-SAT-S-IB/S-IC
Mr. Higgins, PM-SAT-S-IVB
Mr. Odom, PM-SAT-S-II
Mr. Stover, PM-SAT-S-II
Mr. Reaves, PM-SAT-Q
Mr. Wheeler, PM-EP-F
Mr. Johnson, PM-SAT-T
Mr. Cushman, PM-SAT-T (10)
Mr. Marchese, PM-MA-QR

S&E

Mr. Weidner, S&E-DIR
Mr. Richard, S&E-DIR
Dr. Johnson, S&E-R
Mr. Hamilton, MSC-RL

S&E-AERO

Dr. Geissler, S&E-AERO-DIR
Mr. Horn, S&E-AERO-DIR
Mr. Dahm, S&E-AERO-A (2)
Mr. Holderer, S&E-AERO-A
Mr. Dunn, S&E-AERO-ADV
Mr. Elkin, S&E-AERO-AT
Mr. Wilson, S&E-AERO-AT
Mr. Jones, S&E-AERO-AT
Mr. Reed, S&E-AERO-AU
Mr. Guest, S&E-AERO-AU
Mr. Ryan, S&E-AERO-DD
Mr. Cremin, S&E-AERO-M
Mr. Lindberg, S&E-AERO-M (10)
Mr. Baker, S&E-AERO-G
Mr. Jackson, S&E-AERO-P
Mr. Cummings, S&E-AERO-T
Mr. O. E. Smith, S&E-AERO-Y
Mr. J. Sims, S&E-AERO-P
Dr. Lovingood, S&E-AERO-D
Mr. Vaughan, S&E-AERO-Y

S&E-CSE

Dr. Haeussermann, S&E-CSE-DIR
Mr. Hoberg, S&E-CSE-DIR
Mr. Mack, S&E-CSE-DIR
Dr. McDonough, S&E-CSE-A
Mr. Aberg, S&E-CSE-S
Mr. Fichtner, S&E-CSE-G
Mr. Vann, S&E-CSE-GA
Mr. Hammers, S&E-CSE-I
Mr. Wolfe, S&E-CSE-I
Mr. E. May, S&E-CSE-L
Mr. McKay, S&E-CSE-LF
Mr. R. L. Smith, S&E-CSE-V
Mr. Brooks, S&E-CSE-V
Mr. Hagood, S&E-CSE-M (3)

S&E-ASTR

Mr. Moore, S&E-ASTR-DIR
Mr. Stroud, S&E-ASTR-SC
Mr. Robinson, S&E-P-ATM (4487)
Mr. Erickson, S&E-ASTR-SE
Mr. Darden, S&E-ASTR-SDC
Mr. Justice, S&E-ASTR-SDA
Mr. Vallely, S&E-ASTR-SDC
Mr. George, S&E-ASTR-SDI
Mr. Mandel, S&E-ASTR-G
Mr. Ferrell, S&E-ASTR-GS
Mr. Powell, S&E-ASTR-I
Mr. Avery, S&E-ASTR-SC
Mr. Kerr, S&E-ASTR-IRD
Mr. Threlkeld, S&E-ASTR-ITA
Mr. Boehm, S&E-ASTR-M
Mr. Lominick, S&E-ASTR-GMF
Mr. Taylor, S&E-ASTR-R

S&E COMP

Dr. Hoelzer, S&E-COMP-DIR
Mr. Prince, S&E-COMP-DIR
Mr. Fortenberry, S&E-COMP-A
Mr. Cochran, S&E-COMP-R
Mr. Houston, S&E-COMP-RR
Mr. Craft, S&E-COMP-RR

S&E-ME

Mr. Siebel, S&E-ME-DIR
Mr. Wuencher, S&E-ME-DIR
Mr. Orr, S&E-ME-A
Mr. Franklin, S&E-ME-T

S&E-ASTN

Mr. Heimburg, S&E-ASTN-DIR
Mr. Kingsbury, S&E-ASTN-DIR
Mr. Hellebrand, S&E-ASTN-DIR
Mr. Edwards, S&E-ASTN-DIR
Mr. Sterett, S&E-ASTN-A
Mr. Schwinghamer, S&E-ASTN-M
Mr. Earle, S&E-ASTN-P
Mr. Reilmann, S&E-ASTN-P
Mr. Thompson, S&E-ASTN-E
Mr. Fuhrmann, S&E-ASTN-EM
Mr. Cobb, S&E-ASTN-PP (2)
Mr. Black, S&E-ASTN-PPE
Mr. Wood, S&E-ASTN-P
Mr. Hunt, S&E-ASTN-A
Mr. Beam, S&E-ASTN-AD
Mr. Riquelmy, S&E-ASTN-SDF
Mr. Katz, S&E-ASTN-SER
Mr. Showers, S&E-ASTN-SL
Mr. Frederick, S&E-ASTN-SS
Mr. Furman, S&E-ASTN-AA
Mr. Green, S&E-ASTN-SVM
Mr. Grafton, S&E-ASTN-T
Mr. Marmann, S&E-ASTN-VAW
Mr. Lutonsky, S&E-ASTN-VAW
Mr. Devenish, S&E-ASTN-VNP (2)
Mr. Sells, S&E-ASTN-VOO
Mr. Schulze, S&E-ASTN-V (2)
Mr. Rothe, S&E-ASTN-XA
Mr. Griner, S&E-ASTN-XSJ
Mr. Boone, S&E-ASTN-XEK

S&E-QUAL

Mr. Grau, S&E-QUAL-DIR
Mr. Chandler, S&E-QUAL-DIR
Mr. Henritze, S&E-QUAL-A
Mr. Rushing, S&E-QUAL-PI
Mr. Klauss, S&E-QUAL-J
Mr. Hughes, S&E-QUAL-P
Mr. Landers, S&E-QUAL-PC (3)
Mr. Peck, S&E-QUAL-F
Mr. Brien, S&E-QUAL-Q
Mr. Wittmann, S&E-QUAL-T
Mr. Davis, S&E-QUAL-F

S&E-SSL

Mr. Heller, S&E-SSL-DIR
Mr. Sieber, S&E-SSL-S

MS

MS-H
MS-I
MS-IP
MS-IL (8)
MS-D

CC-P

Mr. Wofford, CC-P

KSC

Dr. Debus, CD
Adm. Middleton, AP (5)
Dr. Gruene, LV
Mr. Rigell, LV-ENG
Mr. Sendler, IN
Mr. Mathews, AP
Dr. Knothe, EX-SCI
Mr. Edwards, LV-INS
Mr. Fannin, LV-MEC
Mr. Pickett, LV-TMO
Mr. Rainwater, LV-TMO
Mr. Bell, LV-TMO-3
Mr. Lealman, LV-GDC
Mr. Preston, DE
Mr. Mizell, LV-PLN-12
Mr. O'Hara, LV-TMO
Mr. Brown, AP-SVO-3
Mr. Smith, AP-SVO

EXTERNAL

Headquarters, National Aeronautics & Space Administration
Washington, D. C. 20546

Dr. Mueller, M
Mr. Petrone, MO
Gen. Stevenson, MO (3 copies)
Mr. Hage, MO
Mr. Schneider, MO-2
Capt. Freitag, MC
Capt. Holcomb, MAO
Mr. White, MAR (2 copies)
Mr. Day, MAT (10 copies)
Mr. Wilkinson, MAB
Mr. Kubat, MAP
Mr. Wagner, MAS (2 copies)
Mr. Armstrong, MB
Mr. Mathews, ML (3 copies)
Mr. Lord, MT
Mr. Lederer, MY

Director, Ames Research Center: Dr. H. Julian Allen
National Aeronautics & Space Administration
Moffett Field, California 94035

Director, Flight Research Center: Paul F. Bikle
National Aeronautics & Space Administration
P. O. Box 273
Edwards, California 93523

Goddard Space Flight Center
National Aeronautics & Space Administration
Greenbelt, Maryland 20771
Attn: Herman LaGow, Code 300

John F. Kennedy Space Center
National Aeronautics & Space Administration
Kennedy Space Center, Florida 32899
Attn: Technical Library, Code RC-42
Mrs. L. B. Russell

Director, Langley Research Center: Dr. Floyd L. Thompson
National Aeronautics & Space Administration
Langley Station
Hampton, Virginia 23365

Lewis Research Center
National Aeronautics & Space Administration
21000 Brookpark Road
Cleveland, Ohio 44135
Attn: Dr. Abe Silverstein, Director
Robert Washko, Mail Stop 86-1
E. R. Jonash, Centaur Project Mgr.

Manned Spacecraft Center
National Aeronautics & Space Administration
Houston, Texas 77058
Attn: Director: Dr. Robert R. Gilruth, AA
Mr. Low, PA
Mr. Arabian, ASPO-PT (15 copies)
Mr. Paules, FC-5
J. Hamilton, RF (MSFC Resident Office)
G. F. Prude, CF-33 (3 copies)

Director, Wallops Station: R. L. Krieger
National Aeronautics & Space Administration
Wallops Island, Virginia 23337

Director, Western Operations Office: Robert W. Kamm
National Aeronautics & Space Administration
150 Pico Blvd.
Santa Monica, California 90406

Scientific and Technical Information Facility
P. O. Box 5700
Bethesda, Maryland 20014
Attn: NASA Representative (S-AK/RKT) (25 copies)

Jet Propulsion Laboratory
4800 Oak Grove Drive
Pasadena, California 91103
Attn: Irl Newlan, Reports Group (Mail 111-122)
H. Levy, CCMTA (Mail 179-203) (4 copies)

Office of the Asst. Sec. of Defense for Research and Engineering
Room 3E1065
The Pentagon
Washington, D. C. 20301
Attn: Tech Library

Director of Guided Missiles
Office of the Secretary of Defense
Room 3E131
The Pentagon
Washington, D. C. 20301

Central Intelligence Agency
Washington, D. C. 20505
Attn: OCR/DD/Publications (5 copies)

Director, National Security Agency
Ft. George Mead, Maryland 20755
Attn: C3/TDL

U. S. Atomic Energy Commission, Sandia Corp.
University of California Radiation Lab.
Technical Information Division
P. O. Box 808
Livermore, California 94551
Attn: Clovis Craig

U. S. Atomic Energy Commission, Sandia Corp.
Livermore Br, P. O. Box 969
Livermore, California 94551
Attn: Tech Library

Commander, Armed Services Technical Inf. Agency
Arlington Hall Station
Arlington, Virginia 22212
Attn: TIPCR (Transmittal per Cognizant Act Security Instruction) (5 copies)

Commanding General
White Sands Missile Range,
New Mexico 88002
Attn: RE-L (3 copies)

Chief of Staff, U. S. Air Force
The Pentagon
Washington, D. C. 20330
1 Cpy marked for DCS/D AFDRD
1 Cpy marked for DCS/D AFDRD-EX

Headquarters SAC (DPLBS)
Offutt AFB, Nebraska 68113

Commander
Arnold Engineering Development Center
Arnold Air Force Station, Tennessee 37389
Attn: Tech Library (2 copies)

Commander
Air Force Flight Test Center
Edwards AFB, California 93523
Attn: FTOTL

Commander
Air Force Missile Development Center
Holloman Air Force Base
New Mexico 88330
Attn: Tech Library (SRLT)

Headquarters
6570th Aerospace Medical Division (AFSC)
U. S. Air Force
Wright-Patterson Air Force Base, Ohio 45433
Attn: H. E. Vongierke

Systems Engineering Group (RTD)
Attn: SEPIR
Wright-Patterson, AFB, Ohio 45433

AFETR (ETLLG-1)
Patrick AFB, Florida 32925

EXTERNAL (CONT.)

Director
U. S. Naval Research Laboratory
Washington, D. C. 20390
Attn: Code 2027

Chief of Naval Research
Department of Navy
Washington, D. C. 20390
Attn: Code 463

Chief, Bureau of Weapons
Department of Navy
Washington, D. C. 20390
1 Cpy to RESI, 1 Cpy to SP,
1 Cpy to AD3, 1 Cpy to REW3

Commander
U. S. Naval Air Missile Test Center
Point Mugu, California 93041

AMSMI-RBLD; RSIC (3 copies)
Bldg. 4484
Redstone Arsenal, Alabama 35809

Aerospace Corporation
Reliability Dept.
P. O. Box 95085
Los Angeles, California 90045
Attn: Don Herzstein

Bellcomm, Inc.
1100 Seventeenth St. N. W.
Washington, D. C. 20036
Attn: Miss Scott, Librarian

The Boeing Company
P.O. Box 1680
Huntsville, Alabama 35807
Attn: S. C. Krausse, Mail Stop AD-60
(20 copies)
J. B. Winch, Mail Stop JA-52
(1 copy)

The Boeing Company
P.O. Box 58747
Houston, Texas 77058
Attn: H. J. McClellan, Mail Stop HH-05
(2 copies)

The Boeing Company
P.O. Box 29100
New Orleans, Louisiana 70129
Attn: S. P. Johnson, Mail Stop LT-84
(10 copies)

Mr. Norman Sissenwine, CREW
Chief, Design Climatology Branch
Aerospace Instrumentation Laboratory
Air Force Cambridge Research Laboratories
L. G. Hanscom Field
Bedford, Massachusetts 01731

Lt/Col. H. R. Montague
Det. 11, 4th Weather Group
Eastern Test Range
Patrick Air Force Base, Florida 33564

Mr. W. Davidson
NASA Resident Management Office
Mail Stop 8890
Martin Marietta Corporation
Denver Division
Denver, Colorado 80201

Chrysler Corporation Space Division
Huntsville Operation
1312 N. Meridian Street
Huntsville, Alabama 35807
Attn: J. Fletcher, Dept. 4830
M. L. Bell, Dept. 4830

McDonnell Douglas Astronautics Company
Missile & Space Systems Division/SSC
5301 Bolsa Avenue
Huntington Beach, California 92646
Attn: R. J. Mohr (40 copies)

Grumman Aircraft Engineering Corp.
Bethpage, Long Island, N. Y. 11714
Attn: NASA Resident Office
John Johansen

International Business Machine
Mission Engineering Dept. F103
150 Sparkman Dr. NW
Huntsville, Alabama 35805
Attn: C. N. Hansen (15 copies)

Martin Company
Space Systems Division
Baltimore, Maryland 21203
Attn: W. P. Sommers

North American Rockwell/Space Division
12214 S. Lakewood Blvd.
Downey, California 90241
Attn: R. T. Burks (35 copies)

Radio Corporation of America
Defense Electronic Products
Data Systems Division
8500 Balboa Blvd.
Van Nuys, California 91406

Rocketdyne
6633 Canoga Avenue
Canoga Park, California 91303
Attn: T. L. Johnson (10 copies)

Foreign Technology Division
FTD (TDPSL)
Wright-Patterson Air Force Base, Ohio 45433

Mr. George Mueller
Structures Division
Air Force Flight Dynamics Laboratory
Research and Technology Division
Wright-Patterson Air Force Base, Ohio 45433

Mr. David Hargis
Aerospace Corporation
Post Office Box 95085
Los Angeles, California 90045

Mr. H. B. Tolefson
DLD-Atmospheric Physics Branch
Mail Stop 240
NASA-Langley Research Center
Hampton, Virginia 23365

Mr. Chasteen
Sperry Rand
Dept. 223
Blue Spring Road
Huntsville, Ala.

EXTERNAL (CONT.)

J. E. Trader
NASA Resident Manager's Office
McDonnell Douglas Astronautics Corp.
5301 Balsa Avenue
Huntington Beach, California 92646

L. C. Curran
NASA Resident Manager's Office
North American Rockwell/Space Division
12214 Lakewood Blvd.
Downey, California 90241

L. M. McBride
NASA Resident Manager's Office
North American Rockwell/Rocketdyne
6633 Canoga Avenue
Canoga Park, California 91303

C. M. Norton
NASA Resident Manager's Office
International Business Machines
150 Sparkman Drive
Huntsville, Alabama 35804

N. G. Futral
NASA Resident Manager's Office
North American Rockwell/Space Division
69 Bypass NE
McAllester, Oklahoma 74501

C. Flora
McDonnell Douglas Astronautics Corp.
Sacramento Test Center
11505 Douglas Avenue
Rancho Cardora, California 95670

W. Klabunde
Northrup
6025 Technology Drive
Huntsville, Alabama 35804